CRANFIELD UNIVERSITY

ANNA CHWIALKOWSKA

Electrical rectification from aligned diodes based on the donor-(π-bridge)-acceptor molecules

SCHOOL OF ENGINEERING

PhD THESIS

CRANFIELD UNIVERSITY

SCHOOL OF ENGINEERING

PhD THESIS

Academic Year 2004-2007

ANNA CHWIALKOWSKA

Electrical rectification from aligned diodes based on the donor-(π-bridge)-acceptor molecules

Supervisor: GJ ASHWELL

April 2007

This thesis is submitted in partial fulfilment of the requirements for the degree of Master of Science

Abstract

As traditional devices containing silicon transistors begin to approach their physical limits, new systems composed of organic molecules are being considered for molecular-scale devices of the future. The present work reports on the electrical properties of molecular diodes, especially observations of electrical rectification from molecular systems based on donor-(π-bridge)-acceptor molecules. For this purpose three types of molecular assembly were incorporated and their growth was observed with the quartz crystal microbalance (QCM) technique.

Covalent self-assembly proved to be the most efficient method of forming well-ordered molecular films compared to those obtained via LB and ESA techniques. SAMs of Q3CNQ molecules yielded higher rectification than their LB analogues and achieved rectification ratio of 30 at ± 1V for every sample. On the other hand ESA films, in which molecular alignment of the physisorbed cationic dye was controlled by self-assembly of the anionic component, were probably more disordered, but exhibited higher (and sample-dependent) rectification ratios with a maximum of 450 at ± 1V. QCM also showed the phenomena of trapped water molecules within the physisorbed ESA monolayer that affected molecular order and also the electrical properties of the samples.

Scanning tunnelling microscopy (STM), incorporated for obtaining current-voltage (I-V) characteristics from samples, showed that stearic hindrance has to be taken into consideration when designing donor-(π-bridge)-acceptor rectifiers. Sufficient isolation of donor and acceptor groups by the π-bridge is essential in order to prevent delocalisation of molecular orbitals over the entire molecule. Therefore, implementation of the Aviram-Ratner model of molecular rectification became possible although molecules investigated here did not possess the proposed σ-bridge. Additionally, the rectification effect arising from geometrical asymmetry induced by electrode-linking alkyl chains was shown to be negligible here, which is contrary to other theories of molecular rectification.

Acknowledgements

I am grateful to many people who have been very helpful to me during my time at Cranfield University. First of all, to my supervisor, Prof Geoffrey J. Ashwell, for giving me the opportunity to do the PhD. Secondly, to all my colleagues who tried their best to get me closer to English culture and life-style and Polish friends, who made my time like at homeland. I am also very grateful to Dr Wayne Tyrrell for taking time from the busy schedule to help in experimental work and discuss many issues and dr Anne Wittham for reading this thesis and offering helpful comments.

I especially thank my uncle Andrzej Ziober, who has been like a father to me for all those years and always encouraged me to aspire for more. Finally and most importantly I would like to thank to my husband Rafał, for his support and never-ending love.

List of contents

List of figures

1 Introduction

Nanotechnology is the field of science that deals with the fundamental understanding of physical properties and phenomena of small structures or small-sized materials. The field was suggested in 1959 by a famous physicist, Richard Feynman, who considered a direct manipulation of matter at the atomic scale [1]. He was particularly interested in denser integrated circuits and development of microscopy at the atomic scale.

Currently there are many different opinions about what exactly can be classified within the field of nanotechnology. However, it was assumed that nanomaterials are those with at least one dimension falling in the nanometer scale [2]. In this group are included: nanoparticles, nanorods, nanowires, thin films and bulk materials made of nanoscale building blocks or consisting of nanoscale structures. Although nanotechnology seemed to be very promising, there were many speculations as to its realisation for many years.

The real interest in nanotechnology was fuelled by the invention of the transistor (1947), which was the beginning of rapid improvement in information processing technology [3]. Thanks to the use of some photographic methods and chemical etching, mass production and miniaturisation of transistors became possible. Among dozens of semiconductor devices, metal-oxide-semiconductor field-effect-transistors (MOSFETs) turned out to be dominant in information processing technology. MOSFETs offer many advantages, such as signal balance, fast operation speed and dense packing of the transistors within the integrated circuit. However, the possibility of dimension reduction in order to produce smaller electronic devices [4,5] is the main (economical) merit. Due to their shorter length dimensions, more current can pass across the device, which means faster speeds and at the same time a lower energy of device switching.

The process of miniaturisation of integrated circuits was predicted by 'Moore's law' [6] (see Figure 1.1), which stated that the number of transistors on a chip would double every eighteen months. However, this theory did not consider the physical limitations of transistors and smaller integrated circuits. Currently, transistor technology is located at the end of Moore's law with transistors *ca.* 50 nm [7,8]. Below this number, economical production of transistors with good efficiency is a challenge, as large power dissipation* and high heat production† are impossible to avoid.

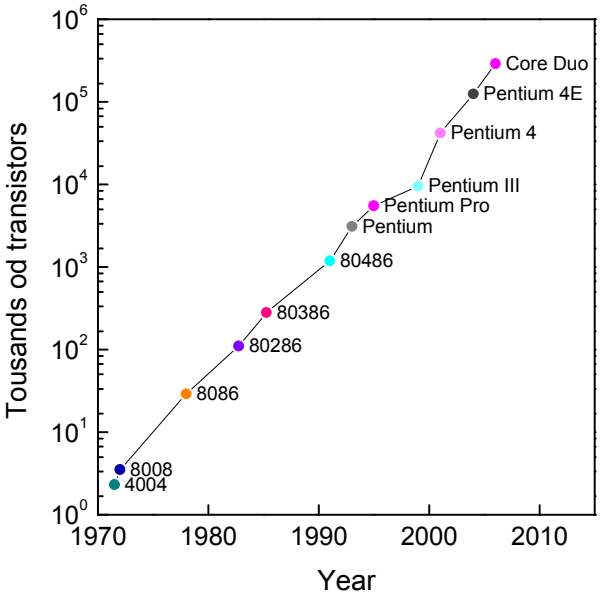

Figure 1.1 The illustration of Moore's law, which states that the number of transistors per square inch on integrated circuits had doubled every year, since the integrated circuit was invented. The data used to construct this plot have been adapted from 9.

* Power dissipation has always been present in the semiconductor transistors but never considered as a threat for transistors above the size of μm. Current semiconductor technology aspires to go far below this size, which is a great benefit because smaller devices mean faster processes. Reduction of the size means smaller voltage, which can be applied to the device and at the same time smaller power consumption. Reduction of the applied voltage carries the consequence of lowering the threshold voltage, which is defined as a (gate) voltage at the depletion (junction) region. However, threshold voltage can only be lowered to a certain point. At this point a transistor can not be completely turned off and work in a special mode (called weak-inversion) with an exponential rise of the current between source and drain. This growth would devour almost 50 % of total power consumption to maintain transistor performance.

† Rise in the density of the transistors on the integrated circuit causes the temperature rise within the circuit, so makes it work slower and not last as long. That is why cooling systems are needed to keep the temperature stable, allowing for maximum work and prevent destruction of the circuit.

In order to make further progress in information technology, several ideas to compose smaller (nanoscale) devices were proposed [10]. Great potential was seen in the shrinking of the size of electronic components down to a single molecule, which can control electron transport. Because molecules are identical, they should have identical properties when used in molecular devices. Thus, one of the advantages to molecular electronics is that component variability can be avoided. This allows the possibility of large molecular arrays of identical and defect-free devices with a molecular density of $10^9 - 10^{13}$ devices m^{-2} [11]. In comparison, current semiconductor devices density is 10^8 devices m^{-2}. The other advantage arises from intramolecular properties of molecules, that are π-conjugated systems, in which conduction can be switched on and off again by changing their molecular conformation. Molecular switching speeds are expected to reach values of over 1 THz [5].

One of the first experiments using molecules to build an electronic device was reported in 1972 [12]. This concerned a sensor using a field effect transistor (FET) configuration with its gate displaced into a liquid electrolyte and an active layer of molecules for molecular recognition. At the same time, Mann and Kuhn first measured the electric properties of organic donor monolayers, doped by guest acceptor molecules [13], which led to the development of a new assembly technique, allowing chemical binding of organic molecules to solid substrates. However, the idea of using just single molecules to build electronic devices was predicted in the early 1970s, when Aviram and Ratner proposed a molecular counterpart of the p-n rectifying diode [14]. At the time, realisation of this proposal was rather difficult, as no information was given on how a molecule could be incorporated into a device or circuit. However, in the early 1980s, two IBM scientists invented a new technique for analysis of the structure of conductive samples – Scanning Tunnelling Microscopy (STM). It was the first step in the development of a whole family of scanning probe microscopies (SPMs), in which 'contact' with a sample was guaranteed by a metallic tip. Since then, several molecular

systems have been investigated theoretically and experimentally leading to molecular electronics becoming a real possibility.

The work being performed in the field of molecular electronics, in science and industry, is focused in two directions. The first relates to the synthesis of new types of organic molecules with different electronic functionalities, whereas the second concerns the invention of new methods to measure electronic properties of molecules and their assemblies. Some of the investigated molecules exhibit properties that are characteristic of two-terminal devices, like switching, rectification or light emission, giving hope for construction of a molecular three-terminal device (transistor).

1.1 Motivation and objectives

According to the Aviram and Ranter model, donor-(σ-bridge)-acceptor molecules were believed to be molecular counterparts of inorganic p-n junctions [14]. As a result of many attempts to synthesise Aviram-Ratner-like molecules, researchers proposed exchanging the σ-bridge for a π-bridge to facilitate synthesis and so obtain a greater number of potential unimolecular rectifiers.

The major objective of this thesis was verification of the mechanism of electron transfer through molecular junctions, based on the studied molecular systems containing donor-(π-bridge)-acceptor chromophores. For this purpose, scanning tunnelling microscopy was utilised for registering current-voltage characteristics of adsorbed monolayers on gold-coated substrates. During the course of the investigations, fifteen chromophores were studied and their structural and electrical properties led to better understanding of the origins of molecular rectification. Some of the theoretical predictions were proved to apply to some systems, whereas others did not, and the reasons are discussed here. Different methods of assembly allowed comparison of electrical properties of molecular films and to obtain the highest to date rectification ratio from donor-(π-bridge)-acceptor-based molecules.

1.2 Outline of dissertation

This dissertation is organised in order to show current progress in molecular electronics, with an emphasis on rectification arising from donor-π-acceptor molecules. In brief:

- Chapter 1; a short introduction to discuss the motives, aims and needs of molecular-based electronics.

- Chapter 2; a review of organic thin film self-assembly methods and tools for structural and optical characterisation of molecules and their assemblies. Although there are many methods, only two of them were described in detail as they were used in this thesis.

- Chapter 3; relates to fabrication of junctions for the purposes of molecular electronics. Despite most of the techniques described here, they will not be utilised in proper devices but contribute to understanding the functional part of molecular devices, *i.e.* electron transfer through a molecular system connected to electrodes.

- Chapter 4; shows the progress in molecular rectification since the Aviram and Ratner proposal. It shows significant examples in both, theoretical and experimental work in molecular rectification. It refers to examples in assembly and device fabrication methods described in chapters 2 and 3.

- Chapter 5; presents molecules utilised for fabrication of molecular films. It also contains a short description of characterisation methods, which in their simplicity tend to explain their functionality and accuracy of their utilisation in current studies.

- Chapter 6; presents the results and discussion of structural and electronic properties of molecular devices, based on molecular films containing

donor-(π-bridge)-acceptor molecules, with applications in molecular rectification. It strongly refers to chapter 4, particularly to theoretical predictions of the source of rectifying behaviour. A part of this chapter describes a novel and sufficient method of layer-by-layer assembly from small molecules and discusses the participation of water (and possible additional ions) in the electron transport process.

- Chapter 7; a summary of experimental work showing the significance and primary contributions of this investigation to the contents of Chapter 4. It also contains recommendations for future research in the area of electrical rectification from donor-(π-bridge)-acceptor molecules.

- Chapter 8; contains a list of publications related to the results desribed in the thesis.

2 Molecular assembly

The first approach to producing organised assemblies was made by Pockels [15] and Rayleigh [16], who observed formation of monolayers of fatty acids on the water surface. These studies were continued by Langmuir, who incorporated precision equipment (Langmuir trough) to study different amphiphilic molecules [17]. He discovered the unique properties of thin films of molecules, which could be aligned at the air-water interface, with the polar functional groups immersed in the water and non-polar chains sticking out of the water. A few years later Katherine Blodgett transferred Langmuir's monolayer to a solid substrate [18]. This allowed deeper investigations into mono- and multilayer properties, resulting in reviewing its spectroscopic [19,20], optical [21,22] and electrical properties. In spite of the possibility of producing films with high precision, the Langmuir-Blodgett (LB) method is not free from drawbacks. Among other disadvantages, poor thermal and mechanical stability have lead to a search for other methods of preparing molecular films, which would be less sensitive to external conditions.

In recent years, two preparation techniques of high precision organic thin films have been very popular. One of them is self-assembly, which may be defined as the spontaneous adsorption of the organic molecules on a solid surface. Such behaviour was first described by Zisman and co-workers in 1946 [23] but the real interest in molecular electronics assembly began with publications of Nuzzo and Allara in 1983, relating to chemisorption of organic disulfides from dilute solutions on gold surfaces [24]. Latest developments in deposition methods have allowed the use of ultrahigh vacuum (UHV) for self-assembly from the gas phase [25]. Development of organic molecular beam deposition (OMBD), also called organic molecular beam epitaxy (OMBE) has adapted UHV for growth of small molecular weight organic molecular crystals [26].

Molecular assembly for nanoelectronic applications demands well-ordered, densely-packed and defect-free films assembled on the substrate. They must be thermally and chemically stable and resistant to mechanical stress. Current progress in molecular assembly offers a variety of organic molecules with different functionalities for formation of a molecular film. Molecular assembly can be divided into groups depending on the type of forces used to control the position of the molecules on the surface of the electrode. This chapter deals with three types of assembly, which were governed by hydrophobicity and hydrophilicity (LB films), chemical reaction (SAMs) and electrostatic interaction (ESA).

2.1 Langmuir-Blodgett monolayers

The LB technique [27,28,29] is a deposition technique, which utilises molecules with amphiphilic properties to make ultrathin organic films. Such molecules contain two parts: a hydrophilic, polar head group and a hydrophobic, nonpolar hydrocarbon tail. Typical examples of amphiphilic molecules are fatty acids; however many examples can be found such as dyes (cyanines, phthalocyanines), charge-transfer complexes (TCNQ, TTF), fullerenes and biological compounds (pigments, peptides, proteins). Amphiphilic molecules, when spread (from the solution of a volatile solvent, such as chloroform, dichloromethane, etc.) at the air-water interface, try to cover the available water surface-area. After evaporation of the solvent molecules, a loosely packed monolayer is formed, which exists in specific equilibrium – hydrophilic ends interact strongly with water (via its dipole moments or by hydrogen bonding), whereas the hydrophobic ends protrude from water. The hydrophobic moiety must be large enough to ensure that the molecule does not dissolve in the water.

The most important indicator of monolayer properties of amphiphilic molecules can be obtained by measuring the surface pressure at constant temperature. Surface pressure can be defined as the surface tension of a liquid covered with molecules, and it can be

recorded during compression of the molecules*. It is usually monitored (and presented) as a function of the area of water surface available to each molecule [27]. A stearic acid isotherm is shown in Figure 2.1 below.

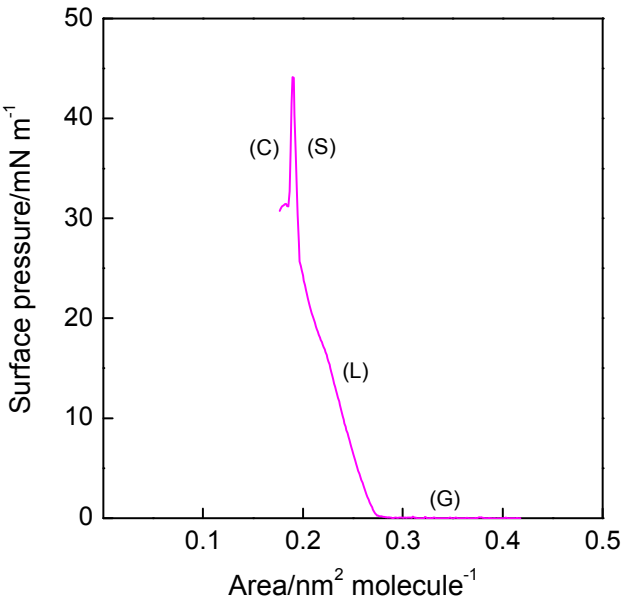

Figure 2.1 The typical surface pressure vs area per molecule isotherm for stearic acid. The isotherm obtained at 21.5° C shows four characteristic features: (G) – region where molecules are in the gaseous state; (L) – called liquid state, in which molecules undergo compression; (S) – solid state, in which molecules form a closely packed monolayer; (C) – collapse of the monolayer into three-dimensional structures, seen as a rapid decrease in the surface pressure.

Deposition of a monolayer of amphiphilic molecules on the solid substrate occurs in two steps. The first is the compression of molecules together with the value of surface pressure required to form a complete and homogeneous monolayer, via a movable barrier. Usually this is midway between the liquid and solid states of the isotherm. When this pressure is reached, the solid substrate moves (with constant speed) in one direction and the computer controlled barrier keeps the surface pressure at the adopted value by constant compression of the molecules until substrate is completely covered

* The term of surface pressure (Π) was introduced to differentiate between the absolute surface tension of a liquid and the instantaneous surface tension of the same liquid covered with a molecular monolayer. Therefore surface pressure is equal to the reduction of the pure liquid surface tension (γ_0) by the film; $\Pi = \gamma_0 - \gamma$, γ – surface tension of the film covered substrate [29].

with molecular film. The illustration of the LB deposition process is shown in Figure 2.2.

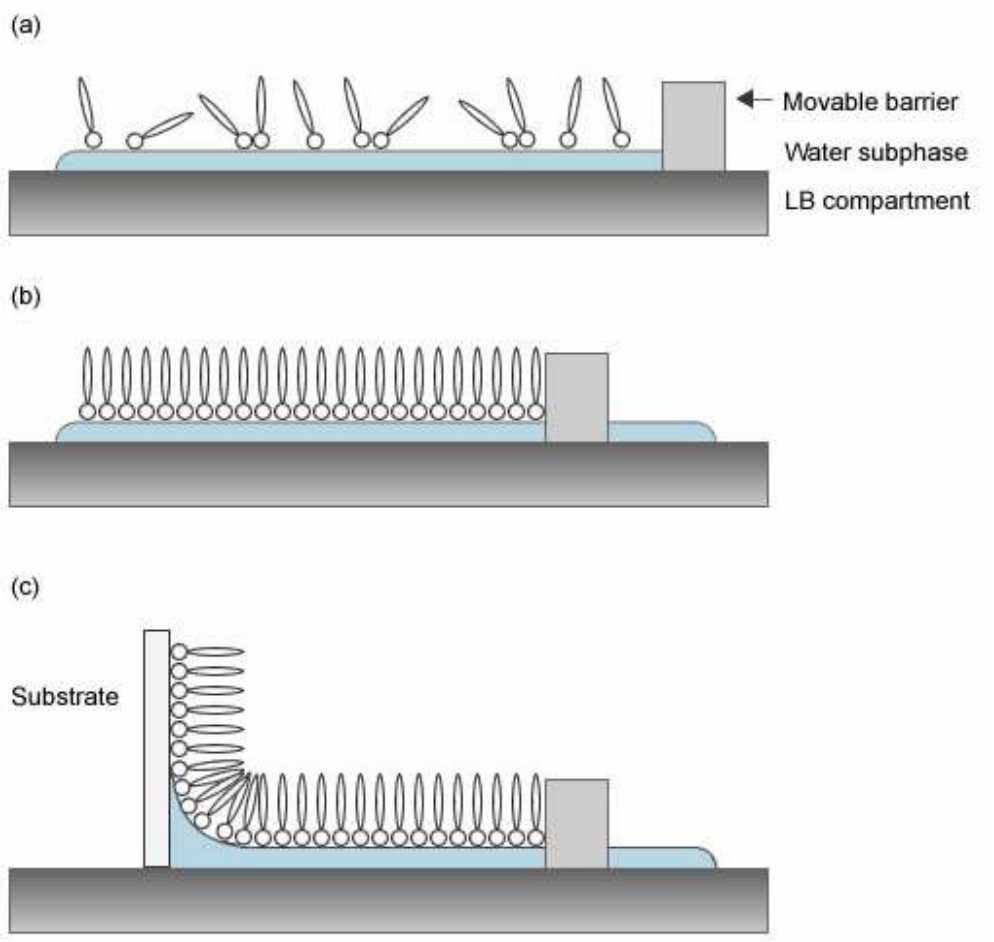

Figure 2.2 Deposition of a monolayer of amphiphilic molecules onto the substrate surface: (a) loose alignment of molecules at the air-water interface after spreading from solution, corresponding to the gaseous phase; (b) compressing molecules with movable barrier to the point molecules stand side-by-side on the subphase; (c) deposition of the monolayer on the movable solid substrate.

The deposition process can be repeated many times resulting in the formation of multilayer structures [30], in which molecules can adopt different configurations: head-to-head or tail-to-tail (called Y-type), head-to-tail (X-type) and tail-to-head (Z-type); see Figure 2.3. Although the arrangement of individual LB monolayers depends on the substrate and the direction of the substrate movement during deposition, the choice

of the arrangements depends on the molecules and its further application. It is even possible to build up superlattice structures using different materials.

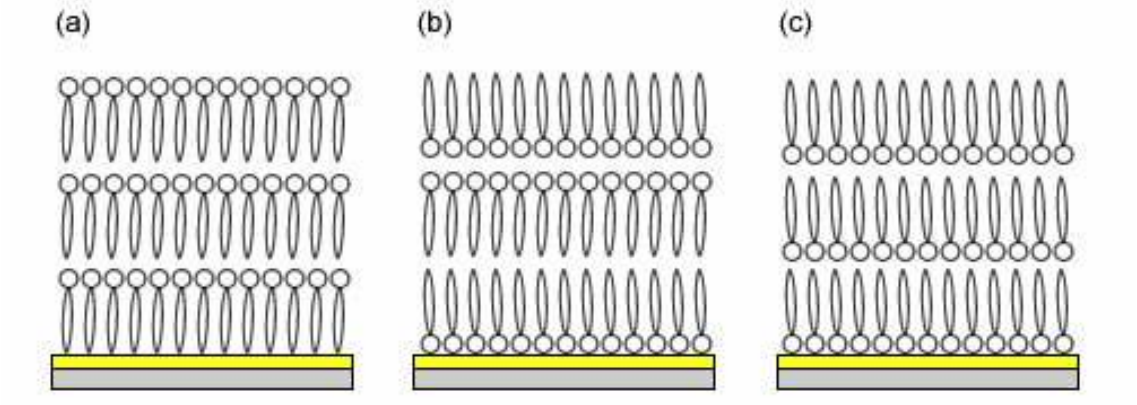

Figure 2.3 Different alignment of molecules within LB films: (a) X-type (head to tail) on hydrophobic substrate; (b) Y-type (alternate) on hydrophilic substrate; (c) Z-type (tail to head) on hydrophobic surface.

The LB technique seems to be a high-precision and easy to use deposition method. There are numerous commercially available instruments for LB deposition and most of them are equipped with automatic systems to control the surface pressure and dipping mechanism. However, there are many external factors that can affect the quality of LB films [29]. Presence of air-bound contamination on the water subphase can change the position of the pressure-area isotherm along the area/molecule axis, and can affect the concentration of molecules constituting film. Vibrations and larger contaminations may cause collapse of the monolayer and therefore change its average thickness.

2.2 Covalent self-assembly

Self-assembled monolayers (SAMs) are molecular structures formed by adsorption of molecules with a strong affinity to the surface on which they organise [25]. They have been extensively studied with the aim of simple self-organising molecular systems with applications in nanofabrication, molecular recognition, corrosion inhibition and biosensors. Much attention was dedicated to structural and chemical properties of self-assembled molecules and the kinetics of the growth of the monolayer.

Deposition of a SAM is rather straightforward and relies on immediate self-organisation of the molecules after their exposure to the solid substrate. It can occur from the gaseous [31,32] or liquid phase [25], depending on the level or control of temperature and cleanliness of the environment. Although the gas phase offers much more stable environmental conditions, it utilises more expensive equipment (vacuum chamber) and so growth from solution is a more popular way for SAM preparation. A schematic view of the self-assembly process from solution is shown in Figure 2.4.

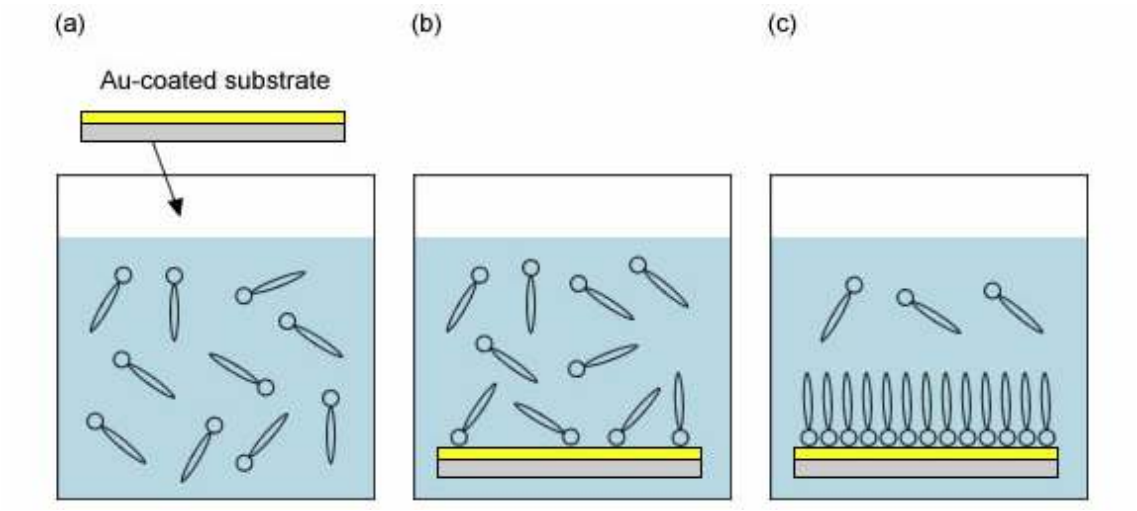

Figure 2.4 Growth of a SAM: (a) immersion of the gold-coated substrate in the dilute solution of surface-active molecule; (b) initial step in formation of a SAM, in which surface-active molecular heads organise towards the substrate; (c) formation of complete, densely packed SAM.

The ability of forming a complete monolayer is dependent on the type of the molecule and its concentration, solvent [33], substrate metal, temperature [34], etc. It was observed that during the first minutes the surface was covered by 80 – 90 %, and although this process was very rapid it produced rather an imperfect layer [35]. However, further exposure of the substrate to the solution of the molecules yielded to repeated desorption and adsorption as molecules tried to attach to all available sites on the substrate, creating a closely-packed structure. SAM formation (mainly first step) was thought to be even more effective if it occurred at temperatures above 25° C [25].

There are several types of self-assembly, which can be divided by the type of molecule and foundation to which they bind. One of the most popular are organosilane compounds, such as $RSiX_3$, R_2SiX_2 or RSiX (where R – functionalised carbon chain, X – Cl or O) can easily assemble on oxidised surfaces (for example SiO_2 [36] or Al_2O_3 [37]) or glass, gold, mica [38]. During adsorption the SiCl part of the molecule reacts in an aqueous environment with the –OH presented in the substrate, resulting in a chemical bond of Si—O—Si to the substrate. Because molecules that are tightly-packed within the monolayer interact with each other, Si—O—Si bonds are also formed between neighbouring molecules, resulting in a mono- or multilayer, polymer-like structure. Despite silane-based molecules assembling on silicon-based surfaces, which are the same as for current semiconductor industry, they do not exhibit effective long-range order. They tend to organise in islands of very closely-packed molecules, with order corresponding to a complete monolayer [39], or they form incomplete (less denser) but homogeneous monolayers [25]. This is dependent on the type of the molecules, particularly the length of the alkyl chain and control of experimental procedure (temperature [40], solvent, rinsing routine [33], and other parameters).

Although less dense than organosilanes, alkanothiolates (see example molecules in Figure 2.5) have become the most investigated groups of molecules for SAMs. It is because of their greater solubility and high speed of 'on surface' reaction. They organise easily on noble metals, such as gold [33,34,38,41,42], silver [43], platinum [44], copper [41,45], indium [46] and mercury [47,48]. Positive feedback was also shown from self-assembly of alkanethiols on GaAs [49], which is known for its good electronic properties, comparable with silicon[*].

[*] From a molecular electronics point of view, silicon is cheaper to obtain and has greater physical strength. It also has a natural insulating layer of oxide, which GaAs does not have. However, GaAs has a higher electron mobility and higher breakdown voltages, which allow higher operating power levels. It can also be used for light emission.

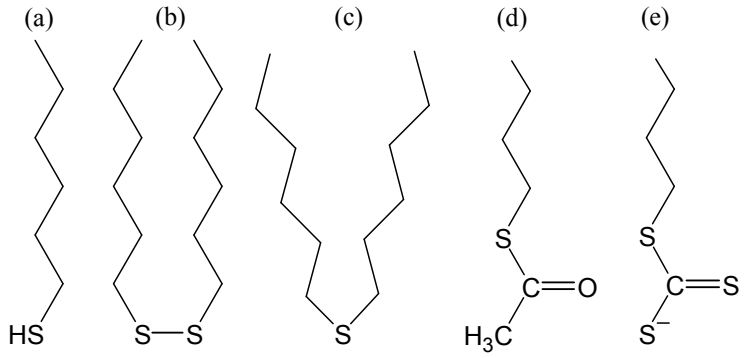

Figure 2.5 Surface-active organic compounds, which can form SAMs by chemical bonding to the metallic substrate: (a) alkanethiol; (b) dialkyl disulfide; (c) dialkyl sulphide; (d) thioacetate; (e) alkyl xianthale.

Gold has an advantage over other metallic electrodes because it does not oxidise under ambient conditions. Its high conductivity allows use in many electronic applications [38], such as with a thin film layer (vapour deposition, electrodeposition, etc.). Gold is commonly used as a substrate in many analytical techniques, such as quartz crystal microbalance (QCM), surface plasmon spectroscopy (SPR) or ellipsometry. Unfortunately, polycrystalline metallic surfaces are not free from structural defects. Roughness of the gold surface can produce defects at gold grain boundaries, step edges and vacancy islands and even some metallic ions. These would significantly affect the alignment of the molecules and disturb the order within a SAM [38]. Some theoretical studies predict disruption of electronic properties [50] in the presence of defects. An alternative material to gold could be palladium [51]. It is characterised by smaller grains (2-3 times than gold), which would effectively decrease the number of defects in SAMs [52] and does not oxidise in air.

The mechanism of adsorption of simple alkanethiols on gold surfaces involves each molecule losing the hydrogen from its thiol group (-SH). At this point the molecule gains a negative charge ($-S^-$), which forms a bond with the metal ion (Au_3^+). A by-product of the reaction is the hydrogen, which ideally should transform into dihydrogen. However, it can also stick to the sulfur and convert a surface thiolate to disulfide [25].

Intensive theoretical studies revealed that it was likely that single sulphur atoms were bound to three atoms of gold. Such chemical bonding corresponds to an energy of ~ 40-45 kcal/mol [53] and is the strongest interaction existing in SAMs. Alkanethiols on gold have fully extended chains, which yields a tilt angle of about 30° from the normal to the substrate. In the case of bulkier molecules, particularly dyes, the tilt angle may be different and depends on the molecular structure and length of the alkyl chain (see chapter 6.2). For example, phenylthioureas were shown to be tilted at the same angle as alkanethiols. It was because they contained an easily twisted long alkyl chain, whereas the rest of the molecule was perpendicular to the surface [54]. For simple oligophene-based molecules, which do not possess an alkyl chain, the tilt angle was in a range from less then 5° [55,56] to up to 33° ±18° [57]. This was dependent upon the substituents and presence (or absence) of hydrogen connected to the sulfur atom linking molecule to the substrate [58].

2.3 Ionic self-assembly

The technique of ionic self-assembly, also called electrostatic self-assembly (ESA), is based upon electrostatic interaction between at least two molecules containing opposite charges. This deposition technique was pioneered by Iler *et al.* [59] and was developed in early 1990s by Decher and co-workers [60,61,62], who discovered that multilayered structures could be formed via sequential immersion of the substrate into aqueous solutions of polyanions and polycations. This assembly method allowed formation of multifunctional and multicomponent thin films with a variety of advantages. This includes the simplicity of fabrication, and structural stability of films. Therefore, this method has attracted many scientists [63,64,65].

Figure 2.6 shows the basic concept behind the ESA method. A positively charged solid substrate is dipped into a polyanion aqueous solution. Electrostatic attraction between them occurs relatively quickly resulting in the self-assembly of the first monolayer.

Deposition of the second monolayer is usually a longer process because the polycation chains penetrate spaces between those previously deposited. Assembly of subsequent monolayers occurs in the same manner, via immersion, and their self-organisation is strongly affected by the underlying layers.

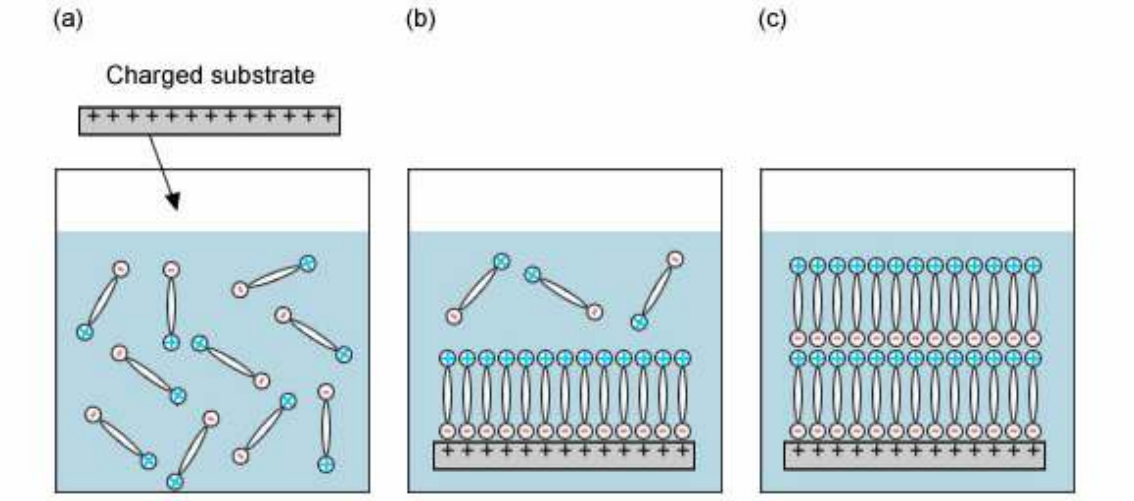

Figure 2.6 ESA procedure for building up multilayer structures via alternate layers of ionically coupled molecules: (a) Immersion of positively charged substrate in the solution of the first component; (b) formation of the first complete monolayer ionically coupled to the substrate and terminated in a negatively-charged group; (c) formation of another monolayer in the same manner as the first one.

There are two important factors involved with the ESA technique in order to obtain well-ordered structures. The first is dipping time, which is dependent on the material used and its concentration. Each material requires a certain amount of time to arrange and ionically bind to the substrate (or following monolayer). The other factor relates to the rinsing routine between depositions of alternate layers, which allows removal of loosely bounded ions with ultra pure water.

Molecules which possess ionic groups of Na^+, SO_3^- and NH_3^+ have been most extensively studied [66]. However, there is a possibility of utilising molecules with different structures and ionic groups. Some examples are shown in Figure 2.7.

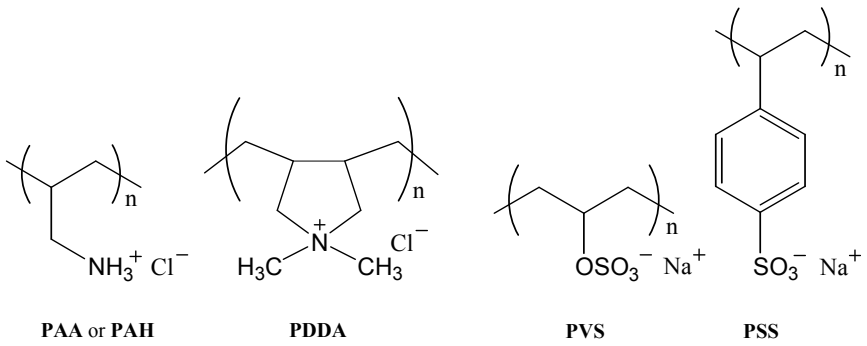

Figure 2.7 Some of the commonly used polyions for ESA deposition: polycations (PAA and PDDA) and polyanions (PVS and PSS). Examples cited from 66.

Apart from polymers, the ESA technique allows deposition of many other molecules. It is mainly known for the immobilisation of biomolecules, such as DNA or proteins [67]. However, organic dyes containing ionic groups can potentially be deposited by ESA technique [68]. They must contain one ionic group that can bind molecules to the substrate and a second ionic group for electrostatic interaction with molecules forming the following layer. Another simple way incorporating self-assembly involves formation of a basic layer and then electrostatic physisorption of molecules of a second material [69,70].

2.4 Monolayer characterisation methods

Exploring electrical behaviour of molecules and monolayers is as important as knowledge about their physical properties and geometry within the molecular junction. Traditional methods of investigating materials are based on optical absorption, which provides information on the structural disorder and presence of impurities in the molecular film. These techniques are significant for monolayer assembly due to their periodicity (in the direction normal to the substrate), which very often determines electrical and optical properties. Among these techniques, the most famous for morphological studies of monolayers and other materials is STM, and their derivative atomic force microscopy family (AFM), utilising atomically sharp tips for contacting a sample. AFM can provide details about magnetic or electrostatic forces of any type of

material [71], whereas with STM only conducting materials can be investigated. However, these two techniques are almost irreplaceable for imagining surfaces with a resolution of less than 1 nm (depending on the tip radius) in any type of environment (UHV, air, liquids). More about STM can be found in chapter 3.3.

For molecules to be useful in nanoscale electronics their purity must be very high. The basic methods for detecting impurities in molecular materials are photoluminescence, X-ray photoelectron spectroscopy (XPS) and Auger spectroscopy [66]. These techniques possess high sensitivity and are able to discern chemical elements down to 0.1 % in concentration. XPS is probably the most utilised for recognition of chemical surfaces of monolayers, and it relies on the electron spectra emitted from core atomic levels under irradiation of X-rays. Although XPS was utilised for investigations of some of the materials described in this thesis, other characterisation techniques were also used to study monolayer films – quartz crystal microbalance (QCM) and surface plasmon resonance (SPR). They will be described in more detail.

QCM and SPR are techniques that can be used to monitor adsorption of the organic materials onto metallic surfaces (electrodes) from solution phase. Their complementary operation was demonstrated by many researchers [72,73] and proved to work more efficiently, compared to the applications of these techniques when used independently. Both QCM and SPR have similar resolution and follow deposition in real time [73], which constitutes a great advantage.

2.4.1 Quartz crystal microbalance

The quartz crystal microbalance (QCM) is well established among techniques used to investigate thin film properties and is based on the piezoelectric effect discovered in 1880 [74]. The first application of the piezoelectric effect was discovered in 1917,

when X-cut plates* of quartz were used to generate and detect sound waves in water [75]. This work led to the development of SONAR and the field of ultrasonics, and also stimulated others to investigate the phenomenon of resonance in piezoelectric crystals. It resulted in production of high-stability quartz crystals with nearly zero frequency drift at around room temperature. The ideal material for quartz resonators must be stable, resistant to high temperatures and insoluble in water. Currently, 10 MHz AT-cut crystals fulfil these requirements [76]. They are cut with respect to the Y-crystallographic axis that corresponds to high stability and utility in a temperature range of 10° C to 50° C. The thickness of the crystal is very important as it determines the resonant frequency on which the accuracy of the calculation of the adsorbed mass is dependent. The sensitivity of the crystal increases with decreasing crystal thickness. Resonant frequency also depends on the structure of the quartz wafer, its shape and its mass [77].

In 1959 Sauerbrey demonstrated the extremely sensitive nature of quartz crystals, that is, the frequency shift of a quartz resonator is directly proportional to the adhered mass [78]. It resulted in the Sauerbrey equation:

$$\Delta f = \frac{-2 f_o^2}{A \cdot \left(\rho_q \mu_q\right)^{0.5}} \cdot \Delta m_q$$

where Δf – measured frequency shift of the quartz crystal, f_o – resonant frequency of the crystal, Δm_q – mass of the material adsorbed on the surface per unit/area (g/cm^3), A – surface area of the resonator, ρ_q – density of quartz and μ_q – shear modulus of the quartz.

* Blank quartz crystals are subjected to a precise cut in order to realise specific performance characteristics. The "cut" refers to the plane and angle under which the crystal is cut that in turn affects the frequency stability.

The Sauerbrey equation was a milestone towards development of quartz crystal sensors to determine mass changes as a result of frequency changes. The applications of quartz crystals can be found in many research environments, *i.e.* electrochemical deposition, corrosion, adsorption, etching, gas sensing, biosensors [77]. In 1985, Kanazawa and co-workers expanded Sauerbrey's description for measurements in a liquid medium [79] and found a linear relationship between the resonant frequency and the square root of the density and viscosity of liquid, which is in contact with the crystal. Recently, research was focused on enhancement of QCM yield by applying new piezoelectric materials and geometry designs to the probes.

2.4.2 Surface plasmon spectroscopy

SPR is a general technique that is used to characterise ultrathin organic films [80,81] deposited onto noble metal surfaces, such as gold [82,83] or silver [84]. SPR allows the film growth to be monitored, by measuring the change in thickness or refractive index and it also allows fully formed film thickness to be calculated. This makes SPR an excellent tool for monolayer characterisation [85,86,87], giving the possibility of estimating molecular size and alignment within monolayers. SPR is also used in conjunction with biosensor technology for characterising and quantifying biomolecular interactions [88].

The basic configuration for SPR utilises a prism on which a p-polarised light beam falls and undergoes refraction (bending). Some of the light still traverses through the prism and some undergoes reflection. When the light beam reaches the end of the prism, it comes across a thin molecular film deposited on metallic surface. At this point total internal reflection occurs on the borderline between glass (dielectric) and metal surfaces. Phonons which penetrate the metal layer excite free metal electrons causing their oscillations, called surface plasmons (or surface plasmon polaritons), which results in a drop of the intensity of reflected light. This phenomena is captured continuously by

the detector whilst scanning the light beam over the range of incident angles and is depicted as angular dependence of the reflection. This dependence is often called an SPR curve or spectrum; see Figure 2.8. The shape of the SPR curve is dependent on the properties of the molecular material (refractive index, thickness, etc.) and the incident angle. In turn, the incident angle is dependent upon the properties of the metal film, the wavelength of the incident light beam and the refractive index of the monolayer: small changes in the dielectric properties or thickness of the deposited monolayer can cause a change in the value of this angle. Analysis (fitting) of the SPR curve is held in agreement with Maxwell's equations and Fresnel's theory of reflections and transmission at the interface [66].

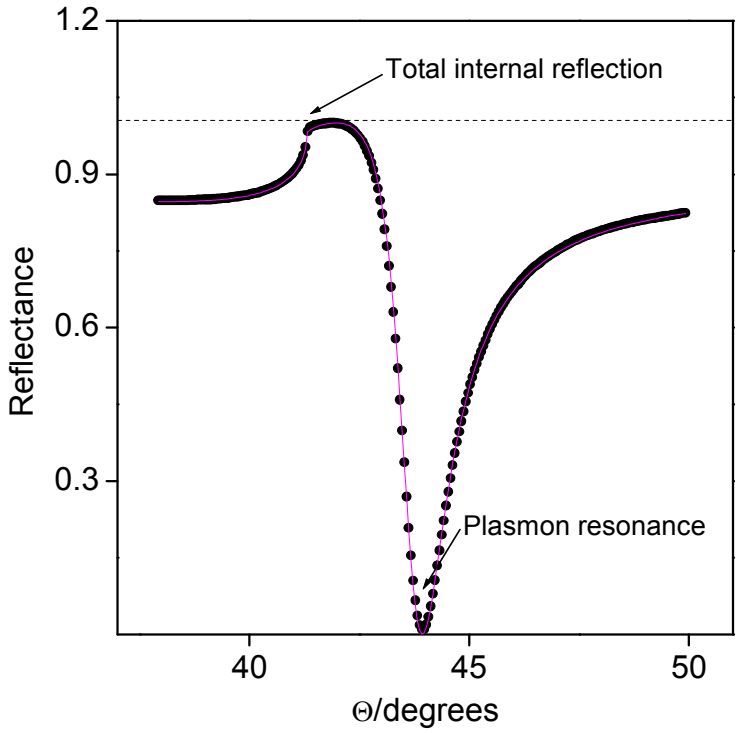

Figure 2.8 SPR curve corresponding to the angular dependence of the reflection of the 47-nm layer of gold on glass substrate. Dots symbolise normalised experimental data whereas fitted curve is an approximation result in respect to the Fresnel's theory; Θ – angle of incidence.

2.5 Summary

Molecular assembly for nanoscale electronics is ruled by two factors: molecular thickness and molecular arrangement. All three previously described techniques can deliver molecular films with unique properties and can be utilised for formation of molecular junctions. However, the ability to manipulate single molecules and assemble them into electronic devices still remains a challenge in molecular electronics. From the manufacturing point of view, a large number of molecules lying side-by side in a thin film has great potential. Ideally, it would be possible to construct a monolayer memory chip (in which each data bit would be represented as a single molecule) and complex switching networks with multilayer chips. However, interconnection raises doubts, due to the lack of techniques to address so many molecules in one go. This situation is straight forward for a bottom electrode (on which molecules assemble), but rather complicated when interconnected to others.

Table 1 summarises the basic features of the techniques described above. It is clear that covalent self-assembly possesses the most merits. SAM formation is self-limited – molecules attach to all of the available sites on the substrate spontaneously, without need for precise equipment (compared to the LB technique) and forms a single molecular layer (except for alkyl-silanes).

Table 1 Comparison of different features of molecular assembly, accessible for organic-based electronics.

	LB films	**SAMs**	**ESA films**
Adhesion	poor (van der Waals forces)	strong (chemical bonding)	strong (electrostatic interaction between oppositely charged molecules)
Film type	mono and multilayers	mainly monolayers	multilayers
Film preparation	demanding (use of special instruments)	simple (immersion)	
Level of order	ordered (but film may tend to thermodynamic steady state)	highly ordered	good (less ordered than LB films and SAMs)
Thickness	from *ca.* 0.5 nm to tens of nm	from *ca.* 0.5 nm to a few nm	from a few to hundreds of nm
Thermal stability	poor	good (depends on material used)	

3 Molecular electronic junctions

A critical issue concerning the fabrication of molecular junctions is the nature of the molecule-electrode interface. Application of voltage across the junction causes redistribution of electrons, and even small changes in the molecular energy levels can significantly affect the current flow through a junction. In some cases distortion of the current is so high that the measured electrical response from the junction can not be considered real. Therefore, understanding how electrons traverse through molecular junctions is a key point in pushing molecular electronics into manufacture and technology.

To fulfil this need, numerous tools have been used to measure electronic properties of both single molecules and their larger assemblies. The simplest is to construct sandwich-like molecular junctions, in which a monolayer is placed between electrodes. Several tools were designed in a manner to mimic one of the electrodes, which evades the problem of the other (usually top) electrode. This remedy is adequate for measurements of electronic properties but might be insufficient to incorporate molecules into real circuits.

In early experiments, the metal-evaporation technique was a standard for fabrication of metallic electrodes and was used to sandwich different types of molecular films. Although convenient, the method has been replaced by others: cross-wires and mercury-drop electrodes, due to better control over the fabrication process. The last two techniques are sufficient for investigations into molecular films, but not single molecules. Because monolayers are likely to suffer from defects [38], mutual interactions of the molecules and molecular conformations, knowledge about behaviour of individual molecules is incontrovertible. Scanning tunneling microscopy (STM), and the relatively new technique of break junctions are now the most commonly used

approaches in single-molecule devices. Ideally, in single-molecule junctions only one molecule should be addressed by electrode(s) but in fact it depends on the structure of the electrode and type of organic material used.

3.1 Electron transfer

Understanding how electrons travel across molecular junctions, particularly at the molecule/electrode interface, is significant if molecules are ever to be employed as key components in molecular-scale devices. In the majority of molecular-based systems, electron transfer is a quantum mechanical phenomenon called tunnelling. This mechanism is based on traversing a finite potential barrier by an electron possessing wavelike properties. The probability of finding an electron on the other side of the barrier is small but non-zero and depends on the thickness of the potential barrier and the availability of unoccupied energy states on the other side of the barrier. Tunnelling current is usually presented in the simplest form, *i.e.* the Simmons equation [89], which shows an exponential dependence between tunnelling and barrier thickness. It can be written as followed:

$$J = B \cdot e^{-\beta d}$$

Where: J = current density (A/cm^2), B = constant, dependent on applied voltage, thickness and height of the energy barrier, β = constant, proportional to a square root of the barrier height and mass of electron (nm^{-1}), d = barrier thickness.

Despite the equation illustrating a direct dependence between J and d, some recent calculations of β for some molecular junctions showed that this equation needs to consider the nature of the contact between electrode and molecule [90]. It was demonstrated that the better the contact is, smaller values of β can be obtained. For example SAMs linked to both electrodes were characterised by the smallest values of β, whereas SAMs mechanically contacted by the tip of conductive AFM or LB films

[91] exhibited the highest values. β, being inversely proportional to the conductance, determines its magnitude and thus higher conductance should be achieved for SAMs in good contact with electrodes. Moreover, in many such junctions conduction is expected to be dominated by superexchange. It is significantly visible for measurements at low temperatures [92]. Another important factor is temperature, which is strongly visible in the hopping mechanism; in which temperature-caused conformational changes lead to electron hopping over the energy barrier between neighbouring localisation sites [92]. This mechanism is characteristic for large barriers and is inversely proportional to the barrier thickness. It is also often quoted in highly-disordered molecular systems [93].

3.2 Monolayer molecular junctions

Utilising vacuum evaporation to deposit a top metal electrode has the main drawback of penetration of the monolayer with energetic metal atoms. This leads to electrical shorting of the junction and obscures the electrical properties of the molecule. Metallic electrode, such as aluminium with a melting point of 660° C is less damaging than non-oxidising gold (1064° C). However, all demand low temperatures and a slow evaporation rate to avoid damage to the molecules within the film.

An example of utilising evaporation as a method of electrode fabrication was performed by Reed *et al*. [94,95]. They intended to realise a single-molecule junction to measure electronic conduction through a SAM of 2'-amino-4-ethynyl-phenyl-4'-ethynylphenyl-5'-nitro-1-benzenethiolate. However, the fabrication process of the molecular junction was rather laborious. Preparation of the Si_3N_4 membrane was time consuming and demanded advanced instrumentation, such as electron beam lithography and reactive ion etching methods, to create a nanopore of 30 – 50 nm in diameter. The nanopore was then filled with gold, via the thermal evaporation and subjected to molecular deposition. The other electrode was deposited on top of the molecular film, via the cold-gold technique of thermal evaporation (see Figure 3.1).

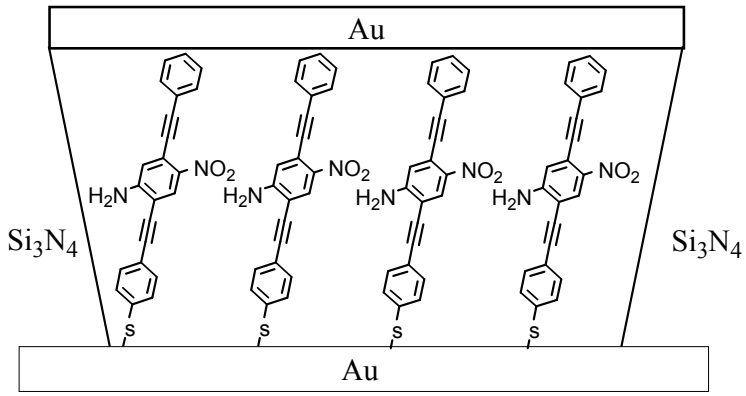

Figure 3.1 Schematic illustration of the mechanically controllable nanopore junction with a SAM of 2'-amino-4-ethynyl-phenyl-4'-ethynylphenyl-5'-nitro-1-benzenethiol and evaporated on top gold electrode, fabricated by Reed and co-workers 95.

In their experiment at temperatures below 60K Reed *et al.* observed negative differential resistance (NDR); Figure 3.2. This phenomenon is due to the decrease in current above a certain threshold voltage. In this case the threshold voltage, in which the current rise broke down, was ~ 2V. Although this type of tunnelling was very similar to resonant tunnelling diodes and I-V characteristics were stable and reproducible, it was not clear whether such behaviour resulted from the molecular structure of the device architecture, particularly that vapour-deposited gold atoms are known to pass through SAMs [96,97].

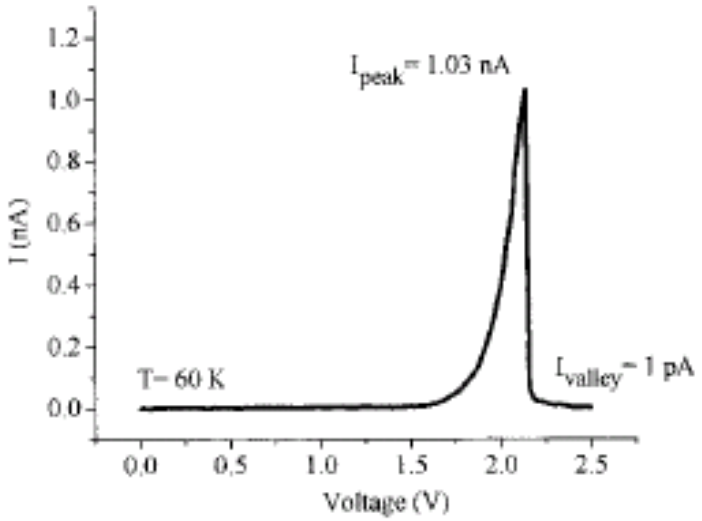

Figure 3.2 I-V characteristics of the nanopore junction showing the NDR behaviour. Copied from 95.

Most of the evaporated electrodes suffer from Schottky barrier formation as a result of metal oxidation after breaking the vacuum. The Schottky effect is due to reduction of the potential barrier at the metal-semiconductor interface and can induce very high electrical asymmetries. These can easily mask the asymmetry arising from the properties of the molecule, or produce asymmetric I-V plots in systems where no rectification would ordinarily be observed. Examples of Schottky barriers are known elsewhere and can be found in measurements of electrical conductance of numerous molecular films. For example, Chang *et al.* [98], who sandwiched napthalene thiol between Pt and evaporated Ti electrodes, observed very steep I-V characteristic with rectification ratios of *ca.* 5×10^5 at ± 2.3 V. Such a high value of rectification ratio is impossible to achieve with a monolayer of thiol, even taking into account the mismatch between work functions of Ti (4.2 eV) and Pt (5.6 eV) electrodes. A similar method of molecular junction fabrication was performed by McCreery *et al*. for a nitroazobenzene-molecule on PPF [99]. Fortunately, it was retracted when further studies (XPS) showed formation of titanium oxide layers (TiO_2 and TiO_3), as a result of the presence of residual gases in the evaporation chamber [100]. Some bulkier materials, such as phthalocyanines [101,102], nanotubes [103] and polymers [104,105] were also not free from formation of a Schottky oxide layer. For example, Pomerantz and co-workers applied an acid-base reaction to attach molecules of copper-phthalocyanine on the surface of HOPG [106]. They observed rectification ratio of 50 at ± 1.2 V. However, it was not considered that cleaning the HOPG by immersion in a solution of CrO_3 in aqueous acetic acid would probably cause a Schottky barrier, and affect I-V plots by raising the asymmetry.

In search of better electrode materials, researchers decided to utilise liquid metal electrodes [107], such as mercury. Typical construction of a mercury probe junction comprises a capillary tube (or syringe) filled with mercury, which can be brought up into mechanical contact with a monolayer deposited on the substrate electrode. The contact occurs in a solution of neutral compound (alkanethiol), which self-assembles on

mercury to prevent penetration into the monolayer [48]. A schematic illustration of Hg-junction is shown in Figure 3.3. Incorporation of two mercury electrodes in order to obtain sandwich-like structure would be advantageous but these would less stable mechanically [48,108].

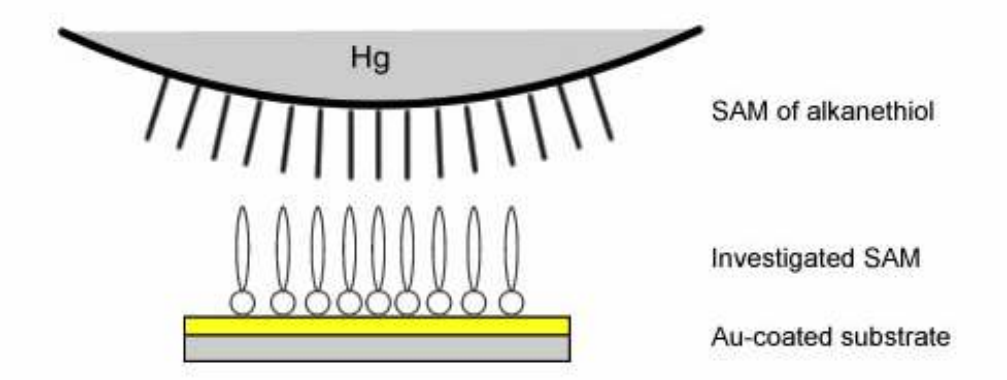

Figure 3.3 Representation of Hg-drop junction in which contact with investigated monolayer on Au-coated substrate is made in the solution of alkanethiol (black rods), firstly assembled on mercury to prevent penetration into the monolayer.

Hg-drop electrodes have the advantage of direct contact with molecules, because similar to gold, it can form thiol-based SAMs [108]. It can not be applied to measurements of LB films, due to the poor adhesion in these layers and high possibility of monolayer damage (surface tension of Hg at room temperature is 485 mN/m). There is also a restriction of temperature range in which conductivity measurements can be performed (between its melting and boiling points, which are -38.87° C and 356.58° C, respectively). Therefore, it is possible to work at room, but not at cryogenic temperatures [109].

An alternative method of molecular junction fabrication involves junctions formed from two gold wires (with known μm diameter) aligned perpendicular to each other. A SAM is deposited on one of the wires, to which a second wire can be brought into contact by finely tuning the deflection current obtained in the presence of a magnetic field. When the two wires are close enough, electron transfer occurs between them as a result of physical contact between the monolayer and deflection wire [110,111] (see Figure 3.4).

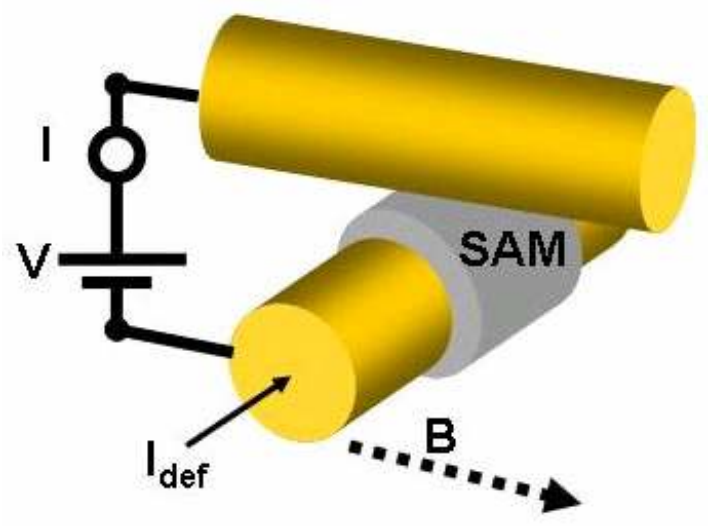

Figure 3.4 A schematic view of the crossed wires method of measuring the I-V characteristics from a SAM, implemented and developed by Kushmerick *et al*. Copied from 110.

This method of measurement of charge transport across monolayers of dithiols was implemented by Kushmerick *et al.* and allowed explanation of many important factors in relation to construction of electronic devices. Comparison of conductance measurements from the crossed wires method and STM for the same family of dithiols showed that conductance of the junction rose linearly with the number of molecules [112]. This was true for conjugated dithiol molecules, such as oligophenylene-ethynylenedithiol (OPE) or oligophenylene-vinylenedithiol (OPV), for which the measured tunnelling current was a factor of 10^3 larger, compared to single-molecule measurements performed by STM. The fabrication of a single-molecule junction was performed via self-assembly of a single dithiol molecule onto gold substrate surrounded by shorter (eleven carbons, C11) thiol molecules. Direct contact was provided by a gold nanoparticle, to which molecules of dithiols linked covalently. However, the factor was different for a simple conjugated 1,12-dodecanedithiol (C12) molecule and amounted to be 220 times larger, when compared to STM results. The difference was attributed to the possible interaction of C11 molecules with the nanoparticle, which would contribute to the overall measured tunnelling current [113]. These measurements proved that

intermolecular charge hopping did not strongly contribute to charge transport in SAM of molecular wires.

3.3 Single-molecule junctions

Major advances in single-molecule junctions came with the invention of the scanning tunnelling microscopy (STM) in 1981. The inventors, Gerd Binnig and Heinrich Rohrer, who aimed for cognition of local structural, electronic and growth properties of thin insulated layers were awarded the Nobel Prize in Physics in 1986. Development of the STM contributed to the development of the whole family of scanning probe microscopies (SPMs) for studying surfaces and surface properties with atomic-scale resolution.

All SPMs are based on the interaction between a sample and the main (essential) feature of the instrument, which is a sharp metallic tip. The tip can be brought into direct electronic contact and its position and movement can be controlled in three dimensions. The most important factor is the distance between the tip and the sample that depends on the interaction type, which is crucial to imaging of sample topography [114,115]. SPMs can operate in different media (air, liquid, gas streams, vacuum) that allow for investigation into different types of structures, such as amorphous or crystalline materials. They allow monitoring of dynamic phenomena, like chemical reactions (catalysis) [116], as well as single molecules [117,118] and larger adsorbates [119].

STM is a technique that involves electron transfer (tunnelling) through a thin potential barrier between two conductors [120,121,122]. Tunnelling is initiated by application of an external bias, which causes positioning of the tip above the surface. Depending on the experimental setup, electron injection can be initiated on either the tip or the surface and then electrons can traverse a potential barrier to reach the other side (sample or tip, respectively). Probability of tunnelling decreases exponentially with the potential barrier thickness (see chapter 3.1), and therefore even a small change in tip-sample distance

results in a large change in the tunnelling current. The energy diagram of the STM molecular junction is presented in Figure 3.5.

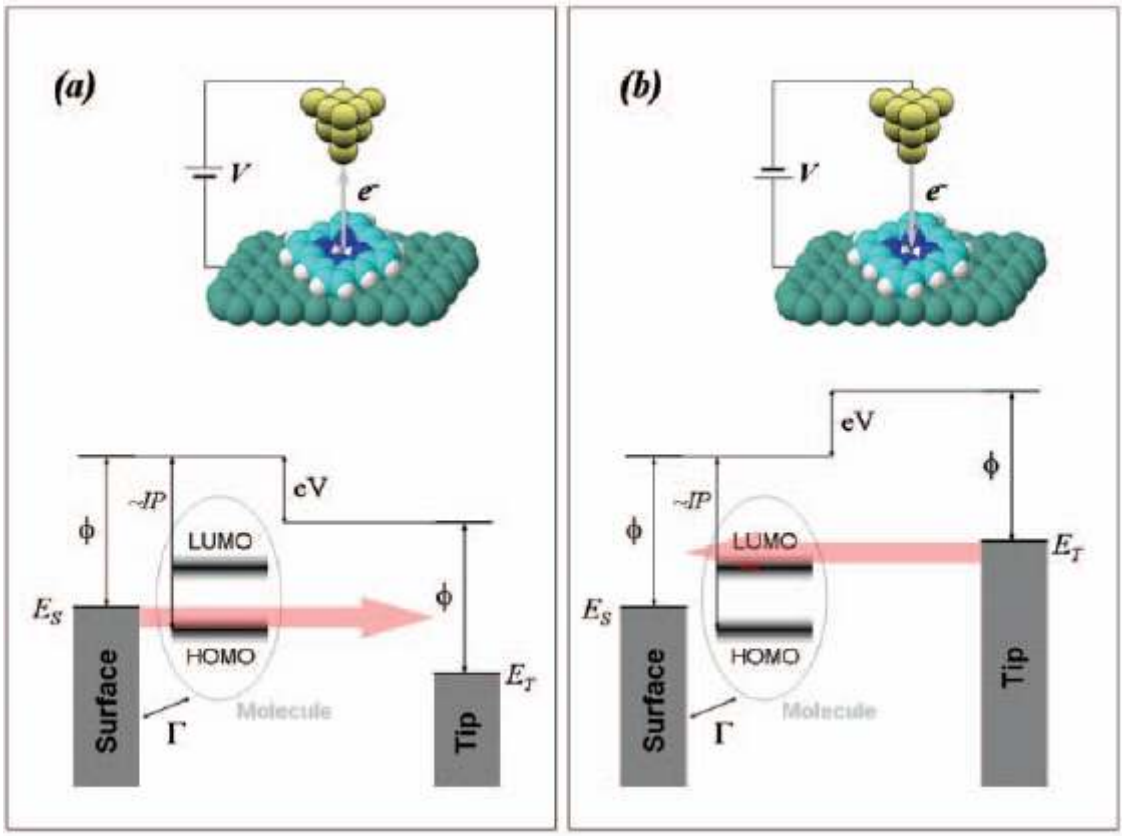

Figure 3.5 An energy diagram for an STM junction, after applying: (a) negative and (b) positive bias voltage to the sample (with respect to the tip). Φ – work function of the Fermi level of the electrode, IP – ionisation potential of a molecule (referring to the HOMO), Γ – electronic coupling, E_T and E_S – Fermi levels of substrate and tip respectively. Copied from123.

It is important to consider how the presence of a molecule significantly influences, and even dominates, electron transport across the junction, when compared to the junction with no molecule [124]. When a sample is biased negatively, electrons travelling from filled surface states to the tip encounter the highest occupied molecular orbital (HOMO) of the molecule, whereas in positively biased samples, the lowest unoccupied molecular orbital (LUMO) is involved. In both cases, the HOMO and LUMO are closer to the Fermi energy level of the surface and tip respectively. Because the tunnelling current between two metallic conductors is proportional to the local density of the electronic

states of the surface at (or near) the Fermi level, ideally the bias voltage can result in direct imaging of the shape of individual molecular orbitals [125].

The importance of the STM technique lies in its high sensitivity, and accuracy for imaging molecular structures. The exponential dependence between tunnelling current and tip-sample barrier is the main factor responsible for nanometer-scale resolution of STM images, which reflect the contour of the local density of electronic states at the surface, being proportional to the tunnelling current [126]. The scanning process relies on the precise raster pattern movement of the tip over the surface in the X and Y directions, whilst at the same time positioning the tip within the tunnelling distance (Z direction). Precision is high; 0.01 nm in the Z-direction and 0.1 nm in the X- and Y-directions. Therefore, STM allows the possibility of imaging topographic and electronic structures, and gives an insight into a variety of chemical and physical properties of molecular-based structures [121,127].

The main challenge in STM measurements is the positioning of the tip: the distance between the tip and the sample has to be precisely controlled without any interference (mechanical, electrical noises, thermal effects) to prevent penetration of the tip into the sample [128]. The control over the tip movement is monitored by the feedback loop, which is responsible for adjusting the position of the tip (with piezoelectric element) to maintain a constant tunnelling current. When the tunnelling current increases, the feedback loop moves the tip away from the surface whereas the tip is brought closer when the tunnelling current decreases. In the case of very smooth (flat) surfaces, there is no need for control over constant tunnelling current. The tip is kept at a constant average Z-distance and STM measures direct tunnelling current.

STM is mainly known from imaging molecular materials and has many applications in the fields of physics, chemistry, materials science and engineering [128]. One of the innovative applications of the STM is manipulation of atoms [129,130].

This is based on the interaction between tip and surface atoms and depends on the tunnelling current, electric potentials, etc. When an STM tip is at the appropriate distance, and a strong enough attractive force is present, it can pick up an atom from the surface then deposit it elsewhere when a repulsive force between the tip and the atom is generated. This creates excellent conditions for measurements of direct single molecular conductance. Proof of this was given by Haiss *et al*. who investigated electrical properties of non-rigid thiol molecules trapped between an STM tip and the substrate [131]. To ensure single molecule contact the constant height mode was used in which molecules spontaneously attached and detached from the tip (see Figure 3.6). This was observed as a current jump in the tunnelling current, which corresponded to physical molecule-tip contact. Because these measurements were made it was possible to observe formation of multi-junctions (STM tip contacted more than a single molecule).

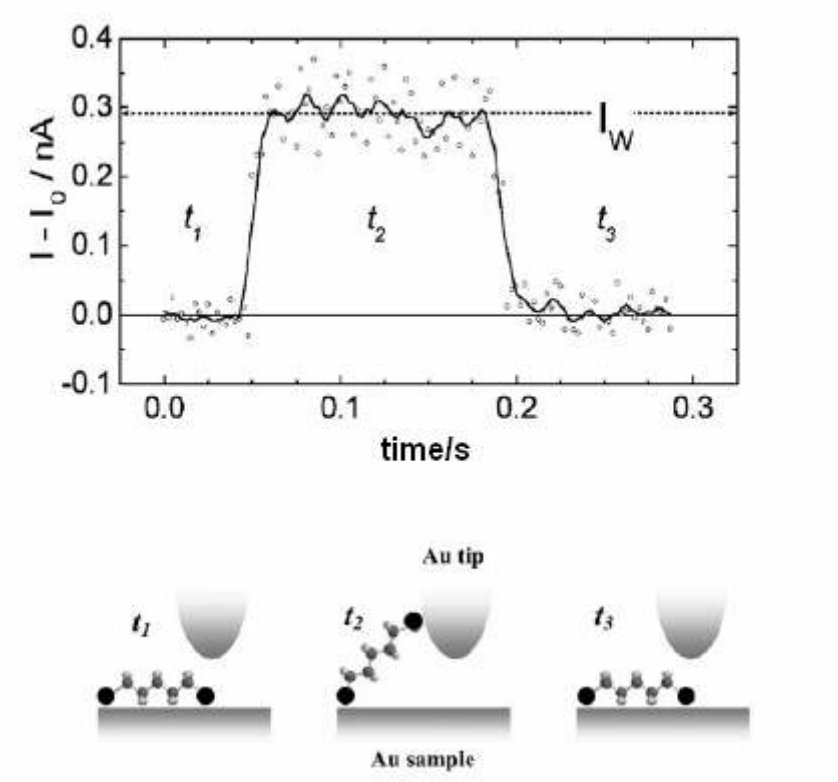

Figure 3.6 Realisation of single molecule conductance: (a) current jump in tunnelling representing; (b) physical STM-molecule contact (t_2). Copied from 131.

On one hand, very close proximity between tip and sample is provided by STM, but it may also cause tip-induced modification of the local electronic environment of the surface. Such a modification would be significant for single-molecule transport measurements and can be enhanced by other interactions within the molecular structure (electrostatic and van der Waals forces of neighbouring molecules). The presence of a vacuum gap between tip and sample does not guarantee direct contact and therefore, may not ensure mechanical and thermal stability, thus analysis of the results can be complicated. This is why in recent years, a number of researchers have used the break junction technique to examine charge transport across single molecule junction [132,133,134]. This method utilises molecules that can chemically bond to the electrode surface and therefore allow direct measurement of junction conductance.

The realisation of a mechanically controlled break junction (MCB) is shown in Figure 3.7. In this technique a gold wire is glued to the substrate apart from a central part (u), with a miniature notch. Continuous bending of the substrate with a piezoelectric actuator, causes elongation of the wire in the central part only and occurs until wire breaks into two parts. The whole process takes place in solution of the adhesive material, so slow elongation allows assembly of densely-packed molecular layers. Once this is achieved, the two half-wires (electrodes) are moved close together to re-establish the contact, which occurs via a single molecule. The only molecules that can achieve this are self-assembled molecular rods, as they are rigid. This ensures stability of the molecule-electrode contact, and they can occupy the available area directly after fracture of the gold wire.

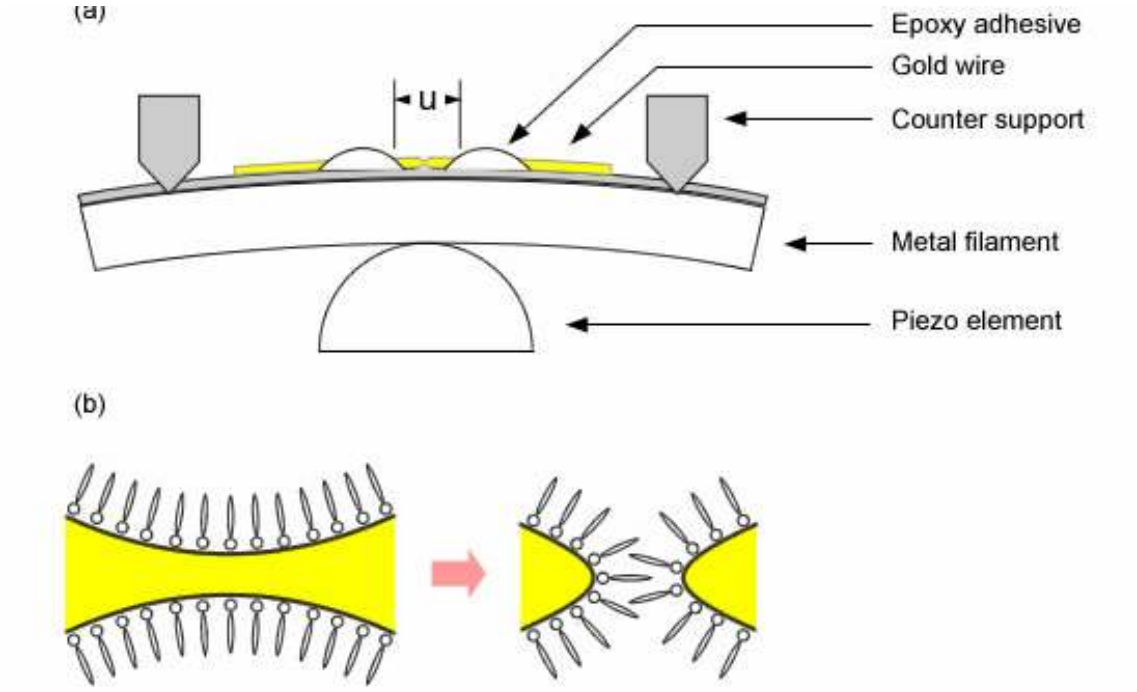

Figure 3.7 Mechanically controlled break junction showing: (a) a split of the gold wire into two electrodes, by bending the elastic substrate with a piezoelectric element; (b) adjusting two electrodes with deposited monolayer. Figure adapted from 133.

Pioneering work in utilising the break junction method was performed by Weber and co-workers. For example, doubling of the current was observed when two identical molecules made contact to both electrodes, rather than an individual molecule [135]. However, when considered measurements of electrical rectification, the main disadvantage of MCB technique lies in its inherent symmetry. Asymmetric molecules can not be incorporated, because when the same molecules deposit on both electrodes, there is a possibility that their electrical properties (rectification) will be cancelled as molecules are aligned oppositely.

3.4 Summary

Although STM and MCB are reliable methods for investigating electrical properties of molecular junctions (stable for many voltage sweeps), they can not be integrated into device geometries. On the other hand, vertical metal-evaporated junctions are an alternative but the shorting and Schottky effects may produce may highly unreliable

results. Unfortunately no technique described in this chapter is perfect, as all exhibit some drawbacks. Table 2 summarises the basic features of the techniques described above. It is clear that all techniques can be applied for investigations molecules being able to covalent bond to the surface.

Table 2 Comparison of different techniques incorporated for analysis electrical properties of single molecules and molecular films.

	Evaporated contacts	**Hg-drop electrode**	**Crossed wires**	**STM**	**MCB**
Electrode preparation	demanding (use of vacuum chamber)	medium (control over drop size)	simple (purchase)	simple (purchase)	demanding (control over bending process)
Number of contacted molecules	numerous molecules (films)			single (but possibly few molecules)	
Contacted assemblies	SAMs, LB films, ESA films	SAMs	SAMs (mainly)	SAMs, LB films, ESA films	SAMs of rigid molecules
Contact type	physical	chemical and physical (via additional thiol layer)	physical and chemical	mainly physical	chemical
Contact stability	good		magnetic field dependent	Vibration dependent, possible thermal drift	good
Electrode re-use	no		yes		no
Main drawbacks	shorting	shorting	adjusting deflection wire	tip positioning	suitable for rigid molecules only

4 Molecular rectification

Rectification is an electronic process that occurs in diodes and can be monitored by observation of current-voltage characteristics. An ideal rectifier allows current to flow in only one direction, which is observed in the form of an exponential curve.

Rectification of current is an essential parameter in fabricating any device for electronic purposes. Traditional MOFSET's can rectify current with a very low forward voltage drop, and also have the advantage of being able to switch at very high speeds. Therefore, molecular equivalents of diodes must exhibit properties of switching and rectification of the current.

The indication used to asses the suitability of a particular molecule for use as a diode is the rectification ratio (RR). This number is estimated from current-voltage characteristics, and is the ratio of the current at two equal but opposite voltages:

$$RR = \left| \frac{I(V_{\max})}{I(-V_{\max})} \right|$$

Traditional diodes, made of semiconductors (*i.e.* silicon) exhibit rectification ratio from a few hundreds [136] depending on doping material. These values can be significantly exceeded and achieve values of approximately 10^6 – 10^7 [137,138] for Schottky-type diodes*. These values must be achievable by molecular rectifiers but, in this case, they depend on the type of molecule and electrode material, rather than the preparation process.

* Schottky diodes are distinguished by high asymmetry of the I-V characteristics and therefore high RRs. Traditional diodes are prepared by doping of the semiconductor material at high temperatures, whereas potential for molecular rectifiers is seen in the ease of preparation (*i.e.* SAMs from solution at room temperature).

4.1 Theoretical predictions

As mentioned earlier, one of the first considerations of a device based on a single organic molecule was the Aviram and Ratner model [14]. This proposed forming a junction by bridging a molecule, possessing electron donating (n-like) and electron withdrawing (p-like) substituents, and therefore constitute a semiconductor-like p-n junction. Although this theory was a step forward it did not consider the whole spectrum of factors affecting conducting properties of molecular devices.

There are several other theories relating to this subject. Much attention was devoted towards incorporating different molecules (see Chapter 4.2). However, the physical effects occurring at the molecule-electrode interface are still under close examination as it was perceived that this is linked to this [139]. The agreement between experimental work and theoretical analysis is somewhat limited [140].

The molecule-electrode interaction has often been examined by the distribution of electrostatic potential across the molecule, which should be sensitive to the position of the chromophore between the electrodes [141,142]. Other theoretical investigations have focused on thermal activated conduction [143,144], which causes conformation changes in molecular structures.

4.1.1 Aviram-Ratner theory

Aviram and Ratner (in 1974) proposed diode-like behaviour from a molecular junction, based on a single asymmetric molecule [14]. It was thought electrons would flow only in one direction in a molecular system. As an ideal candidate they suggested a molecule containing the strong electron acceptor, tetracyanoquinodimethane (TCNQ), and the strong electron donor, tetrathiafulvalene (TTF), separated by a saturated σ-bridge to avoid coupling the molecular orbitals of the donor and acceptor (see Figure 4.1). This molecule has never been synthesised so experimental verification of its potential

rectifying behaviour is difficult to estimate. However, there have been some estimations of the energies required for the molecule to undergo charge transfer from the ground state to the first excited state, and therefore rectify the current. According to Metzger [145], this energy is about 3.5 eV, whereas the reverse process would need an energy of 9.6 eV (calculations were made for the ions at infinite separation).

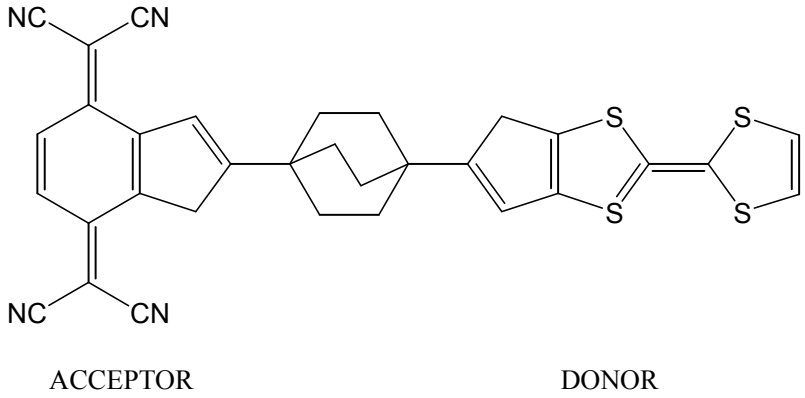

Figure 4.1 Donor-σ-acceptor molecule ("Gedankenmolecül"), proposed by Aviram and Ratner to work as molecular rectifier [14].

The rectifying properties of the Aviram-Ratner molecular device can be understood easily from the energy band diagram, presented in Figure 4.2. For an ideal molecular rectifier the LUMO of the acceptor should lie at (or be slightly above) the Fermi level of the cathode whereas the LUMO of the donor should lie as high as possible above the Fermi level of the anode.

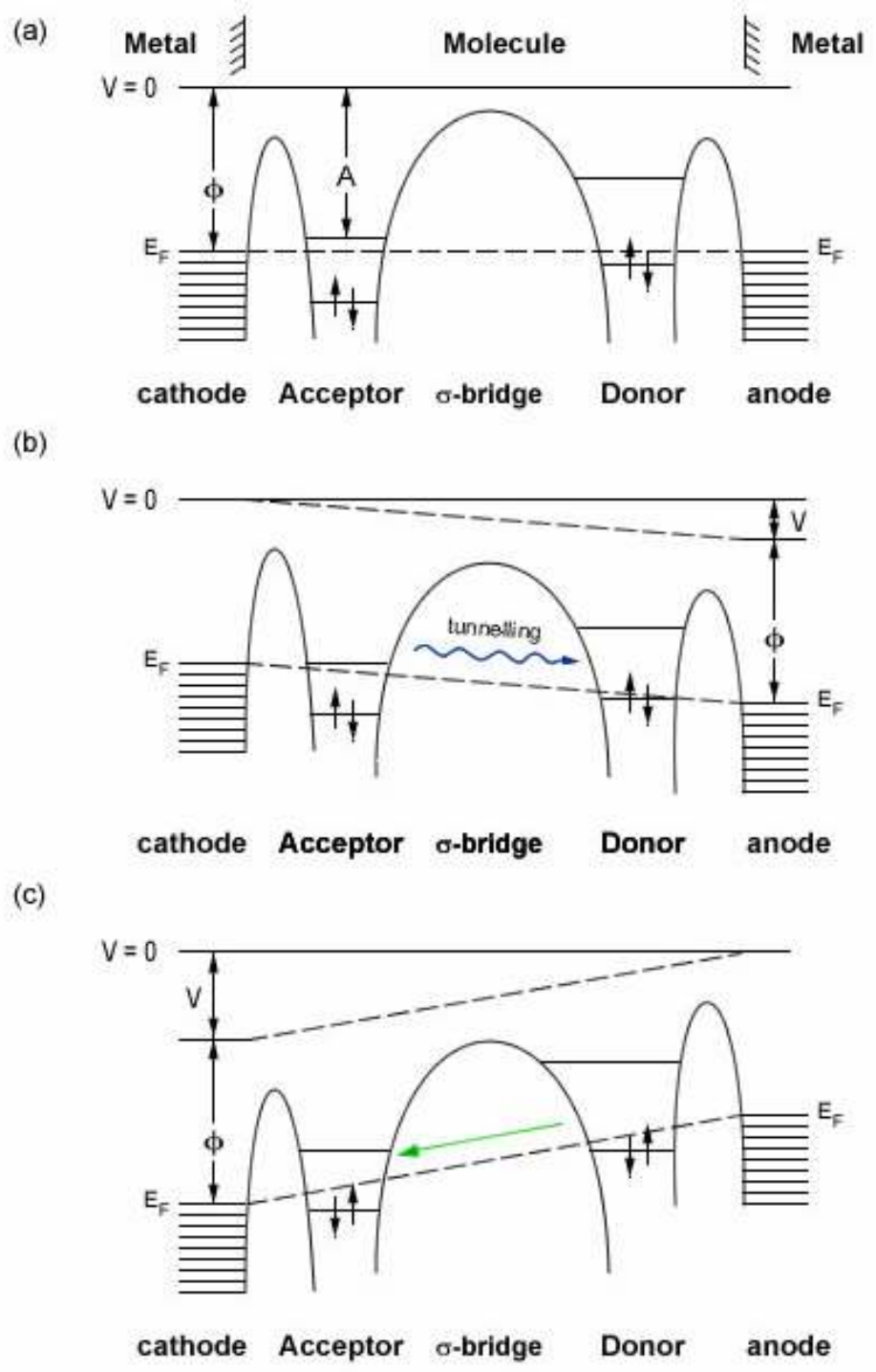

Figure 4.2 Energy diagram of the Aviram-Ratner theory of molecular rectification: (a) D-(σ-bridge)-A molecule placed between the same metallic electrodes with no applied voltage; (b) forward bias causing realignment of molecular orbitals in order to tunnelling within molecular junction make possible; (c) electron-transfer under reverse bias in which the first step is electron transfer from donor (LUMO) to acceptor (HOMO) marked with a green arrow; HOMO – highest occupied electronic orbital, indicated with pair of arrows, E_F – Fermi level of electrodes, Φ – work function of the electrode, A – electron affinity of the acceptor, V – potential applied to the electrode. Figure adapted from 14.

Applying an external field (relatively low) to the junction causes overlapping of the work functions of the electrodes with donor (electron-rich) and acceptor (electron-poor) of the molecule. Under forward bias, an electron travels from the Fermi level of the cathode to the totally (or partially) empty LUMO of the acceptor. The first step is followed by a similar action on the other side of the junction – electron transfer from the occupied HOMO of the donor to the anode. When these orbitals are close enough energetically, an electron tunnels from the (now) occupied LUMO of the acceptor to the empty HOMO of the donor, and the molecular ground state is restored. This electron transfer is irreversible by nature, as the LUMO of the donor is significantly higher in energy than the HOMO of the acceptor, making coupling between them impossible.

However, if the voltage applied to the junction is high enough, the opposite direction of tunnelling would be possible. In this case, under reverse bias, the LUMO of the donor would have to be lowered to the Fermi level of the anode, and the Fermi level of the second electrode would have to be below the HOMO of the acceptor to make electron tunnelling from a donor (LUMO) to an acceptor (HOMO) possible.

Aviram and Ratner believed that the electron affinity of the acceptor should be relatively high (in the range of 1.0 – 2.5 V) and the LUMO of acceptor should be totally (or partially) empty. Whereas the ionisation potential of the donor should be relatively low (between 6.0 – 9.0 V). They also calculated current–voltage characteristic for an arbitrary molecular rectifier, which is presented in Figure 4.3. It possessed typical rectifier characteristics; *i.e.* current asymmetry and a threshold potential, which is dependent on the internal properties of the molecule and its coupling to the electrodes.

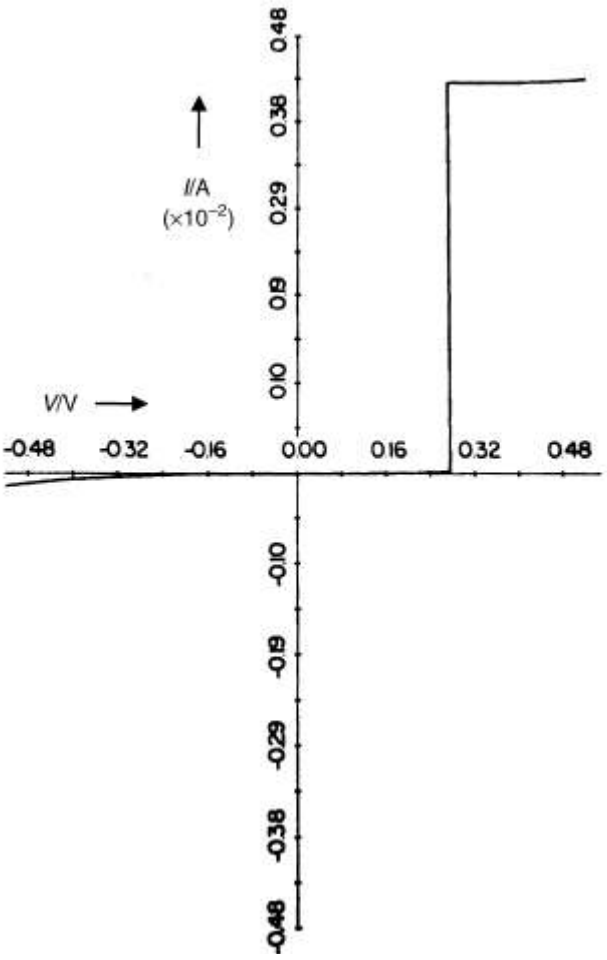

Figure 4.3 Example I-V characteristic of an example molecular donor-σ-acceptor rectifier, proposed by Aviram and Ratner, with the following parameters: I_D = 5.3 eV, A = 5.0 eV, Φ = 5.1 eV. Current expressed in A/cm^2 whereas voltage in volts. Copied from 14.

4.1.2 Kornilovitch theory

In 2002, Kornilovitch *et al.* claimed that rectification with ratios of several hundreds could be expected from a molecule containing 'just one conducting molecular level placed closer to one electrode than to the other' [141]. Therefore, there would be no need to build complicated donor-acceptor molecules. A molecule containing two saturated groups with different lengths that insulated the central phenyl ring from the electrodes was proposed (see Figure 4.4).

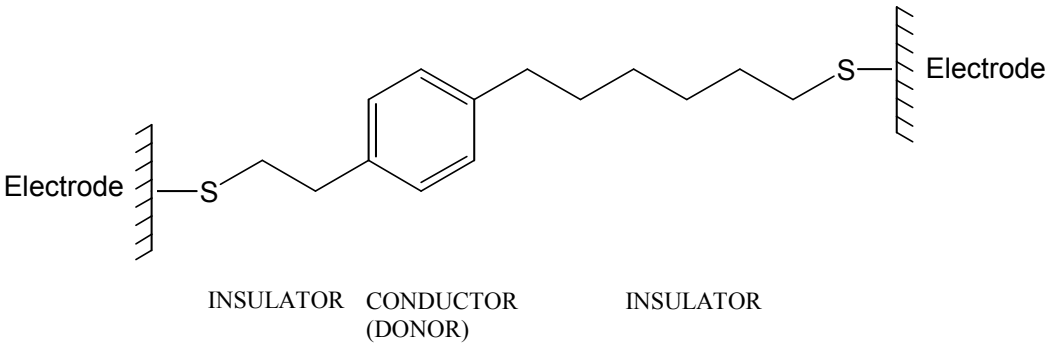

Figure 4.4 An example of a molecular rectifier in the Kornilovitch theory, according to rectification arising from asymmetric positioning of the molecule between electrodes by using two different length alkyl chains [141].

The purpose of asymmetric positioning of the molecule relative to the electrodes was to yield a larger voltage drop on one of the electrodes than on the other. In this case, most of the voltage would drop on the longer insulator, as a result of the proportional dependence of voltage drop and the length of an insulator and therefore electrical rectification would be observed. This situation is presented in Figure 4.5. Applying the voltage to the left electrode caused adjustment of the molecular orbitals with the Fermi levels of the electrodes, which happened faster on the side of molecule containing the longer insulator (anode), as a result of a larger potential drop. Therefore, the LUMO of the phenyl ring, which aligned with a Fermi level, was the only molecular orbital responsible for the rectifying behaviour of the whole molecule, as the HOMO was far below the Fermi level. Under reverse bias, energy of the LUMO would have to reach the Fermi level of the left electrode (cathode). It was predicted that this process would require significantly larger applied bias to allow current through the molecule and therefore rectification of the current could be observed.

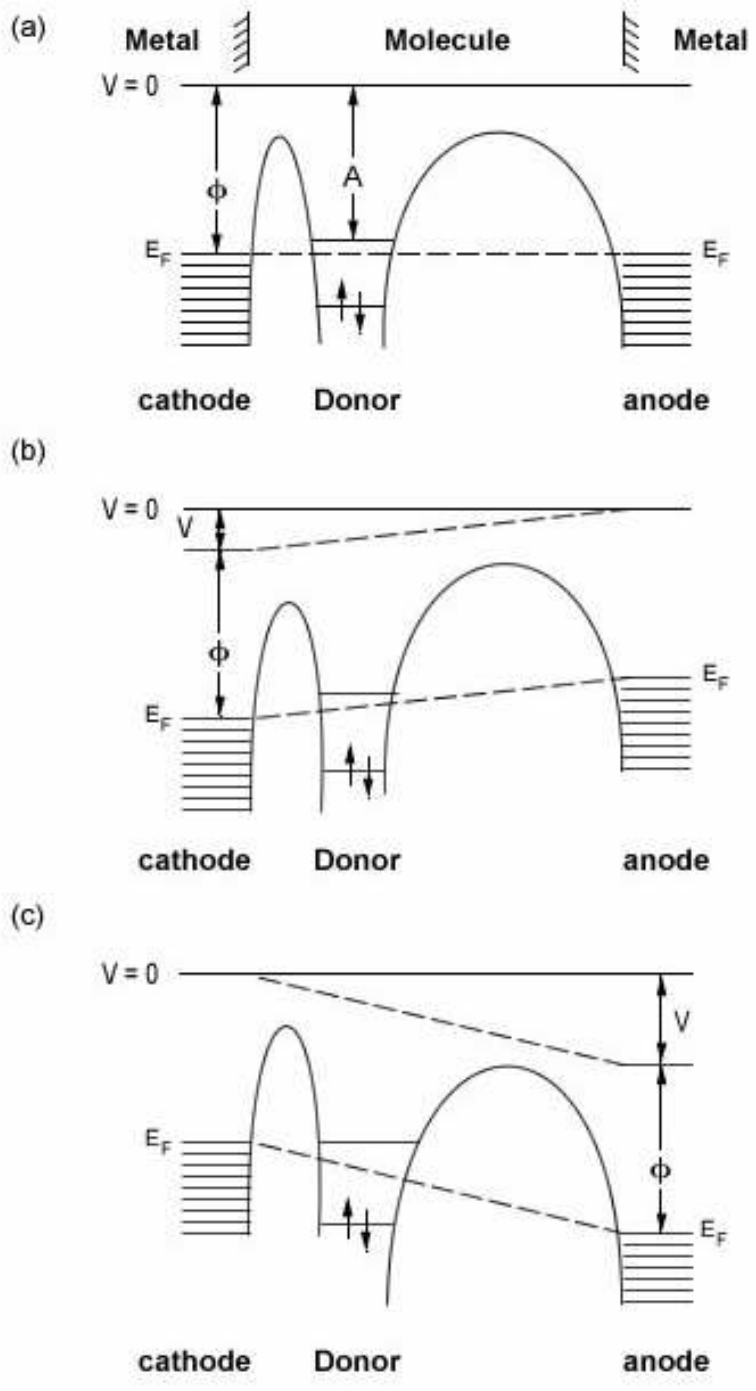

Figure 4.5 Energy diagram showing the realisation of Kornilovitch theory of molecular rectification: (a) asymmetric molecule place between two electrodes; (b) forward bias causes alignment of the LUMO and Fermi level of anode; (b) reverse bias causes matching of the LUMO and cathode. Φ – work function of the electrode, A – electron affinity, V – potential applied to the electrode. Figure adapted from 141.

4.1.3 Related work

In 2000, Ellenbogen and Love proposed a variant of the Aviram-Ratner theory considering the opposite direction of electron transfer; from donor to acceptor [146]. They suggested placing a polyphenylene-based molecular wire, with commonly known electron donating and electron withdrawing substituents to impart push-pull behaviour, between two gold electrodes. The molecular structure is presented in Figure 4.6

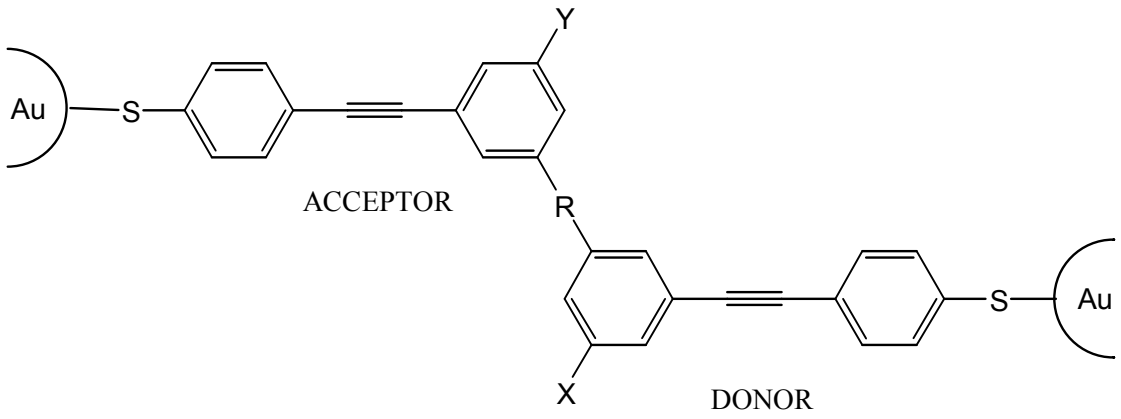

Figure 4.6 Molecular structure of the polyphenylene-based molecule placed between gold electrodes, used in theoretical estimations for Ellenbogen and Love theory [146]. X – donor substituent (NH_2, -OH, $-CH_3$), Y – acceptor substituent ($-NO_2$, -CN, -CHO), R – semi-insulating bridge (CH_2 or CH_2CH_2).

It was proposed that at forward (finite) bias molecular orbital HOMO of donor and LUMO of the acceptor adjust LUMO of both the acceptor and donor moieties of the molecule up to the Fermi level of the cathode. In reverse bias, there was no resonance of the LUMO of the molecule with the Fermi levels of the electrodes. This should give rise to rectification. However, this proposed system has not been verified by any experimental studies.

Kawazoe and co-workers theoretically studied the geometry and electronic structure of a group of D-spacer-A molecular rectifiers, based on mono- or disubstituted benzene rings, covalently linked by an insulating bridge [147]. The molecular structure is reminiscent of an Ellenbogen-Love rectifier: molecules possess ―SH groups for chemical grafting and easy electron injection (from electrode to substrate) and

substituents of —NH_2 and —NO_2, which are electron-donating and electron-accepting subunits; the spacer unit (methylene or dimethylene) was exactly the same. Calculation of molecular orbital energy levels, and spatial orientation of the unoccupied molecular orbitals showed that in this kind of molecule, the LUMO was always localised on the acceptor ring, whereas the HOMO was on the donor ring. However, the localisation of the LUMO on the donor side strongly depends on the number of substituents and the length of the bridge. The potential drop across the tunnelling barrier for a monosubstituted molecule with a methylene bridge was 1.56 eV, whereas for a disubstituted molecule with a dimethylene bridge it was 2.76 eV.

Further verification of the Aviram-Ratner proposal, but for molecular wire, was made by Stokbro *et al.* [148], based on theoretical calculations of I-V characteristics for the molecule chemisorbed between two electrodes. I-V characteristics turned out to be neither symmetric nor rectifying due to different slopes at the same, but opposite-signed, values of voltage at both bias polarities. Authors attributed this property to unfavourable resonance conditions within this particular molecular structure and suggested decreasing the gap between the HOMO of the donor and the LUMO of the acceptor in order to produce a molecular diode.

4.2 Experimental work

Numerous attempts at synthesising and investigating molecules for potential electrical rectifiers, and other molecular devices, have been undertaken. Among them only a few donor-(σ-bridge)-acceptor molecules have been shown to rectify current. However, because of problematic synthetic rules, arising from chemical attachment of in particular the σ-bond, research has been focused on other types of molecules. In particular, D-(π-bridge)-A molecules have been a possible Aviram-Ratner rectifier, as long as the π-bridge is an effective tunnelling barrier. Much work was focused on the study of bulky materials, based on phthalocyanines, nanotubes [149,150], fullerenes [151] and

polymers [152,153]. Special attention has been given to molecular wires, because of their rigid molecular structure and ease of wiring them to electrodes.

Research in molecular rectifiers has been focused on molecules, which can exhibit highly asymmetric I-V characteristics, at small values of applied voltage. Therefore, creation of highly conducting molecular diodes requiring low operating powers should be possible. At this point, building a three-terminal device (transistor) by adjusting a third electrode (gate) would be a final step toward a proper molecular device, assuming complete control over electron flow across a device.

4.2.1 Rectification from D-σ-A molecules

The first observation of rectification in a single organic molecule was made by the authors of the molecular rectification theory [154]. Aviram *et al.* observed asymmetrical I-V characteristics from a SAM of quinone-based molecule deposited on gold (see Figure 4.7). Under negative bias, electron flowed from the tip to the quinone (acceptor), and from the catechol (donor) to the gold surface. However, soon after these results were published, they were retracted as it was concluded that the rectifying behaviour may have been due to proton transfer from the catechol to the quinone. This process produces a semiquinone structure which would be a conductor and so result in enhanced current flow through molecule.

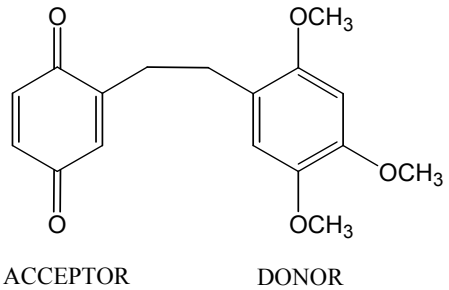

Figure 4.7 Aviram and Ratner donor-σ-acceptor molecule, based on the quinone acceptor and catechol donor [154].

Promising work in synthesising and characterising donor-σ-acceptor molecular rectifiers was performed by Metzger and co-workers in the 1980s [155]. Based on the "Gedankenmolecül" (Figure 4.1) Metzger incorporated TCNQ and different types of donors, which formed LB films for potential Aviram-Ratner-like rectifiers. These results aroused the interest of other research groups in the molecular rectification.

Geddes *et al*. performed further investigations on other donor-σ-acceptor molecules (Figure 4.8). They observed diode-like behaviour from LB films of a DDOP-C-TCNQ molecule, with higher asymmetry at forward bias in the positive quadrant of the I-V plot [156]. I-V characteristics, although reproducible, exhibited high hysteresis, which was attributed to the big difference in work functions of the electrodes (5.65 eV for Pt and 3.66 eV for Mg). Further analysis of this junction revealed Schottky barrier formation between magnesium and BHTCNQ part [157], so this was not an Aviram-Ratner-like electron transfer. The Schottky barrier was due to creation of a magnesium oxide layer as a result of breaking the vacuum, after evaporation of the Mg electrode.

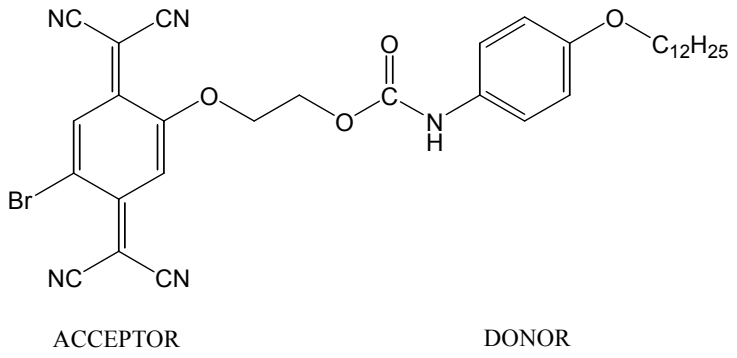

Figure 4.8 D-σ-A molecule of DDOP-C-TCNQ, investigated by Geddes and co-workers [156,157].

Recently, the same molecule was deposited via the LB technique on a gold-coated substrate and its electronic properties analysed with STM [158]. This time, asymmetry was observed in the negative quadrant of the I-V plot. This behaviour was consistent with the alignment of the molecules within the film, with TCNQ near to the bottom electrode (gold). The direction of the current flow followed the Aviram and Ratner

model. However, the same molecule deposited at different surface pressures (previous results were obtained at 15 mN m^{-1}) exhibited anomalous I-V characteristics. For example, films deposited at 10 and 20 mN m^{-1} exhibited symmetric I-V curves whereas asymmetry was observed for the pressure values between 10 and 20 mN m^{-1} [159]. This behaviour could be explained by work performed by Metzger and co-workers, who studied the alignment of similar molecules on the surface of gold-coated HOPG by STM and TEM (Transmission Electron Microscopy). The main difference in the structure was the donor, in which the O—$C_{12}H_{25}$ group was replaced by N—$(C_{12}H_{25})_2$ [160], and the TCNQ acceptor did not contain Br atom. It was found that molecules only exhibited short-range order as they formed islands on the solid substrate, rather than an homogeneous monolayer. Additional structural calculations revealed the possibility of conformational changes of the molecule.

Another successful discovery of a molecular rectifier was made by Mikyama and co-workers [161]. The molecule contained a dinitrobenzene acceptor and a dihydrophenazine donor separated by a methylene σ-bridge (see Figure 4.9). Observed I-V curves displayed rectification ratio of ~ 7 at ±1 V under illumination, and RR of ~ 3 at ±1 V in the dark. These were compared with I-V curves of LB films of arachidic acid, which gave rectification ratio of ~ 1.8 under illumination and 1.6 at ±1 V in the dark. LB films showed light-influenced reproducible rectification in accordance with the Aviram-Ratner model of tunnelling; from the acceptor contacting the bottom electrode (cathode).

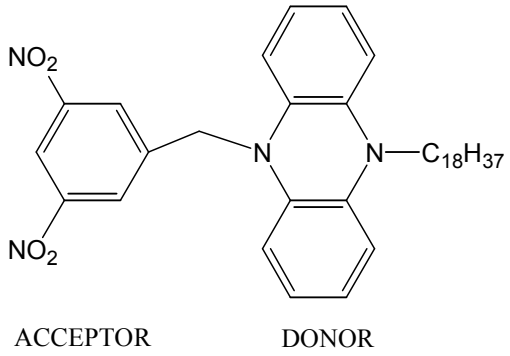

Figure 4.9 Chemical structure of D-σ-A molecule, investigated by Mikayama [161].

There have been many attempts at synthesizing and investigating D-σ-A molecules for potential unimolecular rectifiers [162,163,164]. Recent efforts made by Bryce *et al*. [165] resulted in a D-(σ-bridge)-A diad, containing TTF (strong donor) and fluorene (acceptor). The molecule (Figure 4.10), was deposited as an LB monolayer between an n-doped silicon wafer and evaporated Ti/Al as the top electrode. To prevent penetration of Ti atoms into the film and therefore formation of a Schottky barrier, the monolayer was secured by monolayers of aliphatic chain, and evaporation of the top electrode occurred under very high vacuum (5×10^{-7} Torr). Such a molecular junction revealed the dependence between film-packing and rectification ratios. Films deposited at higher surface pressures, resulted in higher values of rectification ratio, the highest observed being 18 at ±1 V. To confirm this result, a molecule was placed between Au and Hg-drop electrodes in opposite orientations, in two separate experiments. The value of rectification ratio concurred with the previous value, but asymmetry (obtained from I-V curves) was observed in opposite quadrants for the molecule with the same orientation as in the n-Si/molecule/Ti junction. It was thought that this anomalous behaviour may have been caused by the possibility of a change in the ground state of the molecule from neutral to zwitterionic, where TTF becomes an acceptor (gains positive charge) and fluorene a donor.

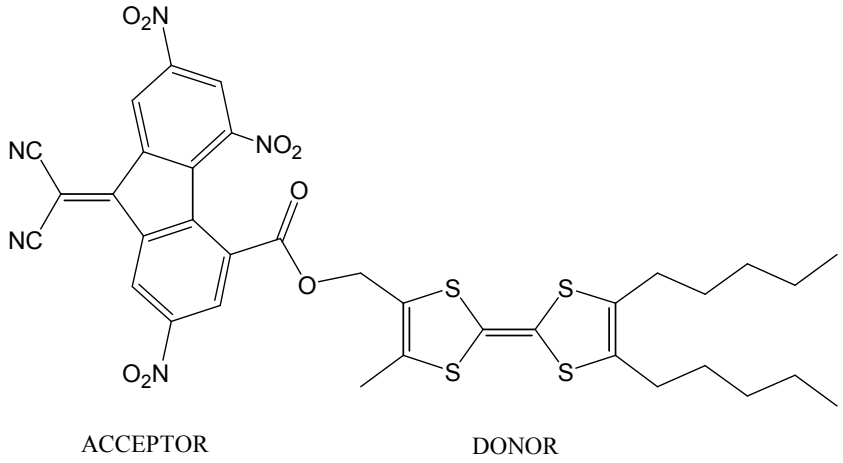

Figure 4.10 Chemical structure of D-σ-A diad, synthesised and investigated by Bryce *et al*. [165]

4.2.2 Rectification from D-π-A molecules

Sambles and Ashwell [166] utilised Geddes' [156,157] experimental procedure for LB films of donor-π-acceptor molecules. Similar results were observed; high Schottky barrier asymmetry and hysteresis of I-V characteristics from mono- and multilayers of $C_{16}H_{33}$-Q3CNQ [166,167] (see Figure 4.11).

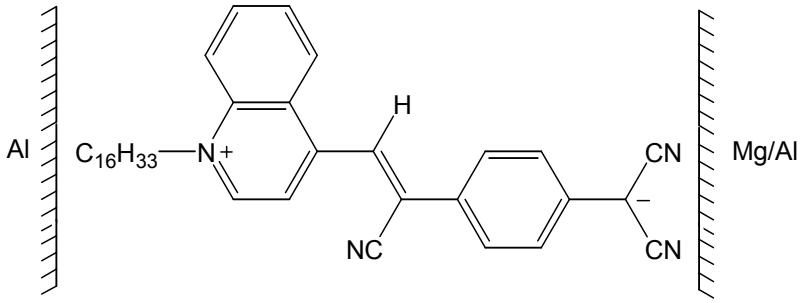

Figure 4.11 Molecular structure of D-π-A $C_{16}H_{33}$-Q3CNQ rectifier, investigated by Ashwell [166] and later Metzger [168], presented in a charge-separated form, placed between metallic electrodes.

To verify these results and explain the mechanism of electron transfer through the molecule, Metzger *et al.* sandwiched the $C_{16}H_{33}$-Q3CNQ molecule between aluminium and magnesium electrodes. To prevent formation of a Schottky barrier, Mg was covered by an additional layer of Al [168]. Using a potentiostat, Metzger observed high asymmetry in positive quadrant of the I-V plot, suggesting electron flow

from 3CNQ to the quinolinium part. According to Metzger description, the mechanism of electron transfer is as the following [168]:

$$M_1\left|D^+ - \pi - A^-\right|M_2 \rightarrow M_1\left|D - \pi - A\right|M_2$$
$$M_1\left|D - \pi - A\right|M_2 \rightarrow M_1\left|D^+ - \pi - A^-\right|M_2{}^+$$

The first equation indicates intramolecular electron transfer by tunnelling through π-bridge whereas second equation represents transfer from D to M_1 and from M_2 to A. This behaviour was assigned to the reverse of the Aviram-Ratner electron transfer through a molecule, in which 3CNQ acts as a acceptor, and quinolinium acts as a donor. According to theoretical calculations, $C_{16}H_{33}$-Q3CNQ molecule exists as a zwitterion in the ground state whilst in the excited state it adapts the quinonoid (neutral) form. Reproducible electric results gave a maximum rectification ratio of *ca.* 20 at ± 1.5 V for a monolayer, and *ca.* 5 at ± 2.0 V for multilayer films.

In spite of confirming the direction of current flow there was doubt about the height of asymmetry arising in the junction, due to possibility of creation of an Al oxide layer on both electrodes [169]. Therefore, Metzger and co-workers incorporated oxide-free gold electrodes for electrical measurements of electron flow through an LB monolayer of $C_{16}H_{33}$-Q3CNQ [170]. I-V characteristics with an average rectification ratio of 7.5 at ±2.2 V, and a maximum of 27.5 at ±2.2 V were obtained. The higher current was seen in the positive quadrant, suggesting an Aviram-Ratner mechanism of rectification. An example of the I-V characteristic is presented in Figure 4.12.

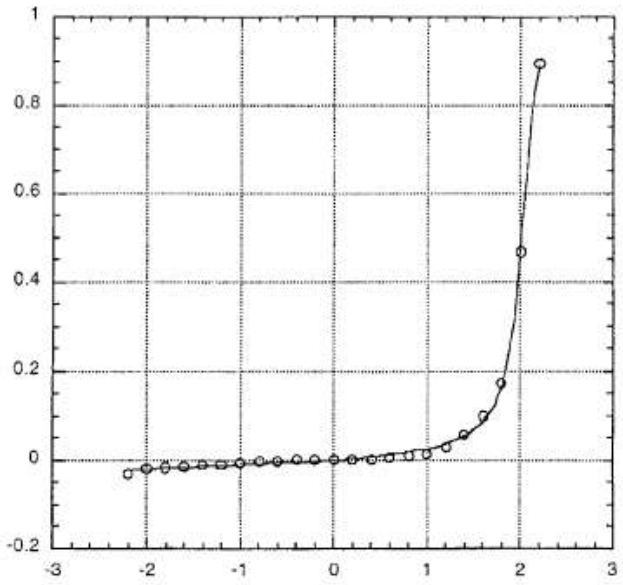

Figure 4.12 I-V characteristic of $C_{16}H_{33}$-Q3CNQ placed between gold electrodes, studied by Metzger *et al.* Rectification ratio for this particular curve was 27.5 at ±2.2 V. Copied from 170.

Krzeminski and Metzger decided to verify these results by applying theoretical calculations of molecular structure and geometry in the molecular junction [171]. This led to the conclusion that the direction of an electron flow was governed by the position of molecular orbitals of the molecule relative to the Fermi levels of electrodes, before bias was applied. The second factor was the presence of the long alkyl chain in a molecular structure, which provides asymmetric positioning of the molecule between the electrodes. An illustration of Krzeminski *et al.* theoretical calculations is presented in Figure 4.13.

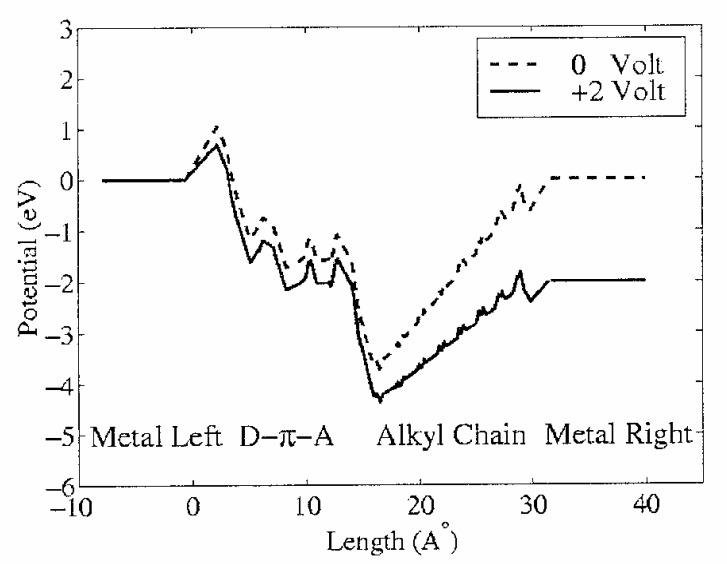

Figure 4.13 Distribution of electrostatic potential across the molecular junction, based on the molecule of $C_{16}H_{33}$-Q3CNQ placed between Al or Au electrodes. Copied from 171.

Applying voltage to the system causes a drop in the electrostatic potential across the molecule. The potential drop has the same (symmetrical) gradient across the D-π-A part whether bias is applied or not. However, for an alkyl chain the difference between the electrostatic potential at 0V or 2V is significant (non symmetrical). This suggested that an alkyl chain plays an important role in the current flow through a molecular junction, because a chromophore is situated closer to one of the electrodes. Therefore, the asymmetry of the I-V characteristics should increase with the length of the alkyl chain. This was in accordance with the Kornilovitch model of rectification, despite molecular structure of $C_{16}H_{33}$-Q3CNQ (donor-spacer-acceptor) being more complicated than theoretical one (see chapter 4.1.2).

The calculation failed to consider the effect of penetration of the gold into the molecular film, which is a common phenomena in fabrication of molecular junctions via the 'cold gold' evaporation technique. The gold penetration could decrease the distance between electrodes (by the reduction of the alkyl length) and thus, effect conduction arising from the chromophore. However, the exact degree of penetration would not be known and could lead to the situation of direct contact of two electrodes in physisorbed

films with a low level of order. The situation is hypothetical and time-dependent but seems to be possible.

Soon after Metzger's publication of rectification form $C_{16}H_{33}$-Q3CNQ between gold electrodes, Okazaki *et al.* reported opposite results for the same system fabricated and studied in the same manner [172]. Higher current was observed in the positive direction, which appeared only in the initial stages of the measurements, and was attributed to the presence of ionic contaminants in the LB film. Further investigations in the broad temperature range of 8 – 281.8 K, showed reproducible and asymmetric I-V curves with higher current in negative quadrant. These results were thought to be due to the possible interaction of the molecules with each other, which would distort current flow through a molecule. This explanation was also suggested later on by other groups [140,141]. However, presence of the alkyl chains may also induce a hopping mechanism, which would govern the overall mechanism of current conduction across the molecular junction.

Development in the field of molecular electronics led to the use of other methods for investigation of electrical rectification in molecular junctions. Metzger [168,173] incorporated STM to image LB films of $C_{16}H_{33}$-Q3CNQ on HOPG substrates. However, it was difficult to interpret the alignment of the molecules on the surface from obtained results as they were unclear. Metzger *et al.* suggested that the molecules can be twisted about 20° from the normal to the substrate.

In 2003, Ashwell and co-workers [174] used STM for investigation of the self-assembled analogue of $C_{16}H_{33}$-Q3CNQ, whose molecular structure is presented in Figure 4.14.

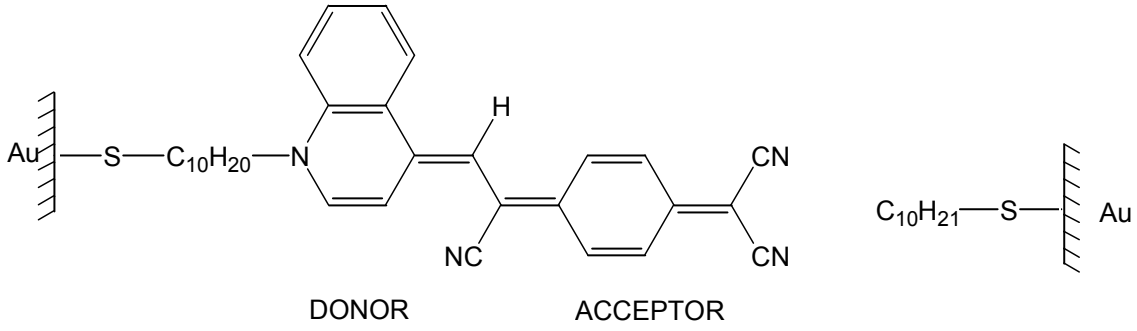

Figure 4.14 SAM of 2-(4-{1-Cyano-2-[1-(10-methanesulfanyl-decyl)-1H-quinolin-4-ylidene]-ethylidene}-cyclohexa-2,5-die nylidene)-malononitrile chemisorbed on gold, investigated by Ashwell *et al.* [174].

Detailed analysis showed a diode-like behaviour for the molecule contacted by a blank gold tip, and a decanethiol-coated gold tip [174]. In both cases, high current in positive direction was observed. Ashwell also used the inverse assembly of the molecule; assembly of the molecule on the tip, contacting an uncoated and decanethiol-coated gold substrate. This time the observed higher current was in the negative quadrant of the I-V plot (see Figure 4.15). This proved that it was possible to control alignment of the molecule in order to control the direction of rectification.

Ashwell *et al.* [174] compared these results with some numerical studies and assumed that this molecule was likely to adapt a quinonoid molecular structure within a SAM, in which the 3CNQ part became the acceptor and quinolinium the donor. These results are contrary to Metzger's previous calculations [168,170,175], in which it was claimed the charge-separated zwitterionic form of $C_{16}H_{33}$-Q3CNQ dominated in LB films. However, they seem to support the Aviram-Ratner model of molecular rectification.

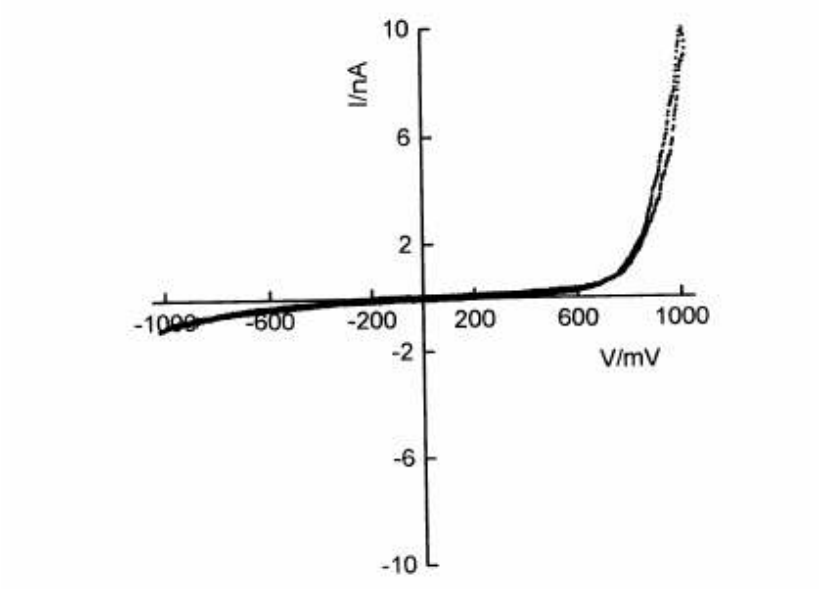

Figure 4.15 I-V characteristic of SAM of self-assembled analogue of donor-π-acceptor molecule, studied by Ashwell *et al*. Copied from 174.

Encouraged by positive results for self-assembled zwitterions Ashwell and co-workers investigated other D-π-A molecules for potential molecular rectifiers [174]. They performed numerous significant investigations for both LB films and SAMs of cationic dyes.

Particularly interesting results were observed when the higher current was changed from the positive to negative quadrant of the I-V plot, as a consequence of anion-induced dipole reversal from aromatic to quinoid form [176]. As can be seen from Figure 4.16, the same anion interacted with the positively-charged heterocycle of the first chromophore, whereas interaction of the second chromophore resulted from different molecular lengths of two ions rather than electrostatics. In this case, the anionic part of the octadecyl counterion was placed closer to the N—$(C_4H_9)_2$ group of the chromophore. These results led to a theoretical analysis of the dependence of molecular dimensions on the location of counterion, which affected the structure of the molecule. However, the main drawback of the experimental method was use of gold-evaporated contacts, which certainly affected the molecular films and influenced

I-V characteristics. Therefore, the maximum rectification ratio of 70 at ±1 V (for chromophore with longer alkyl tail [177]) might not be due to internal properties of the dye.

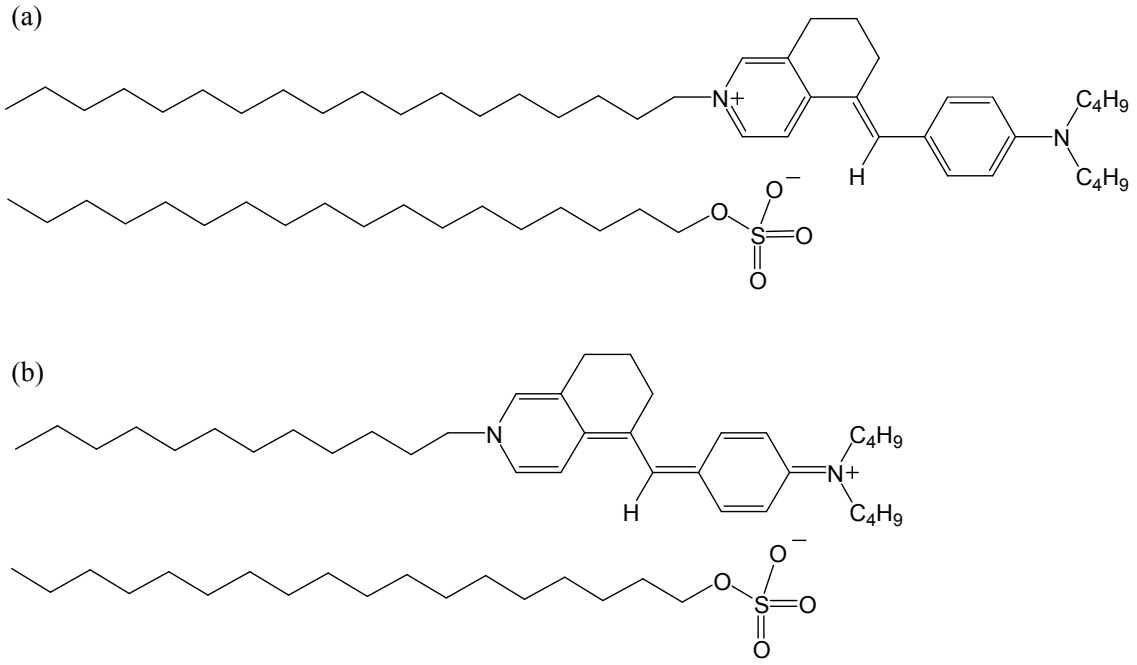

Figure 4.16 Molecular structures of two cationic dyes in; (a) aromatic and (b) quinonoid form, resulting from electrostatic interaction of negatively charged counterion: (a) positively-charged heterocycle; (b) towards N—$(C_4H_9)_2$ group; studied by Ashwell *et al.*[176].

Classical materials for LB films usually possess long alkyl chains, whose presence is essential for alignment of molecules at the air-water interface, can reduce the thermal stability of the LB films [29] and reduce its optical and electrical properties. For some materials it is possible to remove the long-alkyl chain groups after the monolayer deposition [178,179], or even synthesise molecules without long alkyl-chains that still possess amphiphilic properties.

Ashwell, in cooperation with Metzger, developed a 'chevron-shaped' molecule [180,181], in order to reduce the impact of long alkyl chains on the internal current. This molecule (see Figure 4.17) forms stable LB films and when placed between gold electrodes, exhibited rectifying behaviour. The highest observed rectification ratio was

ca. 90 at ±1 V and the direction of electron transfer was assumed to be from bottom gold electrode to the iodide ion (which is known to chemisorb to gold, similar to other halides), which then passed an electron to the pyridinium ring. It was suggested that such high asymmetry of the I-V characteristics must be enhanced somehow, such as a Schottky barrier effect as a possible second mechanism next to interionic electron transfer [181].

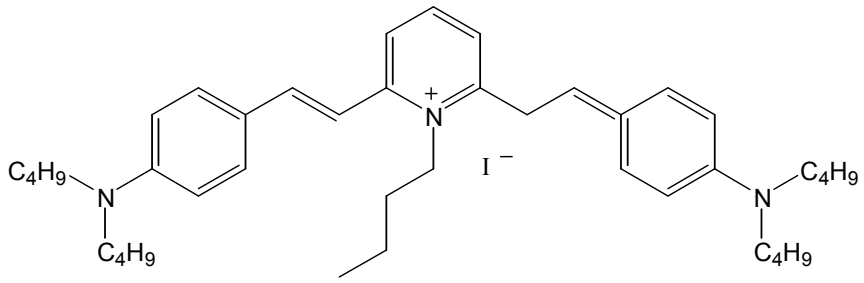

DONOR ACCEPTOR DONOR

Figure 4.17 Molecular structure of a chevron-shaped molecule (1-butyl-2,6-bis-[2-(4-dibutylamino-phenyl)-ethyl]-pyridinium iodide), investigated by Ashwell [180] and Metzger [181].

Recent investigations showed rectification ratio of *ca.* 30 at ±1 V for this molecule contacted by STM Pt/Ir tip [159], which would support explanation of the Schottky barrier formation. However, it was assumed that the arms of the molecule were also engaged in electron transfer, as lengthening the molecule (CH_2—C_6H_6—CH_2) between acceptor and donor on both sides resulted in rectification ratio of 3 at ±1 V [159]. This also might be a result of field-induced reorientation of the molecule on the substrate surface.

Ashwell and Stokes examined the electrical properties of other D-π-A-π-D molecules [182]. An example molecular structure is shown in Figure 4.18. Symmetry of I-V curves for the same squaraine dye with two different chain lengths was observed, which would suggest no contribution to the current arose from non-centric placement of the molecules between the electrodes. Therefore, these results disagree with

the Kornilovitch theory of rectification. However, there was a difference in the value of the current passing through both molecules, and careful estimation of the current at ±1 V revealed that the difference was about 20 times larger for the ten-carbon molecule. With STM it is difficult to predict what would cause this difference (it could be attributed to different measurement conditions or difference in conductivity of samples). Unfortunately, no explanation for this was given by authors.

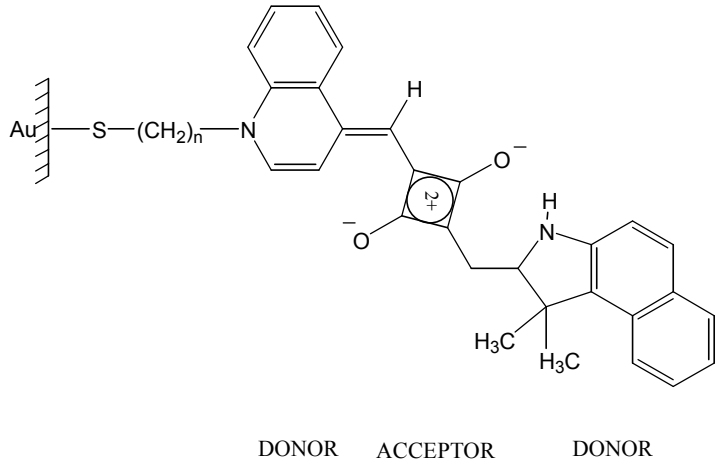

Figure 4.18 Molecular structure of squaraine dye, assembled on the gold substrate, investigated by Ashwell and Stokes [182]; n = 3 or 10, length of the alkyl chain.

In the search for simple D-π-A rectifiers Ashwell and co-workers (examples below) turned their interest to hemicyanine dyes, due to the wide range of possible donor and acceptor groups. Extensive synthesis and electrical studies showed different rectification ratios, which were dependent on the donor-acceptor character of the molecule and led to the conclusion that nonplanarity of the molecular structure influenced the rectifying behaviour.

Examples of three hemicyanines investigated by Aswhell group are presented in Figure 4.19. The first molecule (a) when studied by STM exhibited rectification ratio of no more than 5 at ±1 V [183], second molecule (b) exhibited rectification ratio of 11 – 18 at ±1 V [183] whereas the third molecule (c) possessed rectification ratio of 50 – 150 at ±1 V [184]. The key to explaining such a difference was the steric

hindrance. In the first case the angle between planes of donor and acceptor moieties was about 48°. Whereas the dihedral angle for the second (b) and third molecule (c) was 31° and 61°, respectively. When comparing molecule (a), it was observed that there had to be something more than just a nonplanar structure to obtain rectifying behaviour. The answer was thought to be due to the donor-acceptor character, as the molecular structure of the acceptor in first molecule (a) was completely different. Although rectification from the first molecule was rather minor it was expected to be more asymmetric due to efficient angle (48°) between donor and acceptor planes [183].

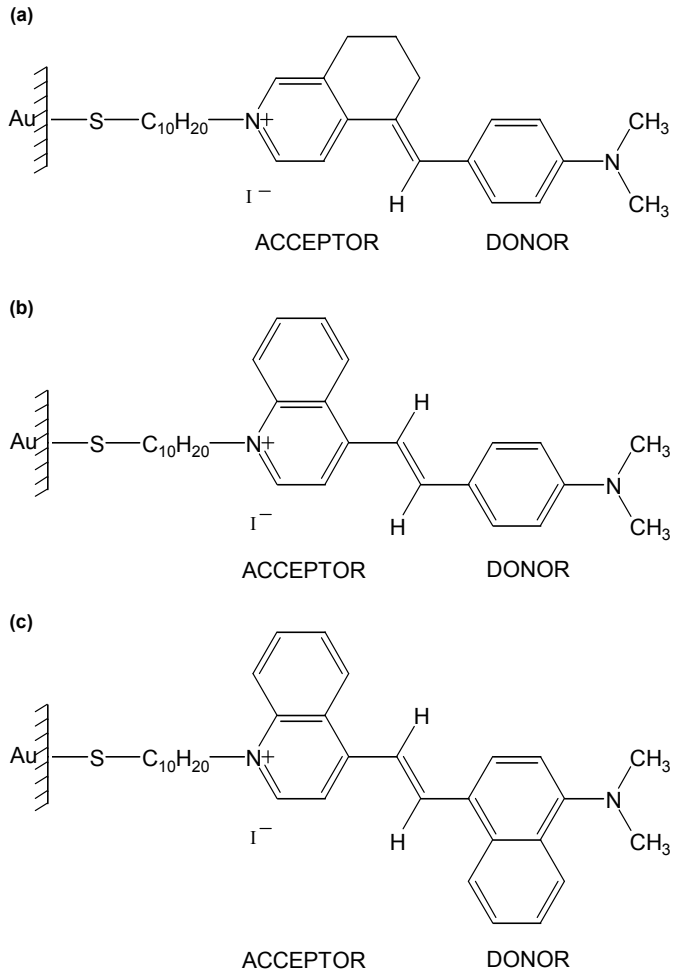

Figure 4.19 SAMs of D-π-A hemicyanines, studied by Ashwell and co-workers. Rectification ratio of: (a) of 5 at ± 1 V [183]; (b) 11 – 18 at ±1 V [183]; (c) 50 – 150 at ±1 V [184].

Electrical behaviour observed in I-V characteristic was consistent and the higher current at forward bias occurred in negative quadrant of the I-V plot for all self-assembled dyes (see example I-V plot in Figure 4.20). It suggested electron transfer from the substrate to the acceptor and from the donor to the STM tip. Therefore this direction of electron transfer was attributed to the Aviram-Ratner model [183].

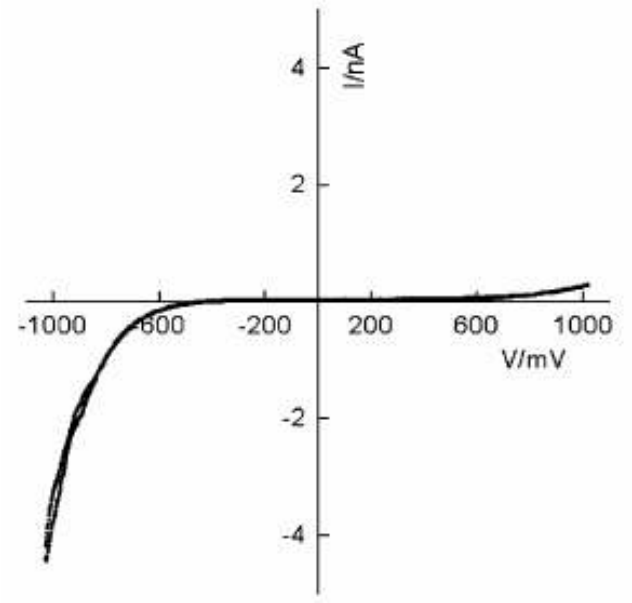

Figure 4.20 I-V characteristics for 1-(10-acetylsulfanyl-decyl)-4-[2-(4-dimethylamino-phenyl)-vinyl]-quinolinum iodide (molecule 2 in Figure 4.19) with rectification ratio of 11 – 18 at ±1 V, studied by Ashwell *et al.* Copied from 183.

4.2.3 Rectification from molecular wires

The crucial factor of molecular wires is their linearity and defined length between components. They are built from conjugated parts separated by single, double and triple C—C bonds (or sometimes aromatic bonds) and conduct current through their π-system. Their future in molecular electronics is seen in designing large matrices of identical (and rigid) molecular structures, such as polymeric wire components [185].

The most popular group of wires are linear conjugated oligomers, which can easily exhibit properties of p-n junctions by precise substitution. It was firstly suggested by

Ellenbogen and Love [146] an an example of this was given by Yu *et al.* in numerous experiments with diblock molecular diodes assembled on gold [186,187,188]. Some of the investigated systems are presented in Figure 4.21.

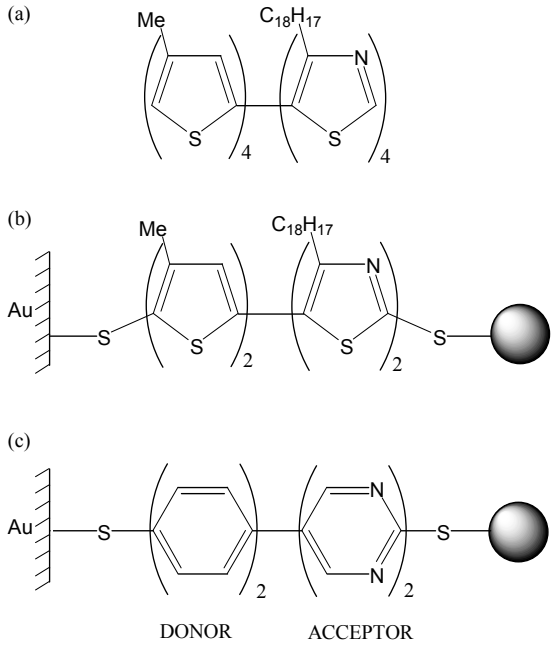

Figure 4.21 Diblock oligomers exhibiting rectifying behaviour in; (a) LB films with rectification ratio of 13 at ± 1.5V; SAMs in contact with Au nanoparticles with rectification ratio of; (b) 5 at ±1.5 V; (c) 4.5 – 9 at ±1.5 V. Studied by Yu *et al*. [188].

All these systems contained electron-rich and electron-poor segments, corresponding to donor and acceptor moieties respectively. Their asymmetric behaviour was rather small and resulted from the weak electron properties of the molecule system. The difference in rectification ratios between the first two molecules most likely resulted from different characters of the forces 'binding' the molecules to the substrate electrode. The rectification ratio was almost twice as high for the third molecule compared to the middle one, which was attributed to the difference in the theoretically calculated dipole moment, that is 6.3 debye and 1.6 debye, respectively.

In an additional experiment Yu *et al.* [188] exposed a SAM (molecular structure in Figure 4.21 c) to a protonation and deprotonation process, which resulted in a change of

rectifying properties (see Figure 4.22). When perchloric acid was used for protonation of the nitrogen, asymmetry of the I-V curves switched position to the negative quadrant with an average rectification ratio of 9.2 at ±1 V. Whereas using sodium ethoxide, I-V curves returned to the initial placement of the asymmetry in the positive quadrant. This phenomena was explained by the reverse of the electronic density of each block with dipyrimidynyl being positively charged.

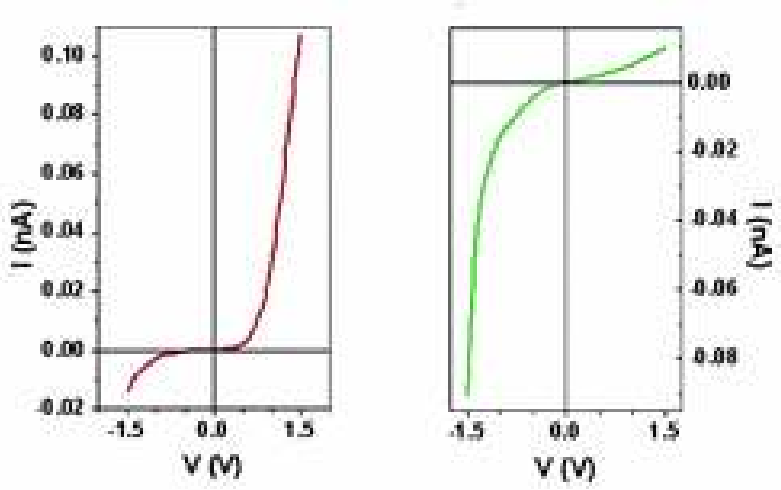

Figure 4.22 Inversion of the rectifying effect in diblock molecule by protonation. Realised by Yu *et al*. Copied from 188.

Kushmerick *et al*. [189] incorporated the cross-wire technique to study the electrical response from some oligophenylene-based molecules (Figure 4.23 a). It was demonstrated that the length of the molecule and the nature of the molecule-electrode bonding were major factors in rectification of the current in molecular junctions. Rectification ratios obtained from experimental I-V characteristics showed the highest values for a three-phenyl molecule with only one anchoring point, then for a phenyl-nitro molecule and a pyridyl molecule. These molecules are 1.95, 1.35 and 1.15 nm long respectively. The fourth molecule with two tailoring points, although the longest (2.02 nm), showed completely symmetrical I-V characteristics. I-V curves are presented in Figure 4.23 b.

(a)

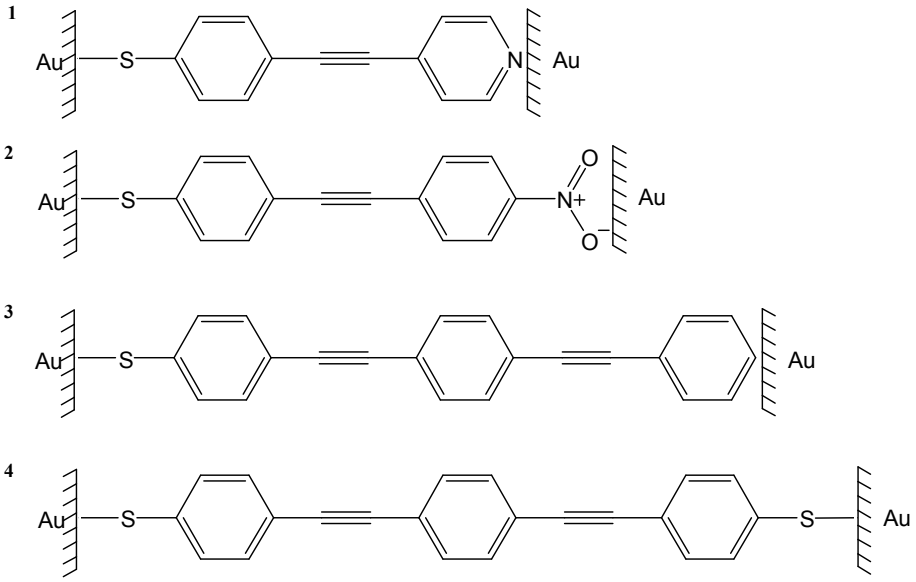

(b)

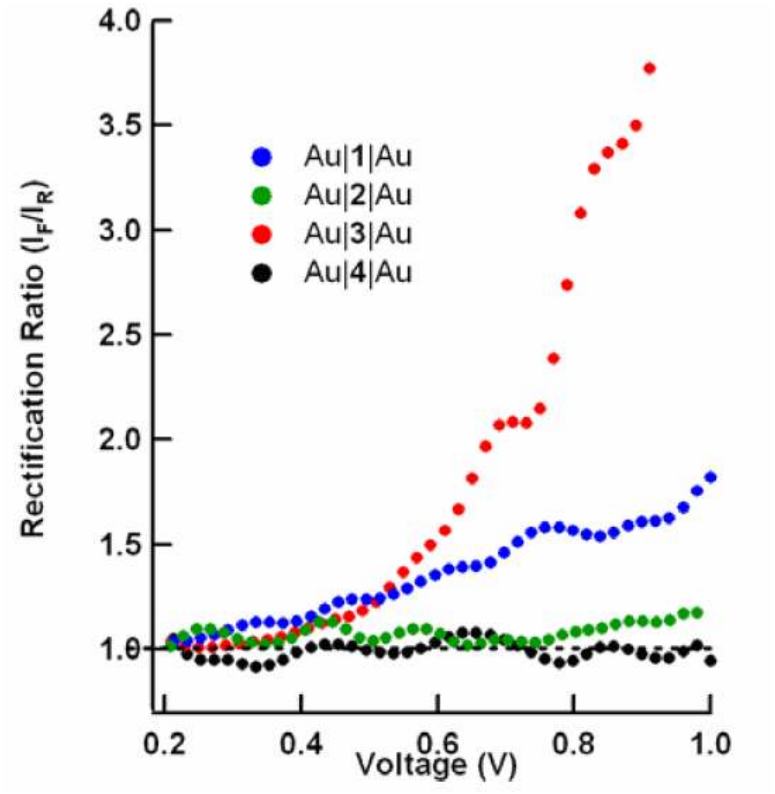

Figure 4.23 Oligophene-based cross-wire molecular junctions investigated by Kushmerick *et al*. [189]: (a) molecular structures; (b) I-V characteristics showing the rise in the asymmetry depending on the molecular length and type of adsorption to the substrate.

Weber *et al.* [190] utilised a mechanically controlled break junction technique for investigation electronic properties of a few molecular rods. Their molecular structures are presented in Figure 4.24.

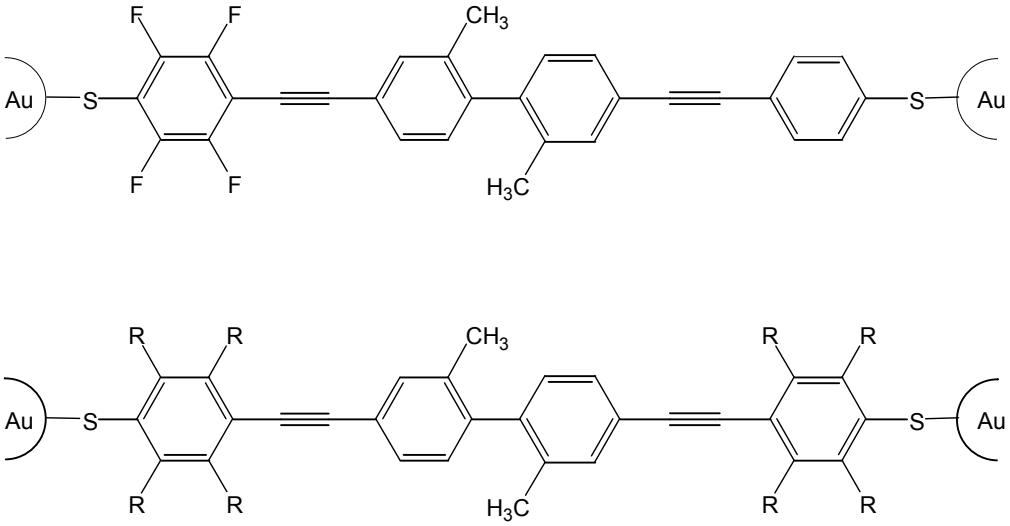

Figure 4.24 Molecular rods for potential molecular rectifiers, constructed by Weber's mechanically controllable break junction method [190]; R = H or F.

Enhanced asymmetry of the I-V characteristics was observed for asymmetric molecules, whereas molecules containing two identical π-units showed minor asymmetry [190]. It was in agreement with Weber's experimental (see chapter 3.3) and led to the conclusion that asymmetry resulted from different heights of the current steps when the bias voltage was increased. These were a consequence of donor-acceptor character of the molecules. The fluorine-part was more conducting (has larger polarisability) than the opposite part of the molecule and therefore the current was larger in the forward bias. These conclusions agree with Aviram-Ratner's dependence of the current on the direction of the applied voltage. However, electrons traversed from donor to acceptor, which is opposite to the predicted Aviram-Ratner route.

4.2.4 Rectification from mixed monolayers

Apart from Metzger and Ashwell, the metal evaporation technique was used by many research groups for fabrication of molecular devices. Fischer and co-workers [191] sandwiched a combination of multilayers of palladium-phthalocyanine (PcPd) and perylene between gold evaporated electrodes as an LB film. Measurements of electron conduction were performed at low temperatures (4.2 K), to suppress possible thermal hopping. Observed I-V curves were asymmetric for combinations of both compounds assembled in one junction, and symmetric for multilayers of single compounds. In addition, Fischer observed a charging effect which he attributed to the Coulomb charging of single molecules (or single molecular stacks).

Rabe *et al.* [192] used STM to investigate alkyl-substituted hexabenzocoronene (HBC, see Figure 4.25) at the graphite-liquid interface. They obtained symmetric I-V characteristics when the STM tip was positioned over an alkyl chain, and asymmetric when the tip was over the π-conjugated part. Rectifying behaviour (rectification ratio of ~ 11 at ± 1.5 V calculated from the published I-V plot) was attributed to the molecule's conjugated system, and therefore could be the first successful rectifier. However, further work with the molecule substituted by a more complicated molecule of athraquinone, showed the opposite rectifying behaviour [193]. The authors attributed this behaviour to resonantly enhanced tunnelling through the HOMO and LUMO of HBC and AQ, respectively.

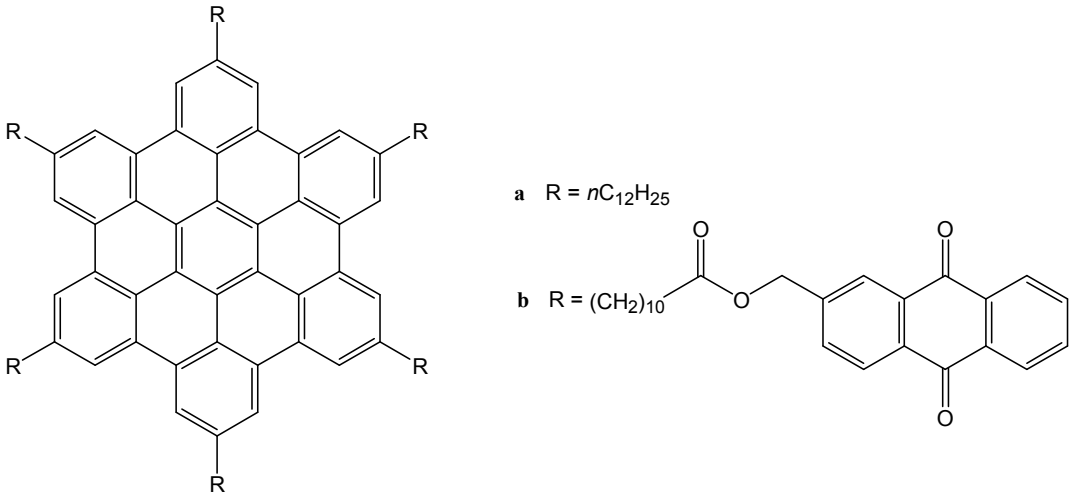

Figure 4.25 Hexabenzocoronene molecule investigated by Rabe *et al.* (a) [192]; (b) [193]

A liquid mercury electrode was incorporated for experimental investigations of TCNQ [47]. A SAM of TCNQ covalently linked to an alkanedisulfide was deposited on Ag or Au electrodes and brought into contact with a SAM of alkanethiol on the Hg electrode. The authors observed higher current in the forward direction, although the system did not have donor-acceptor character, which was attributed to the strong electronic properties of TCNQ. Such a conclusion was conceived from studied electrical properties of similar junctions where TCNQ was replaced with different functional groups: COOH and Fe—$(C_5H_5)_2$. Chabinyc *et al.* [47] excluded formation of a silver oxide layer, or a mismatch between metallic work functions as factors affecting the asymmetry of I-V curves, and observed a decrease in rectification ratio for thicker SAMs on Hg. This would agree with a theory proposed by Kornilovitch [141], that one conducting level aligned asymmetrically with respect to the electrodes was enough to rectify current which additionally could be modulated by the different asymmetric positions. However, this was with strongly disordered films, due to a mismatch between the sizes of thiols and TCNQ, and the van der Waals interaction may have strongly influenced the rectifying behaviour. A molecular system studied by Chabinyc *et al.* exhibited rectification ratio of 10 at ±1 V for a positively biased Hg electrode and is presented in Figure 4.26.

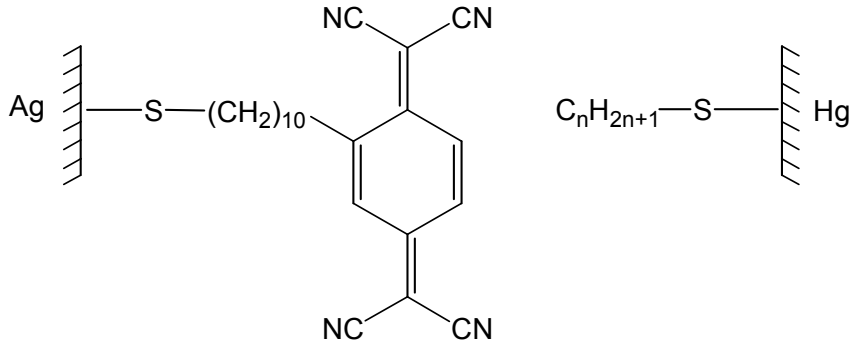

Figure 4.26 Molecular junction incorporating SAM of TCNQ on Ag electrode and SAM of alkanethiol on Hg drop electrode, studied by Chabinyc *et al.* [47]; n = 14, 16, 18, n – number of carbons in alkyl chain.

Much work has been spent studying nanoparticles [194], which are seen as a bridge between bulk materials and molecules, as they can act as interconnections between single molecules and electronic circuits. For example, Reda *et al.* [195] used sequential deposition of a system functionalised with TCNQ and TMPD (tetramethyl-p-phenylenediamine) gold and silver nanoparticles on HOPG. Diode-like behaviour was observed from a multilayered structure with electron flow always in the same direction: from cathode to acceptor (TCNQ), and then donor (TMPD) to anode. To explain this behaviour, the Aviram-Ratner model and the Schottky contact mechanism of current conduction were referred to. The first is not difficult to conclude as the direction of electron transfer and electronic strength of molecules both apply. The suggestion of a second mechanism came from the energy gaps between metal and p-semiconductor ($\Phi_{metal}<\Phi_{semiconductor}$), which in this case would be TCNQ and TMPD respectively. However, another remark was made about the possibility of the $Ag^{+}TCNQ^{-}$ salt forming, especially when rectification ratios significantly differed when silver nanoparticles were incorporated. In this case rectification ratio amounted to 66 at ± 0.075 V, whereas it was rather small for gold, with a maximum of 6.5 at ±1 V.

Ashwell and Berry [196] incorporated two types of deposition to form a rectifying molecular hybrid system (see Figure 4.27). Self-assembly was used to deposit a monolayer of asymmetric squaraine on an Au-coated substrate, whereas

the LB technique formed the second layer, which was composed of a symmetrical squaraine. STM analysis revealed asymmetry of the I-V characteristics for this particular system but both molecules (when studied individually) did not exhibit rectifying behaviour [182,197]. This was attributed to the donor-acceptor interaction between the two layers in the system. It was thought that donor of the unsymmetrical molecule, and A of the symmetrical one were pushed towards the electrodes so that the electron flow was from the tip to the acceptor of molecule in the top layer, then through the SAM to the substrate. Despite the systems visible asymmetry, rectification ratio decreased with time from 12 to 4 at ±1 V. Two explanations were given for this behaviour; rearrangement of the LB-type squaraine in the presence of the electric field, and differences in experimental procedures between samples [198].

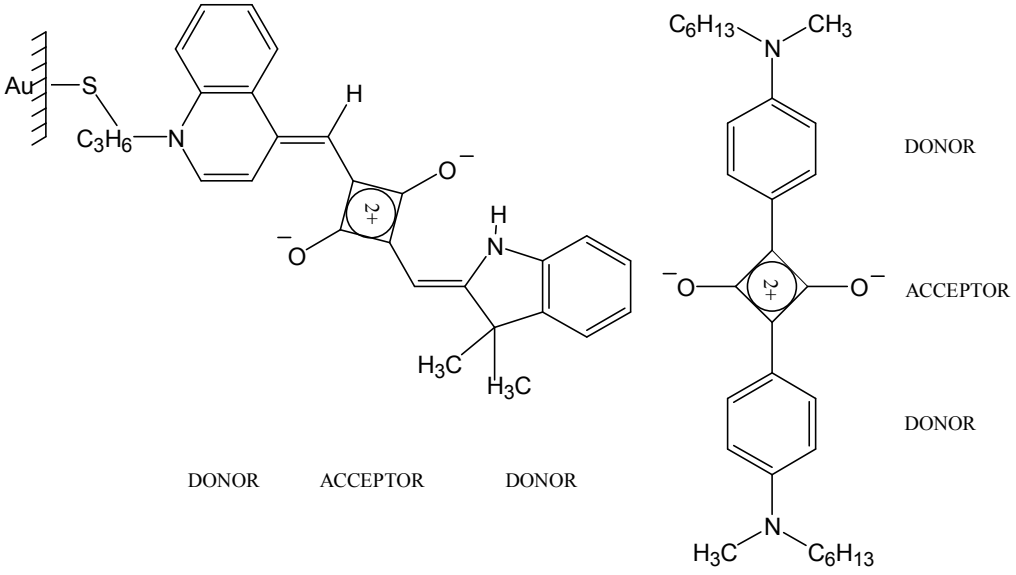

Figure 4.27 Molecular structure of hybrid SAM/LB rectifier, investigated by Ashwell and Berry [196].

Mukherjee and Pal [69] reported molecular rectification from monolayers containing donor and acceptor molecules coupled electrostatically. A molecular junction was formed according to the ESA technique (see chapter 2.3), by dipping a hydrophilic silicon substrate into a polycation bath prior to immersion in phthalocyanine solution. The base layer of donors, on which the acceptor layer (Rose Bengal) was from anionic

solution, was topped with a layer of polymer layer once again to avoid Schottky effects. Molecular structures of main components are shown in Figure 4.28.

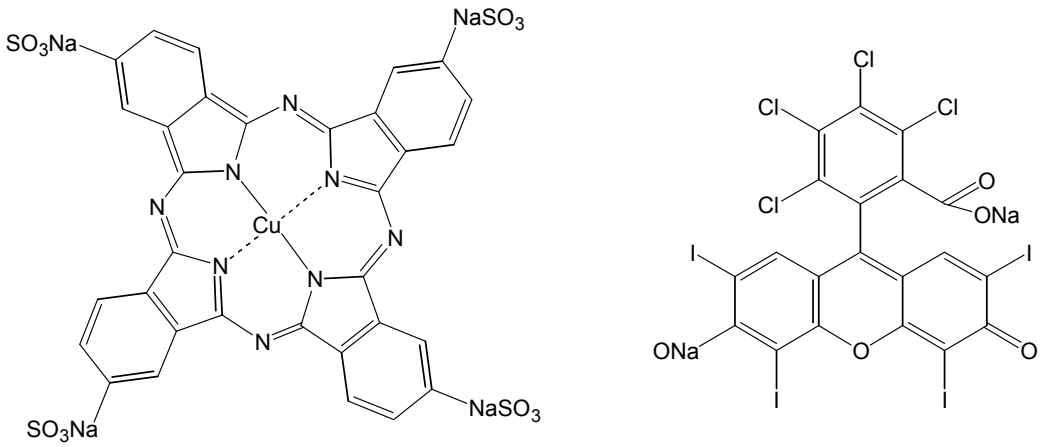

Figure 4.28 Molecular structure of copper phthalocyanine (CuPc, left) and Rose Bengal (RB, right) studied in a molecular donor-acceptor junction formed by ionic attraction of these components with polycationic and polyanionic layers of polymer material (PAH) in between [69].

The authors claimed that electrostatic coupling of molecular components had the advantage of incorporating many other molecules for potential unimolecular rectifiers. Electrical properties of CuPc-RB monolayers were investigated with the Hg drop electrode technique, which recorded asymmetric characteristics with rectification ratio of 30 at ± 1.9V. The asymmetry was verified with electrical measurements of all the separate components, which did not exhibit rectification when studied individually. The direction of the current flow was the reverse of that proposed by Aviram and Ratner [14], from the donor to the acceptor. However, Bryce *et al*. [165] observed a reverse of the electrical asymmetry for D-σ-A molecules when contacted by a Hg electrode in relation to STM results. Therefore, the electrical properties presented here demand further verification.

Ashwell *et al.* [199,200] also studied the electrical behaviour of other electrostatically coupled system, containing CuPc molecules. However, they incorporated covalent self-assembly for deposition of the first components (on solid substrate) to assure an ordered first layer and hence in the whole molecular structure (Figure 4.29 a) [199].

The other component was deposited on top of the first by electrostatic interaction of oppositely charged counterions via immersion. STM analysis showed that the bipyridinium molecule acted as an acceptor, which controls the molecular alignment of copper phthalocyanine in a hybrid structure. Moreover, diode-like behaviour was observed for the system with rectification ratio of 60 – 100 at ±1 V and direction of the current flow was in accordance with the Aviram-Ratner model (see Figure 4.29 b).

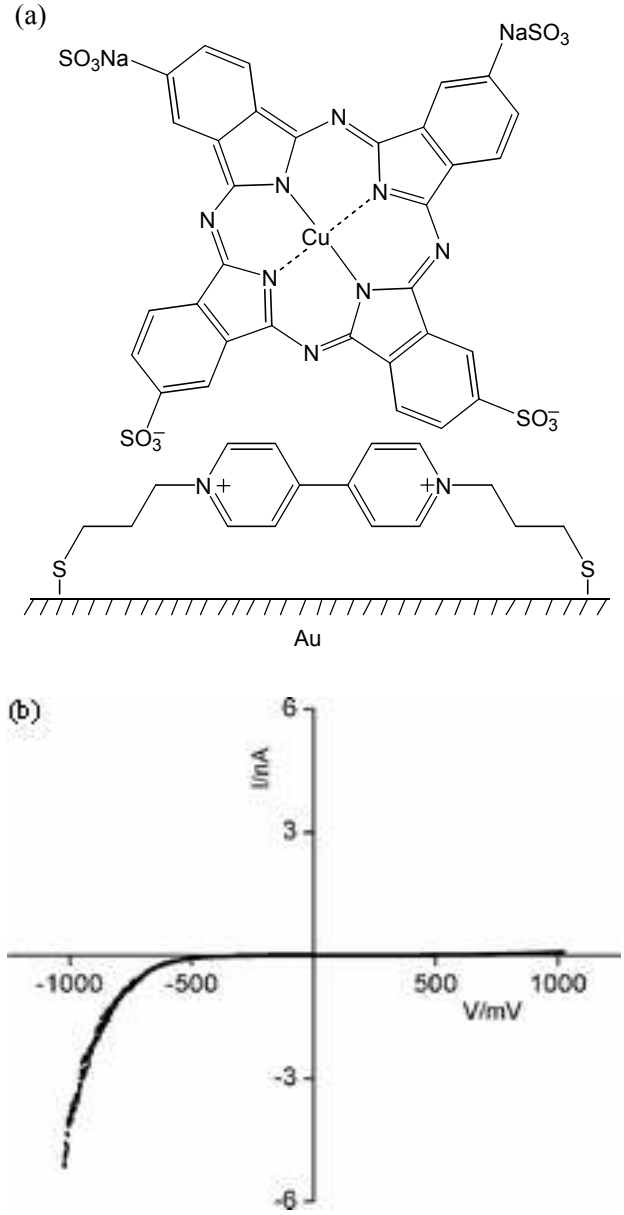

Figure 4.29 Hybrid system investigated by Ashwell *et al.* [199]; (a) molecular structure, incorporated both covalent self assembly of the first component (bipyridinium salt) and electrostatic self-assembly of copper-phtalocyanine as a second component; (b) I-V plot with rectification ratio of 60 – 100 at ±1 V.

Recently, Ashwell and co-workers [200] managed to improve rectification ratio from hybrid systems by replacing a bipyridinium unit with D-π-A molecules; Figure 4.30. Rectification ratios which were obtained for these hybrids were from 15 up to 3000 at ±1 V, dependent on the cationic dye used. It was presumed that, even in mixed monolayers stearic hinderance of D-π-A molecules played a crucial role in triggering rectification. It suggested that the presence of phthalocyanine in the system induced the higher asymmetries, which was what is supported for the results obtained for a planar molecule. It was demonstrated that one-molecular systems with planar molecules do not rectify current [183] because the degree of a stearic hinderance was too small to effectively prevent the planes of donor and acceptor from overlapping, which means a lack of an effective tunnelling barrier for electron flow.

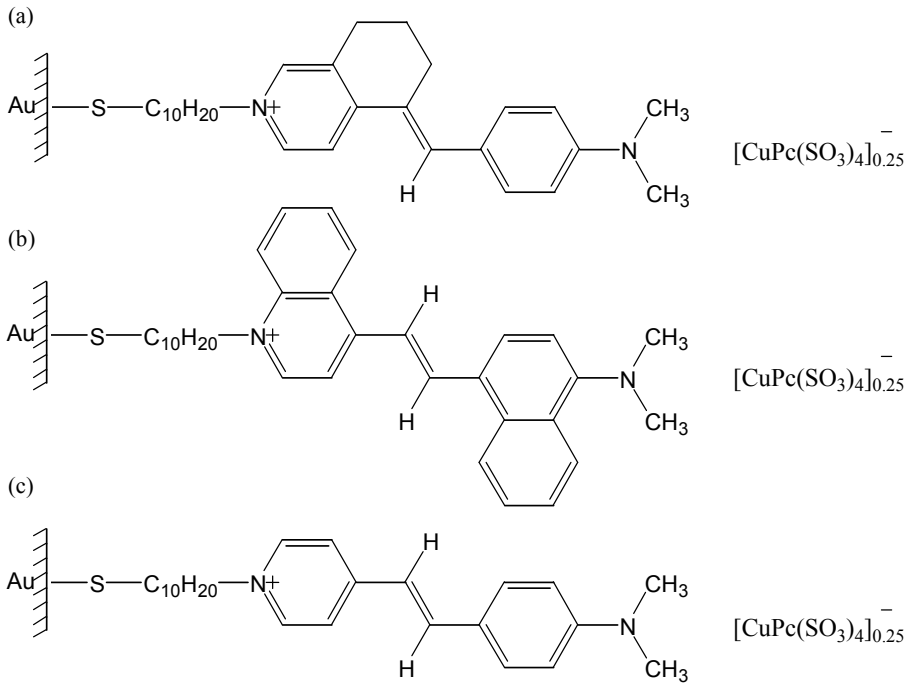

Figure 4.30 Molecular structures of mixed monolayers of cationic dyes and phthalocyanine, studied by Ashwell *et al.*[200] Rectification ratios of presented hybrids were; (a) 3000 at ±1 V; (b) 700 – 900 at ±1 V; (c) 15 – 70 at ±1 V.

5 Experimental

5.1 Studied materials

Overall, the thesis contains seventeen molecules. Due to their molecular structure they are divided in two main groups. The first group relates to D-(π-bridge)-A zwitterionic molecules, synthesised by Dr R.L.H. High. These molecules are noteworthy as they carry positive and negative charges on two different atoms in crystal form. In all investigated zwitterions, the positive charge was delocalised within the heterocycle over the nitrogen atom, whereas the negative charge was spread between two CN groups [169,170,171]. However, in this chapter their molecular structures are presented in the quinoid form. It was assumed that they adapt to this form in SAMs which was experimentally proved by Ashwell *et al.* [174] (see chapter 4.2.2). Investigated zwitterions have been separated into three subgroups; quninolinium (Q3CNQ), pyridinium molecules (P3CNQ) and double-leg Q3CNQ molecules with two possible gold-attachment points (Chapter 5.1.1, 5.1.2 and 5.1.3 respectively).

The second group relates to two-molecular systems based on D-(π-bridge)-A hemicyanine chromophores, whose molecular alignment was proved to be controlled by underlying thiol molecules (purchased from Sigmna-Aldrich Chemical Co., Cillingham, UK). Their molecular structures are shown in Chapter 5.1.4. The hemicyanine dyes were synthesised by Dr M. Amiri (5-(4-dibutylamino-benzylidene)-2-methyl-5,6,7,8-tetrahydro-isoquinolinium iodide, Figure 5.9), Dr A. Whittam (4-[2-(4-dibutyloamino-phenyl)-vinyl]-1-methyl-quinolinium iodide, Figure 5.10) and Dr A. Mohib (4-[2-(4-methoxy-napthalen-1-yl)-vinyl]-1-methyl-quinolinium iodide, Figure 5.11 and 4-[2-(4-dimethyl)-amino-napthalen-1-yl)-vinyl]-1-methyl-quinolinium iodide, Figure 5.12) and their molecular structures are presented in Chapter 5.1.5. The electrical properties of these chromophores in SAMs were studied before [87,183,184,201,202] and they will be compared to those in two-molecular systems.

5.1.1 Quinolinium zwitterions (Q3CNQ)

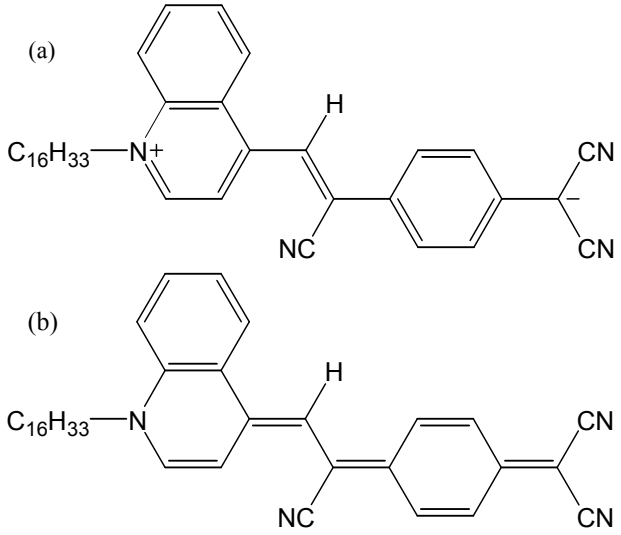

Figure 5.1 Molecule of Z-β-(1-hexadecyl-4-quinolinium)-α-cyano-4-styryldicyanomethanide, (C16H33-Q3CNQ) in: (a) zwitterionic form; (b) quinoid form.

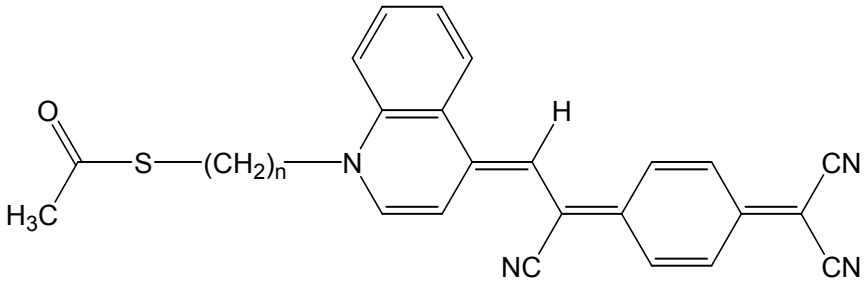

Figure 5.2 Molecule of thioacetic acid S-(10-{4-[2-cyano-2-(4-dicyanomethylene-cyclohexa-2,5-dienylidene)-ethylidene]-4h-quiolin-1-yl}-*n*) ester, *n* = propyl, hexyl, octyl, decyl, dodecyl.

5.1.2 Pyridinium zwitterions (P3CNQ)

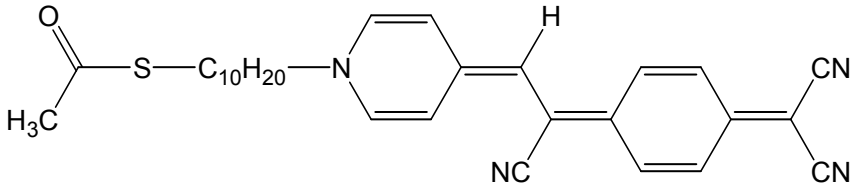

Figure 5.3 Molecule of thioacetic acid S-(3-{4-[2-cyano-2-(4-dicyanomethylene-cyclohexa-2,5-dinelydene)- ethylidene]-4H-pyridin-1-yl}-propyl) ester.

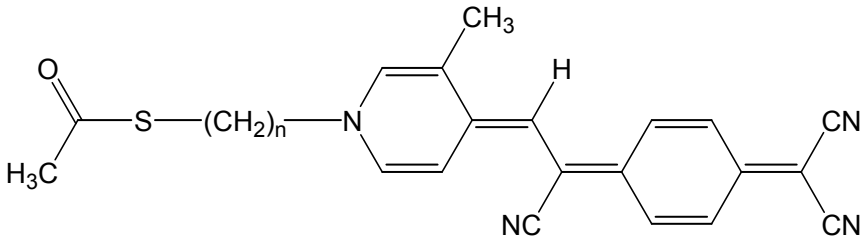

Figure 5.4 Molecule of thioacetic acid S-(3-{4-[2-cyano-2-(4-dicyanomethylene-cyclohexa-2,5-dinelydene)- ethylidene]-3-methyl-4H-pyridin-1-yl}-n) ester, n = propyl, decyl.

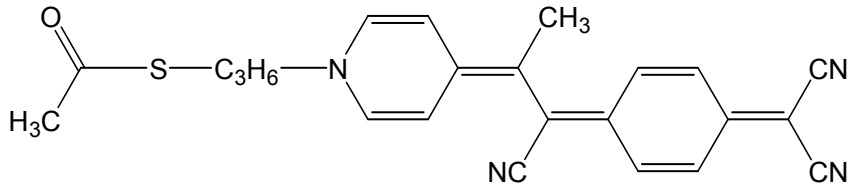

Figure 5.5 Molecule of thioacetic acid S-(3-{4-[2-cyano-2-(4-dicyanomethylene-cyclohexa-2,5-dinelydene)-1-methyl-ethylidene]-4H-pyridin-1-yl}-propyl) ester.

5.1.3 Double-leg zwitterions

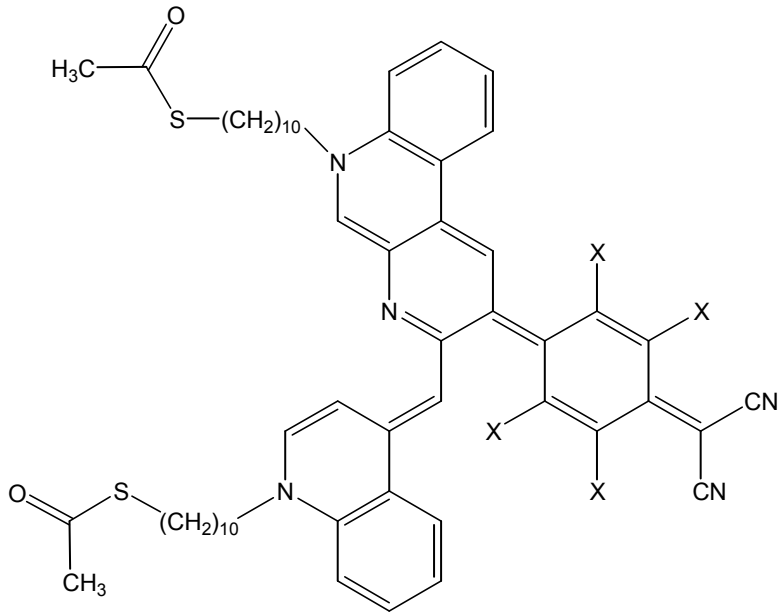

Figure 5.6 Molecule of thioacetic acid 10-[3-(1-(10-acetylsulfanyl-decyl)-1H-quinolin-4-ylidenemethyl]-2-(4-dicyanomethylene-2,3,5,6-tetraX-cyklohexa-2,5-dienylidene)-2H-benzo[f][1,7]naphthyrdin-6-yl]-decyl ester, X = CH_3 or F.

5.1.4 Thiols

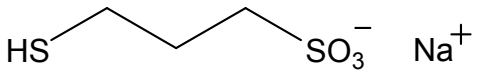

Figure 5.7 Molecule of sodium 3-mercapto-1-propanesulfonate.

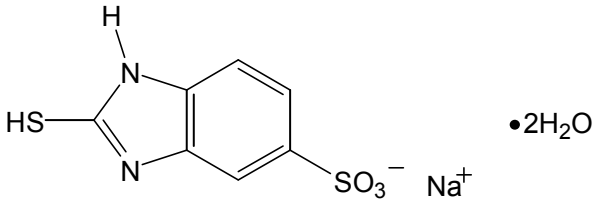

Figure 5.8 Molecule of 2-Mercapto-5-benzimidazolesulfonic acid sodium salt dihydrate.

5.1.5 Hemicyanines

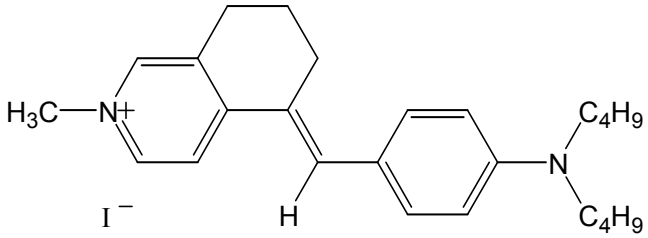

Figure 5.9 Molecule of 5-(4-dibutylamino-benzylidene)-2-methyl-5,6,7,8-tetrahydro-isoquinolinium iodide.

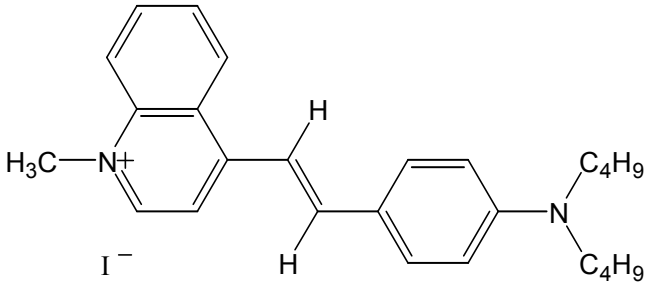

Figure 5.10 Molecule of 4-[2-(4-dibutyloamino-phenyl)-vinyl]-1-methyl-quinolinium iodide.

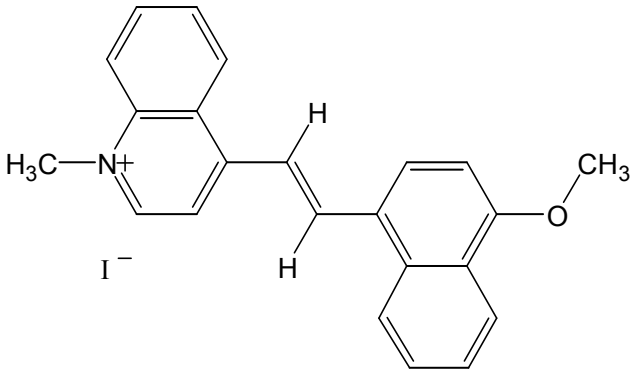

Figure 5.11 Molecule of 4-[2-(4-methoxy-napthalen-1-yl)-vinyl]-1-methyl-quinolinium iodide.

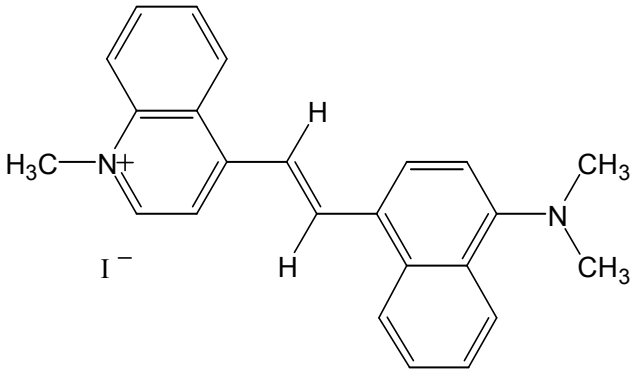

Figure 5.12 Molecule of 4-[2-(4-dimethyl)-amino-napthalen-1-yl)-vinyl]-1-methyl-quinolinium iodide.

5.2 Fabrication techniques

5.2.1 Substrate preparation

Depending on the type of investigation technique to be used, there were three types of substrate used and each of them was subjected to different cleaning and preparation routines.

Hydrophilic slide cleaning was utilised as a treatment for the glass slides (*Blue Star Micro slides)* that were to be used for LB film deposition and obtaining UV-Visible spectrum of LB films:

1) Examination of slides for defects and impurities, then the slides were wiped with tissues soaked in chloroform.

2) Ultrasonic immersion of the slides in general grade isopropanol (IPA) for 10 minutes, followed by ultrasonic immersion in ultrapure water for the same period of time.

3) 24 hour immersion of slides in pirahna solution (30 % H_2O_2 and concentrated H_2SO_4 in ratio 1:1) to remove long-chain hydrocarbons.

4) Thorough rinse with ultra-pure water and step 2 repeated, followed by storage of slides in 30 % H_2O_2 at *ca.* 5° C.

5) Prior to use, the slides were rinsed thoroughly with ultra-pure water and dried in a stream of dry air.

Hydrophobic slide cleaning was implemented for further deposition of SAMs onto gold and their investigations by SPR and UV-Vis spectroscopy. The cleaning procedure was run in similar manner however ultrasonic immersion of the slides in ultra-pure chloroform was also implemented.

HOPG (highly oriented pyrolitic graphite) was used as a base material for electric characterisation. It was chosen because of its smoothness and the possibility of an almost infinite number of graphite layers, which could be easily removed one by one because of graphite's lamellar structure, and its cleaving properties along lateral planes. The freshly cleaved surface of HOPG was prepared by gently peeling off a piece of adhesive tape until the surface that remained was flat.

10 MHz AT-cut quartz crystals (for QCM characterisation) were cleaned in a plasma cleaner (*Plasma Prep 2* manufactured by *Gala Instrument*; Figure 5.13) for 3 minutes

on each side, and then rinsed with at least two types of solvents, dependent on the solvent in which the adhered material was dissolved. Then they were dried in a stream of cool air to avoid any temperature distortion of the quartz crystals.

Figure 5.13 The photograph of Plasma Cleaner, *Plasma Prep 2 by Gala Instrument*, used for cleaning quartz crystals.

The vacuum thermal evaporation of gold was performed on hydrophobic glass slides for SPR and also HOPG substrates in order to fabricate a bottom electrode for STM junctions. This technique is commonly known for deposition of metals with a specific thickness, which may vary from a few to hundreds of nm, depending on the application and thickness-sensitivity of the coater unit.

Thermal coating was realised with the *Edwards 360A unit* in a clean-room environment. Substrates (HOPG and hydrophobic glass slides) were mounted in a holder and placed in a vacuum chamber (see schematic diagram at Figure 5.14), together with gold wire (99.99 % pure, purchased from *Sigma-Aldrich Chemical Ltd.*) of known weight. When the chamber reached a pressure of $< 2\times10^{-6}$ Torr, gold in a molybdenum filament (boat) was evaporated on substrates and continued until the desired value of the gold thickness (*ca.* 47 nm) was reached. Constant deposition rate of 0.1 nm s^{-1} ensured even

distribution of the gold on the substrate surface with the process controlled by the use of a single quartz crystal monitor.

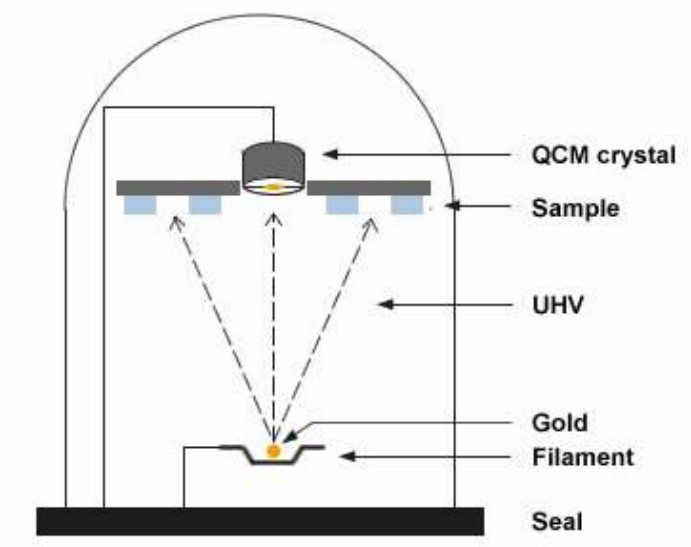

Figure 5.14 Illustration of conventional UHV chamber for thermal evaporation process of metallic thin films. Arrows indicate the direction of gold evaporation.

5.2.2 Monolayer preparation

LB films were obtained using a two-compartment LB trough (*Model 622 NIMA Technology Ltd*.) equipped with a motor-drive dipper mechanism, allowing smooth deposition (see Figure 5.15). Deposition was on hydrophilic glass slides to produce an LB monolayer film. This was performed by a drop-by-drop deposition routine of the molecules from dichloromethane solutions onto the air-water surface. The concentration range varied from 0.01 – 0.05 mg cm^{-3}, and a five minute period was allowed for the solvent to evaporate before compression.otor-drive dipper mechanism, allowing smooth deposition.

Figure 5.15 The photograph of LB trough *Model 622 NIMA Technology Ltd.* used in the experiment.

SAMs of the self-assembling molecules on gold-coated substrates were obtained by immersion of the substrates into acetone (or dichloromethane) solutions of the dyes with concentrations from 0.01 – 0.05 mg cm^{-3}. To facilitate deposition of the molecules, a few drops of ammonium hydroxide were to displace the acetyl groups. It was also found that immersion of substrates for short periods of time, interrupted by rinsing with solvents, delivered better monolayers (denser molecular packing) than films obtained as a result of a single long immersion.

SAMs of purchased thiols on gold-coated substrates and quartz crystals were fabricated by immersion of the substrates in methanol solutions with different concentrations. It was found that concentration of 0.70 – 0.80 mg cm^{-3} of sodium 3-mercapto-1-propanesulfonate and 0.50 – 0.60 mg cm-3 of 2-Mercapto-5-benzimidazolesulfonic acid sodium salt dehydrate was perfect for smooth deposition of the monolayers.

Assembly of hemicyanine dyes on top of thiols was possible due to an electrostatic interaction between the SO_3^- group within the monolayers of thiols and the positively-

charged nitrogen, present in heterocycles. To facilitate the process of ionic attraction of these species, a few drops of water were added to the solutions of the dyes to rinse out Na^+ and Cl^-.

5.3 Measurement methods

5.3.1 Ultraviolet spectroscopy

UV-Vis spectra were obtained in transmission for LB films on glass and SAMs on platinum coated glass substrates using *UV-Vis Super Aquarius 9000 spectrophotometer*. UV-Vis spectroscopy is usually used for identification of conjugated organic compounds (or transition metal ions) which absorb the light within the ultraviolet (200 – 400 nm) and visible region (400 – 700 nm) of the electromagnetic spectrum.

5.3.2 Quartz crystal microbalance

QCM studies allowed calculation of the area occupied by a molecule within the monolayer, when deposited on the gold electrodes of a quartz crystal (see more in chapter 2.4.1). It was assummed that molecules create a perfect monolayer (compete coverage) on the quartz crystal and therefore monolayer was free from any defects.

Caluclation of the area was possible after transformation of the basic Sauerbrey relationship (see chapter 2.4.1), considering all known parameters, to determine the mass and subsequently the area. These parameters are: f_o – fundamental frequency of the crystal (10×10^6 Hz), A – surface area of the resonator (2.059×10^{-5} m^2), ρ_q – density of quartz (2.648×10^6 g m^{-3}) and μ_q – shear modulus of the quartz (2.947×10^{13} g/m s^{-2}). The final equation for measuring the changes of the adsorbed mass on quartz resonator is as follows:

$$\Delta m = -(9.09 \pm 0.01) \times 10^{-10} \Delta f$$

The experimental setup for QCM (see Figure 5.16) consisted of AT-cut quartz crystals with a nominal frequency of 10 MHz, and a thickness of 0.2 mm, connected to the frequency counter to monitor changes in the resonance frequency.

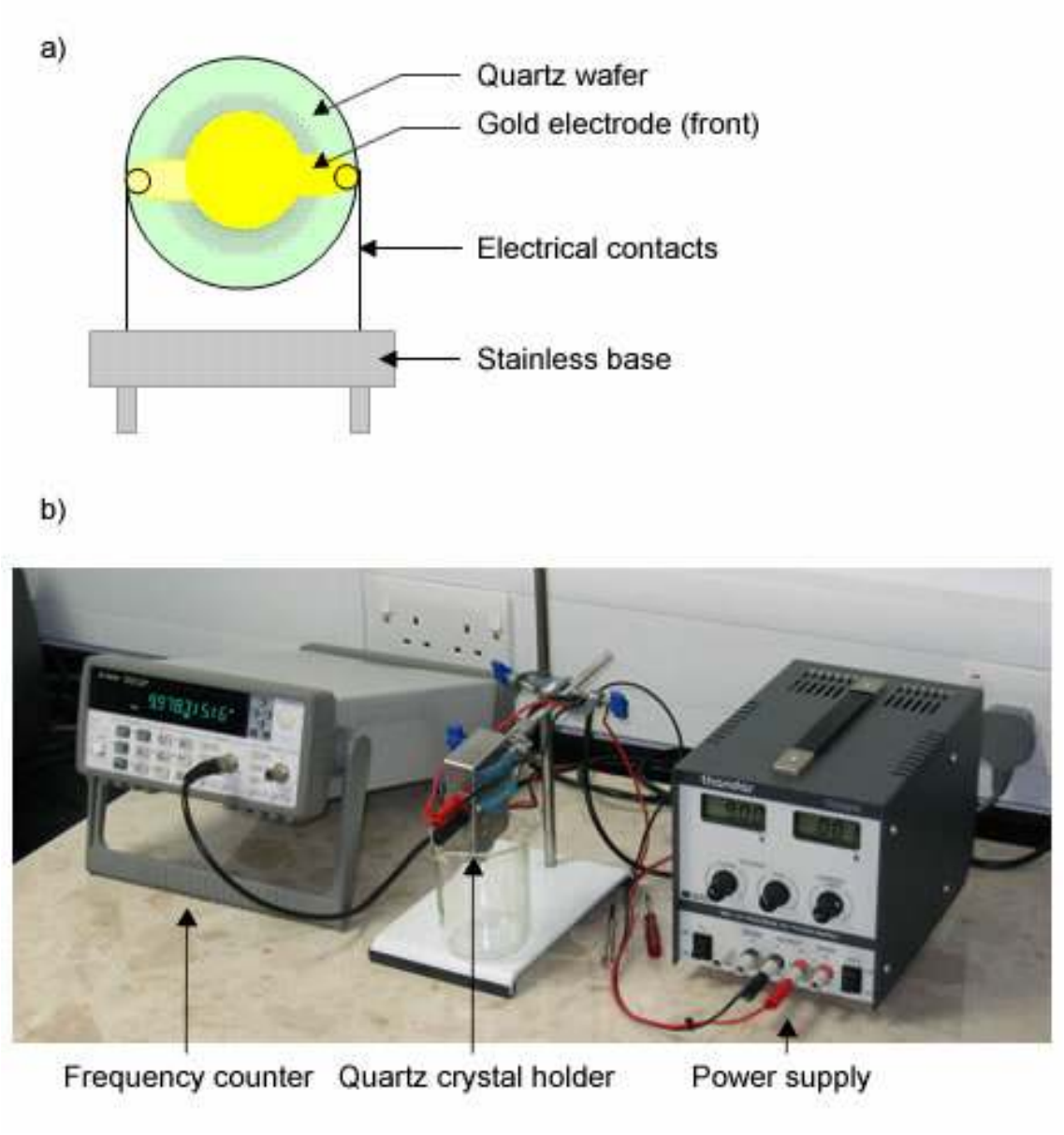

Figure 5.16 QCM apparatus used in the experiment; (a) illustration of quartz crystal (b) wired into electrical circuit in order to perform measurements of quartz crystal frequency change.

The resonant frequency of the blank crystal was measured repeatedly at intervals of 1s. Every measurement was preceded by rinsing and drying, to ensure that the solvent did not affect the process of the deposition of the investigated thin films. It was assumed that molecules had created a complete monolayer when the measurements had reached a plateau value.

5.3.3 Surface plasmon resonance

SPR measurements, used for identification of the thickness of deposited monolayers on gold-coated glass slides, were performed with an apparatus based on the Kretschmann configuration [203] (see Figure 5.17 a). A coated glass slide contacted the prism using index matching fluid* and the reflectance was recorded as a function of angle of the laser beam (θ). The intensity of the reflected beam was rationed to that of a reference to exclude fluctuation from the laser source (λ). In order to obtain reliable results two wavelengths were used for measurements: λ = 632.8 nm (*HeNe laser*) and λ = 532 nm (*frequency doubled Nd:YAG laser)*. Firstly from a blank slide with a 47 ± 2 nm gold layer, then from the same slide with the deposited monolayer.

The illustration of SPR condiguration is shown in Figure 5.17. P-polarised light was passed through the chopper before it was split, so that half was diverted to a reference detector whereas the other half reached the *60° BK7 glass prism*. The prism was mounted on rotational stage which provided various angles (38° - 50°) for p-polarised light to interact with a metallic layer deposited on a glass slide contacting the prism. Uncoupled reflected light was detected by a sample detector and the information about both, reference and sample beams was amplified and processed by the computer program resulting in the production of SPR curve (see chapter 2.4.2)

* Matching fluid which was used was methyl benzoate in order to have the same refractive index as glass slide

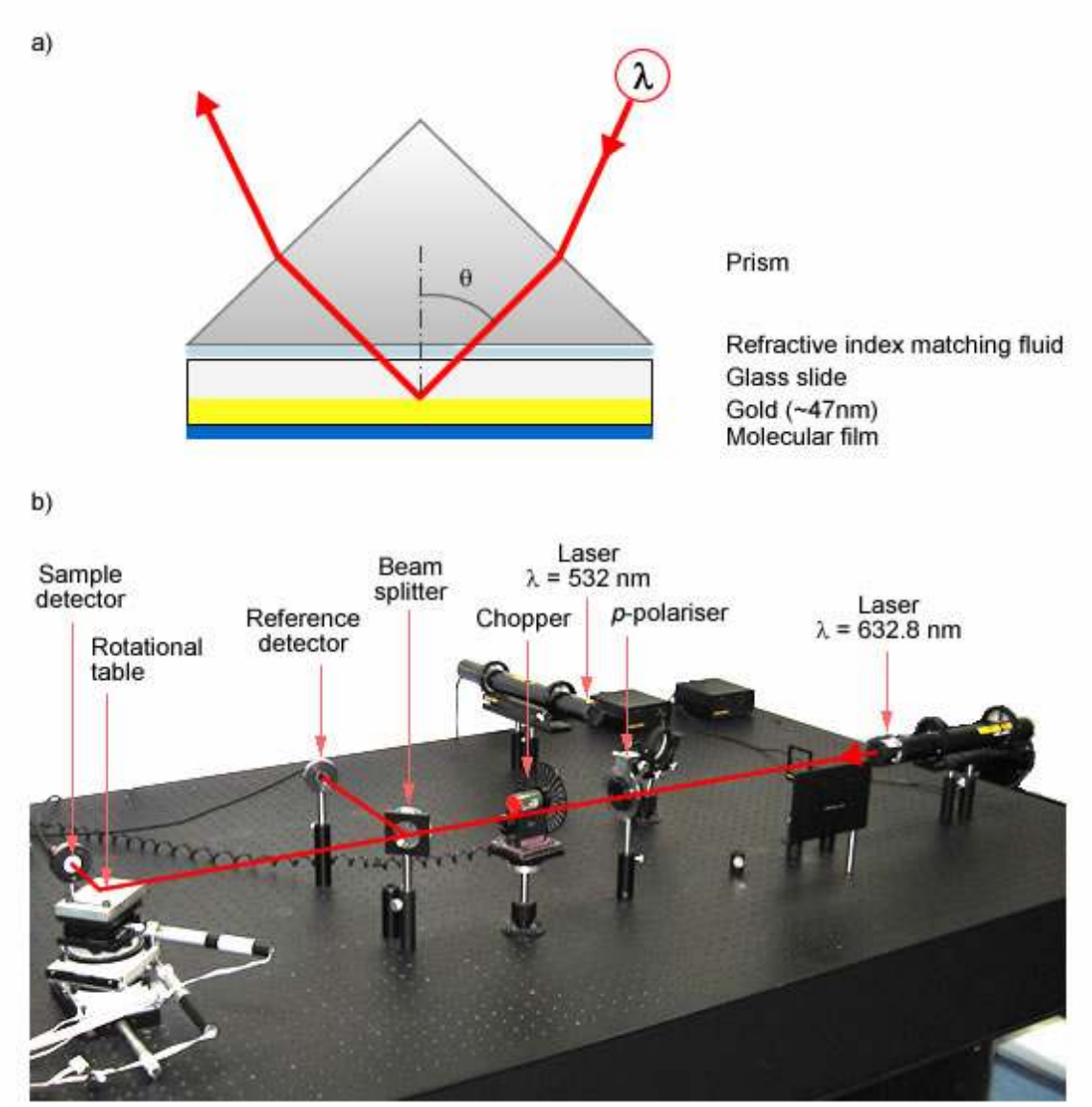

Figure 5.17 Illustration of the SPR optical apparatus applied in current studies; (a) prism arrangement consistent with Kretschmann configuration [203]; (b) the photograph of the SPR setup incorporating two light sources. Red line shows propagation of laser beam through SPR system including polarisation, splitting and detection of the light.

5.3.4 X-ray photoelectron spectroscopy

XPS spectra were obtained from a *Kratos AXIS Ultra* spectrometer equipped with a monochromatic Al X-ray source at 150 W. Survey scans were initiated at 1200 eV and ended at 0 eV, with 1 eV steps and a dwell time of 100 ms. High resolution scans were performed around peaks of particular interest and their quantitative analysis was undertaken using the *Jandel Peakfit* software package. The XPS studies were performed by Dr. Barry Wood at University of Queensland, Brisbane, Australia.

5.3.5 Scanning tunnelling microscopy

Measurements of electronic properties of the molecular films were performed using *MultiMode Nanoscope SPM* by *Veeco International*. The experimental setup for investigations with STM is presented in Figure 5.18.

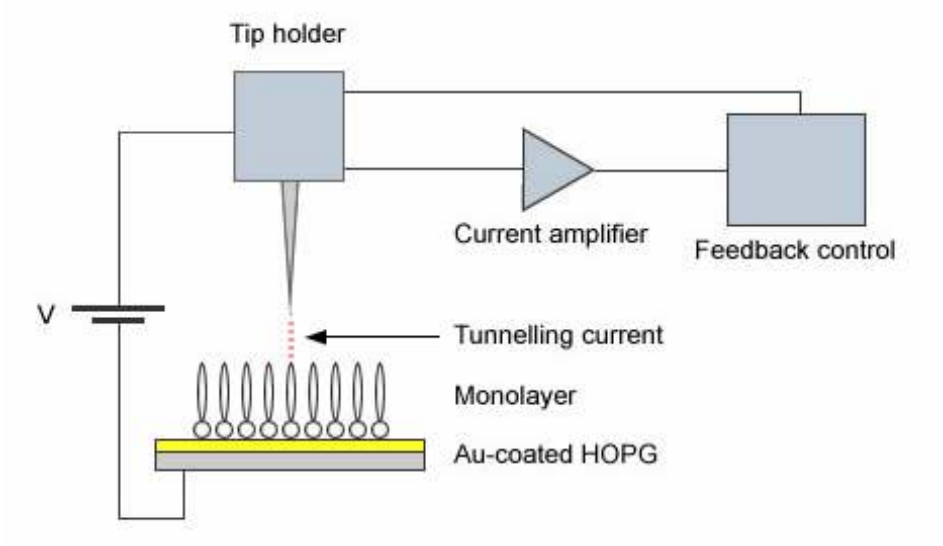

Figure 5.18 Experimental setup for STM used in obtaining I-V characteristics of samples.

The main part of the STM is the atomically sharp tip, which is placed into a holder very tightly to counteract any movement (see Figure 5.19). The holder is a part of the converter unit, which is responsible for minimising any vibrational noise transmission

to the tip. The converter head also contains a build-in preamplifier for tunnelling current to be processed. The tip unit is equipped with a piezoelectric system, which (in order to move the tip over the sample), can shrink or expanse in extremely small distances in the Z-direction (or bend in X or Y-direction), when the voltage bias is applied to it. There are many parameters which influence STM operation (applied bias, scan speed, size of imaged sample, initial tip-sample distance, etc.) and their control is guaranteed by the computer control unit.

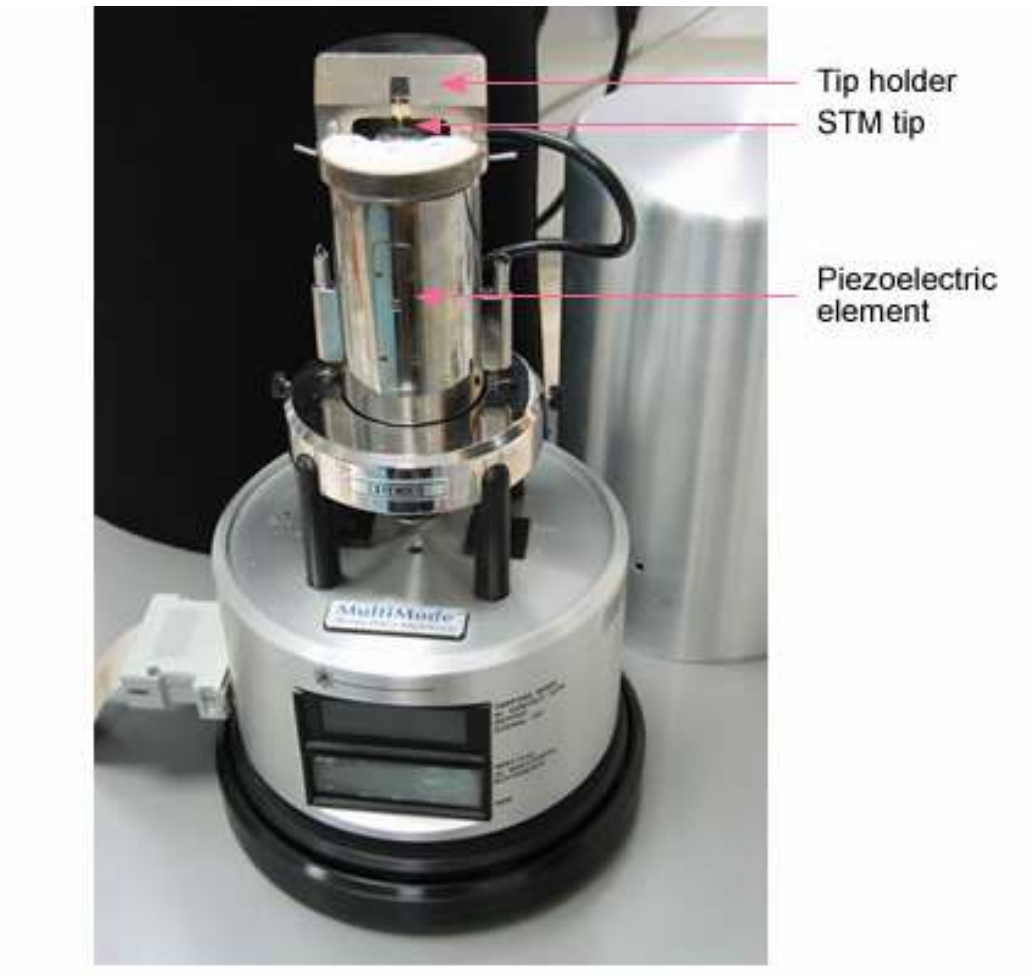

Figure 5.19 Photograph of STM head (*Veeco Instruments)* utilised for electrical measurements.

Parameters initiating the tunnelling were sample-dependent and fell into the range of 30 – 200 mV for bias voltage and 0.1 – 2.0 nA for current setpoint when aiming to observe I-V characteristics. They were measured under constant current mode, as

the sample surface was observed to exhibit some roughness as a result of evaporation of the bottom gold electrode. Part of STM measurements were performed in the constant high mode, for which the parameters were at stated in the Haiss method [131] (see also chapter 3.3).

Electrical measurements were performed at room temperature and in darkness. To ensure a better antivibrational environment, the setup was placed on a vibration isolation table manufactured by *Veeco International*. Samples were probed by two types of tips, which were chosen due to their improved atomic resolution and low reactivity in the air. PtIr tips were purchased from *Veeco International*, whereas Au tips were hand-made by precise cutting of a gold wire that were plasma and solvent cleaned. In cases where the tips were in direct contact with the bottom electrode, it was re-used and cleaned prior to use.

5.3.6 Molecular modelling

Molecular modelling was done using *Cerius Software* (Accelrys, Cambridge) and was applied in order to estimate the length and conformation of the investigated molecules. Amongst many available in the *Cerius MOPAC* package, the AM1 method seemed to be the most reliable for modelling molecules of dyes [204]. When compared with the experimental (X-ray), they appeared to be burdened with smaller mean error of bond lengths [205]. The method allowed modelling and measurement of distances, planes and angles, all structural features characteristic for molecules.

6 Results and discussion

6.1 LB films of Q3CNQ molecules

The precursor of the investigated molecules was $C_{16}H_{33}$-Q3CNQ, which could form LB films with high non-linear optical properties (*i.e.* second-order electrical susceptibility $\chi^{(2)}$ = 180 pm/V) [206]. As already discussed, this dye has also been considered for molecular rectification by many research groups (see Chapter 4.2.2), but the observed rectification was ambiguous due to certain factors, *e.g.* alignment of the molecules, nature of the molecular ground and excited states, etc. Therefore, measurements of the structural and electrical properties were performed again in order to verify all the doubts concerning the origin of the rectification.

Figure 6.1 shows surface pressure-area isotherms of $C_{16}H_{33}$-Q3CNQ molecules, which were deposited at the air-water interface from two dichloromethane solutions with different concentrations. Monolayers obtained from low-concentration solutions (0.008 - 0.012 mg cm^{-3}), formed a purple-coloured monolayer after evaporation of the solvent, and were characterised by an isotherm with three obvious phases. The collapse of this monolayer occurred at a surface pressure of $\pi_c \approx 42$ mN m^{-1}, where the area occupied by the molecule was *ca.* 0.34 nm^2 $molecule^{-1}$. A more concentrated solution (0.2 – 0.6 mg cm^{-3}) produced an isotherm showing more phase-complex structure (possible aggregation or dimer formation), with a plateau region at π = 6 – 8 mN/m, whose size depended on the concentration of the solution. In this case the collapse point was in the range of π_c = 36 – 38 nm^2 $molecule^{-1}$, with the values of area per molecule from 0.30 – 0.36 nm^2 $molecule^{-1}$. The data presented here are similar to previous reported by Ashwell *et al.* [206] who also observed the concentration-dependent isotherm shape for LB films of $C_{16}H_{33}$-Q3CNQ molecules.

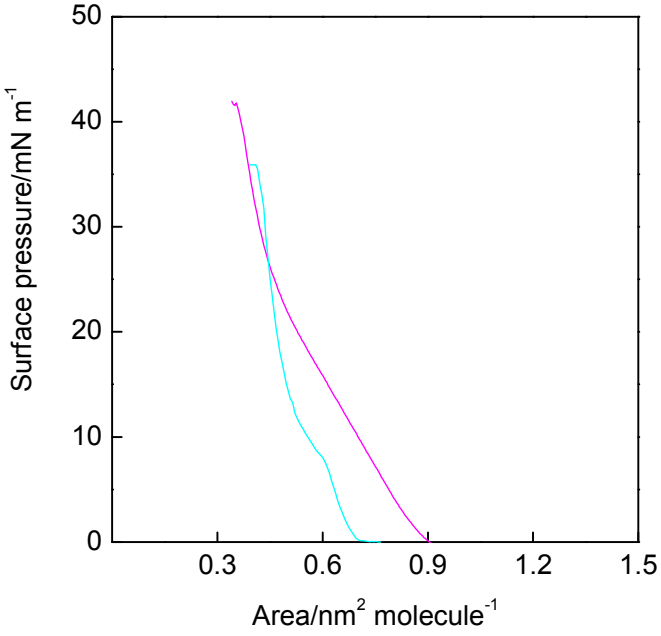

Figure 6.1 Surface pressure *vs.* area isotherms of $C_{16}H_{33}$-Q3CNQ deposited from dichloromethane solution at ambient temperature (23° C), showing two types of behaviour, dependent on the concentration of the solution: 0.011 mg cm^{-3} (magenta) and 0.045 mg cm^{-3}(cyan).

The influence of the concentration on the properties of the monolayer can be easily monitored using UV-Visible spectroscopy. In this case $C_{16}H_{33}$-Q3CNQ monolayers were deposited onto hydrophically treated glass slides, at pressures *ca.* π = 25 mN m^{-1}, which corresponded to the intersection of two isotherms. At this pressure, the molecules remain in the liquid phase regardless of the solution concentration. Visible spectra (see Figure 6.2) showed that films obtained from dilute solution were purple and had a sharp absorption band at 565 nm, whereas those obtained from concentrated solutions were blueish and exhibited a broader absorption band at 610 nm with an additional absorption peak at 670 nm. The difference in absorption spectra probably results from different alignment of the molecules within the monolayers and was previously proven using second-harmonic generation and SPR studies [206].

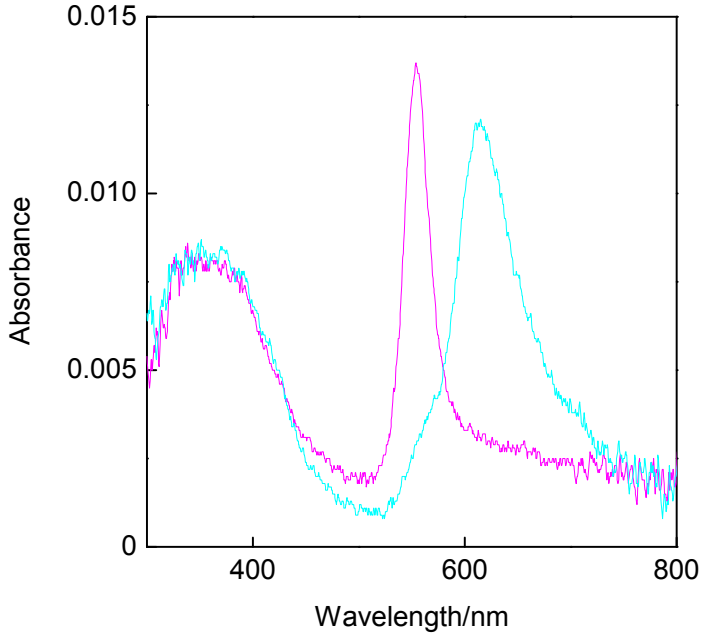

Figure 6.2 UV/visible spectra of LB monolayers of $C_{16}H_{33}$-Q3CNQ deposited on glass slide in transmission, showing two characteristic peaks of absorbance: λ_{max} = 565 nm (magenta) and 610 nm (cyan). Monolayers were deposited at the surface pressure of 25 mN m^{-1} and a speed of 0.6 mm s^{-1}.

SPR studies gave two different values of the film thickness for the two LB phases: 2.3 nm for the purple and 2.8 nm for the blue films, while SHG was active for the purple phase (second-order effective susceptibility of $\chi^{(2)}_{eff}$ = 75 pm/V at 1.064 μm) and almost inactive for the bluish phase. This indicates a non-centrosymmetric arrangement for purple films and centrosymmetric for blue, which concurred with previous data, *i.e.* centrosymmentric arrangement, with probable phase coexistence for short-chain homologues of Q3CNQ dyes (*eg.* $C_{10}H_{21}$-Q3CNQ) [206].

LB monolayer of $C_{16}H_{33}$-Q3CNQ molecule exhibited asymmetric characteristics in opposite quadrants of the I-V plot (see Figure 6.3). A rectification ratio of 8 at ±1 V, with high current in the positive quadrant signifies electron flow from the tip to the substrate, whereas a rectification ratio of 4 at ±1 V with the high current in the negative quadrant corresponds to electron flow from the substrate to the tip. The higher rectification in the positive direction was first seen by Ashwell and Sambles [166,167] in mono- and multilayers of $C_{16}H_{33}$-Q3CNQ when sandwiched between Mg and Pt

electrodes. This experiment was then repeated many times using different electrodes and different deposition techniques in order to eliminate any Schottky barrier [170], and some cases revealed higher current in the negative quadrant [172], similar to data observed in this case. Such anomalous rectifying behaviour was probably caused by high-disorder and phase-coexistence within the LB films. The physisorption of the LB films may not be strong enough to keep the molecules in the same orientation. That is why molecular reorientation, enhanced by the electric field, seems to explain the position of the I-V curves. There is also a possibility that polarisation induced changes in the molecular structure, from the quinoid to the zwitterionic form.

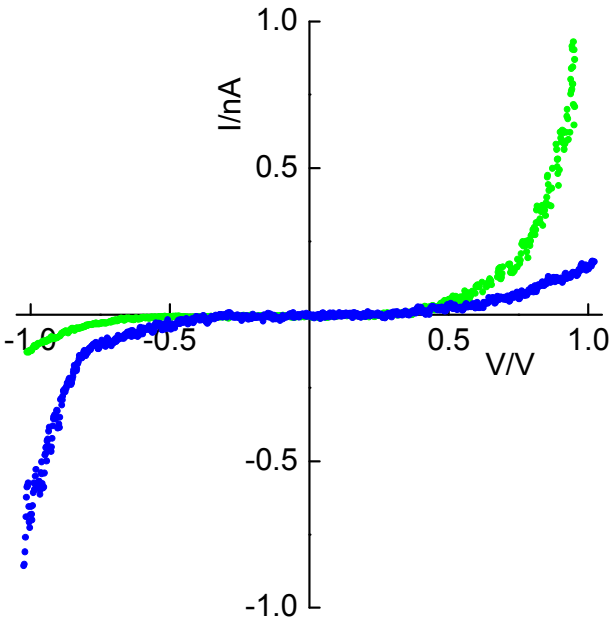

Figure 6.3 I-V characteristics of $C_{16}H_{33}$-Q3CNQ LB monolayers, showing weak rectification in opposite quadrants of the plot Rectification ratio = 8 (green) and 4 (blue) at ±1 V.

The nature of the ground state of Q3CNQ compounds has been the target of many discussions. Broo and Zerner [207,208] calculated the geometry for the Q3CNQ compounds and their pyridinium analogues (P3CNQ). They came to the conclusion that the ground state of both molecules was a resonance mixture between zwitterionic and quinoid forms. A few years later, Pickholtz and dos Santos [209] performed a

theoretical analysis of the relationship between structure and absorption spectra: quinonoid molecules of $C_{16}H_{33}$-Q3CNQ are present in LB films, and it takes a zwitterionic conformation when crystalline and when in acetonitrile solution. Similar experiments, performed by Metzger and co-workers [210], provided the same results when crystalline but opposite for LB films [175]. Investigations of the crystals were confirmed once more, whereas the orientation in LB films has been previously unconfirmed. As crystals, the molecules of $C_{16}H_{33}$-Q3CNQ adopted an antiparallel alignment [211] where the donor and acceptor groups of neighbouring molecules overlapped. Some overlap may also have occurred in the purple LB phase, where in spite of a parallel alignment, the tilt of the molecules (*ca.* 40° [175] from the surface normal) provided space for such a situation to happen (see Figure 6.4).

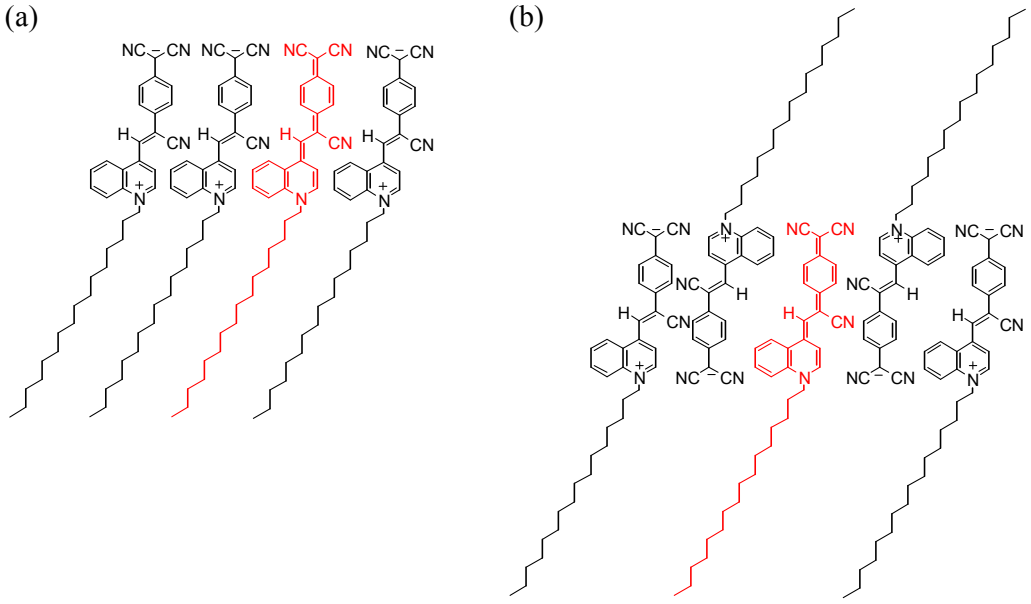

Figure 6.4 Possible molecular alignments of $C_{16}H_{33}$-Q3CNQ molecules within LB films, when bias is applied: (a) parallel alignment; (b) antiparallel alignment of molecules in both zwitterionic (black) and quinonoid (red) states. Antiparallel alignment shows possible interaction of oppositely charged molecules, which could influence (lower) rectifying properties of molecular films.

$C_{16}H_{33}$-Q3CNQ is not an ideal material to study in the context of molecular rectification, mostly because there are so many factors which can influence the electronic behaviour. The way to explain the behaviour and its asymmetry seems to lie

in the orientation of the molecules on the substrate. It is consistent with theoretical predictions, where the conductance of the molecules is strongly dependent on their orientation [14,212,213]. Consequently, self-assembled analogues of $C_{16}H_{33}$-Q3CNQ seem to generate better conditions for investigations and understanding their electrical properties. They are chemically bound to the substrate, and so eliminate field-induced reorientations of the molecules [214] what introduce better order than in the LB films. These results has been already published together with the results for SAMs of Q3CNQ molecules (chapter 6.2) and the information about article localization is given in chapter 8 (publication I).

6.2 SAMs of Q3CNQ molecules

SAMs of Q3CNQ compounds (see Figure 6.5) were obtained by immersion of the substrates into acetone or dichoromethane solutions of dyes with a concentration from 0.01 – 0.02 mg cm^{-3}. To facilitate the deposition process (reducing overall time) a few drops of ammonium hydroxide were added to the dye solution to displace the acetyl groups.

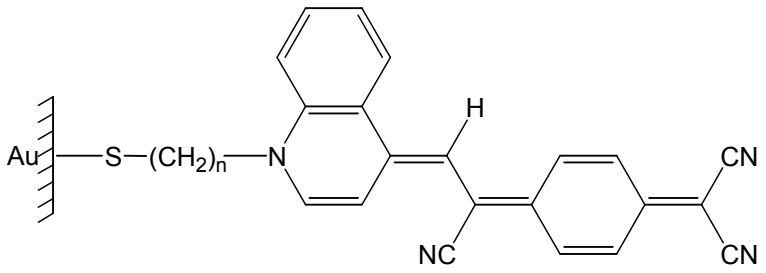

Figure 6.5 SAM of Q3CNQ molecules chemisorbed on gold; Au-S-C_nH_{2n}-Q3CNQ, n = 3, 6, 8, 10, 12

Monolayer characterisation studies, *i.e.* UV-Vis spectroscopy and QCM, proved that the whole series of Q3CNQ materials self-assembled onto gold very easily, with the mean area occupied by the molecules being 0.33 ± 0.03 nm^2 $molecule^{-1}$. Kinetics of SAM growth using dichloromethane was less erratic than observed for acetone solutions. However, for both solvents the mean area was in the same range. Examples of QCM

characteristics are presented in Figure 6.6. The area of 0.33 ± 0.03 nm^2 $molecule^{-1}$, characteristic for all analogues, is consistent with the van der Waals cross-section of the Q3CNQ moiety, which was also modelled using *Cerius* software. It reflects close and vertical packing of the molecules and good order within the films.

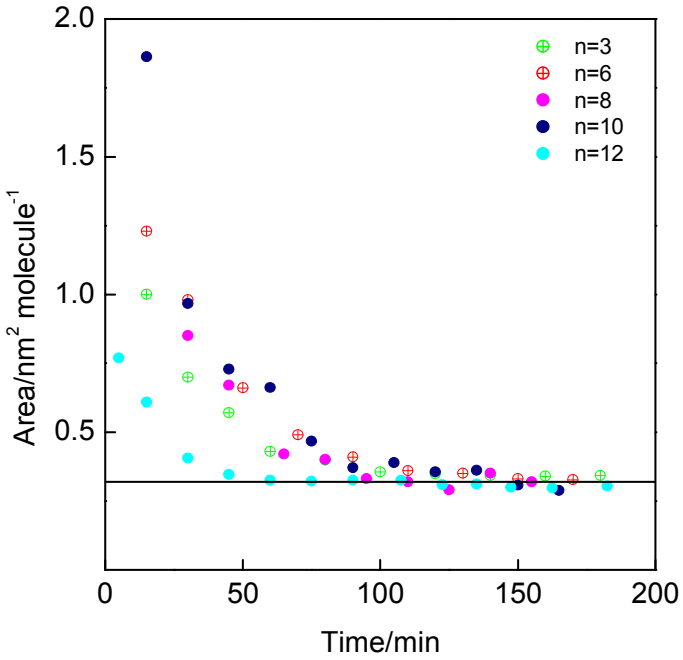

Figure 6.6 Kinetics of SAM formation on gold substrate with five analogues of Q3CNQ molecules; n – the number of methylene groups in the alkyl chain. QCM measurements for n=3 (green), 8 (magenta), 12 (cyan) were obtained by High [215]. Mean area occupied by the molecules, calculated by the 100% coverage of QCM crystal, was 0.33 ± 0.03 nm^2 $molecule^{-1}$.

Analysis of the SPR data, which estimates the thickness of the monolayer, also indicated vertical alignment of the molecules within the film. Figure 6.7 shows that the thickness increased with the length of the alkyl chain, from 1.70 ± 0.1 nm for the Au-S-C_3H_6-Q3CNQ analogue, to 2.44 ± 0.1 nm for the Au-S-$C_{12}H_{24}$-Q3CNQ analogue. Extrapolation to n=1, characteristic for a theoretical molecule with no chain, gives a thickness of *ca.* 1.5 nm, which is consistent with the molecular length between sulfur and the van der Waals surface of the $C(CN)_2$ group, provided by modelling studies. An increase of about 0.08 nm per CH_2 group suggests that the alkyl tail was tilted about 50º from the normal to the substrate to occupy the available area determined

by the wider chromophore cross-section. The angle differs from the value of 40° obtained by Metzger [175] for LB films of $C_{16}H_{33}$-Q3CNQ molecule by XPS technique. The difference in the tilt angle may suggest slightly different packing arrangements in the molecular films due to the different types of force linking molecules to the substrate: van der Waals in LB films and covalent bonding in SAMs.

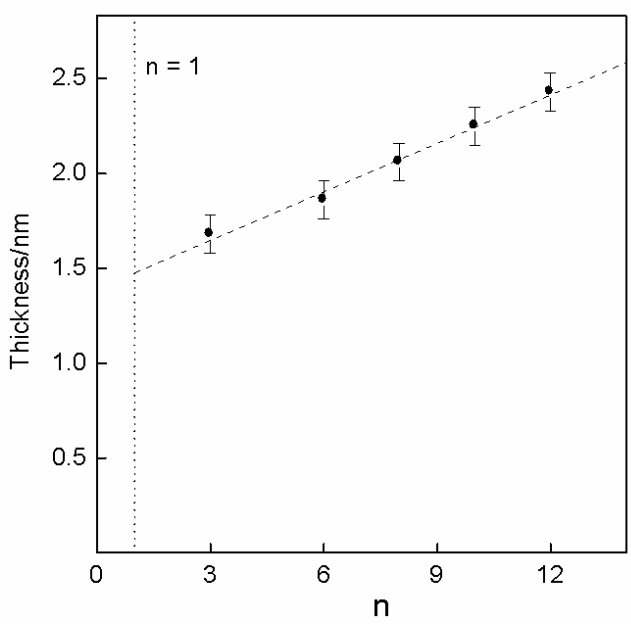

Figure 6.7 Monolayer thickness vs. n (n = the number of methylene groups in the alkyl chain) for Q3CNQ SAMs on gold-coated substrates. Extrapolation to n=1 gives a thickness of *ca.* 1.5 nm, which is consistent with the molecular length between sulfur and the van der Waals surface of the $C(CN)_2$ group. Experimental data were obtained in cooperation with High [215].

I-V characteristics (Figure 6.8) were obtained using Au or PtIr tips and initial tunnelling amounted to *ca.* 100 – 600 pA at 60 mV. All five analogues exhibited asymmetric characteristics with higher current at forward bias in the positive quadrant of the I-V plot. It signified electron flow from tip to substrate via the molecule, where the $C(CN)_2$ group was the acceptor and the heterocycle a donor. It confirmed that the ground state was quinoid rather than charge-separated zwitterionic (proposed by Metzger [170,171,175]), and supports the Aviram-Ratner model [14], and theoretical analysis done by Pickholtz and dos Santos [209].

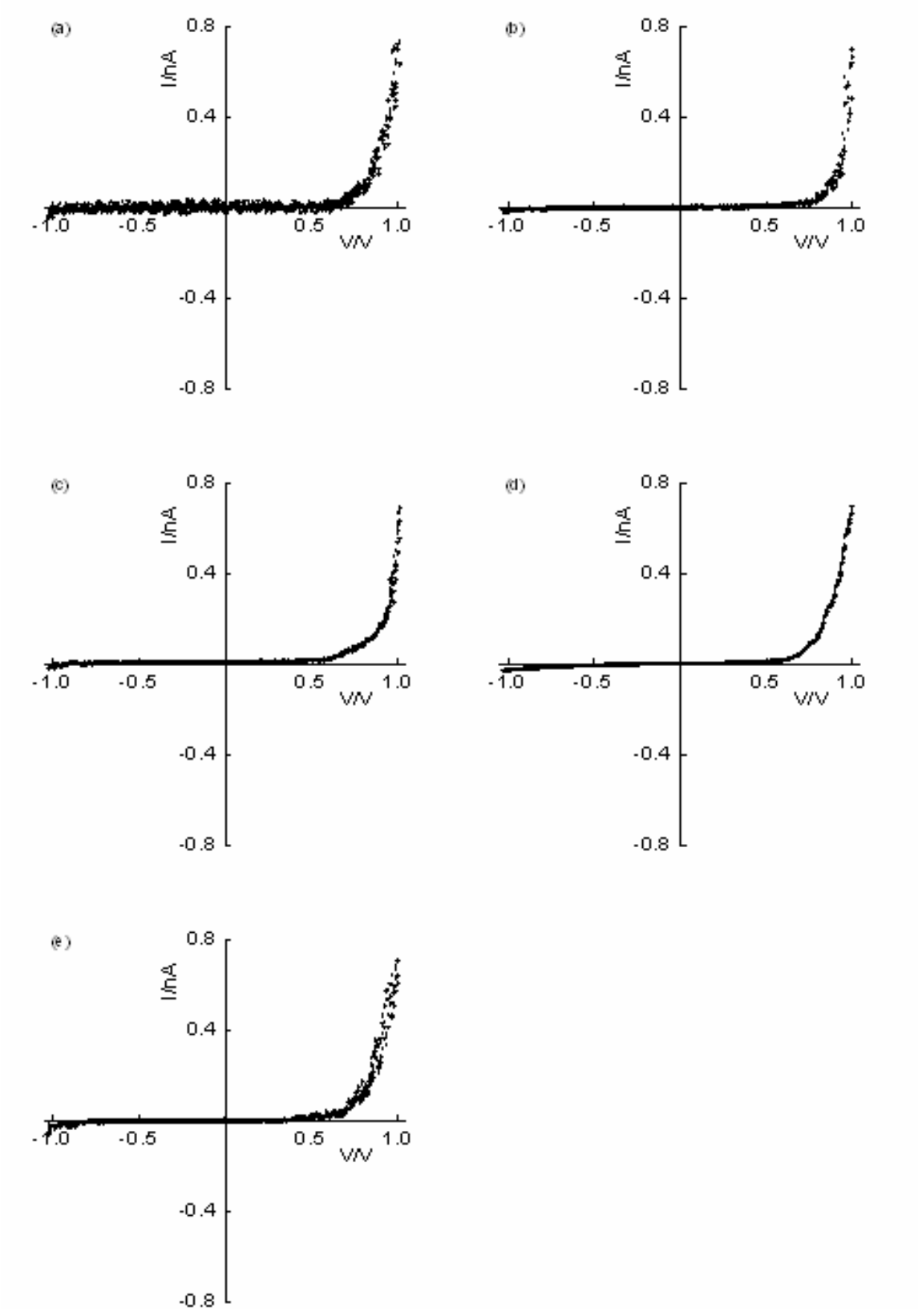

Figure 6.8 Asymmetric I-V plots of Au-S-C_nH_{2n}-Q3CNQ family: (a) n=3; (b) n=6; (c) n=8; (d) n=10; (e) n=12; where n – the number of methylene groups in the alkyl chain. Curve for Au-S-$C_{10}H_{20}$-Q3CNQ molecule was obtained by Hamilton by contacting a molecule with a tip coated with decanethiol [174].

Higher asymmetry of the I-V characteristics was observed for SAMs than for LB films of $C_{16}H_{33}$-Q3CNQ, which indicates better order within the films and the nature of the covalent bonding to the surface preventing molecular flipping under applied bias (characteristic for LB films). This concurs with the area, provided by QCM studies, of 0.33 ± 0.03 nm^2 $molecule^{-1}$, and suggests that in SAMs the molecules are closely packed and were lying side-by side in a parallel manner. The electrical asymmetry proved diode-like behaviour of SAMs of Q3CNQ, and so are ideal candidates for unimolecular rectifiers.

When comparing the I-V curves for the five analogues of Q3CNQ, there would appear to be little change in the shape. The only difference was seen for the Au-S-$C_{10}H_{20}$-Q3CNQ analogue. However, this was probably due to the different measurement method, as the molecule was contacted by a coated (decanethiol) gold tip [174,216]. Therefore, assuming that this molecule should behave the same as the remaining four, the only incompatibility in I-V characteristics occurred in the elbow region at about 0.5 V. This trend can be observed in Figure 6.9, showing the overlap of I-V characteristics for the two extreme analogues; Au-S-C_3H_6-Q3CNQ and Au-S-$C_{12}H_{24}$-Q3CNQ. These results do not support theoretical predictions proposed by Kornilovitch (chapter 4.1.2) and Krzeminski (see chapter 4.2.2). But it does agree with some recent investigations made by Lenfant *et al.* [217] that the current asymmetry arose from the molecular properties and so an increase of the rectification ratio should not be affected by lengthening the alkyl chain. Calculations of the rectification ratio showed that values of 20 – 30 at ±1 V were typical for every member of the Au-S-C_nH_{2n}-Q3CNQ family.

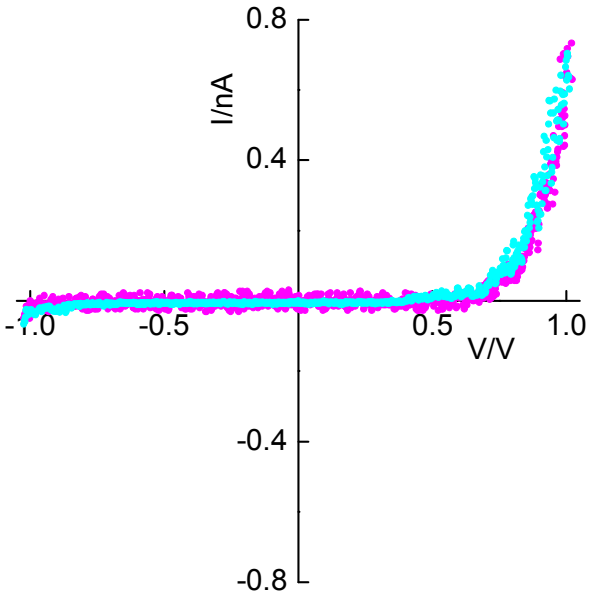

Figure 6.9 I-V plot with the same rectification ratio (~ 30 at ±1 V), showing overlap of two extreme analogues of Q3CNQ molecules: Au-S-C_3H_6-Q3CNQ (magenta) and Au-S-$C_{12}H_{24}$-Q3CNQ (cyan), which suggest that the asymmetric position of the molecule between the electrodes has a negligible effect on the rectifying behaviour of the molecule.

6.2.1 Protonation method

SAMs of Q3CNQ compounds seemed to be stable in the air as I-V measurements of the same sample after two months revealed only a slight suppression of the asymmetry. Therefore, the alignment within the SAM is stable in the air over time. However, the $C(CN)_2$ group can be easily protonated by acidic media, which can affect the donor-acceptor character of the molecule and thus affect the electronic properties. With respect to the quinoid molecular ground state, the molecule should strive to achieve a charge-separated zwitterionic state when protonated. A demonstation of a potential molecular structure after protonation is presented in Figure 6.10. Hydrogen from the HCl is attracted by the dicyanomethanide group (acceptor). At the same time, on the other side of the chromophore, rearrangement of chemical bonds occurs, which results in a cationic structure.

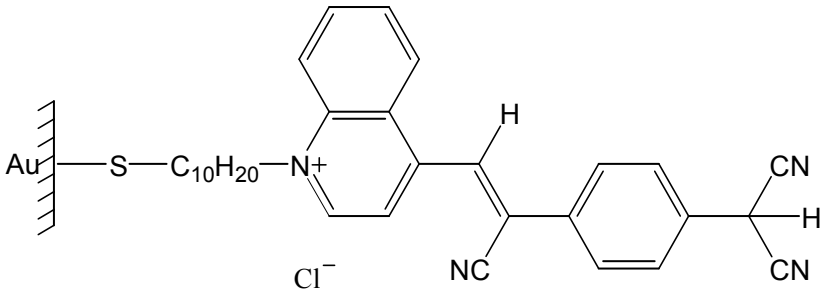

Figure 6.10 Probable molecular structure of Au-S-$C_{10}H_{20}$-Q3CNQ after protonation with HCl vapours.

Consequently, observation of the Au-S-$C_{10}H_{20}$-Q3CNQ molecule after exposure to HCl vapours for 3 – 5 seconds resulted in suppression of the asymmetry of the I-V characteristics (see Figure 6.11). This was connected to a disruption of the intramolecular charge-transfer process (molecule losing its push-pull properties) and was confirmed by protonation of the $SCOCH_3$-$C_{10}H_{20}$-Q3CNQ in solution. UV-Vis spectrum of the solution revealed a vanishing CT band at 570 nm.

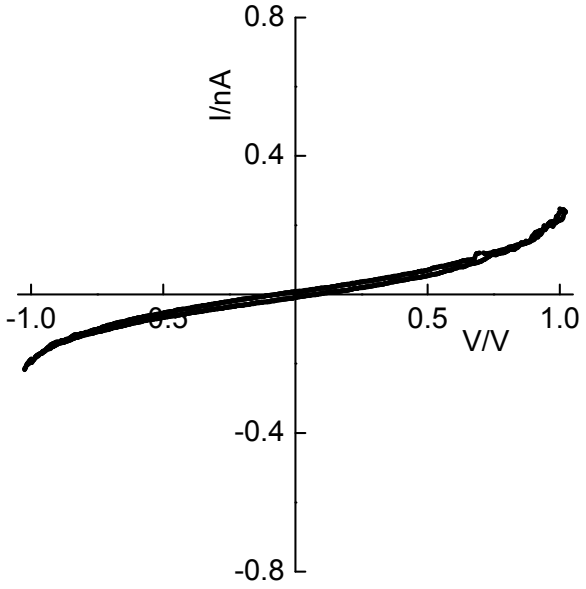

Figure 6.11 Symmetrical I-V characteristic for SAM of Au-S-$C_{10}H_{20}$-Q3CNQ as a result of protonation of the chromophore using HCl vapour.

Similar experimental procedures were used by other researchers for studying the nature of electrical asymmetry. Ashwell *at al.* [174] investigated SAMs of hemicyanine dyes and remarked a change in I-V curves from asymmetric to symmetric as a result of acidic

protonation. Other experiments were performed by Yu *et al.* [188], who observed a reversible change in asymmetry of I-V curves by protonation/deprotonation of some diblock oligomers with $HClO_4$ (see chapter 4.2.3).

The possibility of reversible off-on switching of the diode-like behaviour of the molecule proves that the rectification originates from the D-π-A character of the molecule and so supports the Aviram and Ratner model. Therefore, the Kornilovitch theory that rectification was induced by an asymmetrically positioned conjugated moiety (relative to the electrodes), is not true in the case of Q3CNQ molecules. These revelations have been already published and are of great scientific importance in the molecular rectification field. The details about publications can be found in chapter 8 (publication I).

6.2.2 Single-molecule measurements

To reveal the nature of the ground state, further electrical investigations were performed. Au-S-C_8H_{16}-Q3CNQ (on gold-coated HOPG) was investigated, using Haiss's method [131] of measuring electrical conductivity of single molecules with an STM 'break junction' (see chapter 3.3). The principles of this technique rely on locating the tip just above the surface at a fixed height, which allowed the observation of current jumps each time the tip contacted a single molecule. Such measurements were possible with these molecules in particular since the ―CN groups (placed in the protruding acceptor moiety) exhibit high affinity to the gold. Therefore, direct single contact between the Au STM tip and a molecule was possible.

Samples for an STM 'break junction' were prepared on gold-coated HOPG and probed by an Au tip, which was in plasma cleaner and rinsed with standard solvents. To ensure that the monolayer was present on the gold surface, I-V characteristics were measured first and samples with electrical behaviour similar to the previous study were studied

further. Only two samples were investigated. However, the Au tip probed their surfaces in at least five different areas to prove reproducible electrical behaviour along the whole monolayer.

Single-molecule studies were performed by monitoring the single molecule current as a function of time. For this purpose the tip-sample distance was unchanged by switching from STM mode (constant distance) to constant height mode. Measurements were held at the relatively low surface bias of 0.3 V. A reflection of tip-single molecule contact via the —CN group as a tunneling current jump is shown in Figure 6.12.

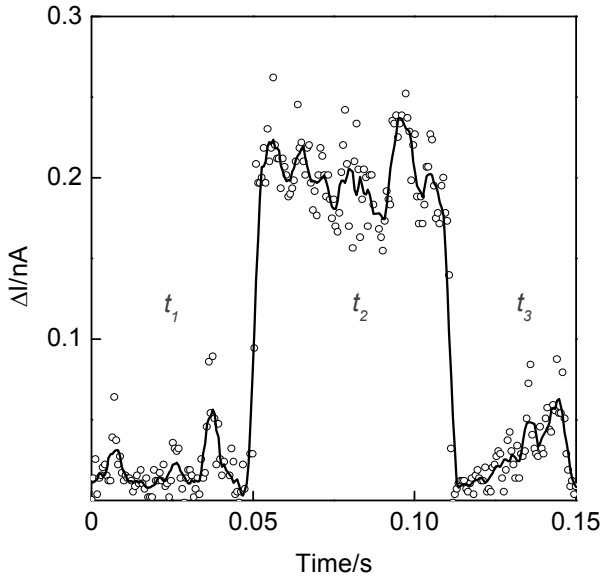

Figure 6.12 Characteristic current jump of Au-S-C_8H_{16}-Q3CNQ observed at forward bias of 0.3V. Open circles correspond to experimental data whereas the solid line (formed from the average of five data points) approximates its shape and height. At t_1 and t_3 molecule is not contacted by the tip whereas at t_2 direct contact occurs leading to the rise of current from 0 to 0.2 nA.

The STM 'break junction' method seemed to work effectively for Au-S-C_8H_{16}-Q3CNQ analogue, as the observed current jumps were reproducible for each place that was probed by an Au tip. The adsorption process persisted for 0.06 ± 0.02 s for the most observable current jump, that is 0.20 ± 0.01 nA at 300 mV. It can be assumed that every time a 0.2 nA current jump appeared, the tip was contacting a single molecule.

Observations of direct molecular contact allowed construction of a histogram showing all recorded current jumps. The histogram of 836 current jumps is shown in Figure 6.13 and its periodic current jump feature can be noticed. As mentioned before, the most observable current jump was 0.2 nA (at 300 mV), which constitutes only 22 % of all registered. This does not seem a lot, but because measurements were taken with a 0.05 s frequency the percentage may not be a true reflection.

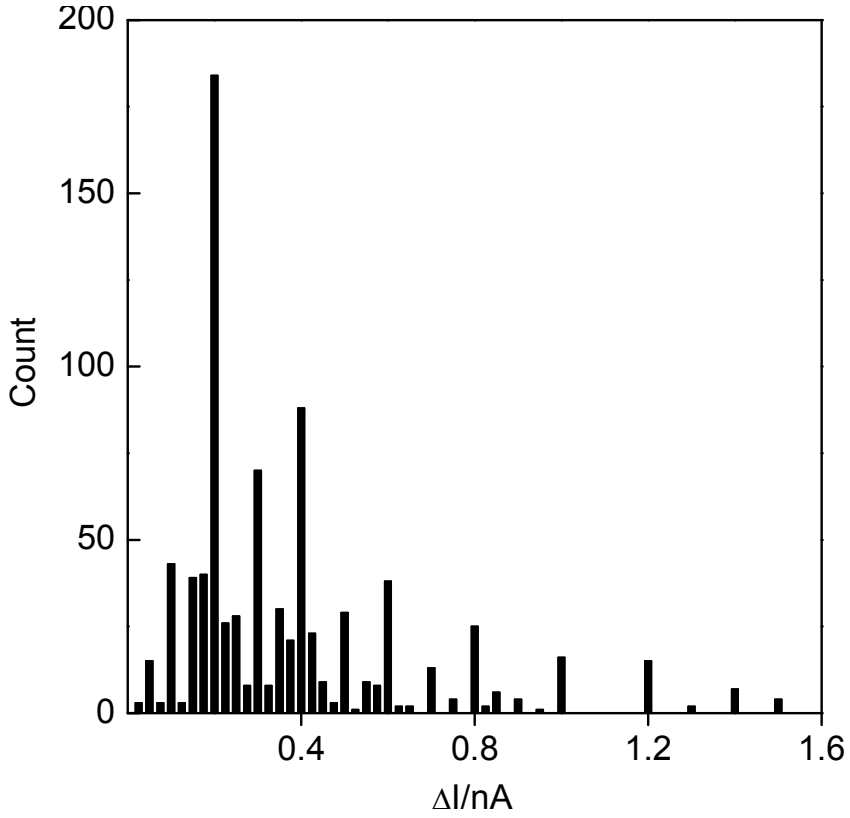

Figure 6.13 Histogram of 836 current jumps shown as a dependence of the frequency appear versus the magnitude of current change.

Figure 6.14 shows the statistics for the most frequent current jumps in which 0.2 nA constitutes more than 50 %. Half of this number was represented by current jumps of 0.4 ± 0.02 nA at 300 mV, which can be attributed to a situation in which the tip probes not one but two molecules. This seems highly probable, as the current value was twice as large when compared with single-molecule contact. So, it could be assumed that for other higher current peaks, the STM tip probes higher numbers of molecules.

In this case a current jump of 0.6 nA ± 0.02 nA at 300 mV could reflect three-molecule contact. The situation is uncertain for the higher current jumps, which constitute 7 and 5 %. Their appearance could be attributed to four and five-molecule contact. However, if these statistics were examined by the magnitude of the current jump in respect of the doubling current, then 0.1 nA, 0.2 nA, 0.4 nA, 0.8 nA current jumps would correspond to singe, two-, three- and four-molecule contact respectively.

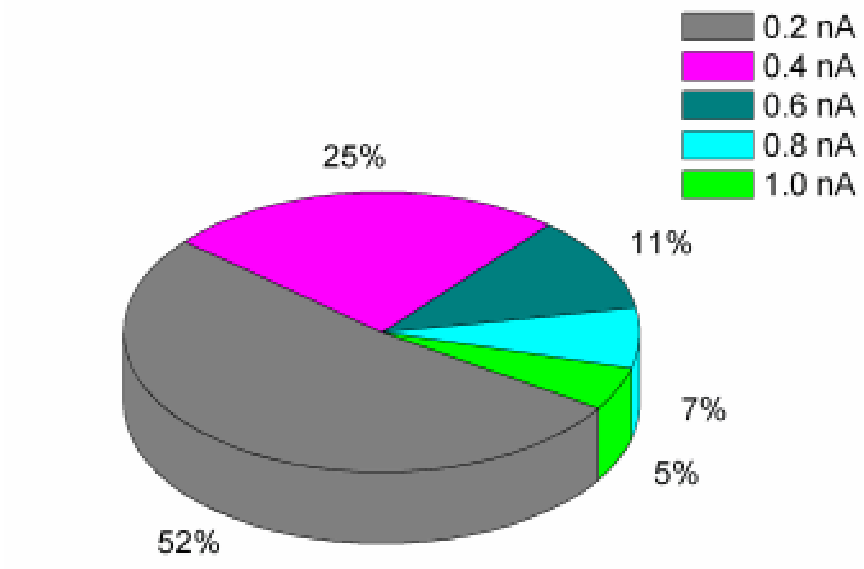

Figure 6.14 Statistics of the most frequent current jumps corresponding to single molecule contact (0.2 nA), two-molecule contact (0.4 nA) and more.

Although, the STM break junction is a relatively new technique, it has been used successfully for measurement of molecular wires [70,131]. The appearance of characteristic multi-contact events resulting in a rise of current jump events was also observed. Haiss [131] and Ashwell [70] observed trapping two, three and more molecules with an STM tip. Therefore, it can be assumed that such contact can definitely appear in molecular D-(π-bridge)-A systems, although it is less favourable than single-molecule contact.

6.2.3 Summary

Reproducible electrical behaviour by measuring I-V characteristics was observed for all Au-S-C_nH_{2n}-Q3CNQ structures. It was proven to be independent on the length of the alkyl-chain, (linking the molecule to the bottom electrode), as each film exhibited similar electrical asymmetry and therefore a similar range of rectification ratios. Furthermore, protonation of the dicyanomethanide group of the acceptor resulted in suppression of the rectifying behaviour suggesting that rectification was strictly connected with the internal donor-acceptor character of the molecule. These revelations resulted in the publication.

Although not discussed here[*], further spectroscopic studies involving Raman and infrared spectra of Au-S-C_8H_{16}-Q3CNQ were performed with the cooperation with Prof. A. Girlando from Parma University, Italy. (Publication in preparation, see V in chapter 8). Spectral analysis of SAMs showed that monolayers deposited on thick gold layers (*ca.* 200 nm) were in the zwitterionic ground state, whereas those formed on thin gold substrates (*ca.* 40 nm) were more neutral (quinoid state). These results suggest that such anomalous behaviour could result from varying surface roughness, which the packing of Q3CNQ molecules can be very sensitive to (compare results for LB films of $C_{16}H_{33}$-Q3CNQ in chapter LB films). Thicker surfaces are probably more jagged and despite molecules being aligned in a parallel manner, they have much more space for tilt and possible mutual interaction. However, detailed clarification of such statements must be supported by surface roughness studies, for example with AFM. It seems a necessity, especially as the difference in the thickness of the gold layers was not large. It may be worthwhile to consider spectroscopic and electrical studies over a broader thickness range. Mrkich *et al.* found that the minimum thickness of gold required to obtain a complete layer was about 12 nm [218]. Additionally, flame annealing will be useful for

[*] Molecules were investigated with STM in exactly the same manner as before with samples that exhibited rectifying behaviour being sent to Italy for further (spectroscopic) studies. Afterwards, the samples were sent back to double check that their electrical properties had not changed over time (3 – 5 months).

roughness studies, as it makes the gold surface smoother [219] and significantly easier to image.

Further electrical measurements, incorporating the STM break-junction method, was used for the first time in the determination of single D-(π-bridge)-A molecules, seemed to work effectively. The electrical properties of Au-S-C_8H_{16}-Q3CNQ molecules, registered as I-V characteristics and current jumps, were reproducible and the polarity for rectification was consistent with that suggested by the Aviram-Ratner model. They also confirmed the nature of the molecular ground state of Q3CNQ molecules in SAMs, appeared to be quinoid.

6.3 SAMs of P3CNQ molecules

The aim of designing pyridinium analogues of zwitterionic compounds was the verification of the impact of steric hinderance in D-(π-bridge)-A molecules on the rectifying behaviour. Results for SAMs of hemicyanine dyes [87,183,184,201], for which I-V characteristics were asymmetric for sterically hindered molecules, and more symmetric for more planar molecules, were the reason for such studies. In comparison to Au-S-C_nH_{2n}-Q3CNQ, these molecules have less stearic hindrance between donor and acceptor groups, which would imply a weaker rectification result. This behaviour has been proved to be true for SAMs of donor-(π-bridge)-acceptor P3CNQ molecules and resulted in a publication (publication II, chapter 8) designated as a 'Hot Article' and as a 'Top Ten Article' by the Royal Society of Chemistry in 2004.

SAMs on gold-coated substrates were prepared in the same manner as for Q3CNQ, compounds, and deposition occurred in acetone solutions with a concentration of *ca.* 0.01 ± 0.002 mg cm^{-3}. The kinetics of the growth of the SAM was monitored by QCM and SPR, whereas electrical properties were monitored by STM using PtIr tips.

6.3.1 Planar pyridinium molecules

Only the ten-carbon analogue (Au-S-$C_{10}H_{20}$-P3CNQ) of this type of molecule was investigated (see Figure 6.15) because the shorter derivative (Au-S-C_3H_6-Q3CNQ) was found to be almost insoluble in all available solvents and its deposition was erratic and difficult to repeat.

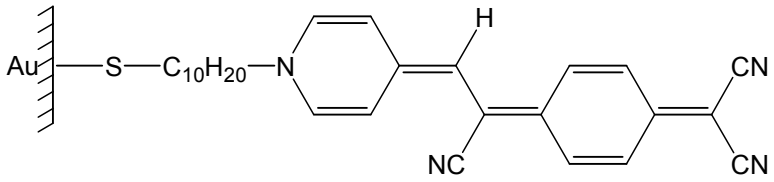

Figure 6.15 SAM of pyridinium molecule chemisorbed on gold; Au-S-$C_{10}H_{20}$-P3CNQ.

QCM studies were performed for five crystals and deposition, similar to Q3CNQ, lasted about three hours with the mean area reaching values of *ca.* 0.27 ± 0.02 nm^2 $molecule^{-1}$ (see Figure 6.16). This value was characteristic for all samples investigated, each of which was prepared from a fresh acetone solution. The value of the mean areas was slightly smaller than for the Au-S-$C_{10}H_{20}$-Q3CNQ. However, this was expected due to the lack of the second benzene ring within the heterocycle. SPR results showed similar behaviour for thickness, which in this case was 1.93 ± 0.2 nm, whereas the thickness of the quinolinium dye amounted to *ca.* 2.20 ± 0.2 nm. This difference proves that the pyridinium chromophore took up less space than the quinolinium moiety, but the molecules were still packed vertically and closely within the monolayer.

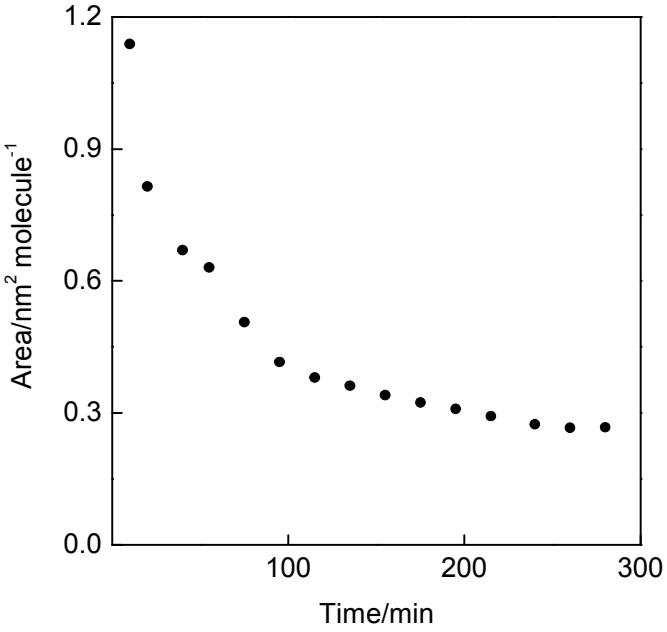

Figure 6.16 Area *versus* immersion time for Au-S-$C_{10}H_{20}$-P3CNQ; 0.27 ± 0.02 nm^2 $molecule^{-1}$ after *ca.* 250 min.

STM studies of Au-S-$C_{10}H_{20}$-P3CNQ were straightforward and the registered I-V plots were symmetrical (see Figure 6.17). Only one sample (from the four studied) presented slight asymmetry (rectification ratio of *ca.* 3.5 at ±1 V) in the negative quadrant of the I-V plot. Such behaviour was characteristic for the STM technique and may be tip-induced rather than molecular in nature. Symmetry of the I-V characteristics was a result of a planar (or nearly planar) structure of the chromophore. Molecular modelling procedures revealed a 5° angle between the donor and acceptor moieties. It seemed to support the theory that electrical rectification was not possible from D-(π-bridge)-A molecules without significant out-of-plane rotation. It also signifies that the Kornilovitch model of molecular rectification arising from asymmetrical coupling molecule to the electrodes did not apply.

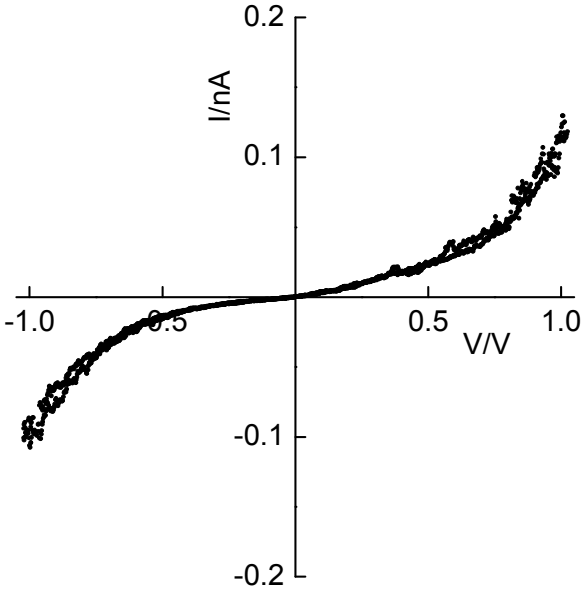

Figure 6.17 Symmetrical I-V characteristics of a planar Au-S-$C_{10}H_{20}$-P3CNQ monolayer.

6.3.2 Lutidinium molecules

Lutidinium molecules (see Figure 6.18), differed from planar Au-S-$C_{10}H_{20}$-P3CNQ by the presence of an extra 3-methyl substituent on the heterocyclic group. They were investigated in the same manner as Q3CNQ molecules.

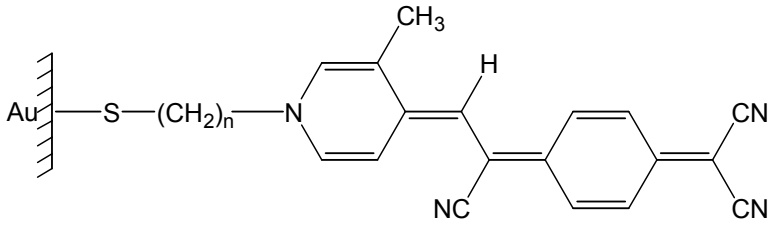

Figure 6.18 SAM of lutidinium molecules; lutidinium Au-S-C_nH_{2n}-P3CNQ, n =3, 10 (n – the number of methylene groups in the alkyl chain).

QCM studies of lutidinium Au-S-$C_{10}H_{20}$-P3CNQ analogue showed that the time required to obtain a complete monolayer was *ca.* 230 mins. This value was similar to those obtained for Au-S-$C_{10}H_{20}$-P3CNQ molecules, and was expected as both analogues possessed the same alkyl chain, which linked them to the substrate. However, the kinetics for the growth of a SAM of lutidinium Au-S-C_3H_6-P3CNQ turned out to be

shorter, which signifies that molecules possessing shorter chains adsorb on the gold surface faster. (This was not observed for the Q3CNQ molecules. Though that might be due to the different concentration of solutions used here to those used by High, see Figure 6.6). However, it was probably caused by heating of the solution to a temperature of *ca.* 35° in order to increase the solubility of the sample in acetone. The kinetics for the growth of a SAM of both lutidinium analogues are presented in Figure 6.19.

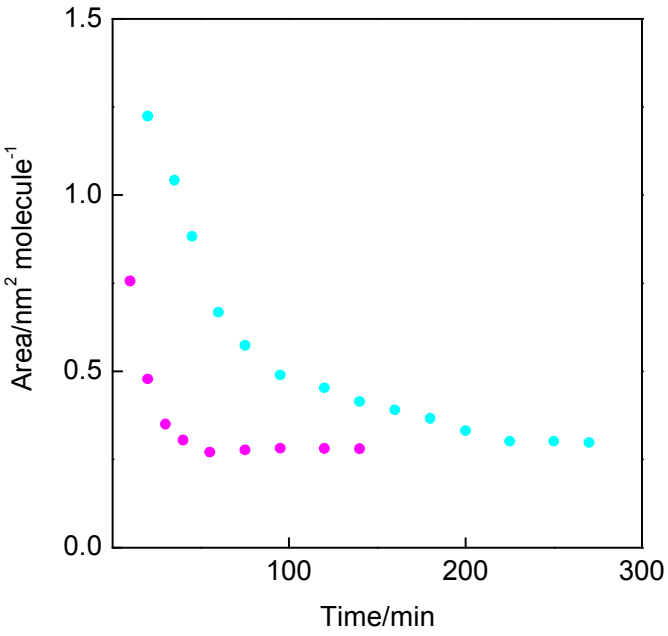

Figure 6.19 Kinetics of SAM deposition for lutidinium Au-S-C_nH_{2n}-P3CNQ, monitored with QCM technique; n = 3 (magenta) and n = 10 (cyan), n – the number of methylene groups in the alkyl chain. Mean area occupied by the molecules amounted to 0.29 ± 0.1 nm^2 molecule^{-1}.

QCM studies provided a value of the area per molecule of lutidinium compounds, which was 0.29 ± 0.1 nm^2 molecule^{-1}. This value constitutes an average of six measurements (three for each molecule) and is an intermediate value between films of Au-S-C_nH_{2n}-Q3CNQ and Au-S-$C_{10}H_{20}$-P3CNQ. This can be attributed to the presence of the 3-methyl substituent on the heterocycle, which expanded the cross-section of the chromophore in comparison with planar Au-S-$C_{10}H_{20}$-P3CNQ structures.

The SPR analysis confirmed an up-right alignment of the molecules within the monolayer, which gave a thickness of 1.7 ± 0.1 nm for lutidinium Au-S-C_3H_6-P3CNQ and 2.2 ± 0.1 nm for lutidinium Au-S-$C_{10}H_{20}$-P3CNQ (SPR data were provided by High [215]). These values are almost identical for the same analogues of Q3CNQ (Au-S-C_3H_6-Q3CNQ and Au-S-$C_{10}H_{20}$-Q3CNQ) and it can be assumed that molecules aligned in the molecular films in a similar fashion to the quinolinium analogues.

STM studies of both molecules showed that the I-V characteristics (see Figure 6.20) were asymmetrical when contacted by PtIr tips with a maximum rectification ratio of 12 at ±1 V, characteristic for both molecules. Rectifying behaviour was similar to that observed for Q3CNQ compounds: higher current at forward bias in the positive quadrant signifying initiation of the electron flow at the tip electrode. The direction of the electron flow seems to be in general agreement with the Aviram-Ratner model.

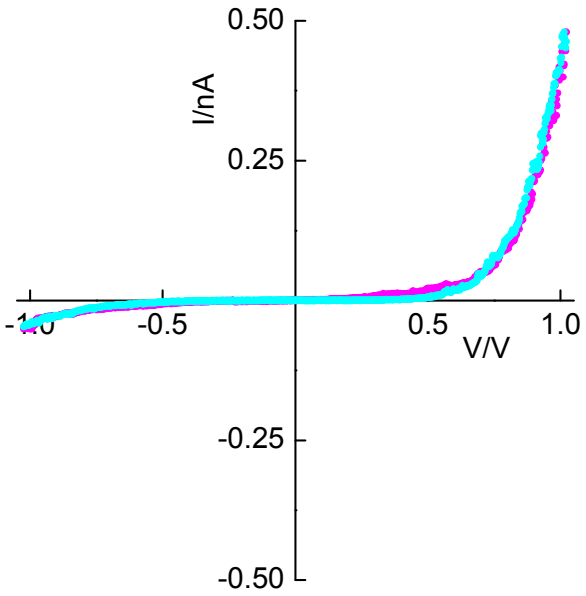

Figure 6.20 Overlapping of I-V characteristics obtained for lutidinium Au-S-C_nH_{2n}-P3CNQ suggesting similar electrical properties; n = 3 (magenta) and n = 10 (cyan), n – the number of methylene groups in the alkyl chain. Maximum observed rectification ratio was 12 at ±1 V.

According to the Kornilovitch theory (see chapter 4.1.2), molecules which are asymmetrically placed with respect to the electrodes should rectify current and its magnitude can be changed by altering the lengths of the insulators connecting the molecule to the electrodes. Although both lutidinium chromophores were coupled to the electrodes asymmetrically, and their alkyl chains were different, I-V characteristics overlapped entirely. Hence, the Kornilovitch proposal appeared to be irrelevant for these zwitterionic molecules. For the purpose of this thesis the curves were normalised. However, the range of the current was 0.5 – 0.8 nA for both analogues.

Further STM investigations concerned protonation of the SAM of lutidinium Au-S-$C_{10}H_{20}$-P3CNQ molecules, which resulted in the suppression of the asymmetry of the I-V curves. Because —$C(CN)_2$ group can be easily protonated, an attempt of deprotonation with basic media was resolved. Ammonia treatment of the SAM for 6 s did not influence the I-V characteristics at all. However, another attempt (on the same sample) for 5 s resulted in the re-establishment of the electrical asymmetry, but the shape of the I-V characteristics was altered (see Figure 6.21).

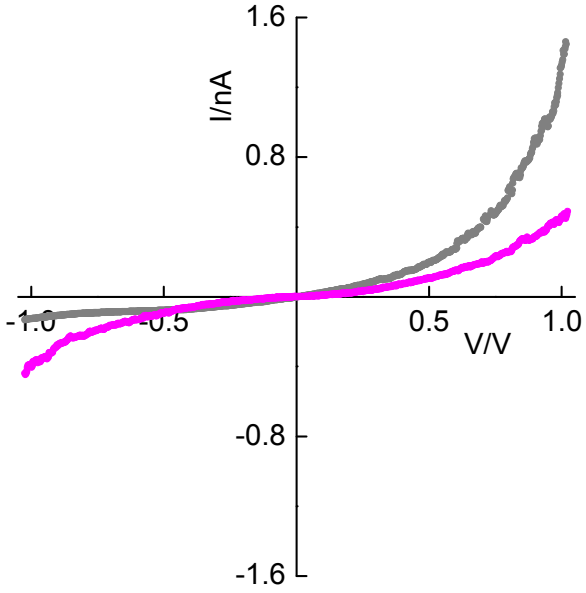

Figure 6.21 Protonation and deprotonation of the SAM of lutidinium Au-S-$C_{10}H_{20}$-P3CNQ with acid and base vapour caused symmetry (magenta) and restored the asymmetry (grey) of the I-V characteristics, respectively.

To verify these results a solution containing molecules of lutidinium $CH_3C(O)S$-$C_{10}H_{20}$-P3CNQ was subjected to acid-base treatment with the results presented in Figure 6.22. A charge-transfer band was located at about 625 nm for lutidinium $CH_3C(O)S$-$C_{10}H_{20}$-P3CNQ in acetonitrile solution. When a few drops of acid were released into solution, the whole molecule lost its push-pull character. It was observed as a reduction in the CT peak intensity (magenta curve) and therefore a loss of the electrical asymmetry. The opposite situation was observed when a few drops of ammonia were added to the dye solution. The CT band was activated and the I-V characteristics became asymmetrical again. However, in this case, the CT band was shifted by *ca.* 30 nm towards the shorter wavelength suggesting that the molecular ground state was now different.

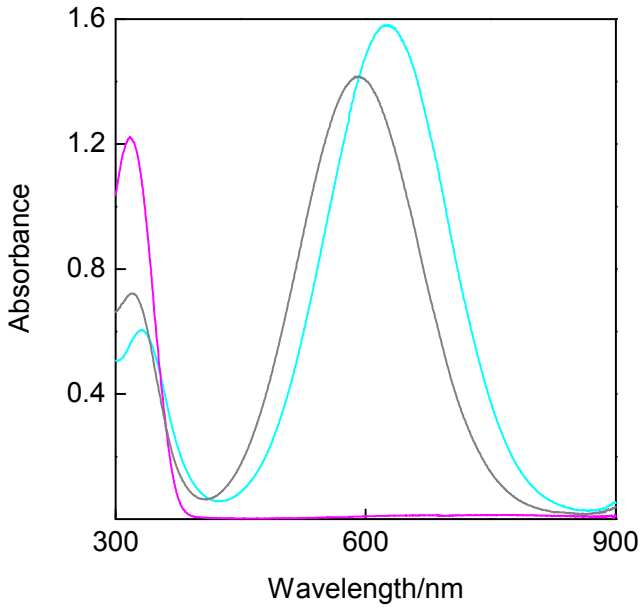

Figure 6.22 Acid-base treatment of lutidinium $CH_3C(O)S$-$C_{10}H_{20}$-P3CNQ molecule in acetonitrile solution resulting in suppression (magenta) of the intramolecular charge-transfer band at 625 nm, characteristic for molecules in clean solvent (cyan). The process can be reversed by adding a few drops of ammonia, to result in the appearance of a charge-transfer band at 595 nm (grey).

When considering the changed shape of the I-V characteristics after treatment of a monolayer with ammonia it could be connected with a different molecular ground state. However, this state must possess push-pull character to influence asymmetry of

the I-V characteristics. This can be explained by creation of the radical anions of the molecule which eventually led to formation of a charge-separated zwitterionic form rather than quinoind. This seemed to be probable as a shift in the absorption band from quinoid to charge-separated was observed previously [175]. The other explanation may lie in the presence of residual amounts of halide from the previous treatment (with acid), which could have reacted with ammonia and created a salt. This salt, if not rinsed with water, could reside within the molecular film and influence the electric properties.

6.3.3 Other pyridinium compounds

Another P3CNQ analogue (see Figure 6.23) was investigated in order to understand the dependence between steric hinderance and electrical proprieties. Similarly to lutidinium Au-S-C_3H_6-P3CNQ was not easily soluble and so was difficult to deposit. Therefore, deposition (with no ammonium hydroxide) of the solution was carried out in order to prepare the monolayers for further studies.

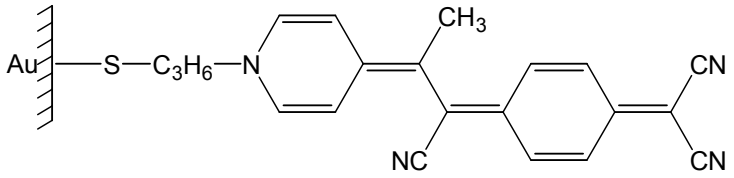

Figure 6.23 SAM of Au-S-C_3H_6-P3(Me)CNQ.

Kinetics of the deposition of $CH_3C(O)S$-C_3H_6-P3(Me)CNQ on gold was monitored with the QCM (see Figure 6.24). Optimum deposition of Au-S-C_3H_6-P3(Me)CNQ on QCM (five different samples) was achieved after *ca.* 7 – 8 hours with the mean area being 0.26 ± 0.03 nm^2 molecule^{-1} (see Figure 6.24). The values were similar to those obtained for the planar analogue of P3CNQ, and relative to the van der Waals cross-section of the chromophore, so indicating vertical packing within the molecular film.

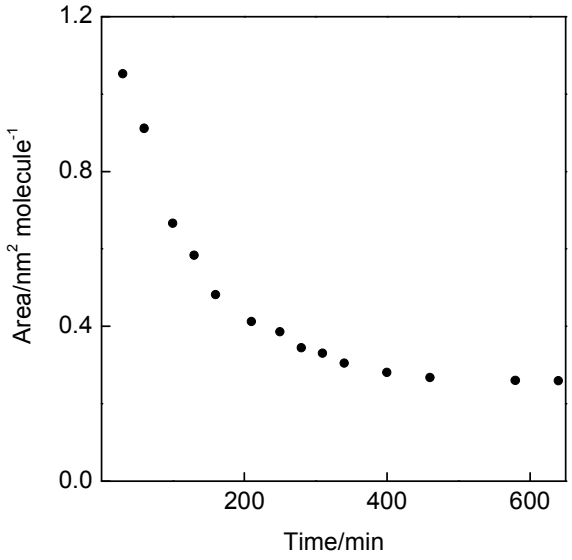

Figure 6.24 Mean area *vs.* immersion time for Au-S-C_3H_6-P3(Me)CNQ; 0.26 ± 0.03 nm^2 molecule^{-1} after *ca.* 8h.

Molecular modelling of this structure showed the torsion angle between donor and acceptor planes to be *ca*. 12°. Similarly to the previous zwitterions, it can be assumed that the Au-S-C_3H_6-P3(Me)CNQ molecule should rectify current, but its magnitude should be smaller according to the internal properties of this molecule. Such behaviour was proven by STM studies of four samples, using both PtIr and Au tips. Direction of electron transport was the same as for all previous zwitterions, confirming that they are very stable structures, in which the mechanism of conduction of the current follows Aviram-Ratner predictions.

Rectification ratio for the measured samples reached was from 7 to 9 at ±1 V and can be compared with planar molecule of Au-S-$C_{10}H_{20}$-P3CNQ, showing that mutual out-of plane rotation of the donor and acceptor moieties was necessary for designing D-(π-bridge)-A rectifiers.

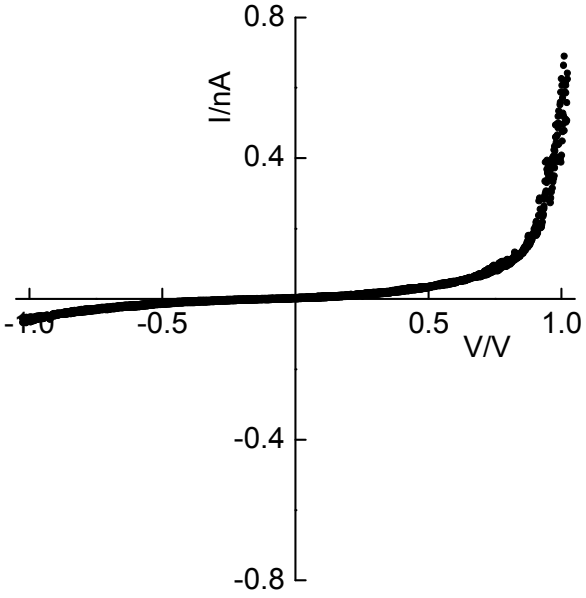

Figure 6.25 Typical I-V characteristics obtained for Au-S-C_3H_6-P3(Me)CNQ monolayer assembled on gold and contacted by Au or PtIr tip. Typical rectification ratio was 7 – 9 at ±1 V.

In order to ascertain if the protonation had similar impact on the Au-S-C_3H_6-P3(Me)CNQ monolayer (as on lutidinium Au-S-$C_{10}H_{20}$-P3CNQ), acid-base treatment was performed on two samples. In both cases a monolayer was easily protonated, which resulted in symmetrical I-V characteristics. However, the reverse process (ammonia) caused disruption of the monolayer with similar I-V characteristics as observed for lutidinium analogue. The CT for the solution of Au-S-C_3H_6-P3(Me)CNQ in acetonitrile solution (see Figure 6.26) band was blue-shifted from 565 nm to 530 nm.

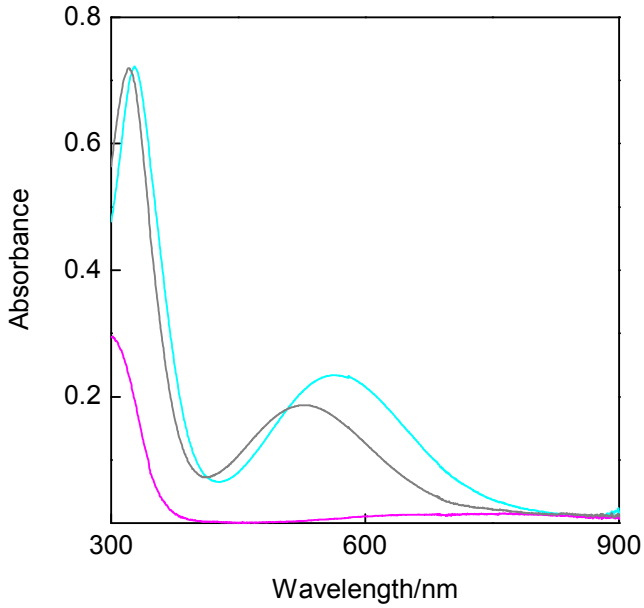

Figure 6.26 UV-Vis spectra showing protonation (magenta) and deprotonation (λ_{max} = 530 nm; grey) effect on molecules of $CH_3C(O)S$-C_3H_6-P3CNQ in the acetonitrile solution. Cyan curve (λ_{max} = 565 nm) corresponds to the molecules in fresh solution.

6.3.4 Summary

SAMs of P3CNQ were observed to behave as molecular diodes, only as long as steric hinderance enforced out-of-plane rotation of the donor and acceptor moieties. Different linking groups (C_3H_6 and $C_{10}H_{20}$) of lutidinium Au-S-C_3H_6-P3CNQ appeared to have no effect on their electrical properties. The direction of the electron flow for all rectifying analogues was in accordance with the Aviram-Ratner model; this was from cathode (tip) to the acceptor, and from the donor to the substrate anode. The switching behaviour was indicative of the disruption of the donor-acceptor combination when the dicyanomethanide group was protonated with acid media. This was accompanied by decolorisation of the solution. All these features are characteristic of all zwitterionic compounds (Q3CNQ and P3CNQ) when assembled in SAMs.

6.4 Double-leg zwitterions

Double-leg Q3CNQ compounds were synthesised unexpectedly in an attempt to investigate molecular rectification from quinolinium zwitterions with different acceptor groups. The synthesis resulted in a series of molecules containing a single acceptor and two donor groups with two potential attachment points [215]. Therefore, there are several ways in which a molecule of double-leg Q3CNQ molecules could align on the surface. During monolayer formation the individual could attach by one, or both legs. Molecular modelling showed that one attachment was preferable, where a molecule was aligned in a similar manner as one-leg Q3CNQ with the alkyl chain tilted and the chromophore perpendicular to the substrate. If a bilayer structure was formed it would occur via creation of an S—S bond at the ends of spare tails (see Figure 6.27) or by partial physisorption of molecules on top of the first monolayer. If so, molecules would adopt a parallel alignment with the protruding Q3CNQ part or, antiparallel alignment in which the Q3CNQ of the second layer orients over Q3CNQ of the first layer.

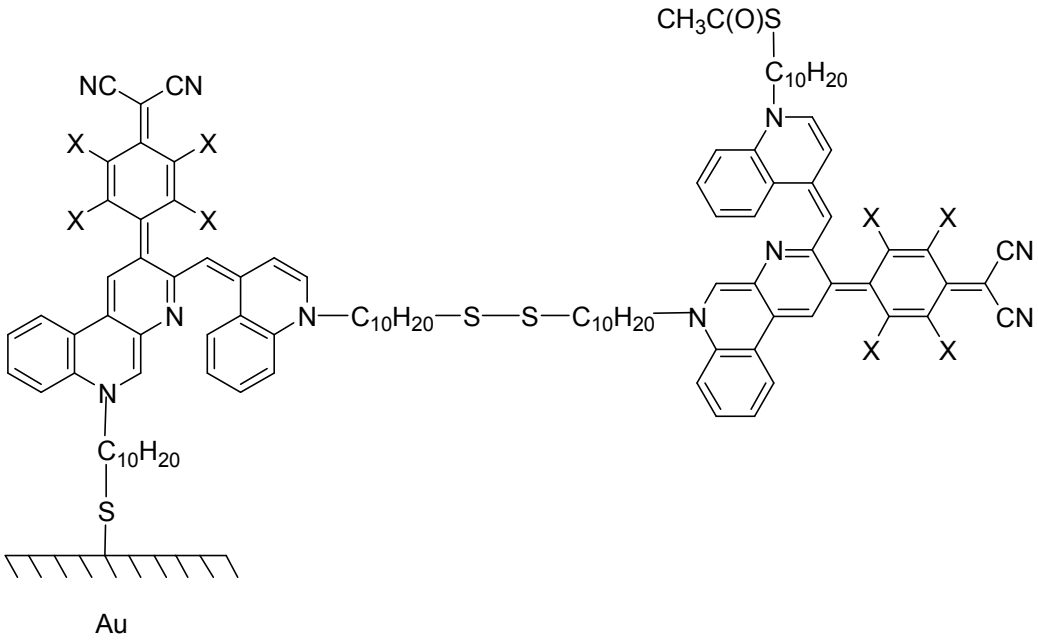

Figure 6.27 Schematic presentation of bilayer formation by double-leg Q3CNQ molecules; X = F ($TCNQF_4$) or CH_3 (TMTCNQ).

The deposition of the TMTCNQ onto QCM and gold-coated HOPG was performed in a similar manner to previous zwitterionic dyes, via use of ammonia to displace the acetyl groups. It resulted in deposition (see Figure 6.28) which reached completion after *ca.* 300 mins. This time was twice as long than that required for Au-S-$C_{10}H_{20}$-Q3CNQ monolayer, when deposited from a solution of the same concentration (0.1 mg cm^{-3}). This would imply that the double-leg molecules need twice as long to form a monolayer. However, the mean area was significantly higher at 1.10 ± 0.01 nm^2 $molecule^{-1}$, compared to 0.33 nm^2 $molecule^{-1}$ for (one-leg) Au-S-$C_{10}H_{20}$-Q3CNQ. This value suggests that a bilayer rather than a monolayer was formed during deposition of TMTCNQ, and SPR studies confirmed this tendency [220]. The thickness of TMTCNQ films was about 3.5 ± 0.2 nm, compared to 2.3 nm for a one-leg monolayer, which constitutes a significant difference (about 30 % rise of in thickness value).

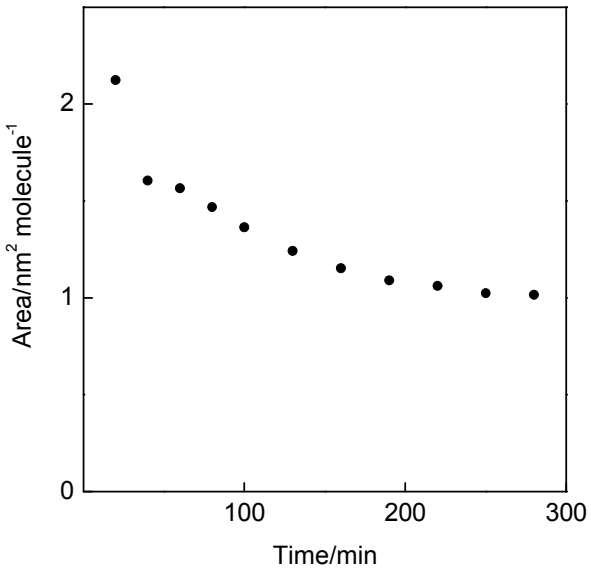

Figure 6.28 Kinetics of SAM deposition of TMTCNQ analogue on QCM. Mean area occupied by the molecule was 1.10 ± 0.01 nm^2 $molecule^{-1}$.

Observation of the the electrical properties of TMTCNQ films showed both symmetrical and asymmetric I-V characteristics (Figure 6.29). They were present in every sample studied and their appearance was dependent on the area of the studied sample. Asymmetrical curves corresponded to the same alignment of chromophores in

the second layer as in the bottom layer, while symmetrical behaviour was due to molecules aligned with the donor group sticking upwards from the second layer. The situation is reminiscent of the anomalous behaviour in LB films of $C_{16}H_{33}$-Q3CNQ, and does not seem to be anything unusual for this type of material.

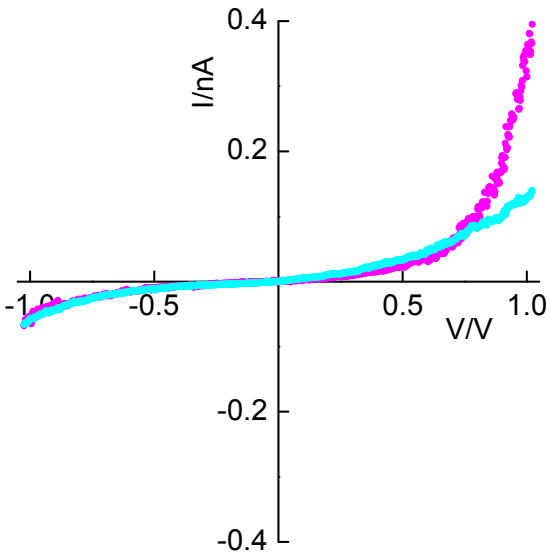

Figure 6.29 I-V characteristic for TMTCNQ analogue of double-leg zwitterions with sample-dependent rectification ratio of 12 at ±1 V (magenta) and 2.5 at ±1 V (cyan) suggesting parallel and antiparallel molecular alignment within bilayer structure.

Ashwell and Mohib [184] observed the creation of the bilayer structure for some SAMs of hemicyanines via S—S bond formation. Molecules (see molecular structure in Figure 4.19 c) created a monolayer with rectification ratio up to 150 at ±1 V, whereas the bilayer structure was characterised by almost symmetrical I-V curves with rectification ratio of 2 at ±1 V. Such a small value of RR suggested antiparallel molecular arrangements. Therefore symmetrical and asymmetrical I-V characteristics of TMTCNQ SAMs analogue can be explained by the antiparallel and parallel alignment of the chromophores within the film.

QCM studies of the $TCNQF_4$ SAMs revealed that the addition of ammonia to the dye solution caused a decrease in the resonant frequency to no more than 20 MHz. Considering this frequency value, calculation of the area for a single molecule

(with only one attachment point), gave a minimum area of *ca.* 2.2 nm^2 $molecule^{-1}$. This may suggest multilayer formation and to avoid it no ammonia was used for further investigations of molecular films. It resulted in longer deposition times and affected the molecular area. From the samples studied (four), an average area 1.0 nm^2 $molecule^{-1}$ (Figure 6.30) was recorded. It may suggest that molecules aligned in exactly the same manner as for TMTCNQ analogues.

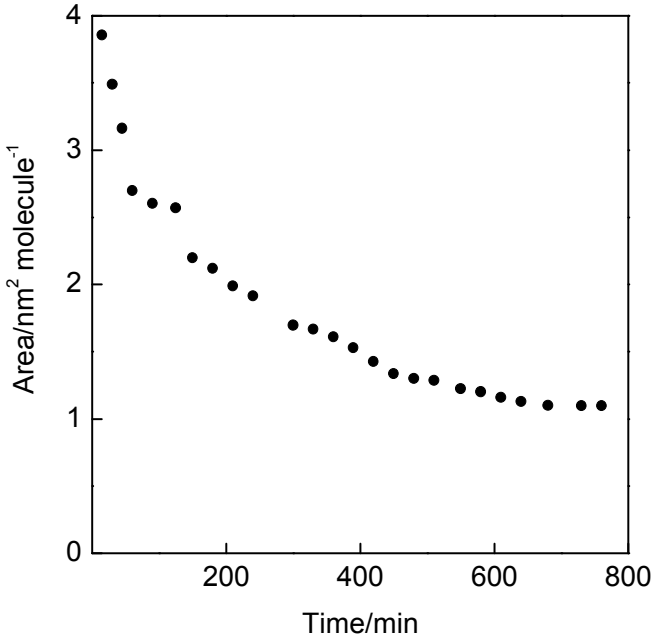

Figure 6.30 Molecular area *vs.* total period of immersion of a QCM in $TCNQF_4$ solution. Area occupied by a molecule in a complete monolayer was *ca.* 1.0 nm^2 $molecule^{-1}$.

Deposition without use of ammonia took longer, but this did allow the production of a clear spectrum of $TCNQF_4$ monolayer on Pt-coated glass slide (see Figure 6.31). Such behaviour was probably connected with ammonia-free forced rearrangement of the molecules, which were packed more closely in $TCNQF_4$ monolayers (compared to TMTCNQ) and therefore easier to detect by the spectrophotometer. UV-Vis spectrum of the monolayer revealed a significant peak at *ca.* 580 nm. This was not too far from the charge-transfer band, characteristic for this molecule in acetonitrile solution *ca.* 590 nm (see Figure 6.33).

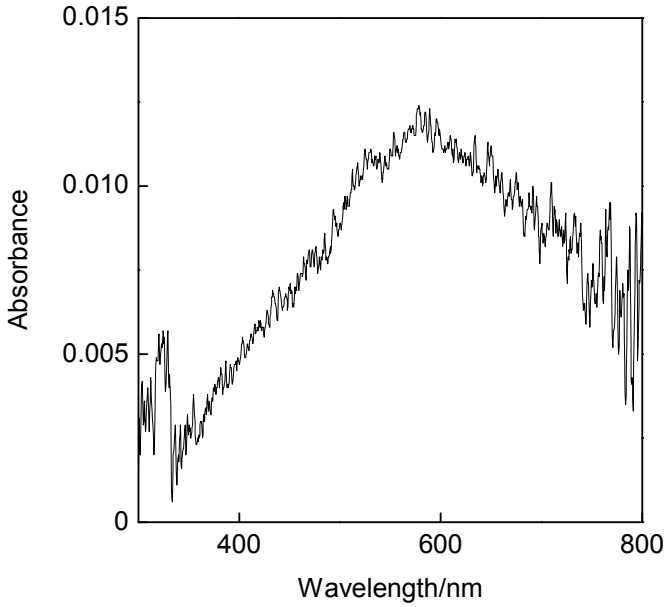

Figure 6.31 UV-Vis spectrum of $TCNQF_4$ molecules, obtained on Pt-coated substrate in transmission. λ_{max} = 580 nm.

Electrical studies of $TCNQF_4$ revealed only asymmetric I-V characteristics, with higher current observed in the positive quadrant of the plot (see Figure 6.32). This signified electron flow from tip to the substrate via SAM, starting from the fluorine acceptor. The range of the observed rectification ratio covered values from 10 to 18 at ±1 V and was sample-dependent. Considering, the closely-packed structure of $TCNQF_4$ in which molecules did not have so much space for rearrangement, the value of 18 at ±1 V may correspond to parallel alignment of the molecules, which were less exposed to polarisation-induced changes. The value of 10 at ± 1V may result from slightly more tilted molecules in the molecular film, which would affect the mutual alignment of the molecules in both mono- and bilayer structure.

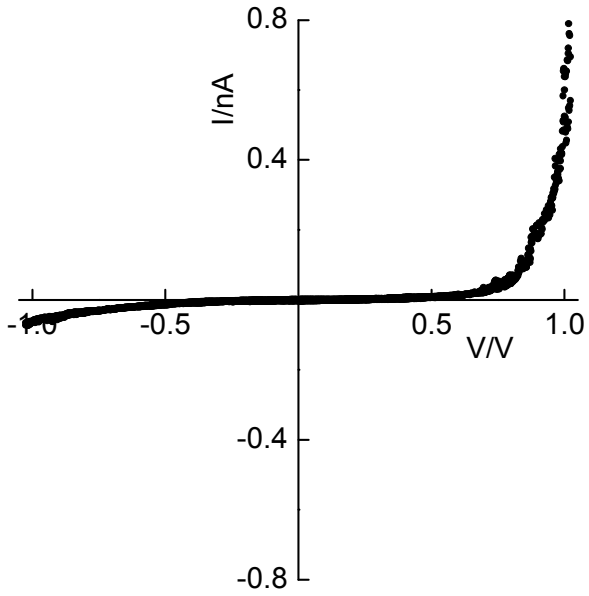

Figure 6.32 Typical asymmetric I-V characteristic observed for SAM of $TCNQF_4$ on gold-coated HOPG. The range of RR was between 10 – 18 at ±1 V.

Chemical switching of the $TCNQF_4$ molecules with acid and base yielded similar behaviour to the rectifying Q3CNQ monolayers. However, $TCNQF_4$ seemed to be more resistant to continuous on-off switching. For the lutidinium Au-S-C_nH_{2n}-P3CNQ analogue, the protonation process may have resulted in the production of a salt, which was difficult to remove from the monolayer and which strongly affected the I-V characteristics. Such behaviour was not observed for the $TCNQF_4$ analogue after three off-on switching cycles of the monolayer on Au-coated substrates and in solution (Figure 6.33). A reason for this may lie in the molecular structure. There is the possibility that during protonation, one of the nitrogens present in the heterocyclic legs was attacked rather than one in the acceptor group. This would be more probable if the molecule possessed a partial radical ion, which was shown to be possible by Metzger *et al.* [175] for one-leg Q3CNQ molecules. In the molecular film, when nitrogen from the donor was attacked as a result of protonation, the molecule would still retain its donor-acceptor character (by having a second donor).

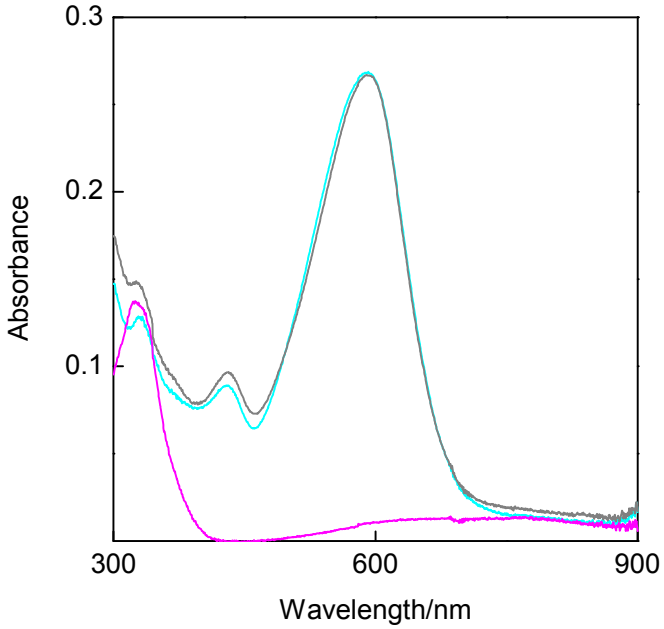

Figure 6.33 UV-Vis spectra of $TCNQF_4$ analogue in solution before HCl exposure (cyan), after HCl exposure (magenta) and after exposure to ammonia (grey); λ_{max} = 590 nm.

6.4.1 Summary

When considering rectification ratio values, the results obtained for both analogues seemed to be reliable. The highest rectification ratio was expected from the $TCNQF_4$ analogue, because it had a stronger fluorine-substituted acceptor then TMTCNQ. Therefore, the ammonia complicity in the level of order in molecular films was a moot point. On the one hand, the QCM results showed similar areas per molecule that would suggest similar molecular alignments. However, the number of the molecules in the molecular film was significantly smaller for TMTCNQ analogues (no UV-Vis spectra) due to ammonia use.

There is a need for further investigations of TMTCNQ and $TCNQF_4$ molecules in order to understand their molecular alignment, chemical nature and electrical properties. Because they are analogues of one-leg compounds it was assumed that they also existed in quinoid molecular ground state, especially when the I-V characteristics showed the higher current in the positive quadrant of the I-V plot.

The protonation of all members of zwitterionic family allow their SAMs to be utilised in developing new systems for gas sensing applications. The organic-based ammonia sensors are very desirable because they can be very sensitive, exhibit fast and reversible response even at room temperatures [221]. These are their main assets when compared to the traditional metal oxide semiconductor based gas sensors which operate at high temperature (350° - 450° C) and hence suffer from the lack of high sensitivity and high selectivity. The other benefit of utilising organic molecules for commercial sensor devices is the low production cost and the organic synthesis can certainly produce large amount of molecules with desired functionalities for sensors applications.

Both, Q3CNQ and P3CNQ molecules were proved to work as ammonia sensors as exposure to ammonia vapours led to the deprotonation of the studied chromophores resulting in the colour change. In particular, double-leg molecules in which reversible operation (off-on switching) could be repeated many times and what is more important be performed at room temperatures. The determination of gaseous ammonia is important in clinical and environmental monitoring, as ammonia is one of the primary irritants to humans [222].

6.5 Ionic films of cationic dyes

The idea of incorporating two molecules into a single molecular system came from the desire to decrease the need for complex synthesis for unimolecular rectifiers. The rectifiers are structurally very complicated molecules and the process of making them can take a multiple step synthesis, often yielding only small amounts of the product. This section shows a new efficient method of preparing ordered monolayers for molecular rectification, which is the first step towards molecular assembly excluding traditional chemical reaction. For this purpose the ionic assembly method of utilising simple cationic D-(π-bridge)-A molecules, rather than polymers, was utilised. A few examples were described in section 4.2.4. However they dealt with different molecular systems (phthalocyanines).

Only four cationic dyes were under investigation and their choice was dictated by their known molecular and electrical properties when deposited as SAMs. These parameters are shown in Table 3, and constitute a reference for the molecular properties investigated in this chapter. There appears to be a correlation between rectification ratio and dihedral angle signifying the importance of the cationic dyes constituting the top layer whereas two different self-assembled thiols were used for formation of the (ordered) bottom anionic surface, relative to the bottom (gold) electrode. Molecules of thiols were studied by the same techniques in order to prove their negligible participation in the electrical properties.

Table 3 Comparison of fundamental parameters, describing structural and electrical properties of cationic hemicyanines in SAMs.

Molecule	Symbol	Dihedral angle (^{0})	Rectification ratio at ± 1V	Area/ (nm^2/$molecule^{-1}$)	Reference
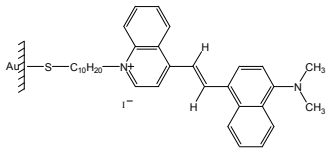	Au-S-$C_{10}H_{20}$-Q^+-π-$C_{10}H_6N(CH_3)_2$	61	50 - 150	0.35 ± 0.03	184
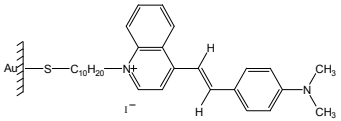	Au-S-$C_{10}H_{20}$-Q^+-π-$C_6H_4N(CH_3)_2$	31	11 - 18	0.32 ± 0.02	183
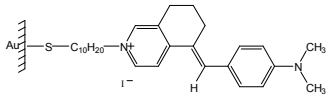	isoquinolinium Au-S-$C_{10}H_{20}$-Q^+-π-$C_6H_4N(CH_3)_2$	48	5 (but expected more)	0.48 ± 0.02	183
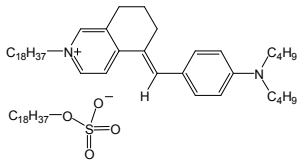	$C_{18}H_{37}$-Q^+-π- $C_6H_4N(C_4H_9)_2$	not provided	70	0.45 ± 0.04	177
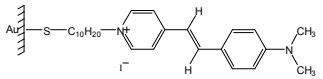	Au-S-$C_{10}H_{20}$-P^+-π-$C_6H_4N(CH_3)_2$	10	1	0.45 ± 0.01	183
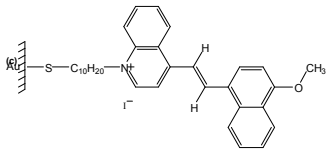	Au-S-$C_{10}H_{20}$-Q^+-π-$C_{10}H_6N(O)CH_3$	not provided	10 - 30	0.40 ± 0.05	201
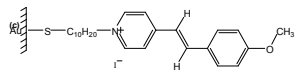	Au-S-$C_{10}H_{20}$-P^+-π-$C_6H_4N(O)CH_3$	not provided	1	0.28 ± 0.03	201

6.5.1 SAMs of anionic molecules

Two different molecules were used to create the anionic surface. They belong to the same group but their molecular structures differ significantly. The purpose of utilising such different molecules was to observe how their structure could influence the electrical behaviour of the prominent part of the molecular system – cationic dye. The molecular structures of both thiols are presented in Figure 6.34.

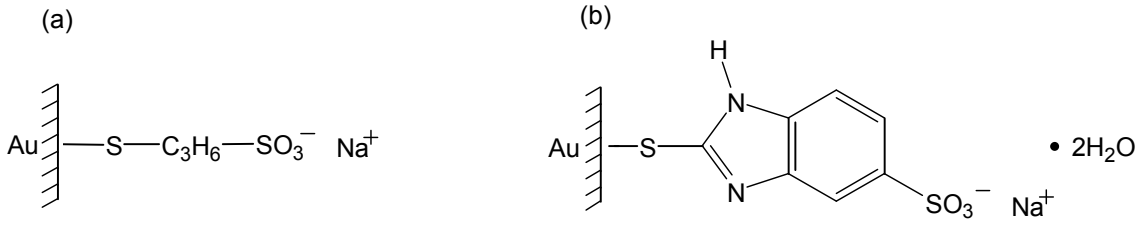

Figure 6.34 SAM of thiols (composing anionic surface) on gold (a) Au-S-C_3H_6-SO_3^- Na^+ and (b) Au-S-$C_7H_4N_2$-SO_3^- Na^+.

Deposition of Au-S-C_3H_6-SO_3^- Na^+ resulted in some difficulties, as even small differences in solution concentration had an impact on the kinetics of deposition onto QCM. A concentration of *ca.* 0.7 mg cm^3 was found to be optimal to obtain smooth characteristics of the growth of the molecular film. Therefore, deposition of Au-S-C_3H_6-SO_3^- Na^+ proceeded from the same solution for every cationic dye.

An illustration of Au-S-C_3H_6-SO_3^- Na^+ deposition is presented in Figure 6.35. The mean area occupied by the molecule was 0.32 ± 0.03 nm^2 $molecule^{-1}$. Relying on the molecular area of cationic dyes contained in Table 3 it can be assumed that that one molecule of a cationic dye should coincide with one molecule of Au-S-C_3H_6-SO_3^- Na^+.

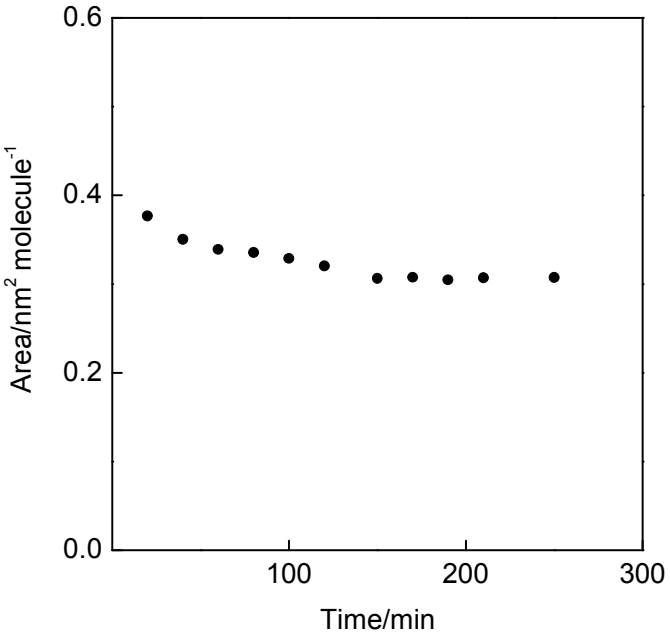

Figure 6.35 Kinetics of growth SAM of Au-S-C_3H_6-SO_3^- Na^+ monitored with QCM. Mean area occupied by the molecule was 0.32 ± 0.03 nm^2 molecule^{-1}.

With regards to the concentration-effect on the quality of the monolayer, STM investigations were executed on quartz crystals. However, they were burdened with a higher level of noise, which affected the shape and stability of the I-V characteristics. Therefore, most of the STM studies were performed on gold-coated HOPG substrates and calculations of the rectification ratio were taken only for I-V curves obtained for films on this substrate. In order to ensure that molecules assembled in the same manner, a quartz crystal was immersed together with the graphite substrate during deposition.

An example I-V characteristic of anionic component on gold is presented in Figure 6.36. All curves (from three samples contacted by PtIr or Au tip) were symmetrical. The only minor difference was in the current on the Y-axis, which was within the range of 0.1 – 0.2 nA, depending on the sample and the initial current setpoint parameters.

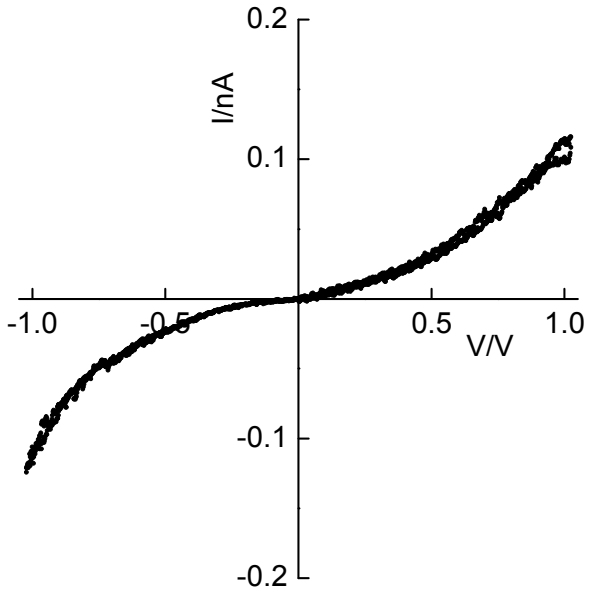

Figure 6.36 Symmetrical I-V characteristics for Au-S-C_3H_6-SO_3^- Na^+, obtained with STM and PtIr tips.

The two-layer SPR analysis for a SAM of Au-S-C_3H_6-SO_3^- Na^+ on a gold-coated substrate gave a thickness of 0.70 ± 0.05 nm. Although this value was burdened with a high error it was not so much different from the value obtained with molecular modelling, 0.75 nm (the distance between sulphur and oxygen situated at the very far from the sulphur in —SO_3 group). Unfortunately, the position of the Na^+ in the monolayer was not known but is needed to exact estimation of the SPR thickness.

The other thiol molecule, Au-S-$C_7H_4N_2$-SO_3^- Na^+ · $2H_2O$ (Figure 6.34 b) was structurally more complicated, as it contained a conjugated system. SPR gave a thickness of 1.80 ± 0.02 nm but this value was too high to be true. Molecular modelling showed that molecule is almost rigid (slight banana-shape) and lies on the gold surface rather than stands perpendicularly to the surface. Therefore, further SPR analysis of Au-S-C_3H_6-SO_3^- and Au-S-$C_7H_4N_2$-SO_3^- -based hybrids was not undertaken.

QCM investigations showed that the area per molecule for Au-S-$C_7H_4N_2$-SO_3^- Na^+ · $2H_2O$ was 0.48 ± 0.03 nm^2 $molecule^{-1}$ (see Figure 6.37). This was higher when compared to Au-S-C_3H_6-SO_3^- Na^+ and calculations included the area of the water

molecules, which makes this compound a hydrated salt (when water was not included in the calculations; the molecular area was 0.44 ± 0.03 nm^2 $molecule^{-1}$). The higher value may signify higher disorder within the cationic layer, when deposited due to the presence of water in the SAM structures.

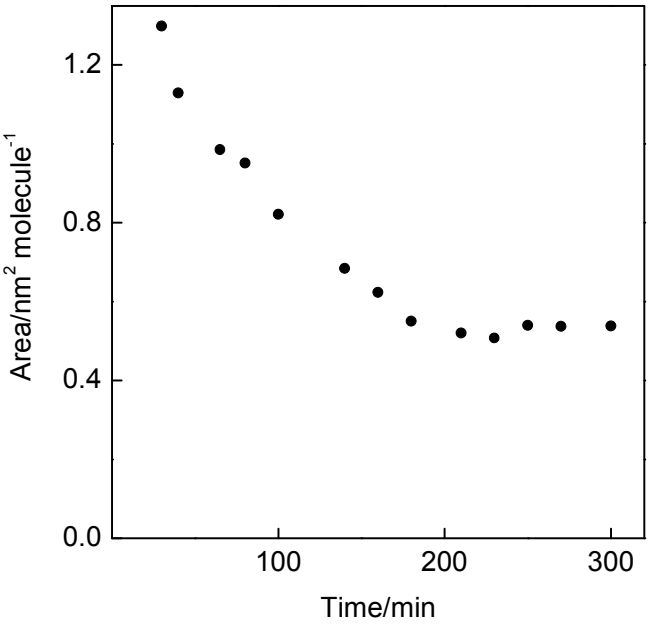

Figure 6.37 Kinetics of SAM deposition for Au-S-$C_7H_4N_2$-SO_3^- Na^+ , monitored with QCM. Mean area occupied by the molecules was 0.48 ± 0.03 nm^2 $molecule^{-1}$.

Yeun *et al.* [223] proposed that in water-saturated structures, the current was carried by ions rather than tunnelling electrons. On the other hand, Heim *et al.* [224] suggested that building a water bridge between sample and tip only occurred in a highly water-saturated environment, which suggested that even in such systems tunnelling due to the molecule was possible. For example, Pt surfaces have a tendency to build up a water bridge in high humidities (above 55 %), whereas a similar effect was observed for Au surfaces at humidities above 75%. In conclusion, because water films possess their own high conductivity [224,225] that strongly affects the density of electronic states at (or near) the Fermi level, the presence of water can influence the conductivity of the entire STM junction. Therefore, it could conceal the electric response from

the molecule and hence significantly affect the ionically coupled molecular films (coupling occurs in aqueous media). These deliberation (on water-affected current flow through molecular junction) will be quoted in Chapter 6.5.3.

STM investigations yielded two types of behaviour for molecules of Au-S-$C_7H_4N_2$-SO_3^- Na^+ assembled on gold-coated graphite. Depending on the sample, I-V characteristics were symmetric or slightly asymmetric with rectification ratio of no more than 3.5 at ±1 V. These curves are presented in Figure 6.38.

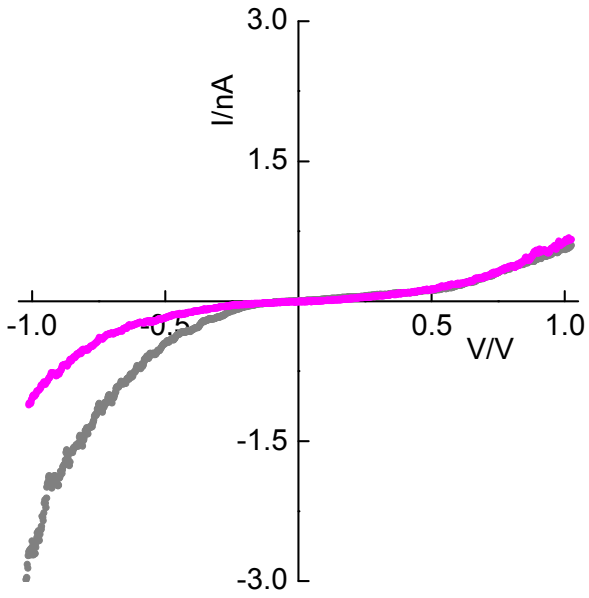

Figure 6.38 I-V curves for Au-S-$C_7H_4N_2$-SO_3^- Na^+ molecules obtained with STM, showing expected symmetrical characteristics and slightly unsymmetrical tip-induced effects.

If all I-V curves presented in Figure 6.38 were asymmetric, then it would be possible that the molecule could rectify current on its own. Indeed, a molecule possessing the —NH group in its structure, would impact slight donating character. If so, the Kornilovitch theory of a molecule possessing only one conducting part (donor) would be fulfilled here (at least partially, as the degree of asymmetrical positioning of the molecule between electrodes was not known exactly). However, the tip-induced asymmetry of the I-V characteristics was highly probable here due to the tip-sample

electrostatic interaction in an aqueous environment and this is taken for granted, when (i) compared with electrical properties of cationic dyes ionically coupled to Au-S-$C_7H_4N_2$-SO_3^- Na^+ (ii) the tip induced rectification is usually no greater than 2 – 4.

6.5.2 Cationic D-π-A dyes on Au-S-C_3H_6-SO_3^- Na^+

Ionically coupled films were obtained in two steps; initially the SAM of HS-C_3H_6-SO_3^- Na^+ was deposited from methanol solution onto a gold-coated substrate. The second step was creation of the cationic monolayer on top of the anionic surface (by dipping the substrate with the thiol SAM in a solution of the dye). During deposition Na^+ from thiol and I^- from the dye create a salt, which was suspended in the aqueous environment of the solution. The salt did not disturb the ionic attraction between the thiol and the dye, as it was rinsed out from the structure with ultra-pure water (deposition interrupted by sequential rinsing with water). All hemycyanine dyes were investigated in the same manner, as ionic self-assembly seemed to have great potential in molecular assembly.

To assess the effectiveness of the rinsing process, XPS analysis was implemented for one of the hybrid systems. The molecular structure of this system is presented in Figure 6.39. XPS confirmed the presence of the most characteristic atoms. For Au-S-C_3H_6-SO_3^- Na^+; sulphur (S 2p) at 162 eV and 167 eV, oxygen (O 1s) at 528 eV. Whereas the cationic layer was represented by a nitrogen peak at 391 eV (N 1s). The presence of sodium was not observed but a negligible amount of iodide was present in the monolayer with a peak at 614 eV (I 3d).

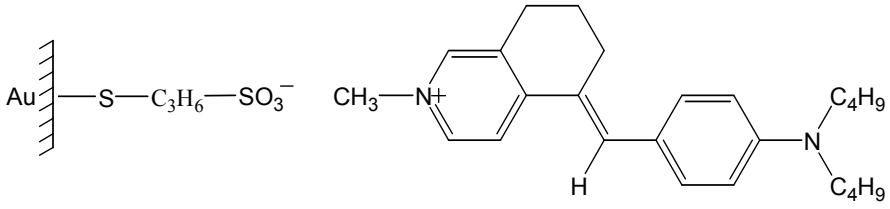

Figure 6.39 Molecular structure of the hybrid containing isoquinolinium-acceptor-based Q^+-π-$C_6H_4N(C_4H_9)_2$ dye deposited on top of the alkanethiol molecule of Au-S-C_3H_6-SO_3^- Na^+ via mutual ionic attraction. Q^+ - 5,6,7,8-tetrahydro-isoquinolinium (acceptor).

The metathesis process was monitored with QCM apparatus and deposition of the cationic dye revealed a value of 0.30 ± 0.01 nm^2 $molecule^{-1}$ after 5h of intensive physisorption interrupted by sequential rinsing with water, methanol and ethanol. Figure 6.40 shows deposition of the hybrid monolayer on the anionic surface and the comparison of two molecular areas are presented. It can be assumed that the molecular areas of the two components were the same, and so the alignment of the molecules within the second layer was controlled.

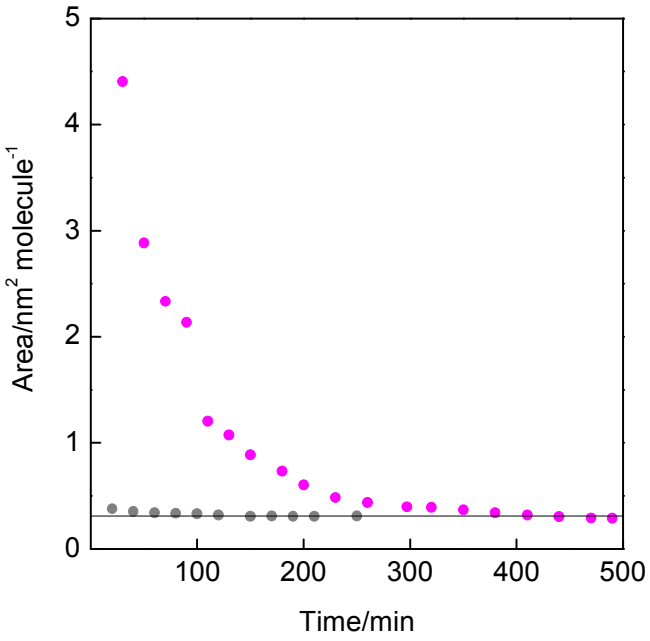

Figure 6.40 Mean area *vs*. immersion time for cationic cationic isoquinolinium Q^+-π-$C_6H_4N(C_4H_9)_2$ (magenta), which is limited by underlying anionic molecules of Au-S-C_3H_6-SO_3^- (grey); 0.30 ± 0.02 nm^2 $molecule^{-1}$. Parallel line shows matching of the molecular areas of both components.

UV-Vis spectroscopy also provided essential information about the presence of a physisorbed cationic layer in the hybrid structure on Pt-coated glass. Figure 6.41 certainly shows a characteristic absorption band at 490 nm. However, the intensity of the peak (absorbance) was an order of magnitude less than for SAMs of similar D-π-A molecules (see isoquinolinium Au-S-$C_{10}H_{20}$-Q^+-π-$C_6H_4N(CH_3)_2$, Table 3). This could be caused by a smaller amount of the cationic dye present in the molecular structure as a result of physisorption. Because they are ionically coupled to the bottom

layer, the whole structure could be affected by the presence of structural defects caused by residual metal ions or dust from the air.

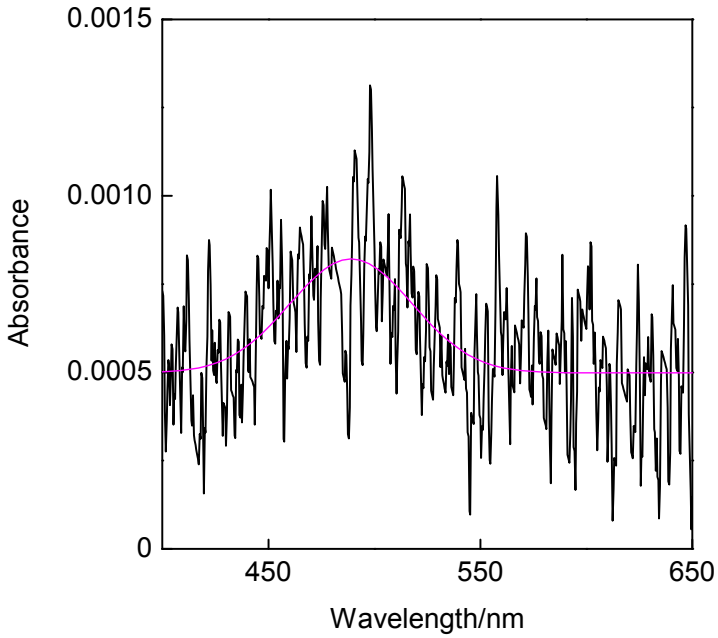

Figure 6.41 UV-Vis spectrum of a hybrid structure, containing cationic dye of isoquinolinium Q^{+}-π-$C_6H_4N(C_4H_9)_2$ on top of anionic Au-S-C_3H_6-SO_3^- component, obtained in transmission on Pt-coated glass slide. Distinct absorption at 490 nm was obtained by Gaussian approximation (*Origin 61 Software*).

Electrical studies of the STM junction containing isoquinolinium Q^{+}-π-$C_6H_4N(C_4H_9)_2$ showed reproducible electric behaviour of the system with higher current in the negative quadrant of the I-V plot (Figure 6.42); the bias was defined by the sign of the substrate electrode. This was in agreement with the direction of the current flow for SAMs of the ten-carbon analogue (Table 3, isoquinolinium Au-S-$C_{10}H_{20}$-Q^{+}-π-$C_6H_4N(CH_3)_2$) and the direction of electron tunnelling was from the gold-coated substrate to the contacting tip (in accordance with the Aviram-Ratner model). However, STM studies also failed to show periodicity in the images of the structure, probably resulting from a high degree of disorder in the cationic layer. Calculations of the rectification ratio from five samples displayed a broad range from 20 up to 450 at ± 1V. The lower values were usually obtained just a few hours after deposition, which increased with time. The highest values of rectification ratio

(*ca.* 400 at ± 1V) constituted almost 20 % of the highly asymmetric I-V characteristics (when RR was above 100 at ± 1V) and occurred between 24 – 40 hours after deposition. The rise of the rectification ratio values could not be explained by the STM cycling effect [165], as the higher values were observed either, just after engaging the tip over the monolayer surface, or in cycles. This behaviour seems to be due to the properties of the molecular junction itself. It is reminiscent of the behaviour observed for Schottky-type electrodes, where metal oxidation enhanced the asymmetry of I-V curves.

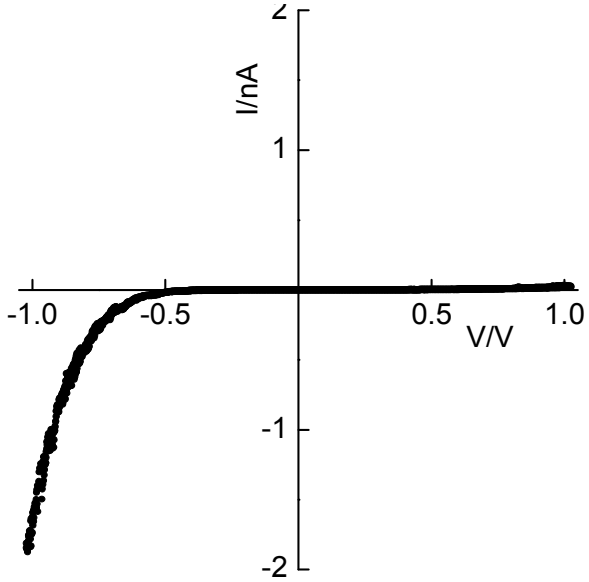

Figure 6.42 I-V characteristic obtained for bilayer formed by ionically coupled molecules of Au-S-C_3H_6-SO_3^- and isoquinolinium-based Q^+-π-$C_6H_4N(C_4H_9)_2$, using STM Au tip. The highest observed RR was 450 at ±1 V.

Comparison of the rectification ratios of the ionic hybrid with rectification ratios of 'traditional' molecular films shows a big gap between them. The values in the range of 8 – 22 at ±1 V for LB films of the iodide salts of amphiphilic derivatives [226], 70 at ±1 V were observed for mixed LB films with octadecyl sulfate ($C_{18}H_{37}$-Q^+-π-$C_6H_4N(C_4H_9)_2$, Table 3), and 5 at ±1 V for SAMs contacted by a decanethiolate-coated STM tip (isoquinolinium Au-S-$C_{10}H_{20}$-Q^+-π-$C_6H_4N(CH_3)_2$, Table 3). However, the higher values were expected for SAMs [183] as the molecule possessed a substantial steric hinderance. Cerius modelling calculated the torsion angle

between donor and acceptor moieties to be *ca.* 51° (see Figure 6.43). Reduced values of rectification ratio for LB films and SAMs may be connected to the replacement of the iodide counterion under an external field, which favours travel along the longer axis of the chromophore and therefore yields the quinonid form [176,226]. Thus, the monolayer may contain a mixture of the molecules in both states, ground and dipole-reversed. Such a phenomenon (triggered by anion-induced polarisation), was also observed for other cationic dyes in molecular films, mostly for LB films [176,226].

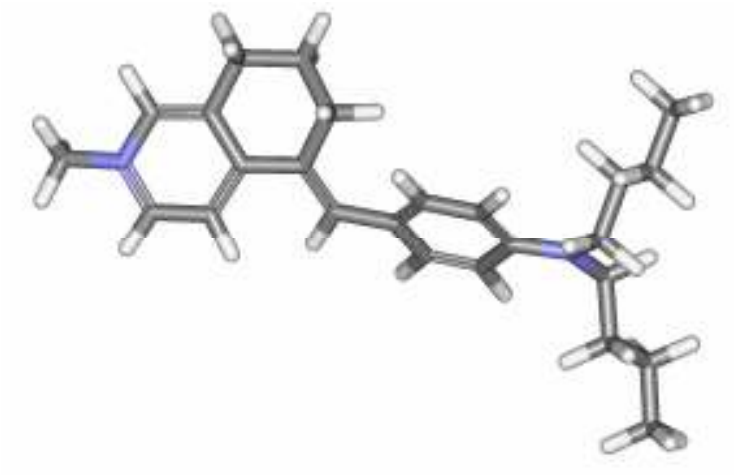

Figure 6.43 Modelled structure of isoquinolinium Q^{+}-π-$C_6H_4N(C_4H_9)_2$ molecule by energy minimisation obtained with *Cerius* AM1 method, showing molecular steric hinderance for which dihedral angle was *ca.* 51°.

Consecutive dyes were investigated in a similar manner to the previous hybrid system, as ionic self-assembly seemed to have a great potential in molecular assembly for electronics applications.

The molecular structure of another hybrid is presented in Figure 6.44. Because the previous cationic dye has exactly the same donor group the molecular formula assigned to this molecule would be the same. To differ between both hybrids the name of the acceptor will be used if necessary.

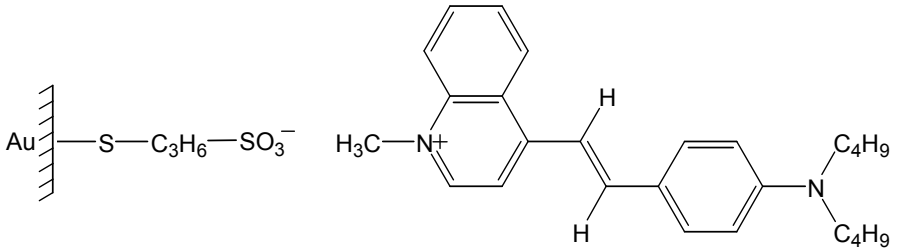

Figure 6.44 Molecular structure of the hybrid containing quinolinium-acceptor-based Q^+-π-$C_6H_4N(C_4H_9)_2$ dye deposited on top of the alkanethiol molecule of Au-S-C_3H_6-SO_3^- Na^+ via mutual ionic attraction. Q^+ – 1-methyl quinolinium (acceptor).

QCM analysis of three samples provided an average area per molecule of 0.29 ± 0.02 nm^2 $molecule^{-1}$ for quinolinium Q^+-π-$C_6H_4N(C_4H_9)_2$ molecules adsorbed on an anionic monolayer. The area approximates to the van der Waals cross-section of the chromophore and is similar to the same chromophore in SAMs (Table 3, quinolinium Au-S-$C_{10}H_{20}$-Q^+-π-$C_6H_4N(CH_3)_2$). A complete monolayer was obtained after *ca.* 6 hours and the area was comparable to the mean area of anionic component (Figure 6.45), suggesting that one anionic structure of Au-S-C_3H_6-SO_3^- is addressed by one molecule of cationic dye.

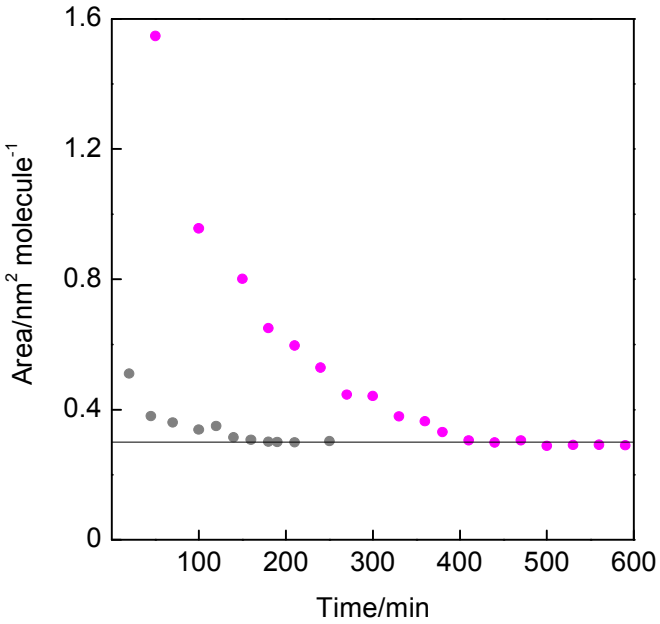

Figure 6.45 Mean area *vs.* immersion time for cationic cationic quinolinium Q^+-π-$C_6H_4N(C_4H_9)_2$ (magenta), which is limited by underlying anionic molecules of Au-S-C_3H_6-SO_3^- (grey); 0.29 ± 0.02 nm^2 $molecule^{-1}$. Parallel line shows matching of the molecular areas of both components.

Unfortunately, attempts at obtaining a visible spectrum of quinolinium Q^+-π-$C_6H_4N(C_4H_9)_2$-based hybrid failed, possibly due to the thickness of the coated platinum layer. Relying on previous studies, the absorbance of monolayers obtained by physisorption from solutions was very low, it can be assumed that the absorbance of the platinum in the range of 0.5 was too high for the spectrophotometer to differentiate the spectrum of the monolayer. The difference in the absorbance between Pt and the cationic layer exceeded three orders of the magnitude.

STM analysis confirmed the rectifying behaviour of the quinolinium-based Q^+-π-$C_6H_4N(C_4H_9)_2$ with higher current at negative bias (see Figure 6.46). This would suggest that electron flow was from the bottom electrode (Au-coated HOPG) through the anionic surface to the acceptor (Q^+) of the cation, and then from the donor ($C_6H_4N(C_4H_9)_2$) to the tip. The direction of electron transfer is exactly the same as for isoquinolinium-based Q^+-π-$C_6H_4N(C_4H_9)_2$. Although all three samples of quinolinium Q^+-π-$C_6H_4N(C_4H_9)_2$ exhibited asymmetry of the I-V characteristics, no very high rectification ratios (as for previous system) were observed for any of them.

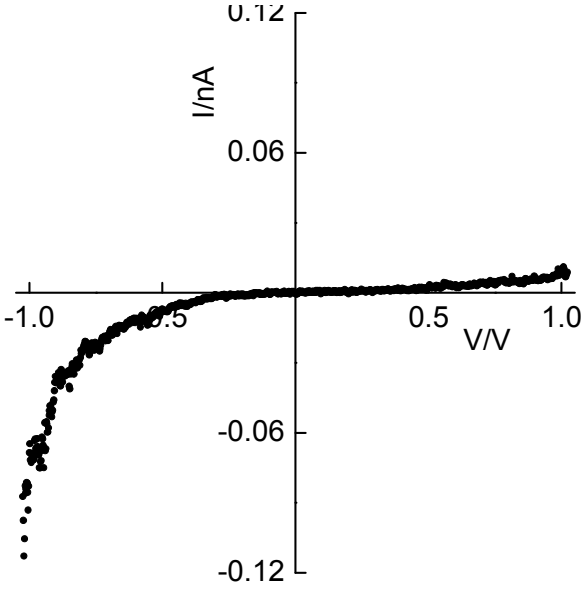

Figure 6.46 I-V characteristic obtained for bilayer formed by ionically coupled molecules of Au-S-C_3H_6-SO_3^- and quinolinium-based Q^+-π-$C_6H_4N(C_4H_9)_2$, using STM Au tip. Typical rectification ratio was 10 – 14 at ±1 V.

Molecular modelling showed that quinolinium Q^+-π-$C_6H_4N(C_4H_9)_2$ molecule had the smallest dihedral angle of all the cationic dyes studied here, which were *ca.* 24° (see Figure 6.47) and so high rectification ratios were not expected from this molecule. The rectification ratio was 12 – 16 at ±1 V and the highest values were obtained at 30 hours after deposition. These values were in the same rectification ratio range as for the chromophore in SAM (Table 3, quinolinium Au-S-$C_{10}H_{20}$-Q^+-π-$C_6H_4N(CH_3)_2$); 11 – 18 at ±1 V.

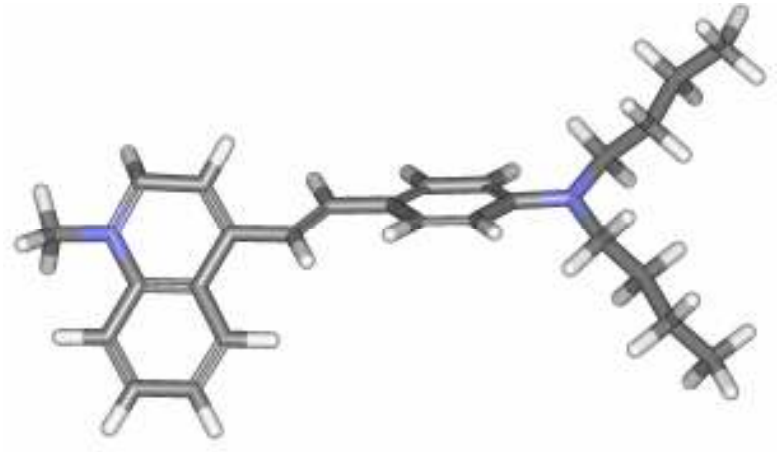

Figure 6.47 Modelled structure of quinolinium Q^+-π-$C_6H_4N(C_4H_9)_2$ molecule by energy minimisation obtained with *Cerius* AM1 method, showing molecular steric hinderance for which dihedral angle was *ca.* 24°.

Similar electrical behaviour (to previous system) was observed for following structure, in which a methoxy analogue of the naphthalene-1-yl dye (Q^+-π-$C_{10}H_6OCH_3$) was ionically coupled to the Au-S-C_3H_6-SO_3^- surface (see Figure 6.48). This cationic dye possessed a methoxy substituent, which being a donor imparted the push-pull behaviour on this molecule.

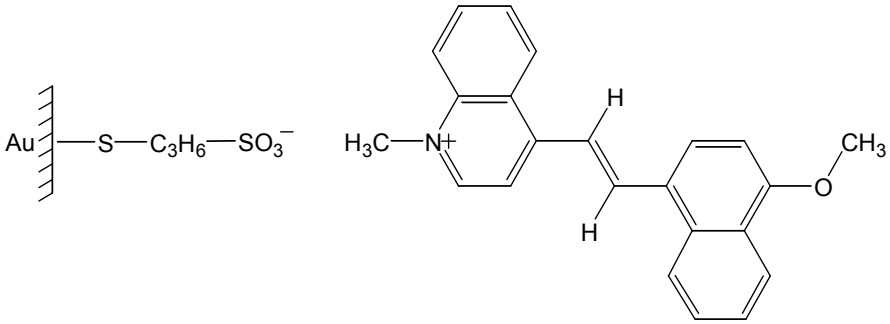

Figure 6.48 Molecular structure of the hybrid containing quinolinium-acceptor-based Q^{+}-π-$C_{10}H_6O(CH_3)$ dye deposited on top of the alkanethiol molecule of Au-S-C_3H_6-SO_3^{-} Na^{+} via mutual ionic attraction. Q^{+} – 1-methyl-quinolinum (acceptor).

QCM analysis confirmed that the area of the cationic layer was limited by the area of the underlying anionic molecule. Meticulous calculations revealed a value of 0.32 ± 0.02 nm^2 $molecule^{-1}$. A higher value of molecular area (when compared with previous systems) was expected, because of the bulkier methoxynaphthalene donor. QCM results are presented in Figure 6.49.

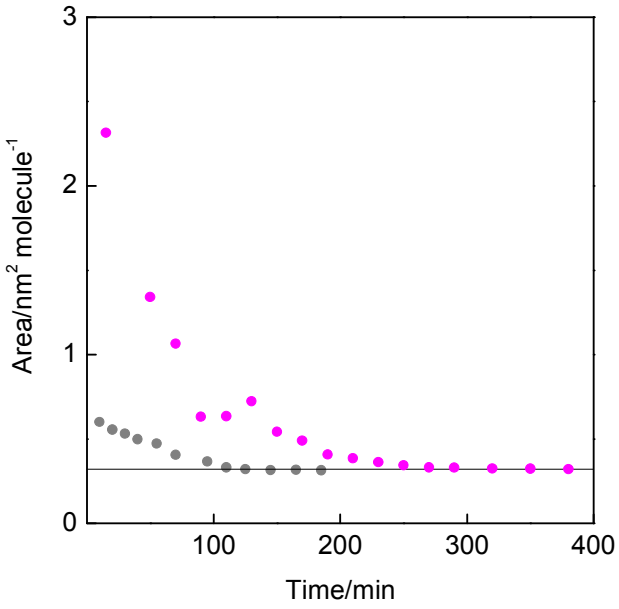

Figure 6.49 Mean area *vs*. immersion time for cationic dye of Q^{+}-π-$C_{10}H_6OCH_3$ (magenta) , which is limited by underlying anionic molecules of Q^{+}-π-$C_{10}H_6OCH_3$ (grey); 0.32 ± 0.02 nm^2 $molecule^{-1}$. Parallel line shows matching of the molecular areas of both components.

STM investigations of two samples were troublesome and engaging the tip was difficult, even when the current setpoint parameters were changed. The first decent I-V characteristics were observed after 19 hours since monolayer deposition with higher current in the negative quadrant of the I-V plot (see an example in Figure 6.50).

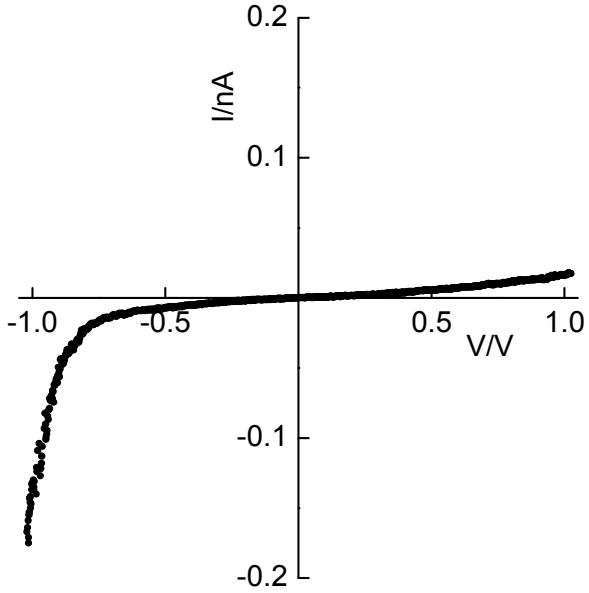

Figure 6.50 I-V characteristic obtained for bilayer formed by ionically coupled molecules of Au-S-C_3H_6-SO_3^- and Q^+-π-$C_{10}H_6OCH_3$ using STM Au tip. Typical rectification ratio was 10 – 14 at ±1 V.

The range of the rectification ratio values was comparable with the values obtained for Q^+-π-$C_6H_4N(C_4H_9)_2$ incorporating quinolinium acceptor. However, the dihedral angle, calculated by Cerius software (see Figure 6.51), was 52°, which suggested the possibility of obtaining higher rectification ratios. The same chromophore in SAMs exhibited rectification ratio of 30 at ±1 V (Table 3, Au-S-$C_{10}H_{20}$-Q^+-π-$C_{10}H_6NOCH_3$) and so another sample was prepared. Despite problems in engaging the tip, asymmetrical I-V characteristics were observed after 19 hours with a rectification ratio of 10 at ±1 V. A day later, the rectification ratio increased up to 14 at ±1 V, but a few curves with rectification ratio of 30 at ±1 V were also observed. The percentage of curves with rectification ratio of 30 at ±1 V was less than 5 %. So, it can be assumed

that cationic molecules in ESA monolayer obtain similar properties (molecular alignment and electrical properties) to SAMs over time.

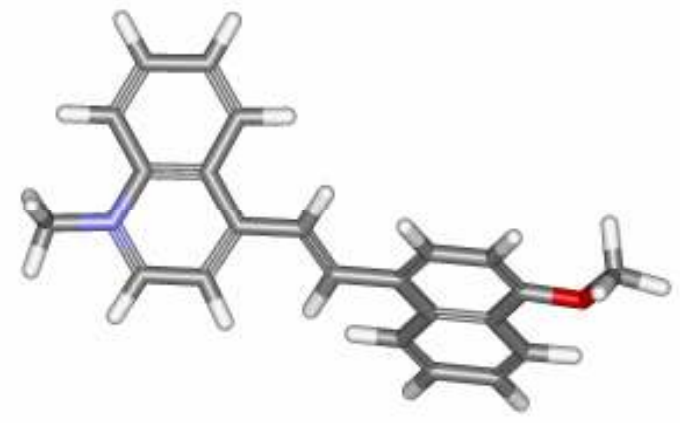

Figure 6.51 Modelled structure of Q^{+}-π-$C_{10}H_6OCH_3$ molecule by energy minimisation obtained with *Cerius* AM1 method, showing molecular steric hinderance for which the dihedral angle was *ca.* 52^0.

The importance of the stearic hinderance on the rectifying properties of the D-π-A self-assembled analogues of A^{+}-π-$C_{10}H_6OCH_3$ was previously reported by Ashwell *et al.* [201]. Molecules with planar structures (Table 3, Au-S-$C_{10}H_{20}$-P^{+}-π-$C_6H_4NOCH_3$) exhibited symmetrical I-V characteristics whereas those in which sufficient out-of-plane rotation was presented (*i.e.* Au-S-$C_{10}H_{20}$-P^{+}-π-$C_6H_4N(CH_3)_2$ and Au-S-$C_{10}H_{20}$-P^{+}-π-$C_6H_4NOCH_3$ in Table 3) exhibited asymmetrical I-V characteristics.

The Q^{+}-π-$C_6H_4N(C_4H_9)_2$ molecule incorporating isoquinolinium acceptor and the Q^{+}-π-$C_{10}H_6OCH_3$ possessed similar dihedral angles; 51° and 52° respectively but their rectification ratios were different for the same voltage range. It can be attributed to the strength of the electronic properties of the donor of the molecule, which is better for the isoquinolinium Q^{+}-π-$C_6H_4N(C_4H_9)_2$ dye.

Another bulky system was studied, with a dimethylaminonaphthalene group being a stronger donor than methoxy (see Figure 6.52). Therefore this hybrid was expected to achieve a higher rectification ratio.

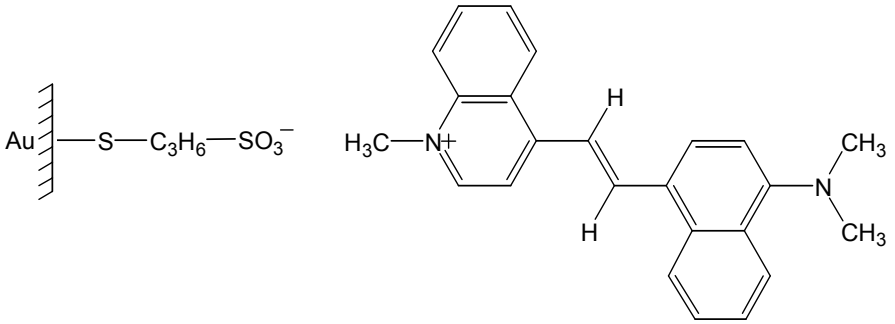

Figure 6.52 Molecular structure of the hybrid containing quinolinium-acceptor-based Q^+-π-$C_{10}H_6N(CH_3)_2$ dye deposited on top of the alkanethiol molecule of Au-S-C_3H_6-SO_3^- Na^+ via mutual ionic attraction. Q^+ – 1-methyl quinolinium (acceptor).

Deposition of the Q^+-π-$C_{10}H_6N(CH_3)_2$ dye on the anionic surface of Au-S-C_3H_6-SO_3^- revealed a mean area of 0.32 ± 0.01 nm^2 $molecule^{-1}$ after *ca.* 8h of immersion. This value was identical to the area occupied by a molecule of Au-S-C_3H_6-SO_3^- Na^+, *i.e.* 0.32 ± 0.01 nm^2 $molecule^{-1}$. Thus, it can be assumed that one molecule of the dye aligned with one molecule of the anionic thiol. The comparison of the area occupied by the molecules of both components is presented in Figure 6.53.

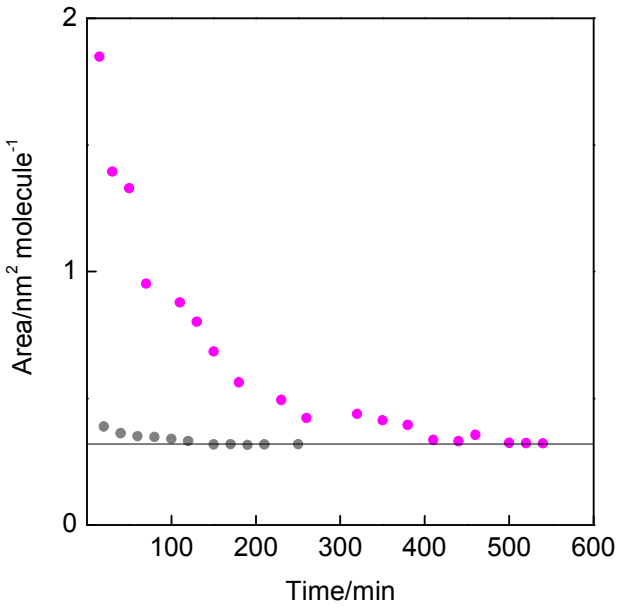

Figure 6.53 Mean area *vs*. immersion time for cationic dye of Q^+-π-$C_{10}H_6N(CH_3)_2$, which is limited by underlying anionic molecules of Au-S-C_3H_6-SO_3^- (grey); 0.32 ± 0.01 nm^2 $molecule^{-1}$. Parallel line shows matching of the molecular areas of both components.

UV-Vis spectroscopy was used on Au-S-C_3H_6-SO_3^- Q^+-π-$C_{10}H_6N(CH_3)_2$ on Pt-coated glass. This yielded an absorption band at about 450 nm (see Figure 6.54). The placement of this peak was consistent with the absorption band obtained for SAMs of the same dye [184]. However, absorbance of the bilayer was an order of magnitude smaller than for the Au-S-$C_{10}H_{20}$-Q^+-π-$C_{10}H_6N(CH_3)_2$, which may suggest poor order within the cationic monolayer in the hybrid structure (as physisorption is a weaker force than chemisorption).

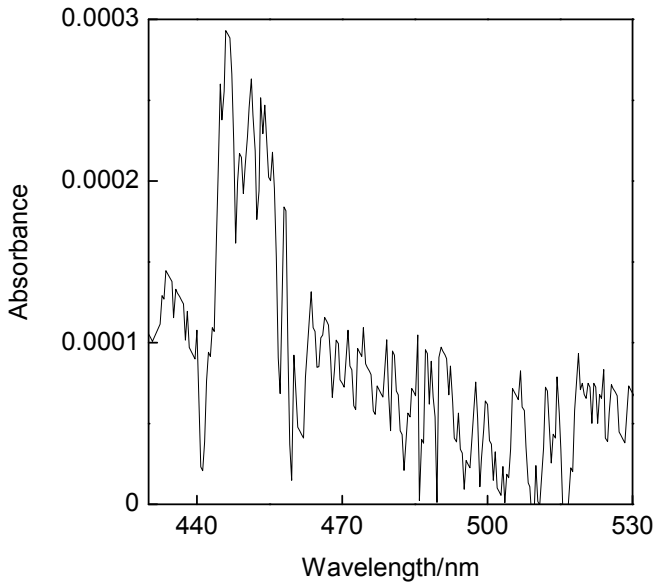

Figure 6.54 Visible spectrum of the cationic dye of A^+-π-$C_{10}H_6N(CH_3)_2$ an anionic surface of Au-S-C_3H_6-SO_3^- obtained in transmission.

STM investigations of three samples showed rectifying behaviour of Au-S-C_3H_6-SO_3^- Q^+-π-$C_{10}H_6N(CH_3)_2$ hybrid when contacted by a PtIr tip (see Figure 6.55). Similar to isoquinolinium Q^+-π-$C_6H_4N(C_4H_9)_2$-based bilayer, all samples exhibited various asymmetry of the I-V characteristics and the highest rectification ratio of 100 – 200 at ±1 V obtained 32 – 38 hours after deposition. The lower range of the rectification ratio was from 30 to 60 at ±1 V and was characteristic for molecular films probed after 6 – 12 hours after deposition. Rectification ratios obtained for ionically coupled molecules slightly extended the range obtained for SAMs contacted by a decanethiolate

link; 50 – 150 at ±1 V (Au-S-$C_{10}H_{20}$-Q^+-π-$C_{10}H_6N(CH_3)_2$ in Table 3). The phenomenon of rise in rectification ratio over time was characteristic for all four hybrids and can be attributed to the realignment of the cationic molecules on the anionic surface under applied electric field.

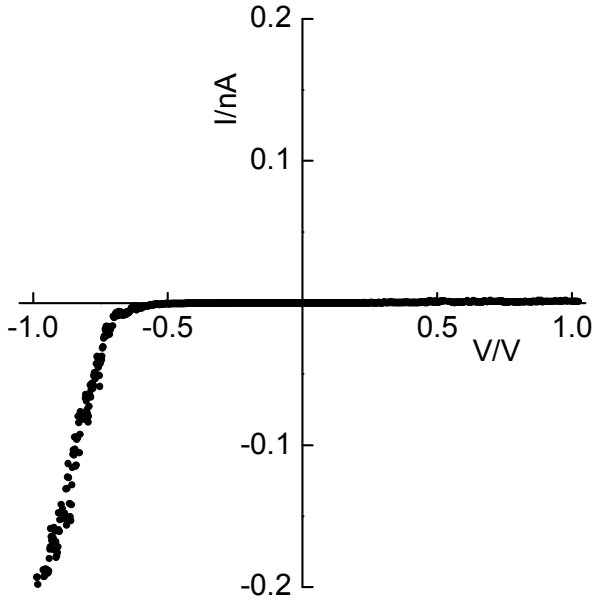

Figure 6.55 I-V characteristic obtained for bilayer formed by ionically coupled molecules of Au-S-C_3H_6-SO_3^- and Q^+-π-$C_{10}H_6N(CH_3)_2$ using STM Au tip. The highest rectification ratio was *ca*. 200 at ±1 V.

The assumption of higher rectification ratios expected from the same molecule containing different donor groups was successful. Rectification ratios from Au-S-C_3H_6-SO_3^- Q^+-π-$C_{10}H_6N(CH_3)_2$ were higher than from Au-S-C_3H_6-SO_3^- Q^+-π-$C_{10}H_6OCH_3$ although the dihedral angle for both chromophores was similar. Molecular modelling of the Q^+-π-$C_{10}H_6N(CH_3)_2$ dye also showed steric hinderance of the chromophore with a torsion angle value of *ca.* 56°. The modelled structure is presented in Figure 6.56 and the image shows significant out-of-plane rotation of the molecule.

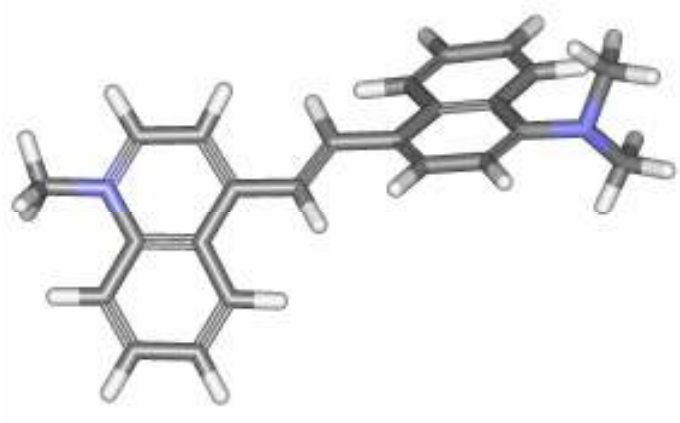

Figure 6.56 Modelled structure of A^{+}-π-$C_{10}H_6N(CH_3)_2$ molecule by energy minimisation obtained with *Cerius* AM1 method, showing molecular steric hinderance for which dihedral angle was *ca.* 56°.

6.5.3 Cationic D-π-A dyes on Au-S-$C_7H_4N_2$-SO_3^- Na^+

The aim in investigating hybrid structures equipped with bulkier anionic layer of Au-S-$C_7H_4N_2$-SO_3^- was to verify the structural- and water-influence on the electrical properties of the molecular film. For this purpose only two hybrids were investigated, and were related to the cationic dyes that exhibited highest rectification ratios when physisorbed on an anionic surface of Au-S-C_3H_6-SO_3^- Na^+. The molecular structure of the first hybrid is presented in Figure 6.57.

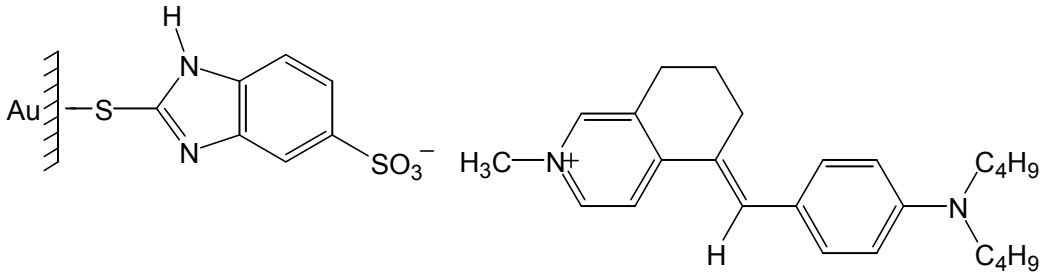

Figure 6.57 Molecular structure of bilayer containing anionic thiol derivative of Au-S-$C_7H_4N_2$-SO_3^- and isoquinolinium analogue of Q^{+}π-$C_6H_4N(C_4H_9)_2$ which were coupled electrostatically. Q^{+} – 5,6,7,8-tetrahydro-isoquinolinium (acceptor).

Molecular films were prepared in the same manner as the Au-S-C_3H_6-SO_3^- -based bilayers and they were deposited from the solutions with a concentration from 0.15 to 0.20 mg cm^{-3}. Despite the fact that the anionic molecules possessed water

molecules in the structure, a few additional drops of water had to be added to the solution of the dye to initiate deposition of the physisorbed monolayer. When water was not added to the solution, the QCM analysis failed to deliver good monolayer characteristics. The result of the QCM analysis with and without water is presented in Figure 6.58.

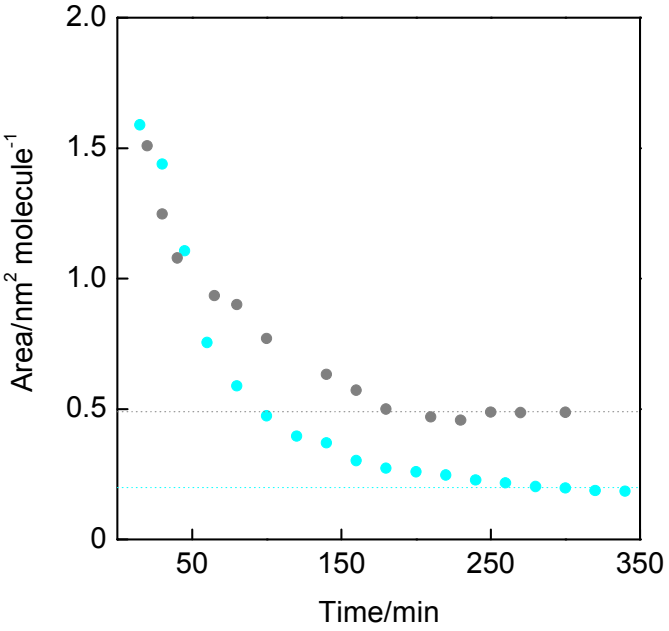

Figure 6.58 Mean area *vs*. immersion time for cationic cationic quinolinium Q^+-π-$C_6H_4N(C_4H_9)_2$ (cyan), and underlying anionic molecules of Au-S-$C_7H_4N_2$-SO_3^- (grey); 0.20 ± 0.01 and 0.48 ± 0.05 nm^2 molecule^{-1}.

The mean molecular area of bilayer structure amounted to 0.20 ± 0.01 nm^2 molecule^{-1}. This value was significantly smaller than the molecular area of underlying anionic molecules, that is 0.48 ± 0.03 nm^2 molecule^{-1}. Differences in molecular areas of both components suggest that molecules of water can be trapped within bilayer structure. It is impossible for the same cationic dye Q^+π-$C_6H_4N(C_4H_9)_2$ to have such significantly different molecular areas: 0.30 nm^2 molecule^{-1} when assembled on Au-S-C_3H_6-SO_3^- and 0.20 nm^2 molecule^{-1} on Au-S-$C_7H_4N_2$-SO_3^- (despite the fact of that molecular area of cationic dye is limited by the area of underlying anionic lattice).

STM analysis of seven samples of Au-S-$C_7H_4N_2$-SO_3^- $Q^+\pi$-$C_6H_4N(C_4H_9)_2$ bilayer yielded ambiguous results, all of which were highly hysteretic and constituted 50 to 100 % of all I-V characteristics registered for each sample. Only four samples (from seven measured) exhibited 'normal-shaped' I-V characteristics, and this dual behaviour is presented in Figure 6.59.

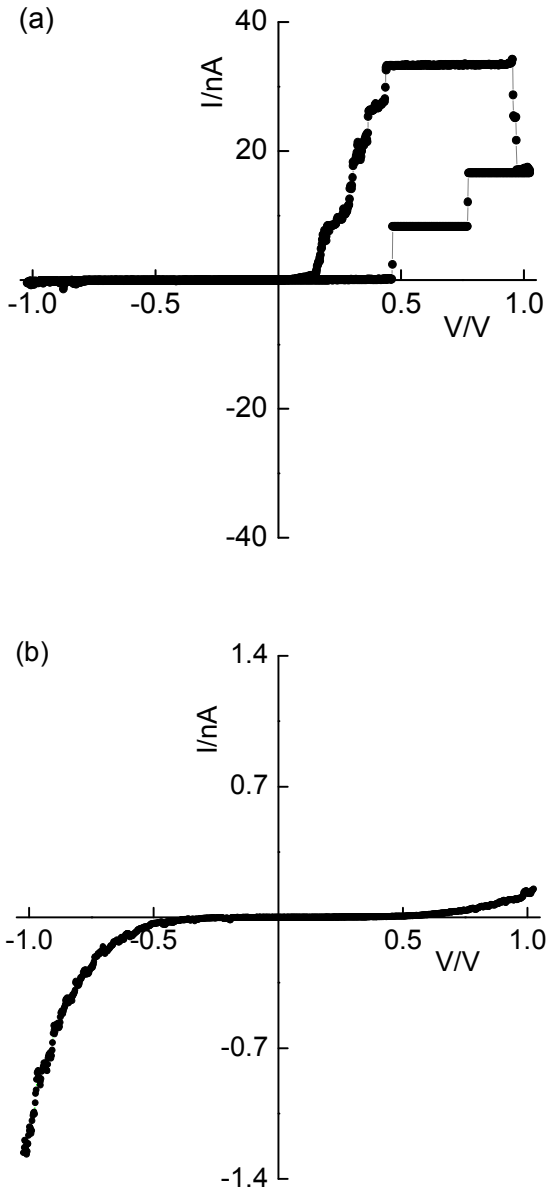

Figure 6.59 Electrical behaviour of aligned diode composed with ionically coupled molecules of Au-S-$C_7H_4N_2$-SO_3^- and isoquinolinium Q+π-$C_6H_4N(C_4H_9)_2$, represented by I-V characteristics: (a) with high asymmetry and hysteresis suggesting ionic flow or leakage; (b) of tunnelling with typical rectification ratio of 10 – 15 at ±1 V.

The shape and current magnitude of the first I-V characteristics (a) may be a reflection of ionic flow from the STM tip contacting the residual water molecules (meniscus is created between the tip and water molecules, as mentioned before in Chapter 6.5.1; p. 128) and thus reflects the leakage current. Such behaviour was consistent for both forward and reverse bias, and occurred independently from the initial setpoint parameters. The magnitude of current; 40 – 200 nA also suggested other mechanism of electron transport were involved, other than tunnelling.

The shape of the second I-V plot (see Figure 6.59 b) probably represents tunnelling between cationic dye and tip. This conclusion was drawn from the rectification that was similar to the range obtained for other molecular rectifiers. For example tunnelling current of *ca.* 0.05 to 2 nA at ± 1V was observed for D-(π-bridge)-A zwitterions. Therefore direct interaction of anionic and cationic components in aqueous environment, may still have occurred. However, in this case the number of cationic molecules was probably smaller than for the Au-S-C_3H_6-SO_3^--based hybrids, as it was impossible to obtain a visible spectrum (even for very thin layers of Pt coated slides). Rectification ratio characteristics for tunnelling were mainly in the range of 10 – 15 at ±1 V, which is almost 20 order less than for the same chromophore assembled on Au-S-C_3H_6-SO_3^-. However, one sample did yield several asymmetric I-V characteristics for which rectification ratio was 30 at ± V (five curves) and 50 at ±1 V (two curves from a more than a hundred registered).

In order to verify previous electrical results the second bilayer was formed. This one contained bulky Q^+-π-$C_{10}H_6N(CH_3)_2$ electrostatically bind to the anionic surface of Au-S-$C_7H_4N_2$-SO_3^- (see Figure 6.60).

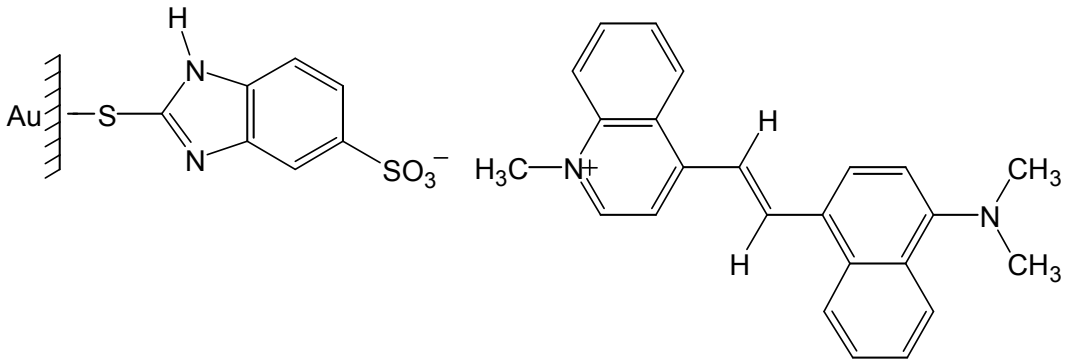

Figure 6.60 Molecular structure of self-assembled bilayer containing monolayer of Au-S-$C_7H_4N_2$-SO_3^- anions to which cationic dye of Q+-π-$C_{10}H_6N(CH_3)_2$ can be electrostatically coupled.

Calculation of the area, obtained form the QCM measurements of three samples showed similar behaviour to previous Au-S-$C_7H_4N_2$-SO_3^--based bilayer, with the value of molecular area being only 0.20 ± 0.02 nm^2 $molecule^{-1}$ (see Figure 6.61).

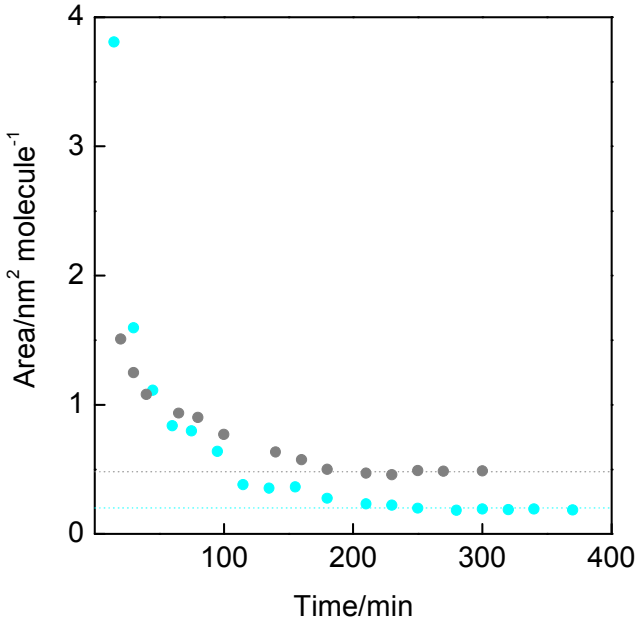

Figure 6.61 Mean area *vs.* immersion time for cationic cationic Q^+-π-$C_{10}H_6N(C_4H_9)_2$ (cyan), and underlying anionic molecules of Au-S-$C_7H_4N_2$-SO_3^- (grey); 0.20 ± 0.01 and 0.48 ± 0.05 nm^2 $molecule^{-1}$.

Investigations of the electrical behaviour of the bulkier hybrid on a gold-coated substrate with a PtIr tip also showed dual behaviour (see Figure 6.62).

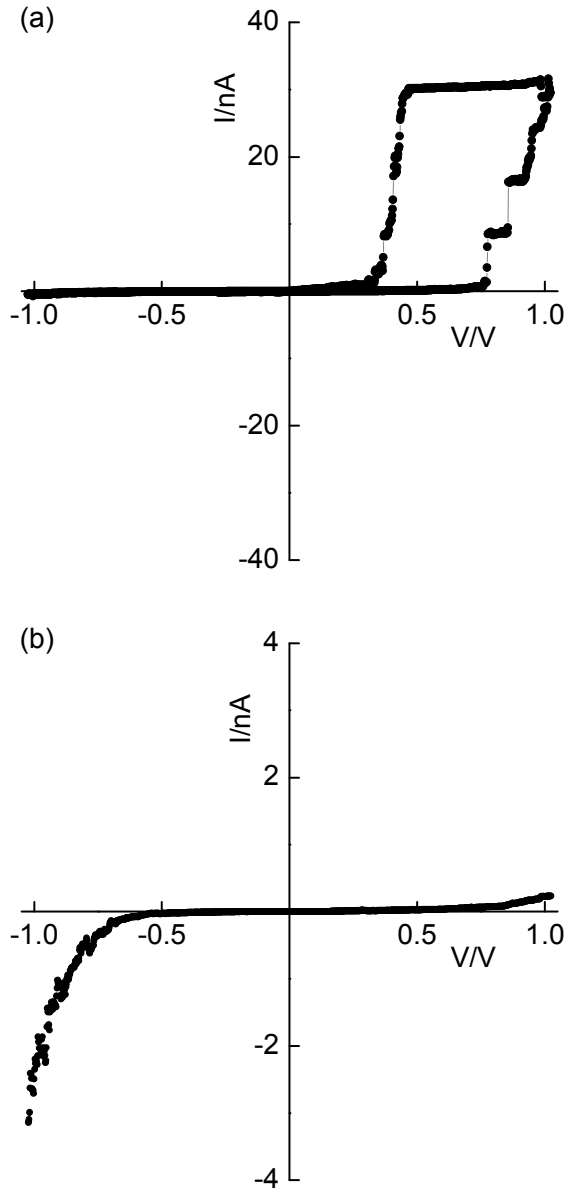

Figure 6.62 Electrical behaviour of ionically coupled molecular hybrid of Au-S-$C_7H_4N_2$-SO_3^- and Q^+-π-$C_{10}H_6N(CH_3)_2$ represented by I-V characteristics: (a) with high asymmetry and hysteresis suggesting ionic flow or leakage; (b) of tunnelling with typical rectification ratio of 8 – 15 at ±1 V.

The hysteresis-like I-V characteristics (their appearance was independent from forward and reverse bias) were observed when the tip was contacting the same point on the surface for a long time. That meant that the initial current flow was probably tunnelling, which was exchanged (or enhanced) by ionic flow when the applied working field redistributed ions along the molecule resulting in water contacting the tip directly. The same phenomena might have occurred in the case of the previous bilayer, although this was not noticed (due to the huge amount of hysteretic I-V plots).

Rectification ratio calculated for non-hysteretic I-V plots (in the range of 8 – 15 at ±1 V; Figure 6.62 b). They probably represent pure tunnelling mechanism what can be concluded from the magnitude of the rectification (*ca*. 0.1 – 0.4 nA dependent on sample and current setpoints).

6.5.4 Summary

The ionic assembly process (ESA) is straightforward since it depends on the electrostatic interaction of two components in solution. It can be assumed that by appropriate selection of components (molecules with similar molecular areas), electrostatic interaction can create multi-component assemblies of small molecules. Ionically coupled films seem to possess good order, however no investigations were performed to compare it with other assemblies (SAMs). Inability to obtain UV-Vis spectra of the most hybrids (except two) on Pt-coated glass slides and the magnitude of the absorbance seem to suggest smaller number of cationic molecules in electrostatically-coupled films.

STM measurements of bilayers on Au-coated substrates revealed the higher current in the negative quadrant of the I-V plot, which suggested electron transfer from the substrate via anionic surface to the acceptor and then from the donor to the STM tip. Therefore the direction of the electron flow could be attributed to the Aviram-Ratner

model. However, high rectification ratios (higher than in SAMs) observed for systems with Au-S-C_3H_6-SO_3^- anion suggest that that it may result from push-pull character of the molecule and be enhanced by the electrostatic interaction of the cationic chromophore with an anionic surface. These revelations has been recently published (see chapter 8, publication III) and benefit from the rectification ratio of 450 at ±1 V for Q^+-π-$C_6H_4N(C_4H_9)_2$ molecule, which is the highest to date for donor-(π-bridge)-acceptor molecular system.

Unfortunately, there is little evidence to support the thesis of water, present in molecular films, affecting the electrical properties. (The idea came up with the QCM kinetics curve which could not reach a plateau region as it continuously dropped). However such explanation was given in order to explain the shape of the hysteretic I-V characteristics, which were characteristic for the Au-S-$C_7H_4N_2$-SO_3^- (which was deposited as a hydrated to compose anionic surface) but not Au-S-C_3H_6-SO_3^-. However, if it was true there is a necessity to counteract the water trapping effect. This can be achieved by drying samples in a desiccator environment and deposition in higher than room temperature to ensure that the hydrated salt will loose its water.

7 Conclusions and recommendations

For all rectifying zwitterion-type SAMs a higher current was observed at forward bias in the positive quadrant of the I-V plot. Relying on the Aviram-Ratner model, it can be assumed that on one side of the device electrons flowed from the tip to the LUMO of the acceptor, and from the HOMO of the donor to the substrate on the other side. This process was followed by an electron transfer between acceptor and donor to restore the molecular ground state (see example molecule in Figure 7.1). In zwitterionic molecules the —$C(CN)_2$ group acted as an acceptor, whereas the heterocycle was a donor. This confirmed theoretical analysis of Pickholtz and dos Santos, as molecules within the monolayer adopted a quinoid, rather than a charge-separated zwitterionic form, in order to minimise the repulsion energy of a parallel side-by-side arrangement of aligned dipoles. The quinoid ground state was also confirmed to be present in Q3CNQ monolayers assembled on thin layers of gold with spectroscopic techniques.

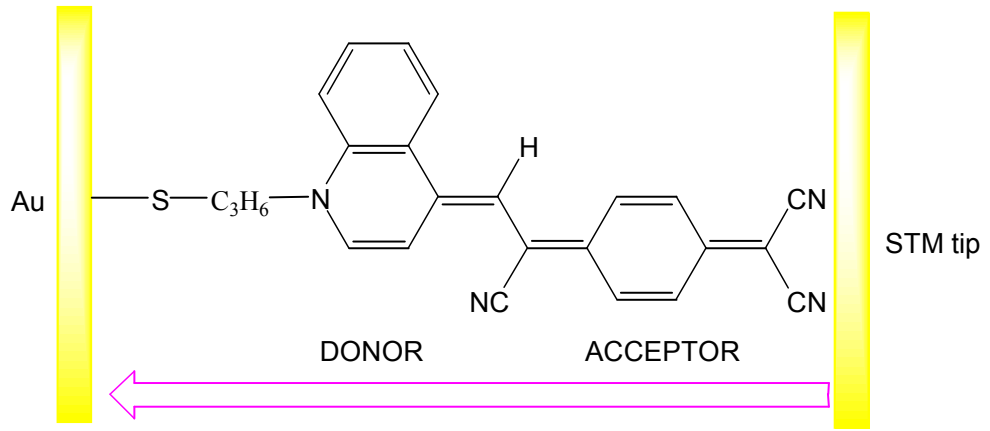

Figure 7.1 SAM of zwitterionic molecule deposited on gold (Au-S-C_3H_6-Q3CNQ) and contacted with STM tip. Arrow signifies the preferred direction of the electron flow across the junction.

Electrical studies of the quinolinium and lutidinium compounds demonstrated that the length of the alkyl chain did not influence the rectifying behaviour of the molecule, as defined by the magnitude of the rectification ratio and the shape of I-V characteristics. Rectification ratios were approximately the same for Q3CNQ, and two analogues of lutidinium compounds; *ca.* 30 at ±1 V and 12 at ±1 V, respectively. I-V characteristics were almost identical and only a slight difference in shape was observed in the elbow region (at *ca.* 0.5 V). Therefore, it can be assumed that the D-(π-bridge)-A character of the molecule was responsible for the greater part of the electrical asymmetry, which supports the Aviram-Ratner theory and disproves the Kornilovitch theory (electrical rectification from asymmetric positioning between electrodes). This was also supported by the results obtained from chemical protonation of the rectifying molecules resulting in a change of the asymmetric I-V characteristics into symmetric, regardless of the length of the alkyl linking the molecule to the surface. The symmetric I-V plots for the planar Au-S-$C_{10}H_{20}$-P3CNQ analogue with weak push-pull properties also backs this up.

Observations of current jumps during the electrical study of Au-S-C_8H_{16}-Q3CNQ molecule should be a standard technique which all Q3CNQ and P3CNQ molecules should be subjected to. It could help with the caluclations of conductance of single molecules. However, The STM break-junction method was used for the first time to measure the current arising from tip-single D-(π-bridge)-A molecule contact and the results were feasible.

Comparing all molecular diodes presented in this thesis, it can be assumed that high electrical rectification is possible for D-(π-bridge)-A dyes, which are sterically hindered. Whereas dyes with planar chromophores, where the donor and the acceptor are effectively coupled do not rectify. Sterically hindered out-of-plane rotation was probably sufficient to isolate the push and pull moieties and thus prevent overlap of their molecular orbitals. The only molecule that did not rectify was the planar

Au-S-$C_{10}H_{20}$-P3CNQ analogue. This molecule was almost planar and so it was assumed that the quinoid ground state and zwitterionic excited state were degenerate resonant forms, and so the I-V characteristics are symmetric. Therefore, it can be assumed that designing Aviram-Ratner like unimolecular rectifiers with π-bridges and steric hinderance is a necessity together with strong push-pull properties.

A new effective method of assembling molecular D-(π-bridge)-A diodes was found that allowed reaching the highest rectification ratio to date from D-(π-bridge)-A molecules. The method was based on the ionic assembly of cationic D-(π-bridge)-A molecules on anionic surfaces of simple thiols and excluded the use of chromophores containing a self-assembling thiol group. The anionic surface was a layer of sodium 3-mercapto-1-propanesulfonate thiol, whose molecular area was comparable with that of all four chromophores. It was thought that every anionic thiol attracted only one cationic dye, so the systems were highly-ordered. STM measurements showed the higher current at forward bias in negative quadrant of the I-V plot and the rectification ratio was at least the same or higher (for example Au-S-C_3H_6-SO_3^- Q^+-π-$C_{10}H_6OCH_3$ and Au-S-C_3H_6-SO_3^- Q^+-π-$C_{10}H_6N(CH_3)_2$ respectively) than for the same chromophores deposited by conventional self-assembly. Therefore, it can be assumed that electrostatic interaction of two components could enhance the rectifying properties of monolayers. The direction of the current flow occurred in accordance with the Aviram-Ratner model (see example molecule in Figure 7.2), however verification of whether the mechanism was only tunnelling was difficult to determine.

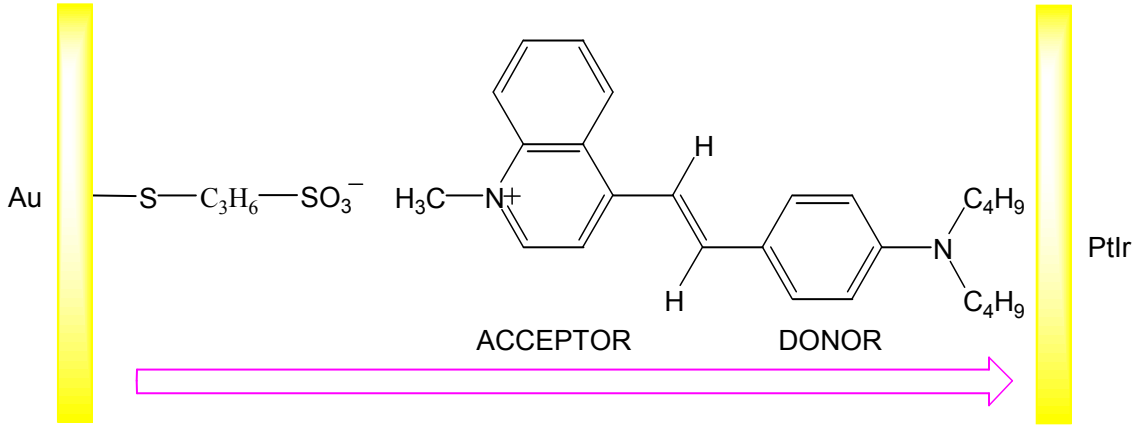

Figure 7.2 Aligned molecular diode Au-S-C_3H_6-SO_3^- Q^+-π-C_6H_4 $N(C_4H_9)_2$ deposited on gold and contacted with STM tip. Arrow signifies the preferred direction of the electron flow across the junction. Q^+ – acceptor, 1-methyl-quinolinium.

In designing molecular systems based on ionic coupling, the molecular dimensions should play a crucial role in the selection of components for multilayered structures. The results for the bulkier anionic surface (Au-S-$C_7H_4N_2$-SO_3^-) compared to Au-S-C_3H_6-SO_3^- showed that components with different area per molecule produced disorder in the following layers. This could contribute to water (or other solvents) being trapped, which can substantially modify electron transport, due to the effects of media polarisation (that dominate traditional molecular electron transfer) and molecule-electrode interactions.

The method of assembling cationic D-π-A molecules on anionic surfaces seems to have great potential in developing assemblies for molecular electronics applications. It will allow the construction of diode-like lattices of alternate donors and acceptors by a simple immersion method. The advantage of this is rectification ratios which can be higher than for conventional SAMs built from the same components. However, this method requires more advanced studies, which acknowledge the structural and optical properties of ionically coupled systems.

In summary, results presented in this thesis deal with a major challenge in molecular-scale electronics, which is the understanding of the alignment and electrical properties of the molecules assembled into molecular junctions with particular interest placed in the molecular rectification mechanism.

8 Publications

The list of publications related to the results described in this thesis:

I. G.J. Ashwell, A. Chwialkowska and L.R.H. High, "Au-S-C_nH_{2n}-Q3CNQ: self-assembled monolayers for molecular rectification", *Journal of Materials Chemistry*, **2004**, *14*, 2389 – 2394.

II. G.J. Ashwell, A. Chwialkowska and L.R.H. High, "Rectifying Au-S-C_nH_{2n}-P3CNQ derivatives", *Journal of Materials Chemistry*, **2004**, *14*, 2848 – 2851. *Designated as a "Hot Article" and as a "Top Ten Article" by the Royal Society of Chemistry and also reviewed by P. Earis, Chemistry World,* ***2004****, 1(11), 16.*

III. G.J. Ashwell and A. Chwialkowska, "Controlled alignment of molecular diodes via ionic assembly of cationic donor-(π-bridge)-acceptor molecules on anionic surfaces", *Chemical Communications*, **2006**, *7*, 1404 – 1406.

IV. G.J. Ashwell, K. Moczko, M. Sujka, A. Chwialkowska, L.R.H. High and D.J. Sandman, "Molecular diodes and ultra-thin organic rectifying junctions: Au–S–C_nH_{2n}–Q3CNQ and TCNQ derivatives", *Physical Chemistry Chemical Physics*, **2007**, *9*, 996 – 1002.

V. A. Girlando, C. Sissa, F. Terenziani, A. Painelli, A. Chwialkowska and G.J. Ashwell, "In situ spectroscopic characterisation of rectifying molecular monolayer self-assembled on gold", in preparation for Royal Society of Chemistry journal.

References

[1] T. Hey and P. Walters, "The new quantum universe", Cambridge Univversity Press, **2003**.

2 G. Cao, "Nanostructures and nanomaterials: synthesis, properties and applications", Imperial College Press, London **2004**.

[3] I.M. Ross, "The Invention of the Transistor", *Proceedings of the IEEE*, **1998**, *86*, 7 – 28.

[4] R.H. Dennard, F.H. Gaensslen, N.-H. Yu, V.L. Rideout, E. Bassous and A.R. LeBlanc, "Design of ion-implanted MOSFET's with very small physical dimensions", *Proceedings of the IEEE*, **1999**, *87*, 668 – 678.

[5] Y. Wada, T. Uda, M. Ludwyche, S. Kondo and S. Heike, "A proposal of nanoscale devices based on atom/molecule switching", *Journal of Applied Physics*, **1993**, *74*, 7321 – 7328.

[6] G. E. Moore, "Cramming more components onto integrated circuits", *Electronics*, **1965**, *38*, 114 – 117.

[7] S. Thompson, "A 90 nm logic technology featuring 50 nm strained silicon channel transistors, 7 layers of Cu interconnects, low k ILD and 1 μm^2/SPAM cell ", *International Devices Meeting, IEDM Technical Digest*, **2002**, 61 – 64.

[8] R.M. Ramanathan and R. Willoner, 'Silicon innovation: Leaping from 90 nm to 65 nm', Technical report at *Technology@ Intel Magazine,* Intel Corporation, **2006**.

[9] Intel Corporation, "Moore's Law" (web page: http://www.intel.com/technology/mooreslaw/).

[10] G. Maruccio, R. Cingolani and R. Rinaldi, "Projecting the nanoworld: concepts, results and perspectives of molecular electronics", *Journal of Materials Chemistry*, **2004**, *14*, 542 – 554.

[11] N.K. Chaki, M. Aslam, J. Sharma and K. Vijayamohanan, "Applications of self-assembled monolayers in materials chemistry", *The Proceedings of the Indian Academy of Sciences (Chemical Science)*, **2001**, *113*, 659 – 670.

[12] P. Berveld, N.F. de Rooij and J.M. Zemel, "Physcial mechanisms for chemically sensitive semiconductor devices", *Nature*, **1978**, *273*, 438 – 443.

[13] B. Mann and H. Kuhn, "Tunnelling through fatty acid salt monolayers", *Journal of Applied Physics* **1971**, *42*, 4398 – 4405.

[14] A. Aviram and M. Ratner, "Molecular rectifiers", *Chemical Physics Letters*, **1974**, *29*, 277 – 283.

[15] A. Pockels, "Surface tension", *Nature*, **1891**, *43*, 437 – 439.

[16] L. Rayleigh, "Investigations in capillarity", *Philosophical Magazine*, **1899**, *48*, 321

[17] I. Langmuir, "The constitution and fundamental properties of solids and liquids. II. Liquids", *Journal of the American Chemical Society*, **1917**, *39*, 1848 – 1902.

[18] K.B. Blodgett, "Films built by depositing successive monomolecular layers on a solid surface", *Journal of the American Chemical Society*, **1935**, *57*, 1007 – 1022.

[19] M. A. Carpenter, C.S. Willand, T.L. Penner, D.J. Williams and S. Mukamel, "Aggregation in hemicyanine dye Langmuir-Blodgett films: Ultraviolet-Visible absorption and Second-Harmonic Generation studies", *Journal of Physical Chemistry*, **1992**, *96*, 2801 – 2804.

[20] N.A. Bell, C.S. Bradley, R.A. Broughton, S.J. Coles, D.E. Hibbs, M.B. Hursthouse, A.K. Ray, D.J. Simmonds and S.C. Thorpe, "Comparison of the structure property relationships in LB films of zwitterionic TCNQ adducts", *Journal of Materials Chemistry*, **2005**, *15*, 1437 – 1445.

[21] G.J. Ashwell, "Langmuir-Blodgett films: molecular engineering of non-centrosymmetric structures for second-order lonear optical applications", *Journal of Materials Chemistry*, **1999**, *9*, 1991 – 2003.

[22] G.J. Ashwell and G.A.N. Paxton, "Multifunctional Properties of *Z*-β-(*N*-hexadecyl-4-quinolinium)-α-cyano-4-styryldicyanomethanide: a molecular rectifier, optically non-linear dye, and ammonia sensor", *Australian Journal of Chemistry*, **2002**, *55*, 199 – 204.

[23] W.C. Bigelow, D.L. Pickett and W.A. Zisman, "Oleopphobic monolayer. Films adsorbed from solution in non-polar liquids", *Journal of Colloid and Interface Science*, **1946**, *1*, 513 – 538.

[24] R.G. Nuzzo and D.L. Allara, "Adsorption of bifunctional organic disulfides on gold surface", *Journal of the American Chemical Society*, **1983**, 105, 4481 – 4483.

[25] F. Schreiber, "Structure and growth of self-assembling monolayers", *Progress in Surface Science*, **2000**, *65*, 151 – 126.

[26] S.R. Forrest, "Ultrathin organic films grown by organic molecular beam deposition and related techniques", *Chemical Reviews*, **1997**, *97*, 1793 – 1896.

[27] G. Roberts, "Langmuir-Blodgett films", Plenum Press, New York, **1990**.

[28] M. Petty, M. Bryce and D. Bloor, "An Introduction to Molecular Electronics", Edward, Great Britain, **1995**.

[29] M.C. Petty, "Langmuir-Blodgett films: An introduction", Cambridge University Press, **1996**.

[30] P.S. Vincent and G.G. Robers, "Electrical and photoelectrical transport properties of Langmuir-Blodgett films and a discussion of possible device applications", T*hin Solid Films*, **1980**, *68*, 135 – 171.

[31] A. Eberhardt, P. Fenter and P. Eisenberg, "Growth kinetics in self-assembling monolayers: a unique adsorption mechanism", *Surface Science*, **1998**, *397*, L285 – L290.

[32] G.E. Poirier and E.D Pylant, "The self-assembly mechanism of alkanethiols on Au (III)", *Science*, **1996**, *272*, 1145 – 1148.

[33] C.D. Bain, E.B. Troughtoyt, Y.-T. Tao, J. Evall, G.M. Whitesides and R.G. Nuzzo, "Formation of monolayer films by the spontaneous assembly of organic thiols from solution onto gold", *Journal of the American Chemical Society*, **1989**, *111*, 321 – 335.

[34] R. Yamada, H. Wano and K. Uosaki, "Effect of the temperature on structure of the self-assembled monolayer of decanethiol on Au (111) surface", *Langmuir*, **2000**, *16*, 5523 – 5525.

[35] D.K. Schwartz, "Mechanism and kinetics of self-assembled monolayer formation", *Annual Review of Physical Chemistry*, **2001**, *52*, 107 – 137.

[36] D.L. Allara, A.N. Parikh and F. Rondelez, "Evidence for a unique chain organisation in long chain silane monolayers deposited on two widely different solid substrates", *Langmuir*, **1995**, *11*, 2357 – 2360.

[37] N. Tillman, A. Ulman, J.S. Schildkraut and T.L. Peller, "Incorporation of phenoxy groups in self-assembled monolayers of trichlorosilane derivatives. Effects on film thickness, wettability, and molecular orientation", *Journal of the American Chemical Society*, **1988**, *110*, 6136 – 6144.

[38] A. Ulman, "Formation and structure of self-assembled monolayers", *Chemical Reviews*, **1996**, *96*, 1533 – 1554.

[39] K. Bierbaum and M. Grunze, "Growth of self-assembled n-alkytrichlorolsilane films on Si (100) investigated by atomic force microscopy", *Langmuir*, **1995**, *11*, 2143 – 2150.

[40] A. Glaser, J. Foisner, G. Friedbacher and H. Hoffmann, "Low-temperature investigation of the growth mechanism of alkylsiloxane self-assembled monolayers", *Analytical and Bioanalytical Chemistry*, **2004**, *379*, 653 – 657.

[41] P.E. Laibinis, G.M. Whitesides, D.L. Allara, Y.T. Tao, A.N. Parikh and R.G. Nuzzo, "Comparison of structure and wetting properties of self-assembled monolayers of n-Alkanethiols on the coinage metal surfaces, Cu, Ag, Au", *Journal of the American Chemical Society*, **1991**, *113*, 7152 – 7167.

[42] Y.T. Kim and A.K. Bard, "Imaging and etching of self-assembled n-octadecanethiol layers on gold with the scanning tunneling microscope", *Langmuir*, **1992**, *8*, 1096 – 1102.

[43] M.M. Walczak, C. Chung, S.M. Stole, C.A. Widrig and M.D. Porter, "Structure and interfacial properties of sponataneously adsorbed n-alkanethiolate monolayers on evaporated silver surfaces", *Journal of the American Chemical Society*, **1991**, *113*, 2370 - 2378.

[44] S. Lee, J. Park, R. Ragan, S. Kim, Z. Lee, D.K. Lim, D.A.A. Ohlberg and R.S. Williams, "Self-Assembled monolayers on Pt (111): Molecular packing structure and strain effects observed by scanning tunneling microscopy" *Journal of the American Chemical Society*, **2006**, *128*, 5745 – 5750.

[45] H. Ron, H. Cohen, S. Matlis, M. Rappaport and I. Rubinstein, "Self-assembled monolayers on oxidised metals: superior n-alkanethiol monolayers on copper", *Journal of Physical Chemistry B*, **1998**, *102*, 9861 – 9869.

[46] Y. Liu, X. Fan, D. Yang, C. Wang, L. Wan and C. Bai, "Tunnelling characteristics of octadecyl derivatives on tin and indium electrodes", *Langmuir*, **2004**, *20*, 855 – 861.

[47] M.L. Chabinyc, X. Chen, R.E. Holmlin, H. Jacobs, H. Skulason, C.D. Frisbie, V. Mujica, M.A. Ratner, M.A. Rampi and G.M. Whitesides, "Molecular rectification in a metal-insulator-metal junction based on self-assembled monolayers", *Journal of the American Chemical Society*, **2002**, *124*, 11730 – 11736.

[48] K. Slowinski, H.K.Y. Fong and M. Majda, "Mercury-mercury tunnelling junctions. 1. Electron tunnelling across symmetric and asymmetric alkanethiolate bilayers", *Journal of the American Chemical Society*, **1999**, *121*, 7257 – 7261.

[49] C.W. Sheen, J.X. Shi, J. Martensson, A.N. Parikh and D.L. Allara, "A new class of organized self-assembled monolayers: alkane thiols on GaAs (100)", *Journal of the American Chemical Society*, **1992**, *114*, 1514 – 1515.

[50] B. Larade and A.M. Bratovsky, "Effect of the impurities on transport through organic self-assembled molecular films from first principles", *Physical Review B*, **2005**, *72*, art. no. 035440.

[51] J.C. Love, D.B. Wolfe, M.L. Chabinyc, K.E. Paul and G. Whitesides, "Self-assembled monolayers of alkanethiolates on palladium are good etch resists", *Journal of the American Chemical Society*, **2002**, *124*, 1576 – 1577.

[52] J.C. Love, L.A. Estroff, J.K. Kriebel, R.G. Nuzzo and G. Whitesides, "Self-assembled monolayers of thiolates on metals as a form of nanotechnology", *Chemical Reviews*, **2005**, *105*, 1103 – 1169.

[53] L.H. Dubois, B.R. Zegarski and R.G. Nuzzo, "Fundamental studies of microscopic wetting on organic surfaces. 2. Interaction of secondary adsorbates with chemically textured organic monolayers", *Journal of the American chemical Society*, **1990**, *112*, 570 – 579.

[54] Y. Ning, H. Xie, H. Xing, W. Deng and D. Yang, "Comparison of self-assembled monolayers of n-Alkanethiols and Phenylthioureas on the surface of gold", *Surface and Interface Analysis*, **1998**, *24*, 667 – 670.

[55] A.A. Dhirani, R.W. Zehner, R.P. Hsung, P. Guyot-Sionnest and L.R. Sita, "Self-assembly of conjugated molecular rods: A high-resolution STM study", *Journal of the American Chemical Society*, **1996**, *118*, 3319 – 3320.

[56] G. Yang, Y. Xian, C. Engtrakul, L.R. Sita and G.Y. Liu, "Arenethiols from ordered and incommensurate self-assembled monolayers on Au (111)", *Journal of Physical Chemistry B*, **2000**, *104*, 9059 – 9062.

[57] J.J. Stapleton, P. Harder, T.A. Daniel, M.D. Reinard, Y. Yao, D.W. Price, J.M. Tour and D.L. Allara, "Self-assembled oligo(phenylene-ethylene) molecular electronic switch monolayers on gold: structures and chemical stability", *Langmuir*, **2003**, *19*, 8245 – 8255.

[58] K Walzer, E Marx, NC Greenham, RJ Less, P.R. Raithby and K. Stokbro, "Scanning tunneling microscopy of self-assembled phenylene", *Journal of the American Chemical Society*, **2004**, *126*, 1229 – 1234.

[59] R.K. Iler, "Multilayers of colloidal particles", *Journal of Colloid and Interface Science*, **1996**, *21*, 569 - 594.

[60] G. Decher, J.D. Hong and J. Schmidt, "Buildup of ultrathin multilayer films by a self-assembly process: III. Consecutively alternating adsorption of anionic and cationic polyelectrolytes on charged surfaces", *Thin Solid Films*, **1992**, *210/211*, 831 – 835.

[61] Y. Lvov. F. Essier and G. Decher, "Combination of polycation/polyanion self-assembly and Langmuir-Blodgett transfer for construction of superlattice films", *Journal of Physical Chemistry*, **1993**, *97*, 13773 – 13777.

[62] G. Decher, Y. Lvov and J. Schmidt, "Proof of multilayer structural organization in self-assembled polycation-polanion molecular films", *Thin Solid Films*, **1994**, *244*, 772-777.

[63] K.N. Lenahan, Y. Liu, Y. Wang and R.O. Claus, "Electrostatic self-assembly processes for noncentrosymmetric thin films and devices", *Proceedings of SPIE*, **1999**, *3675*, 104 – 112.

[64] Y. Zhang and W. Cao, "Self-assembly of small molecules: an approach combining electrostatic self-assembly technology with host-guest chemistry", *New Journal of Chemistry*, **2001**, *25*, 483 – 486.

[65] C. Deng, M.Li, Q. Xie, M. Liu, Y. Tan, X. Xu and S. Yao, "New glucose biosensor based on a poly(o-phenylendiamine)/glucose oxidase-glutaraldehyde/Prussian blue/Au electrode with QCM monitoring of various electrode-surface modifications", *Analytica Chimica Acta*, **2006**, *557*, 85 – 94.

[66] A. Nabok, "Organic and inorganic nanostructures", Artech House Publishers, Boston, **2005**.

[67] Y. Lvov, and H. Mohwald, "Protein Architecture. Interfacing Molecular Assemblies and Immobilization Biotechnology", *Marcel Dekker*, New York, **2000**.

[68] S. Das and A.J. Pal, "Layer-bylayer self-assembling of a low molecular weight organic material by different electrostatic adsorption process", *Langmuir*, **2002**, *18*, 458 – 461.

[69] B. Mukherjee and A.J. Pal, "Rectification in molecular assemblies of donor-acceptor monolayers", *Chemical Physics Letters*, **2005**, *416*, 289 – 292.

[70] G.J. Ashwell, B. Urasinska, C. Wang, M.R. Bryce, I. Grace and C.J. Lambert, "Single-molecule electrical studies on a 7 nm long molecular wire", *Chemical Communications*, **2006**, *15*, 4706 – 4708.

[71] B. Bhushan and H. Fuchs, "Applied Scanning Probe methods III. Characterisation", *Springer*, **2004**.

[72] F. Caruso, T. Serizawa, D.N. Furlong and Y. Okahata, "Quartz crystal microbalance and surface plasmon resonance study of surfactant adsorption onto gold and chromium oxide surfaces", *Langmuir*, **1995**, *11*, 1546 – 1552.

[73] L.E. Bailey, D. Kambhampati, K.K. Kanazawa, W. Knoll and C.W. Frank, "Using surface plasmon resonance and the quartz crystal microbalance to monitor in situ the interfacial behvior of thin organic films", *Langmuir*, **2002**, *18*, 479 – 489.

[74] A. Ballato, "Piezoelectricity: history and new thrusts", *Ultrasonics Symposium, Proceedings to the IEEE*, **1996**, *1*, 375 – 381.

[75] C.F. Brockelsby, "Some applications of ultrasonics" *Journal of Scientific Instruments*, **1963**, *40*, 153 – 157.

[76] D.A. Buttry and M.D. Ward, "Measurement of interfacial processes at electrode surface with the electrochemical quartz crystal microbalance", *Chemical Reviews*, **1992**, *92*, 1355 – 1379.

[77] C.K. O'Sullivan and G.G. Guilbault, "Commercial quartz crystal microbalances – theory and applications", *Biosensors & Bioelectronics*, **1999**, *14*, 663 – 670.

[78] G. Sauerbrey, "Use of oscillator quartz crystals for weighing thin layers and micro-waighing", *Z. Physik*, **1959**, *155*, 206 – 222.

[79] K.K. Kanazawa and J.G. Gordon II, "Frequency of quartz microbalance in contact with liquid", *Analytical Chemistry*, **1985**, *57*, 1770 – 1771.

[80] Z. Kretschman, "The determination of the optical constants of metals by excitation of surface plasmons", *Z. Physik* **1971**, *241*, 313 – 324.

[81] E. Burstein, W. P. Chen, Y. J. Chen, A. Harstein, "Surface polaritons – propagating electromagnetic modes at interfaces", *Journal of Vacuum Science and Technology*, **1974,** *11*, 1004 – 1024.

[82] K.A. Peterlinz and R. Georgiadis, "In situ kinetics of self-assembly by surface plasmon resonance spectroscopy", *Langmuir*, **1996**, *12*, 4731 – 4740.

[83] T.T. Ehler, N. Malmberg and L.J. Noe, "Characterisation of self-assembled alkanethiol monolayers on silver and glod using surface plasmon spectroscopy", *Langmuir*, **1997**, *101*, 1286 – 1272.

[84] A. Hatta, S. Suzuki and W. Suetaka, "Polarization-modulation electronic absorption study of copper phtalocyanine films on silver by surface plasmon resonance spectroscopy", *Applied Surface Science*, **1989**, *40*, 9 – 18.

[85] I. Pockrand, J.D. Swalen, J.G. Gordon II and M.R. Philpott, "Surface plasmon spectroscopy of organic monolayer assemblies", *Surface Science*, **1997**, *74*, 237 – 244.

[86] G.J. Ashwell, A.A. Maxwell and A. Green, "Unconventional Langmuir-Blodgett films: alignment of an optically nonlinear dye where the donor and π-electron bridge are hydrophobic and the acceptor is hydrophilic", *Journal of Materials Chemistry*, **2002**, *12*, 2192 – 2196.

[87] G.J. Ashwell, G.A.N. Paxton, A.J. Whittam, W.D. Tyrrell, M. Berry and D. Zhou, "Merocyanine dyes: self-assembled monolayers", *Journal of Materials Chemistry*, **2002**, *12*, 1631 – 1635.

[88] J. Homola, S. S. Yee, G. Gauglitz, "Surface plamon resonance sensors: review", *Sensors and Actuators B,* **1999**, *54*, 3 – 15.

[89] J.G. Simmons, "Generalized formula for the electric tunnel effect between similar electrodes separated by a thin insulating film", *Journal of Applied Physics*, **1963**, *34*, 1793 – 1804.

[90] L.A. Bumm, J.A. Arnold, T.D. Dunbar, D.L. Allara and P.S. Weiss, "Electron transfer through organic molecules", *Journal of Physical Chemistry B*, **1999**, *103*, 8122 – 8127.

[91] D. Vuillaume, S. Lenfant, "The metal/organic monolayer interface in molecular electronic devices", *Microelectronic Engineering*, **2002**, *70*, 539 – 550.

[92] Y. Selzer, M.A. Cabassi, T. Mayer and D.L. Allara, "Temperature effects on conduction through a molecular junction", *Nanotechnology*, **2004**, *15*, 483-488.

[93] G.R. Hutchison, M.A. Ratner and T.J. Marks, "Hopping transport in conductive heterocyclic oligomers: reorganisation energies and substituent effects", *Journal of the American Chemical Society*, **2005**, *127*, 2339 – 2350.

[94] M.A. Reed, C. Zhou, C.J. Mullen, T.P. Burgin and J.M. Tour, "Conductance of molecular junction", *Science*, **1997**, *278*, 252 – 254.

[95] J. Chen, M.A. Reed, A.M. Rawlett and J.M. Tour, "Large on-off ratios and negative differential resistance in a molecular electronic device", *Science*, **1999**, *286*, 1550 – 1552.

[96] A.V. Walker, T.B. Tighe, O.M. Cabarcos, M.D. Reinard, B.C. Haynie, S. Uppili, N. Winograd and D.L. Allara, "The dynamics of noble metal atom penetration through methoxy-terminated alkanethiolate monolayers", *Journal of the American Chemical Society*, **2004**, *126*, 3954 – 3963.

[97] Z. Zhu, T.A. Daniel, M. Maitani, O.M. Cabarcos, D.L. Allara and N. Winograd, "Controlling gold atom penetration through alkanethiolate self-assembled monolayers on Au {111} by adjusting terminal group intermolecular interactions", *Journal of the American Chemical Society*, **2006**, *128*, 13710 – 13719.

[98] S. Chang, Z. Li, C. N. Lau, B. Larade, R. S. Williams, "Investigation of a model molecular-electronic rectifier with an evaporated Ti-metal top contact", *Applied Phyics Letters*, **2003**, *83*, 3198 – 3200.

[99] R. McCreery, J. Dieringer, A. O. Solak, B. Snyder, A.M. Nowak, W.R. McGovern and S. DuVall, "Molecular rectification and conductance switching in carbon-based molecular junction by structural rearrangement accompanying electron injection', *Journal of the American Chemical Society*, **2003,** *125*, 10748 – 10758.

[100] R. McCreery, J. Dieringer, A. O. Solak, B. Snyder, A.M. Nowak, W.R. McGovern and S. DuVall, "Molecular rectification and conductance switching in carbon-based molecular junction by structural rearrangement accompanying electron injection', *Journal of the American Chemical Society*, **2004,** *126*, 6200.

[101] W. Hu, Y. Liu, Y. Xu, S. Liu, S. Zhou and D. Zhu, "The application of Langmuir-Blodgett films of a new asymmetrically substituted phthalocyanine, amino-tri-tert-butyl-phthalocyanine, in diodes and in all organic field effect transistors", *Synthetic Metals*, **1999**, *104*, 19 – 26.

[102] A.K. Mahapatro and S. Ghosk, "Schottky energy barrier and charge injection in metal/copper-phthalocyanine/metal structures", *Applied Physics Letters*, **2002**, *80*, 4840 – 4842.

[103] H.M. Manohara, E.W. Wong, E. Schlecht, B.D. Hunt and P.H. Siegel, "Carbon nanotube Schottky diodes using Ti-Schottky and Pt-ohmic contacts for high frequency applications" *Nano Letters* **2005**, *5*, 1469 – 1474.

[104] J. Bastein, A. Assadi, S. Soderholm, J. Hellberg and M. Moge, "Fabrication and characterisation of Schottky barrier diodes with tetracyanoquinodimethane doped with bis (β-naphthyl)-tetra-thiafulvalene", *Synthetic Metals*, **1996**, *82*, 97 – 101.

[105] R.K. Gupta and R.A. Singh, "Fabrication and characteristics of Schottky diode based on composite organic semiconductors", *Composites Science and Technology*, **2005**, *65*, 677 – 681.

[106] M. Pomerantz ,A. Aviram, R.A. McCorkle, L. Li and A.G. Schrott, "Rectification of STM current to graphite covered with phthalocyanine molecules", *Science*, **1992**, *255*, 1115 – 1118.

[107] O.M. Magnussen, B.M. Ocko, M. Deutsch, M.J. Regan, P.S. Pershan, D. Abernathy, G. Grubel and J-F. Legrand, "Self-assembly of organic films on a liquid metal", *Nature*, **1996**, *384*, 250 – 252.

[108] R.L. York, P.T. Nguyen and K. Slowinski, "Long-range electron transfer through monolayers and bilayers of alkanethiols in electrochemically controlled Hg-Hg tunnelling junctions", *Journal of the American Chemical Society*, **2003**, *125*, 5948 – 5953.

[109] M.A. Rampi and G.M. Whitesides, "A versatile experimental approach for understanding electron transport through organic materials", *Chemical Physics*, **2002**, *281*, 373 – 391.

[110] J.G. Kushmerick, D.B. Holt, J.C. Yang, J. Naciri, M.H. Moore and R. Shashidhar, "Metal-molecule contacts and charge transport across monomolecular layers: measurement and theory", *Physical Review Letters*, **2002**, *89*, art. no. 086802.

[111] J.G. Kushmerick, J. Naciri, J.C. Yang and R. Shashidhar, "Conductance scaling of molecular wires in parallel", *Nano Letters*, **2003**, *3*, 897 – 900.

[112] J.G. Kushmerick, D.B. Holt, S.K. Pollack, M.A. Ratner, J.C. Yang, T.L. Schull, J. Naciri, M.H. Moore and R. Shashidhar, "Effect of bond-length alternation in molecular wires", *Journal of the American Chemical Society*, **2002**, *124*, 10654 – 10655.

[113] A. S. Blum, J.G. Kushmerick, S.K. Pollack, J.C. Yang, M. Moore, H. Naciri, R. Shashidhar and B.R. Ratna, "Charge transport and scaling in molecular wires", *Journal of Physical Chemistry B*, **2004**, *108*, 18124 – 18128.

[114] G. Binning and H. Rohrer, "Scanning tunnelling microscopy – from birth to adolescence", *Reviews of Modern Physics*, **1987**, *59*, 615 – 625.

[115] H. Rohrer, "Scanning tunnelling microscopy: a surface science tool and beyond", *Surface Science*, **1994**, *299/300*, 956 – 964.

[116] J.O. Besenhard, U. Krebber, J. K. H. Hörber, N. Kanani, H. Meyer, "A STM study of Pd-catalyst for electroless Cu deposition on nonconductors by means of a modified graphite substrate", *Journal of the Electrochemical Society*, **1989**, *136*, 3608 – 3610.

[117] C. Joachim, J.K. Gimzewski, R.R. Schlitter and C. Chavy, "Electronic transparence of a single C_{60} molecule", *Physical Review Letters* **1995**, *74*, 2102 – 2105.

[118] X. Xiao, B. Xu and N.J. Tao, "Measurements of single molecule conductance: benzenedithiol and nemzemedimethanethiol", *Nano Letters*, **2004**, *4*, 267 – 271.

[119] B. McCarthy, J.N. Coleman, R. Czerw, A.B. Dalton, H.J. Byrne, D. Tekleab, P. Iyer, P.M. Ajayan, W.J. Blau and D.L. Carroll, "Complex nano-assemblies of polymers and carbon nanotubes", *Nanotechnology*, **2001**, *12*, 187 – 190.

[120] E.Meyer, H,Hug, R. Bennewitz, "Scanning Probe Microscopy: The Lab on a Tip (Advanced Texts in Physics S.*)", Springer-Verlag*, Berlin, **2003**.

[121] P. Samori, "Scanning probe microscopies beyond imagining", *Journal of Materials Chemistry*, **2004**, *14*, 1353 – 1366.

[122] R.M. Feenstra, "Scanning tunnelling spectroscopy", *Surface Science,* **1994**, *299/300*, 965 – 979.

[123] T. Müller, "Scanning tunnelling microscopy: A tool for studying self-assembly and model systems for molecular devices", application note by Veeco Instruments Inc., downloaded from: http://veeco.com/products/details.php?cat=1&sub=1&pid=271&option=4&#navIII.

[124] D. M. Eigler, P.S. Weiss and E.K. Schweizer, "Imaging Xe with a low-temperature scanning tunnelling microscope", *Physical Review Letters*, **1991**, *66*, 1189 – 1192.

[125] J. Repp and G. Meyer, "Scanning tunnelling microscopy of adsorbates on isulating films. From the imaging of individual molecular orbitals to the manipulation of the charge state", *Applied Physics A: Materials Science & Processing*, **2006**, *85*, 399 – 406.

[126] C. Bai, "Scanning tunneling microscopy and its applications", Springer Series in Surface Science, Springer and Shanghai Scientific and Technical Publishers, **2000**, vol. 32.

[127] H.P. Lang, M. Hegner, E. Meyer and Ch. Gerber, "Nanomechanics from atomic resolution to molecular recognition based on atomic force microscopy technologu", *Nanotechnology*, **2002**, *13*, R29 – R36.

[128] C.J. Chen, "Introduction to Scanning Tunneling Microscopy, Oxford Series in Optical and Imaging Sciences, Oxford University Press, USA **1993**.

[129] L.J. Whitman, J.A. Stroscio, R.A. Dragoset and R.J. Celotta, "Manipulation of adsorbed atoms and creation of new structures on room-temperature surfaces with a scanning tunnelling microscope", *Science*, **1991**, *251*, 1206 – 1210.

[130] M.F. Crommie, C.P. Lutz and D.M. Eigler, "Confinement of electrons to quantum corrals on a metal surface", *Science*, **1993**, *262*, 218 – 220.

[131] W. Haiss, R.J. Nichols, H. van Zalinge, S.J. Higgins, D. Bethell and D.J. Schiffrin, "Measurement of single molecule conductivity using spontaneous formation of molecular wires", *Physical Chemistry Chemical Physics*, **2004**, *6*, 4330 – 4337.

[132] C.J. Muller, B.J. Vleeming, M.A. Reed, J.J.S. Lamba, R. Hara, L. Jones II and J.M. Tour, "Atomic probes: a search for conduction through a single molecule", *Nanotechnology*, **1996**, *7*, 409 – 411.

[133] J. Reichert, R. Ochs, D. Beckmann, H. B. Weber, M. Mayor and H.V. Löhneysen, "Driving current through single organic molecules", *Physical Review Letters*, **2002**, *88*, 176804 – 176808.

[134] J. Reichert, H. B. Weber, M. Mayor, and H. v. Löhneysen, "Low temperature conductance measurements on single molecules", *Applied Physics Letters*, **2003**, *82*, 4137 – 4139.

[135] M. Mayor and H.B. Weber, J. Reichert, M. Elbing, C. von Hanisch, D. Beckmann and M. Fischer, "Electric current through molecular rod – relevance of the position of the anchor groups", *Andegwandte Chemie International Edition*, **2003**, *42*, 5834 – 5838.

[136] Q. Wang, S. Ward, A. Duda, J. Hua, P. Stradins, R.S. Crandall, H.M. Branz, F. Jeffrey, H. Lou, C. Perlov, W. Jackson, P. Mei and C. Taussing, "Low temperature thin-film silicon diodes for consumer electronics", *Amorphous and Nanocrystalline Silicon Science and Technology*, **2005**, *862*, 709-714.

[137] Guliants, C. Ji, Y.J. Song and W.A. Anderson, "A 0.5-μm-thick polycrystalline silicon Schottky diode with rectification ratio of 10^6", *Applied Physics Letters*, **2002**, *80*, 1474 – 1476.

[138] Q. Wang, S. Ward, A. Duda, J. Hu, P. Stradins, R.S. Crandall, H.M. Branz, C. Perlov, W. Jackson, P. Mei and C. Taussing, "High current density thin-film silicon diodes grown at low temperature", *Applied Physics Letters*, **2004**, *85*, 2122 – 2124.

[139] A.A. Kornyshev and A.M. Kuznetsov, "A new type on in situ single-molecular rectifier", *A European Journal of Chemical Physics and Physical Chemistry*, **2006,** *7*, 1036 – 1040.

[140] A. Nitzan and M.A. Ratner, "Electron transport in molecular wire junctions", *Science*, **2003**, *300*, 1384 – 1389.

[141] P.E. Kornilovitch, A.M. Bratovsky and R. S. Williams, "Current rectification by molecules with asymmetric tunnelling barriers", *Physical Review B*, **2002**, *66*, art. no. 165436.

[142] V. Mujica, M.A. Ratner and A. Nitzan, "Molecular rectification: why is it so rare?", *Chemical Physics*, **2002**, *281*, 147 – 150.

[143] Y. Selzer, M.A. Cabassi, T.S. Mayer and D.L. Allara, "Thermally activated conduction in molecular junctions", *Journal of the American Chemical Society*, **2004**, *126*, 4052 – 4053.

[144] A. Troisi and M.A. Ratner, "Conformational molecular rectifiers", *Nano Letters*, **2004**, *4*, 591 – 595.

[145] R.M. Metzger, "Unimolecular electrical rectifiers", *Chemical Reviews*, **2003**, *103*, 3808 – 3834.

[146] J.C. Ellenbogen and J.C. Love, "Architectures for molecular electronic computers: 1. Logic structures and an adder designed from molecular electronic diodes", *Proceedings of the IEEE*, **2000**, *88*, 386 – 426.

[147] C. Majumder, H. Mizuseki and Y. Kawazoe, "Molecular scale rectifier: theoretical study", *Journal of Physical Chemistry A*, **2001**, *105*, 9454 – 9459.

[148] Stokbro K., J. Taylor and M. Brandbyge, "Do Aviram-Ranter diodes rectify?", *Journal of the American Chemical Society*, **2003**, *125*, 3674 – 3675.

[149] P.G. Collins, A. Zettl, H. Bando, A. Thess and R.E.Smalley, "Nanotube nanodevice", *Science*, **1997**, *278*, 100 – 102.

[150] Z.Wei, M. Kondratenko, L.H. Dao and D.F. Perepichka, "Rectifying diodes from asymmetrically functionalised single-wall carbon nanotubes", *Journal of the American Chemical Society*, **2006**, *128*, 3134 – 3135.

[151] S.S. Gayathri and A. Patnaik, "Electrical rectification form fullerene[60]-dyad based metal-organic metal junction", *Chemical Communications*, **2006**, *18*, 1977 – 1979.

[152] I.H. Campbell, D.L. Smith, C.J. Neef and J.P. Ferraris, "Charge transport in polymer light-emitting diodes at high current density", *Applied Physics Letters*, **1999**, *75*, 841 – 843.

[153] M. Chen, D. Nilsson, t. Kugler, M. Berggren and T. Remonen, "Electric current rectification by an all-organic electrochemical device", *Applied Physics Letters*, **2002**, *81*, 2011 – 2013.

[154] A. Aviram, M. Ratner and M. Pomerantz, "Evidence of switching and rectification by a single molecule effected with a scanning tunneling microscope", *Chemical Physics Letters*, **1988**, *146*, 490 – 495.

[155] R.M. Metzger, C.A. Panetta, N.E. Heimer, A.M. Bhatti, E. Torres, G.F. Blackburn, S.K. Tripathy and L.A. Samuelson, "Toward organic rectifiers: Langmuir-Blodgett films and redox properies of the N-(4-n-dodecyloxyphenyl) and N-(1-pyrenyl) carbamates of 2-bromo-5-(2[1])-hydroxyethoxy)-TCNQ", *Journal of Molecular Electronics*, **1986**, *2*, 119 – 124.

[156] N.J. Geddess J.R. Sambles, D.J. Jarvis, W.G. Parker and D.J. Sandman, "Fabrication and investigation of asymmetric current-voltage of a metal Langmuir-Blodgett monolayer metal structure", *Applied Physics Letters*, **1990**, *56*, 1916 – 1918.

[157] N.J. Geddess J.R. Sambles, D.J. Jarvis, W.G. Parker and D.J. Sandman, "The electrical properties of metal-sandwiched Langmuir-Blodgett multilayers and monolayers of a redox-active organic molecular compound", *Journal of Applied Physics*, **1992**, *71*, 756 – 768.

[158] G. J. Ashwell, K. Moczko, M. Sujka, A. Chwialkowska, L.R.H. High and D.J. Sandman, "Molecular diodes and ultra-thin organic rectifying junctions: Au-S-C_nH_{2n}-Q3CNQ and TCNQ derivatives", *Physical Chemistry Chemical Physics*, **2007**, *9*, 996 – 1002.

[159] M.K. Sujka, unpublished results till PhD thesis **2007**, Cranfield University, Cranfield, UK

[160] P. Wang, J.L. Singleton, X.-L. Wu, M. Shamsuzzhoha, C.A. Panetta, J.W. Kim, N.E. Heimer, S. Stafstrom, W.R. Salaneck, O. Ignasias, and T. Hjertberg, "Scanning tunnelling microscopy and transmission electron microscopy of Langmuir-Blodgett films of three donor-smigma-acceptor molecules: BDDAP-C-HETCNQ, BDDAP-C-HPTCNQ and BDDAP-C-HBTCNQ", *Synthetic Metals*, **1993**, *55 – 57*, 3824 – 3829.

[161] T. Mikayama, M. Ara, K. Uehara, A. Sugimoto, K. Mizuno and N. Inoue, 'Nanometre-scale photoelectric characteristic of a molecular device monolayer', *Physical Chemistry Chemical Physics*, **2001**, *3*, 3459 – 3462.

[162] S. Scheib, M.P. Cava, J.W. Baldwin and R.M. Metzger, "In search of molecular rectifiers. The donor-σ-acceptor system derived from triptycenequinone and tetrathiafulvalene", *Journal of Organic Chemistry*, **1998**, *63*, 1198 – 1204.

[163] L.D. Wescott and D.L. Mattern, "Donor-σ-acceptor molecules incorporating a nonadecyl-swallowtailed perylenediimide acceptor", *Journal of Organic Chemistry* **2003**, 68, 10058 – 10066.

[164] H. Li, E.A. Homan, A.J. Lampkins, I. Ghivirgia and R.K. Castellano, "Synthesis and self-assembly of functionalised donor-σ-acceptor molecules", *Organic Letters*, **2005**, *7*, 443 – 446.

[165] G. Ho, J.R. Heath, M. Kondratenko, D.F. Perepichka, K. Arseneault, M. Pezolet and M.R. Bryce, "The first studies of a tetrathiafulvalene-σ-acceptor molecular rectifier", *Chemistry – A European Journal*, **2005,** *11*, 2914 – 2922.

[166] A.S. Martin, J.R. Sambles, and G.J. Ashwell, "Identification of the process producing observed rectifying characteristics of metal/Langmuir-Blodgett film/ metal structures", *Thin Solid Films*, **1992**, *210/211*, 313 – 316.

[167] A.S. Martin, J.R. Sambles, and G.J. Ashwell, "Molecular rectifier", *Physical Review Letters*, **1993**, *70*, 218 – 221.

[168] R. M. Metzger, B. Chen, U. Höpfner, M.V. Lakshmikantham, D. Vuillaume, T. Kawai, X. Wu, H. Tachibana, T.V. Hughes, H. Sakurai, J. W. Baldwin, C. Hosch, M.P. Cava, L. Brehmer and G.J. Ashwell, "Unimolecular electrical rectification in hexadecylquinolinium tricyanoquinodimethanide", *Journal of the American Chemical Society*, **1997**, *119*, 10455 – 10466.

[169] D. Vuillaume, B. Chen and R.M. Metzger, "Electron transfer through a monolayer of haxadecylquinolinium tricyanoquinodimethanide", *Langmuir*, **1999**, *15*, 4011 – 4017.

[170] R.M. Metzger, T. Xu and I.R. Peterson, "Electrical rectification by a monolayer of haxadecylquinolinium tricyanoquinodimethanide measured between macroscopic gold electrodes", *Journal of Physical Chemistry*, **2001**, *105*, 7280 – 7290.

[171] C. Krzeminski, C. Delure, D. Allan, D. Vuillaume and R.M. Metzger, "Theory of electrical rectification in a molecular rectifier", *Physical Reviews B*, **2001**, *64*, art. no. 085405.

[172] N. Okazaki, J.R. Sambles, M.J. Jory and G.J. Ashwell, "Molecular rectification at 8K in an Au/ $C_{16}H_{33}$-Q3CNQ LB film/Au structure", *Applied Physics Letters*, **2002**, *81*, 2300 – 2303.

[173] X-.L. Wu, M. Shamsuzzoha, R.M. Metzger and G.J. Ashwell, "Scanning tunnelling microscopy and high-resolution transmission electron microscopy of $C_{16}H_{33}$-Q3CNQ, hexadecylquinolinium tricyanoquinomethanice", *Synthetic Metals*, **1993**, *55 – 57*, 3836 – 3841.

[174] G.J. Ashwell, R. Hamilton and R.L.H. High, "Molecular rectification: asymmetric current-voltage curves from self-assembled monolayers of a donor-(π-bridge)-acceptor dye", *Journal of Materials Chemistry*, **2003**, *13*, 1501 – 1503.

[175] T. Xu, T.A. Morris, G.J. Szulczewski, R.R. Amaresh, Y. Gao, S.C. Street, L.D. kispert and R.M. Metzger, "A spectroscopic study of hexadecylquinolinium tricyanoquinomethanide as a monolayer and in bulk", *Journal of Physical Chemistry B*, **2002**, *106*, 10374 – 10381.

[176] G.J. Ashwell and D.S. Gandolfo, "Molecular rectification: dipole reversal in a cationic donor-(π-bridge)-acceptor dye", *Journal of Materials Chemistry*, **2002**, *12*, 411 – 415.

[177] G.J. Ashwell and D.S. Gandolfo, "Molecular rectification using gold/(LB film)/gold structure", *Journal of Materials Chemistry*, **2001**, *11*, 246 – 248.

[178] Y. Nishikata, M. Kakimoto, A. Morikawa, and Y. Imai, "Preparation and characterization of poly(amide-imide) multilayer films", *Thin Solid Films*, **1988**, *160*, 15 – 20.

[179] Y. Nishikata, M. Kakimoto, and Y. Imai, "Preparation and properties of poly(p-phenylene-vinylene) Langmuir-Blodgett film", *Thin Solid Films*, **1989**, *179*, 191 – 197.

[180] G.J. Ashwell and M. Amiri, "Alignment of chevron-shaped molecules for photonic and electronic applications", *Journal of Materials Chemistry*, **2002**, *12*, 2181- 2183.

[181] J.W. Baldwin, R.R. Amaresh, I.R. Peterson, W.J. Shumate, M.P. Cava, M.A. Amiri, R. Hamilton, G.J. Ashwell and R.M. Metzger, "Rectification and nonlinear optical properties of a Langmuir-Blodgett monolayer of a pyridinium dye", *Journal of Physcial Chemistry B*, **2002**, *106*, 12158 – 12164.

[182] G.J. Ashwell and R.J. Stokes, "Do alkyl tunnelling barriers contribute to molecular rectification?", *Journal of Materials Chemistry*, **2004**, *14*, 1228 – 1230.

[183] G.J. Ashwell, W.D. Tyrrell and A.J. Whittam, "Molecular rectification: self-assembled monolayers in which donor-(π-bridge)-acceptor moieties are centrally located and symmetrically coupled to both gold electrodes", *Journal of the American Chemical Society*, **2004**, *126*, 7102 – 7110.

[184] G.J. Ashwell and A. Mohib, "Improved molecular rectification from self-assembled monolayers of a stearically hindered dye", *Journal of the American Chemical Society*, **2005**, *127*, 16238 – 16244.

[185] S. Sitha and K. Bhanuprakash, "Role of aromatic π-bridge on electron transport property in a donor-bridge-acceptor system: A computational study on frontier molecular orbitals", *Journal of Molecular Structure: Theochem*, **2006**, *761*, 31 – 38.

[186] M-.K. Ng and L. Yu, "Synthesis of amphiphilic conjugated diblock oligomers as molecular diodes", *Angewandte Chemie International Edition*, **2002**, *41*, 3598 – 3601.

[187] P. Jiang, G.M. Morales, W. You and L. Yu, "Synthesis of diode molecules and their sequential assembly to control electron transport", *Angewandte Chemie International Edition*, **2004**, *43*, 4471 – 4475.

[188] G.M. Morales, P. Jiang, S. Yuan, Y. Lee, A. Sanchez, W. You and L. Yu, "Inversion of the rectifying effect in diblock molecular diodes by protonation", *Journal of the American Chemical Society*, **2005**, *127*, 10456 – 10457.

[189] J.G. Kushmerick, C.M. Whitaker, S.K. Pollack, T.L. Schull and R. Shashidhar, "Tuning current rectification across molecular junction", *Nanotechnology*, **2004**, *15*, 489 – 493.

[190] M. Elbing, R. Ochs, M. Koentopp, M. Fischer, C. von Hanisch, F. Weigend, F. Evers, H.B. Weber and M. Mayor, "A single-molecule diode", *Proceedings of the National Academy of Sciences of the United States of America*, **2005**, *102*, 8815 – 8820.

[191] C. M. Fischer, M. Burghard, S. Roth, and K. V. Klitzing, "Organic quantum-wells: molecular rectification and single electron tunnelling," *Europhysics Letters*, **1994**, *28*, 129 – 134.

[192] A. Stabel, P. Herwig, K. Mullen and J.P. Rabe, "Diodelike current-voltage curves for a single molecule-tunneling spectroscopy with submolecular resolution of an alkylated, *peri*-condensed hexabenzocoronene", *Angewandte Chemie International Edition*, **1995**, 34, 1609 – 1611.

[193] F. Jackel, Z. Wang, M.D. Watson, K. Mullen and J.P. Rabe, "Nanoscale array of inversely biased molecular rectifiers", *Chemical Physics Letters*, **2004**, *387*, 372 – 376.

[194] M.C. Daniel and D. Astruc, "Gold nanoparicles: Assembly, supramolecular chemistry, quantum-size-related propereties, and application towards biology, catalysis, and nanotechnology", C*hemical Reviews*, **2004**, *104*, 293 – 346.

[195] T. Reda, A.F. Collings, C. Barton and P. Lukins, "Functionalized nanoparticle films with rectifying conduction properties", *Journal of Physical ChemistryB*, **2003**, *107*, 13774 – 13781.

[196] G.J. Ashwell, and M. Berry, "Hybrid SAM/LB device structures: manipulation of the molecular orientation for nanoscale electronic applications", *Journal of Materials Chemistry*, **2005**, *15*, 108-110.

[197] G. J. Ashwell, G.S. Bahra, C.R. Brown, D.G. Hamilton, C.H.L. Kennard and D.E. Lynch, "2,4-Bis[4-(*N*,*N*-dibutylamino)phenyl] squaraine: X-ray crystal structure of a centrosymmetric dye and the second-order non-linear optical properties of its non-centrosymmetric Langmuir–Blodgett films", *Journal of Materials Chemistry*, **1996**, 6, 23 – 26.

[198] M. Berry, "Nanoscale architecture for molecular electronic applications", PhD thesis **2002**, Cranfield University, Cranfield, UK.

[199] G.J. Ashwell, J. Ewington and B.J. Robinson, "Organic rectifying junctions fabricated by ionic coupling", *Chemical Communications*, **2006**, *6*, 618 – 620.

[200] G.J. Ashwell, B. Urasinska and W.D. Tyrell, "Molecules that mimic Schottky diodes", *Physical Chemistry Chemical Physics*, **2006**, *8*, 3314 – 3319.

[201] G.J. Ashwell, A. Mohib and J.R. Miller, "Induced rectification from self-assembled monolayers of sterically hindered π-bridged chromophores", *Journal of Materials Chemistry*, **2005**, *15*, 1160 – 1166.

[202] S.S. Shah, R. Ahmad, S.W.H. Shah, K.M. Asif and K. Naeem, 'Synthesis of cationic hemicyanine dyes and their interactions with anionic surfactants', *Colloids and Surfaces A: Physicochemical and Engineering Aspects*, **1998**, *137*, 301 – 305.

[203] Z. Kretschmann, "The determination of the optical constants of metals by excitation of surface plasmons", *Z. Physik*, **1971**, *241*, 313 – 324.

[204] D.P. Piet, D. Danovitch, H. Zuilhof and E.J.R. Studholter, "Ionization potentials of porphyrins and phthalocyanines. A comparative benchmark study of fast improvements of Koopman's Theorem", *Journal of the Chemical Society Perkin Transactions 2*, **1999**, 1653 – 1661.

[205] H.S. Freeman, G.C. Lickfield, M.J. Drews, M.B. Polk, S. Kumar, D. Hinks, T. Chen, X. Hu, L. Cleveland and J. Lye, "A molecular orbital approach to molecular design", *National Textile Center Annual Report*, **1995**, *22*, 283 – 293.

[206] G.J. Ashwell, G. Jefferies, E.J.C. Dawnay, A.P. Kuczynski, D.E. Lynch, Y. Gongdata and G.D. Bucknall, "Linear and non-linear optical properties of the different Langmuir-Blodgett Phases of C_nH_{2n+1}-Q3CNQ", *Journal of Materials Chemistry*, **1995**, 5, 975 – 980.

[207] A. Broo and M. C. Zerner, "Electronic structure of dnor-spacer-acceptor molecules of potential interest for molecular electronics. III. Geometry and device properties of P3CNQ and Q3CNQ", *Chemical Physics*, **1995,** *196*, 407 – 422.

[208] A. Broo and M. C. Zerner, "Electronic structure of dnor-spacer-acceptor molecules of potential interest for molecular electronics. IV. Geometry and absorption spectrum of CH_3-αP3CNQ", *Chemical Physics*, **1995,** *196*, 423 – 436.

[209] M. Pickholtz and M.C. dos Santos, "AM1/CI study of molecular rectifier", *Journal of Molecular Structure (Theochem)*, **1998,** *432*, 89 – 96.

[210] R. M. Metzger, N. E. Heimer and G. J. Ashwell, "Crystal and molecular structure and properties of picolytricyanoquinodimethan, zwitterionic donor-pi-acceptor adduct between Li^+TCNQ^- and 1,2-dimethylpyridinium iodide ", *Molecular Crystals and Liquid Crystals*, **1984,** *107*, 133 – 149.

[211] N. A. Bell, D. J. Crouch, D. J. Simmonds, A.E. Goeta, T. Gelbrich and M.B. Hursthouse, "Structural and solvatochromic studies of series of tricyanoquinodimethane-based zwitterions", *Journal of Materials Chemistry*, **2002,** *12*, 1274 – 1279.

[212] S.N. Yaliraki, M. Kemp and M.A. Ratner, "Conductance of molecular wires: influence of molecule-electrode binding", *Journal of the American Chemical Society*, **1999** *121*, 3428 – 3434.

[213] L.E. Hall, J.R. Reimers, N.S. Hush and K. Silverbrook, "Formalism, analytical model and a prioro Green's-function-based calculations of the current voltage characteristics of molecular wires", *Journal of Chemical Physics*, **2000**, *112*, 1510 – 1521.

[214] K. Han, X. Lu, J. Xu, S. Ma and W. Wang, „Second harmonic generation investigation on molecular orientation in Langmuir-Blodhett films pooled by an electric field", *Optical Communications*, **1998**, *152*, 371 – 375.

[215] R.L.H. High, "Synthesis and self-assembly of rectifying molecules, PhD thesis **2005**, Cranfield University, Cranfield, UK.

[216] R. Hamilton, "Materials for molecular electronics fabricated by Langmuir-Blodgett techniques and self-assembly", PhD thesis **2002**, Cranfield University, Cranfield, UK.

[217] S. Lenfant, C. Krzeminski, C. Delure, G. Allan and D. Vuillaume, "Molecular rectifying diodes from self-assembly on silicon", *Nano Letters*, **2003**, *3*, 741 – 746.

[218] M. Mrksich, C.S. Chen, Y. Xia, L.E. Dike, D.E. Ingber and G.M. Whitesides, "Controlling cell attachment on contoured surfaces with self-assembled monolayers of alkanethiolates on gold", *Proceedings of the National Academy of Sciences of the United States of America* **1996**, *93*, 10775 – 10778.

[219] Z. Hou, N.L. Abbott and P. Stroeve, "Electroless gold on a substrate for self-assembled monolayers", *Langmuir*, **1998**, *14*, 3287 – 3297.

[220] K. Moczko, unpublished results PhD thesis **2007**, Cranfield University, Cranfield, UK.

[221] S.A. Krutovertsev, S.I. Sorokin, A.V. Zorin, Ya.A. Letuchy and O.Yu Antonova, "Polymer film-based sensors for ammonia detection", *Sensors and Actuators B*, **1992**, *7*, 492 – 494.

[222] T. Grady, T.Butler, B.D. MacCraith, D. Diamond and M.A. McKervey, "Optical sensor for gaseous ammonia with tuneable sensitivity", *The Analyst*, **1997**, *122*, 803 – 806.

[223] J. Yaun, S. Shao and C. Gao, "Alternative method of imaging surface topologies of nonconducting bulk specimens by scanning tunneling microscopy", *Physical Review Letters*, **1991**, *67*, 863 – 866.

[224] M. Heim, R. Eschrich, A. Hillebrand, H.F. Knapp, R. Guckenberger and G. Cevc, "Scanning tunneling microscopy based on the conductivity of surface adsorbed water. Charge transfer between tip and sample via electrochemistry in a water meniscus or via tunneling?", *Journal of Vacuum Science and Technology B*, **1996**, *14*, 1498 – 1502.

[225] M.B. Song, J.M. Jang and C.W. Lee, "Electron tunneling and electrochemical current through interfacial water inside an STM junction", *Bulletin of the Korean Chemical Society*, **2002**, *23*, 71 – 74.

[226] G.J. Ashwell, B.J. Robinson, M.A. Amiri, D. Locatelli, S. Quici and D. Roberto, "Dipole reversal in Langmuir-Blodgett films of an optically nonlinear dye and its effect on the polarity for molecular rectification", *Journal of Materials Chemistry*, **2005**, *15*, 4203 – 4205.